DELFT UNIVERSITY OF TECHNOLOGY

MASTER THESIS

CIE5061-01

Industrial Floors

Research on the structural behaviour

Author:
Maik ODIJK - 4095561

Supervisors:
TU Delft
René BRAAM
Max HENDRIKS
Lambert HOUBEN

Pieters Bouwtechniek Utrecht
Robin SCHIPPER

October 29, 2019

TU Delft
Delft University of Technology

Pieters BOUWTECHNIEK

Preface

This thesis is submitted to obtain the Master of Science degree at the Delft University of Technology. To obtain this degree, an investigation is conducted on the structural behaviour of an industrial floor constructed on grade. The research is carried out at Pieters Bouwtechniek B.V. Utrecht where the question was raised on how to improve the design and quality of industrial floors.

I would like to thank my supervisors for their support during my research. I am very pleased with the guidance of Robin Schipper at Pieters bouwtechniek B.V. who gave me the opportunity and trust to let me perform my thesis at the company. He helped me with valuable practical insights and support to finish this research. I would also like to thank all the colleague's for there support, help and most important the warm welcome and great working ambiance. During my stay I have gained valuable experience both on the research subject and the general engineering work.

For the development of the non-linear finite element model, I would like to thank the engineering department of DIANA FEA B.V. in Arnhem for there help to set-up the model. Special thanks to Ab van den Bos for sharing his expertise on industrial floors and FEA.

Next I would like to thank my supervisors at the Delft University of Technology for assisting me in the process. For the first part of the research Dick Hordijk provided me with guidance and structure to start my research. The guidance on the development of the finite element model was great by Max Hendriks. The practical input during the meetings by Lambert Houben were very helpful. My special thanks is for René Braam who not only support me during this thesis but also during my complete study. His support over the years gave me the confidence to finalise the master program.

Finally, I want to thank family and friends for their mental support during the research. Especially, I want to express my sincere thanks to my girlfriend, Hanna, for her support and believe during the moment when I needed them the most.

Maik Odijk
4095561

Abstract

This research focuses on the structural behaviour of an elastic supported reinforced concrete slab. Over the years, there is a tendency to realise industrial floors with large joint-spacings. The downside of a slab on grade with a large joint-spacing is that the risk of (uncontrolled) cracking due to a shrinkage load is higher, which often results in durability issues. In practice, the slabs on grade are generally designed and constructed based on experience by specialised floor companies and often with less than the theoretical minimum required reinforcement. This research aims to close the gap between theory and practice and to gain insight into the structural behaviour. Moreover, reducing the number of damages in slabs on grade.

In the first part of this thesis, the stress development and crack risk in a restrained concrete slab on grade exposed to shrinkage is analysed. The restrained shrinkage stress in the concrete member is mainly influenced by the time-dependent properties of concrete and the degree of restraint of the slab. The most relevant degree of restraint for a jointless slab is by soil friction and depends on the slab length, soil properties and the vertical load like self-weight. From the sensitivity analysis in this research, it is shown that the middle section is fully restrained for slab lengths or joint spacings of 40 to 80 meters long for practical ranged values. The relaxation effect in concrete, based on the creep behaviour, reduces the restrained shrinkage stress over time. Stress reductions of 40% to 70% were found for practical values in the analysis after one year of shrinkage loading.

The crack risk in indoor slabs on grade is the highest between two and twelve months after casting according to the findings in practice and this thesis. The early-age crack risk is relatively low for an indoor slab on grade compared to a concrete pavement because of the significant less influences of the environment. The crack risk can be reduced by composing a concrete mixture with a low relaxation coefficient ψ, low concrete shrinkage e_{cs}, low Young's modulus E_{cm}, a high concrete cracking stress capacity σ_{cr} and by reducing the degree of restraint of the slab.

Secondly, the cracking behaviour of a fully restrained concrete tensile member with only reinforcement near the surface is analysed with analytical models and a finite element model. For modelling cracking in a restrained member initiated by an imposed deformation in the finite element model, the random field application is required. The random field application generates the spatial variation of the tensile strength of the concrete material. The random field simulates weak zones in the concrete member where crack localisation will be initiated. The downside of the random field application is that the crack pattern in the model is predetermined. The cracking behaviour is analysed for a shrinkage load, a point load and for both loads combined. In all the analyses, it is found that cracking in a slab on grade always results in a not fully developed crack pattern. A not fully developed crack pattern is characterised by the forming of additional cracks instead of widening of the existing cracks when the load increases.

When cracking due to a shrinkage load in fully restrained members occurs, the imposed load decreases, which reduces the tensile force in the uncracked zone. Force reductions up to 73% were calculated after cracking in a five-meter long restrained slab. For an eccentrically top reinforced member, the first crack occurs at the bottom fibre and is uncontrolled. The tensile force in the reinforcement, in combination with the eccentrical position, induces a negative bending moment in the uncracked zone of the slab on grade. In combination with the restrained shrinkage load, this results in an axial tensile force and a negative bending moment in the uncracked zone after cracking. Over time, the shrinkage load increases and a flexural crack can be initiated at the slab surface.

A point load induces a positive bending moment at the position of the load and a smaller negative bending moment next to the point load. After cracking due to the point load, an axial compressive force and an increased negative bending moment are present in the uncracked zones next to the point load. The sensitivity analysis on the behaviour by the point load showed that the principal stresses in the slab could be reduced by increasing the subgrade modulus k_{mod}, the slab height h or by lowering the concrete stiffness E_{cm} of the slab.

The load combination analysis showed that an axial tensile force and a negative bending moment are present in the uncracked zones. It is found that a higher point load only increased the slab deflection and the number of flexural surface cracks and not the crack width. However, a higher shrinkage strain load did slightly

increased the maximum crack width but mainly increased the number of cracks. Therefore, it is concluded that the slab on grade remains in the cracking phase for the combined loading situation.

Both in this research and the literature, it is stated that crack width calculations of a restrained concrete slab imposed by a shrinkage load results only in indicative values. The analysis of the cracking behaviour showed that cracking at the surface is induced by an axial tensile force in combination with a negative bending moment. Therefore, estimation of the crack width can best be performed with the *CUR-65* model based on an enhanced cracking bending moment of the slab on grade.

Because accurate crack width calculations are not possible, recommendations are made on how to reduce the crack widths in a jointless slab on grade. A slender slab with a low concrete tensile strength is advised to reduce the internal cracking force and bending moment. Also, it is found that a lower shrinkage load leads to a smaller crack width. Therefore, a shrinkage reducing concrete mixture is advised. Moreover, high bonding properties between the reinforcement and concrete reduce the crack width, which can be realised with reinforcement with a small diameter $\varnothing$ and mesh-size. Finally, reinforcement is the most effective in controlling surface cracks when placed in the top fibre of the slab. It is concluded that for a slab on grade, replacing the conventional reinforcement with steel fibre reinforcement does not reduce the required amount of reinforcement for controlling surface cracks.

Summary

Over the years, the demand for large industrial floors has increased and, because joints often result in performance issues, there is a tendency to realise floors with large joint-spacings. Industrial floors constructed on grade, now referred to as a slab on grade, is continuously supported by the soil. Therefore, the slab on grade can be realised more slender compared to a slab on piles. A slender slab result in a more economical floor and is, therefore, more desirable in the highly competitive market. The downside of a slab on grade with large joint-spacing is that the risk of uncontrolled cracking due to shrinkage is higher. In practice, the slabs on grade are generally designed and constructed based on experience by specialised floor companies. Detailed calculations of the crack width are often not provided. Instead, only an indication of the crack width is given. A remarkable finding in this thesis is that the slabs on grade are often constructed with less than the theoretical minimum required reinforcement. In theory, the low amount of reinforcement is not sufficient for controlling cracks. Research is performed to gain insight into the stress and cracking behaviour of slab on grades. The results of the research can be used to design and construct an uncracked or crack controlled slab on grade, thereby closing the gap between theory and practice.

Stress behaviour
In the first part of this thesis, the stress development in a restrained concrete slab on grade is analysed. The slab on grade shrinks due to the chemical concrete properties and environmental influences. When the shrinkage of the slab is restrained, stresses develop in the concrete. The stress development in the restrained member is mainly influenced by the time-dependent properties of concrete and the degree of restraint. The influence of these parameters is analysed in this research with the use of practical ranged properties.

Degree of restraint
The governing restraints in slab on grade occur due to the surrounding structure like foundation strips or pads and the soil friction. When the slab is connected to surrounding structures, it can fully restrain the slab over the total length. Restrained shrinkage stresses will then be present everywhere. It is advised to construct the slab on grade detached from its surrounding structures to reduce the degree of restraint. The soil friction induces no restraint at the slab edges and is maximum in the middle section of the slab. The degree of restraint by soil friction depends on the slab length, soil properties and the vertical load like self-weight. From the sensitivity analyses in this research, it is shown that the middle section is fully restrained for slab lengths or joint spacings of 40 to 80 meters long for practical ranged values. Nowadays, these joint spacings are often realised in slabs on grade. In the literature, it is stated that the shrinkage profile is most times a combination of a uniform and a gradient strain. The gradient strain induces a rotation of the slab on grade, which is also restrained by the vertical loading. The analysis showed that the rotation is fully restrained at joint spacings of six to ten meters.

Concrete relaxation
Besides the degree of restraint, the stress development is mainly influenced by the concrete relaxation effect. The relaxation effect, based on the creep behaviour, relaxes the restrained shrinkage stresses over time and is quantified by the relaxation coefficient ψ. In the analysis of the relaxation effect in ageing concrete, stress reductions of 40% (ψ=0.6) to 70% (ψ=0.3) were found after one year of shrinkage loading. The age of the concrete at the moment of loading mainly influences the concrete relaxation coefficient. Therefore, early age loading has significantly less influence on the long-term stresses in concrete slab compared to the same loading at a later moment in time. It is concluded in this research that for design calculations, the long-term stresses can best be estimated by taking into account the relaxation coefficient ψ given in the *CUR-36*, a Dutch recommendation for the design of slab on grade.

Crack risk
In the second part of the thesis, the crack risk in a slab on grade is analysed. When the restrained shrinkage stresses reach the cracking stress of concrete, cracking is likely to occur. The crack risk in indoor slabs on grade is the highest between two and twelve months after casting according to the findings in practice. The same time-range is found in the analysis of this research. Compared to a slab on grade cast outdoors, where cracking occurs after a few days due to the significant influence of the daily temperature drops, the early-age cracking risk is significantly lower for an indoor slab on grade. The daily temperature influence for an indoor slab is significantly less. The moment of cracking of an indoor slab mainly depends on the seasonal temperature

influence (e.g., the moment of casting) and the amount of concrete shrinkage. The crack risk can be reduced by composing a concrete mixture with a low relaxation coefficient ψ, low concrete shrinkage e_{cs}, low Young's modulus E_{cm} and a high concrete cracking stress capacity σ_{cr}. If the degree of restraint R is reduced, only a part of the restrained shrinkage stresses will be generated, and therefore, reduces the crack risk of the slab on grade. In a large jointless slab on grade, it can be assumed that there is always a fully restrained section present and that cracking is likely to occur during the slab's lifetime. Therefore, the cracking behaviour in a fully restrained slab on grade is analysed with the use of a finite element model in great detail in this thesis.

F.E.M.
The fully restrained section of the slab on grade is modelled in *DIANA FEA* and transient crack analyses are performed. For modelling cracking initiated by imposed deformation in a fully restrained member, the random field application is used in the finite element model. The random field application generates the spatial variation of the tensile strength of the concrete material. The random field simulates weak zones in the concrete member. In these weak zones, crack localisation is initiated. The downside of the random field application is that the crack pattern is predetermined in the model. In addition, there are no recommended parameters given in the standard norms for the generation of a realistic random field of the concrete properties. Besides the use of the random field application, it is also important to take into account the long-term bond-slip properties of the reinforcement in the finite element model. Furthermore, different post-processing checks of the crack width are compared and it is found that the average crack width per element is the best method for the determination of the crack width in the model.

Cracking behaviour
The cracking behaviour analysis focused on a fully restrained concrete tensile member with only reinforcement near the top surface. The cracking behaviour in the fully restrained tensile member by a shrinkage load, point load and combined loading are analysed. The transient analysis represents a slab on grade, which undergoes five years of shrinkage after casting. In the analysis, it is found that cracking in a slab on grade always results in a not fully developed crack pattern. A not fully developed crack pattern is characterised by the forming of additional cracks instead of widening of the existing cracks when the load increases. When cracking due to a shrinkage load in fully restrained members occurs, the imposed load decreases. After cracking, the cracked surfaces move towards the uncracked zone. Thereby, the imposed shrinkage strain in the uncracked zone reduces. The reduction of the imposed strain load results in a reduction of the tensile stresses in the uncracked zone, which results in a lower tensile force in the reinforcement. This force reduction effect is referred to as crack relaxation and is, in this thesis, quantified by the crack relaxation coefficient ψ_{crack}. This effect is analysed in this research and it is found that the crack relaxation effect can be significant in members with a short restrained length $L_{restraint}$, low reinforcement ratio ρ_s or a low concrete-reinforcement bonding quality. Force reductions up to 73% (ψ_{crack}=0.27) were calculated after cracking in a five-meter long restrained slab.

For an eccentrically top reinforced member, the first crack occurs in the unreinforced bottom section because the force resistance N_{cr} is lower when no reinforcement is present. The crack at the bottom fibre is uncontrolled and rapidly develops towards the top fibre. There, the reinforcement is present to control the crack by transferring the stresses through the crack into the concrete. The tensile force in the reinforcement in combination with the eccentrical position of the reinforcement induces a negative bending moment in the uncracked zones. In combination with the restrained shrinkage load, an axial tensile force and a negative bending moment are present after cracking with the result that the maximum tensile stress in the uncracked concrete is located at the top fibre. Over time, the shrinkage load increases and additional cracking can occur at the surface of the slab on grade. If the shrinkage load is high enough and the concrete stress reaches the cracking stress, a flexural crack is initiated at the slab surface. These cracks reduced the axial tensile force and negative bending moment to some extent due to the crack relaxation effect. Over time, the shrinkage strain continues to develop and more flexural cracks at the surface can be formed. In Fig: , the stress behaviour is shown per load step for the crack development in the eccentrically reinforced restrained slab on grade loaded by a uniform strain load.

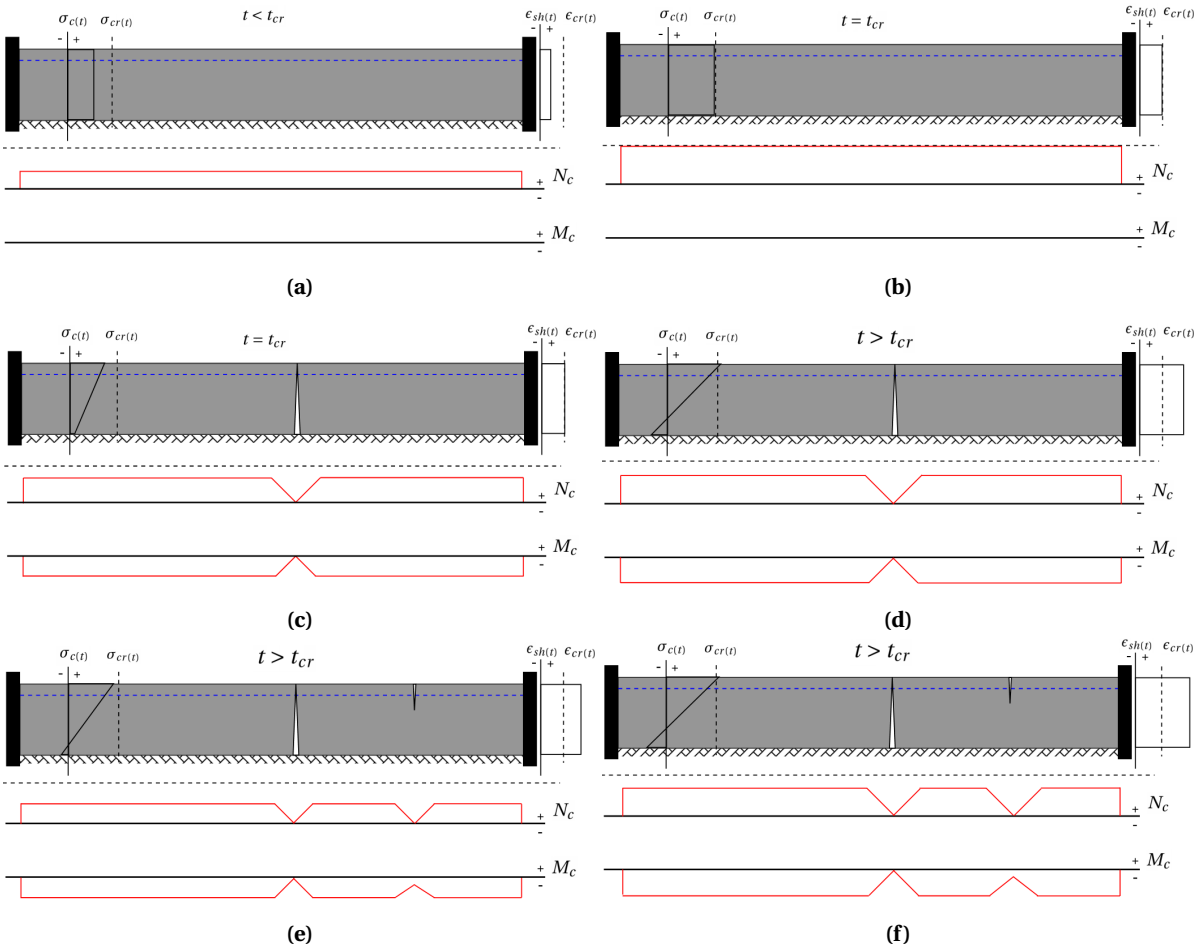

Figure 1: Cracking behaviour in restrained slab due to shrinkage

The stress behaviour in a slab on grade loaded by a point load is different from the restrained shrinkage load. The point load induces a positive bending moment at the position of the load and a negative bending moment next to the point load. The point load does not induce an axial force in the uncracked slab on grade. When the point load is high enough, cracking can be initiated at the bottom fibre at the location of the point load. Due to the crack, the local stiffness reduces and the rotation in the restrained slab increases. This leads to the horizontal movement of the cracked surfaces towards the edges of the restrained slab. This restrained horizontal movement, induced by the point load and the crack, results in an axial compressive force in the slab. The rotation in the slab also increases after the formation of the crack, which results in an increment of the negative bending moment in the uncracked zones. After cracking an axial compressive force and an increased negative bending moment is present in the uncracked zones of the slab on grade. If the point load is high enough, this negative bending moment can initiate flexural cracking at the surface. It is found that, even for high external point loads, the slab on grade is in the not fully developed crack pattern. In Fig: the stress behaviour is shown for the crack development in the eccentrically reinforced restrained slab on grade loaded by a point load.

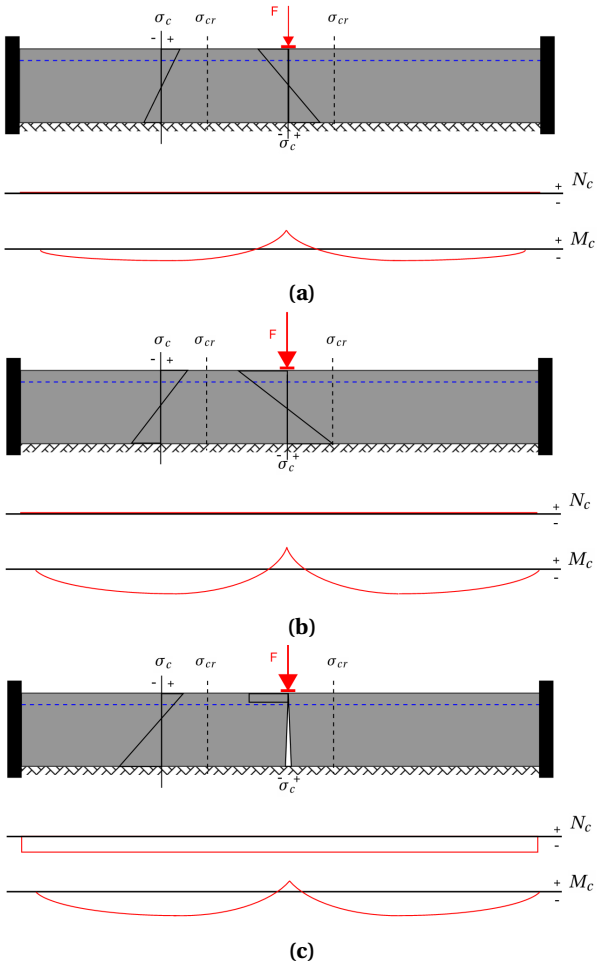

Figure 2: Cracking behaviour in restrained slab due to point load

Furthermore, in the performed linear sensitivity analysis of a point load on a slab on grade, it is found that the stresses in the slab can be reduced by increasing the subgrade modulus k_{mod}, the slab height h or by lowering the concrete stiffness E_{cm} of the slab. Besides reducing the stresses in the slab on grade, it is found that a higher subgrade modulus also significantly reduces the deflection of the slab at the position of point load.

The final analysis of the stress behaviour is the load combination of restrained shrinkage with four point loads simulating the back-to-back racking. Equal to the previous analyses, an axial tensile force and a negative bending moment are present in the uncracked zones next to the racking. When the first crack is initiated at the position of the racking, the tensile force is lower due to the beneficial compressive force from the point loads. It is found that when the first crack is not initiated at the position of the racking, a through crack occurs in the zone next to the racking with a significantly larger crack width. A maximum surface crack width after five years of 0.36 mm compared to 0.15 mm is found in the finite element analysis for the situation where first cracking occurs next to and at the position of the racking. Furthermore, the analysis showed that a higher point load only increased the deflection and the number of surface flexural cracks and not the crack width. A larger shrinkage load also increased the number of cracks, but also slightly increased the maximum crack width. Even-though the crack width slightly increases with an increase of strain load, the slab on grade is still in the not fully developed crack pattern for the combined loading situation.

Crack width analysis

It is now known that, for all loading situations, the slab on grade remains in the not fully developed crack pattern. Cracking at the surface is induced by an axial tensile force in combination with a negative bending moment. In the literature, it is often stated that accurate crack width calculations are not possible and a considerable variation of results is found. This research reaches the same conclusion after the comparison of different crack width models for the not fully developed crack pattern. Therefore, it is concluded that the crack width calculation of a slab on grade results in an indicative value. From the analysis, it is found that the crack width can best be estimated with the adapted *Van Breugel* model given in the Stu*fib*-11 report and the *CUR-65* model based on an enhanced cracking bending moment of the slab on grade. The cracking bending moment M_{cr} of the slab is multiplied with a factor 1.4, which is based on practical findings. This factor represents the presence of the tensile force in the member after cracking, the ageing of the concrete and additional shrinkage strain by the environment.

In the crack width analysis of this research, it is shown that the analytical design models result in conservative crack widths when compared with the crack widths found in the N.L.F.E.A.. The ratio of the maximum crack width for the combined loading situations between the finite element model results and the analytical model results of *CUR-65* and Stu*fib*-11 are respectively 1,87 and 1,90. For both models, a lower- and upper bound ratio of 1,2 and 2,4 is found. In the most unfavourable situation of the through crack in the section next to the racking load, the analytical models *CUR-65* and Stu*fib*-11 resulted in a ratio of respectively $\frac{0.39}{0.36} = 1,08$ and $\frac{0.41}{0.36} = 1,14$.

Because accurate crack width calculations are not possible, recommendations are made on how to reduce the crack widths in the slab on grade. The cracking forces and moment of the concrete slab on grade has to be kept small. This is done by reducing the slab height and the concrete tensile strength. The analysis showed that a lower shrinkage load leads to a smaller crack width in the slab on grade. Therefore, a shrinkage reducing concrete mixture is advised. Finally, it is found that better bonding properties between the reinforcement and concrete reduce the crack width. Also, by placing the reinforcement close to the surface, it becomes more efficient in controlling a surface crack of the slab. Therefore, reinforcement with a small diameter ∅ and mesh-size placed near the top fibre is recommended. The downside of reducing the concrete tensile strength can be that the abrasion and impact resistance is then lower. The risk of damage by other loading types can, therefore, be higher and can be undesired regarding durability.

Steel fibre reinforcement

The structural behaviour of concrete changes from brittle to a more ductile one when fibre reinforcement is added to the mixture. The residual tensile strength property of the steel fibre concrete mixture significantly increases. For slabs on grade, steel fibres are not efficient compared to conventional mesh reinforcement. Strain hardening steel fibre reinforced concrete is required to realise a crack controlling slab reinforced only with steel fibres. This requires a high amount of steel fibres. In practice, this amount is often assumed as >85 $\mathrm{kg\,m^{-3}}$. Commonly designed slabs on grade with conventional mesh reinforcement is in the range of 44 to 56 $\mathrm{kg\,m^{-3}}$. Besides the high amount of fibres, due to the random variation of the fibres, the structural integrity in a steel fibre reinforced concrete slab can not everywhere be guaranteed.

Contents

1. Introduction

1.1 Scope

The Dutch landscape is slowly changing because more and more big grey boxes emerge from the horizon. Changing of the landscape is, of course, slightly exaggerated, but it can not be denied that these boxes build mainly for Distribution Center (*D.C.*) are increasing in numbers and size. The demand for new *D.C.* is coming from the growing and changing the retail market. Mainly due to e-commerce, a more centralised distribution of products is preferred by costumers. The Netherlands, especially the south, is a trendy country for large distribution companies to settle due to the tax regulations, high-quality infrastructure and its location in Europe. In 1996 there was a total of ten million m^2 of storage area, which, twenty years later, has almost tripled to 28.8 million m^2. Besides the increment in *D.C.*, there is also a trend of increasing the size of a *D.C.*. In 2017 more than 25% of the newly developed *D.C.* were larger than 40.000 m^2. The largest is a build-to-suit *D.C.* of 170.000 m^2 [1]. That is an equivalent of 34 soccer fields. Besides the increment in area, the storage systems are also becoming more efficient. Higher and denser racking can result in higher loading and more strict requirements for the industrial floor (*I.F.*). For all these large industrial buildings, a high-quality floor is always required. An *I.F.* looks like a relatively simple structural element to design and construct, but in reality, the behaviour is complex.

Figure 1.1: Distribution centre under construction [2]

Over the years, the design philosophy of the *IF's* has changed significantly. In the past, many slabs were designed with saw-cut joints every 5-8 meters to eliminate shrinkage problems. Saw-cut joints are used as crack inducers to relief the shrinkage stresses. Therefore, the influence of shrinkage was neglected in the structural design. The saw-cut joints are very likely to deteriorate and that edges lift up due to curling, Fig: 1.2. The causes of curling are addressed in the next chapter. These problems cause performance issues. When Material Handeling Equipement (*M.H.E.*) is crossing a joint, vibrations, shocks and high local stresses occur in the floor. The damaged joints lead eventually to damaged *M.H.E.*, lower productivity and physical complains by employers. By eliminating the number of joints, the risk of joint deterioration is reduced. The downside is that by increasing the joint spacing, shrinkage problems are becoming more relevant in the structural design. Due to the joint issues and other serviceability and regulation demand, the end-users wishes a jointless industrial floor. 'Jointless' floors are possible but it often results in a high amount of reinforcement to control the cracks. A lot of reinforcement results in an expensive structure that makes this concept in a highly competitive market difficult to sell.

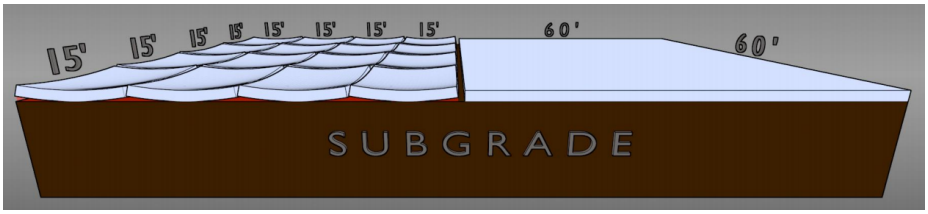

Figure 1.2: Curling effect of sawcut joints v.s. jointless slab

Steel fibres are often added to the concrete mixture when shrinkage issues are present. In some situations, steel fibres can completely replace ordinary reinforcement in industrial floors. Steel fibres can result in significant cost savings. Numbers show that steel fibres are very popular in floor construction. 65% of the total produced steel fibres are used in floor constructions[3].

Important for every structure is its foundation. From all the *IF's*, 70% is constructed directly on grade. The other foundation method is with piles. Slab on Grade (*S.o.G.*) can generally be realised more slender compared to a Slab on Piles (*S.o.P.*) because of continuous support. The downside can be the long-term and differential settlement, which are difficult to predict. The foundation method affect the stress behaviour of the concrete slab. By realising jointless floors, the floor becomes restrained by its surroundings. Due to the restraints, the Imposed Deformation (*I.D.*) is becoming more relevant and the stress behaviour becomes more complex. The time-dependent and non-linear effects in concrete like stress relaxation can have influences on the behaviour. The combinations of all these influences make calculation and design of a *I.F.* complex. Nowadays, there is a trend to use complex Non-Linear Finite Element Analysis (*N.L.F.E.A.*) to estimate the behaviour in concrete structures.

The engineer has to make many decisions in the design process to deliver a durable floor. Very large, high-quality floors have to be realised in a cost-efficient manner. To come up with an economical solution, the engineer needs to have a good understanding of the behaviour and design method of *S.o.G.*. Therefore, research on the behaviour can be helpful for the design of jointless *S.o.G.*. This research will investigate the behaviour of reinforced concrete slabs on grade to contribute to the design methods and final quality of the product.

1.2 Problem statement

The scope described some general problems and subjects regarding *S.o.G.* and the growing interest of an engineering company in designing and constructing large concrete floors. In the problem statement, the research is delimited by formulating different research subjects. The subjects are based on the degree of restraint, concrete mixture, stress and cracking behaviour and *N.L.F.E.A.*. Finally, the research question is formulated, which covers all the sub-questions.

The focus of the research will be on the subjects: *jointless, slabs on grade, steel fibre reinforcement, imposed deformation, degree of restraint, N.L.F.E.A., concrete relaxation, stress behaviour, crack width* and *not fully developed crack pattern.*

Damages

The floor is an essential element for the productivity in industrial buildings like the *D.C.*. A high-quality floor result in higher efficiency at the workplace [4]. A high-quality floor is, unfortunately, not always the case. Complete failure of the floor does not happen often but a damaged concrete floor is very common[5]. In Sweden, it is reported that 20% of all damaged concrete structures are floor slabs. It is found that 35% of the floor damages are from shrinkage related problems [6]. These damages affect the performance of the floor and result in complaints by the end-user. Reparation and maintenance are required to maintain the serviceability of the floor. Production will slow down. This can bring high financial cost to the property owners/end-user [7]. The result is a discussion between the designer, constructor and client about the extra cost and quality of the floor. Simple questions like; How could this happen? What went wrong? How could this be prevented? are often raised, but simple answers can not always be given. Therefore, a better understanding of the behaviour of *I.F.* is required to answer these simple but tough questions.

The change from small to large joint spacing result in a different stress behaviour and the degree of restraint becomes more significant in jointless slabs. Designing a *S.o.G.* is complex, mainly due to the restrained shrinkage load named *I.D.*. When the imposed stresses are not taken into account in the design, excessive cracking up to 3 mm wide can occur in the floor. The imposed deformations are the main reason for the uncontrolled and undesired crack behaviour [8][9]. Many parameters influence the restrained shrinkage cracks. The most important factors are the amount and development speed of shrinkage, time-dependent concrete material properties, concrete relaxation due to creep and the degree of restraint. When the restrained shrinkage strains are not considered in the design, problems are likely to occur.

Degree of restraint

The degree of restraint for *S.o.G.* can come from many aspects. The frictional restraint of the sub-base is often assumed to be governing. The quantification of the restraint is difficult because it depends on the non-linear soil-structure interaction, amount of loading and slab length. Designing a soil-structure interaction requires knowledge from both fields. The anisotropic and load time-dependent soil properties make designing the soil-structure interaction a difficult task. The degree of restraint is also affected by the reinforcement and other surrounding elements. Large jointless slab can be fully restrained. When fully restrained, the concrete structure is statically undetermined, which changes the behaviour of the slab. Therefore, it is essential to quantify the degree of restraint for the design of jointless *S.o.G.*.

Stress behaviour

The stress behaviour in the fully restrained slabs is not commonly known. Standard design methods are often based on statically determined structures. The stress behaviour of a fully restrained member is generally described with the use of the *TU Delft* tensile or flexural member. It should be investigated if this model can also be implemented for the fully restrained slab loaded by *I.D.*. For most crack width analysis, the development of the stresses in the concrete and reinforcement is required. It is difficult to determine how many stresses are

present in the fully restrained member loaded with shrinkage. Calculation models have to be found to determine the concrete and reinforcement stresses. Also, the effect of cracking should be taken into account. It is known that cracking reduces the stiffness of concrete structures, which affects the stress behaviour. Therefore, the effect of the cracking on the stress behaviour should also be analysed.

Concrete mixture

As mentioned before, the stresses from the *I.D.* mainly depend on the time-dependent concrete properties. The stress behaviour in the floor also depends on the highly variable environmental factors. Environmental effects mainly influence the shrinkage and temperature load. The extent of these influences has to be analysed. Ageing of concrete and non-linear viscosity behaviour like creep has to be taken into account for realistic stress calculations in the concrete. It is stated that moisture-related stresses are potentially greater than temperature related. Especially for indoor ground slab were environmental effects are minimised by the building. Moisture related stresses are often developed slowly, so concrete relaxation often reduces them significantly[10]. Many simplified stress calculation methods and relaxation functions are developed over the years. The proper implementation of this effect in practical design procedures have to be determined and analysed. The composition of the concrete mixture can modify the time-dependent properties like shrinkage and strength of concrete. The effects of the concrete properties on the stress behaviour have to be analysed to get more insight.

Cracking behaviour

In industrial floor, the reinforcement is used to increase the load-bearing and to control the cracks. For large *S.o.G.*, continuous reinforcement is required for eliminating joints. The required amount of reinforcement, to control the cracking, is often discussed. The calculation of the most economical reinforcement solution is complicated because many factors influence the behaviour. In practice, constructors often apply less than the theoretical minimum required of reinforcement based on experience without proper substantiation. The amount of reinforcement in a *S.o.G.* is many times a discussion between the constructor and designer. An explanation has to be found to clarify the differences between theory and practice. Besides the amount of reinforcement, the floor design is often a combination of many nation standards, some design methods borrowed from last project manual and a few heavily promoted products from business partners[4]. Good measures and instructions regarding detailing of slabs-on-ground are available in the literature, but a fundamental knowledge of how the *S.o.G.* behave during the shrinkage process when influenced by external restraints is not properly documented. Understanding this behaviour is, however, deemed crucial in order to be able to minimise problems caused by shrinkage cracking[6].

A relatively new development is the use of steel fibre as reinforcement in the concrete. Steel fibres can reduce or replace the nominal reinforcement and can contribute to crack control. The downside is that the calculation methods for Steel Fibre Reinforced Concrete (*S.F.R.C.*) are not widely known and the properties are not yet fully standardise. Designing with steel fibres is still in its infancy. Besides, there is no standardised crack width calculation method for *S.F.R.C.* and hybrid structures. More information on the calculation methods for hybrid reinforcement is required.

It is found that crack width design calculations for imposed deformations result in a wide scatter of results [11][12]. The scatter is due to the many different calculation methods for the crack width. The calculation method depends on the cracking phase of the concrete structure. A crack due to imposed deformation will most likely result in a Not Fully Developed Crack Pattern (*N.F.D.C.P.*) and external loads in a Fully Developed Crack Pattern (*F.D.C.P.*). Besides the cracking phase, the crack width also depends on the slab dimensions, shrinkage load and concrete properties. Insight on the effects of the parameters is desired for a better understanding of the cracking behaviour.

All structures have to be designed to withstand a certain external load. The external load often determines the size of the structural elements. The calculation methods of the stresses in a slab given in the provisions are based on elastic and plastic theory. In literature it is found that these methods are conservative[13][14]. It can

be desirable to calculate the stresses for the external loads more precise because of the competitive market combined with the increasing loads.

N.L.F.E.A. is a tool that can be used for calculating complex structural behaviour. The complete structure and its properties have to be modelled and assumed. The assumption made in the model has a significant effect on the result and errors are easily made. The analyst always stays responsible for the result, and therefore educated guesses have to be made[15]. Expert Finite Element Model (*F.E.M.*) knowledge is required to performed a reliable cracking analysis with the transient effect of creep and shrinkage. Especially for crack development in the *N.F.D.C.P.*.

The stress behaviour of *S.o.G.* depends on many factors. Many assumptions have to be made for calculating the stresses. After many years of studies and experience, engineers can make theses assumptions very well. Nevertheless, some factors are still unknown. During the construction of the structure, many assumed properties can be influenced and damages can appear. Proper execution of the structure is, therefore, always a major factor in the end-quality. Also, for slabs on grade the construction is of great importance. Therefore, recommendations will be given for all the (structural) elements.

The shortcomings of the design for *S.o.G.* are defined as followed:

- The degree of restraint is difficult to quantify.
- Non-linear and viscous effects of concrete influence the stress behaviour of *S.o.G.*.
- Environmental effects influence the stress behaviour of *S.o.G.*
- Cracking changes the stress behaviour in concrete structures.
- Large scatter of crack width values due to the many crack width models.
- Floor design is often based on experience.
- Uncontrolled cracking is common in industrial *S.o.G.*.
- Designing with structural fibre reinforcement is not common practice.
- *N.L.F.E.A.* for fully restrained tensile member loaded by *I.D.* is complex.

The statements result in the following general questions for *I.F.* on grade.

- *What is the degree of restraint of large jointless S.o.G.?*
- *What is the stress behaviour in restrained S.o.G. loaded by I.D. and/or point loads?*
- *What is the cracking behaviour in restrained S.o.G. loaded by I.D. and/or point loads?*
- *What is the influence of concrete relaxation on the stress and cracking behaviour?*
- *Can cracking be prevented in jointless S.o.G.? And if not, how can cracking be controlled in an economical matter?*
- *What is the influence of steel fibres on the behaviour in S.o.G. and how can it be implemented into the structural design?*
- *How can I.D. and external loading be combined in the design procedures of jointless S.o.G.?*
- *Can F.E.M. be implemented in the structural design of S.o.G.?*

The general questions can be combined into the main research question:
What is the structural behaviour of an elastic supported concrete slab loaded by an imposed deformation and point loads?

1.3 Aim of the research

The research focuses on the design method of jointless industrial floors reinforced with conventional or hybrid reinforcement loaded by imposed deformations. The research aims to get insight into the stress and cracking behaviour in *S.o.G.* for a better understanding of the structural behaviour. The main goal is to describe the behaviour in the slab and to find an accurate and practical design procedure for large jointless *S.o.G.* loaded by shrinkage. Therefore, an investigation into the degree of restraint, concrete technology and cracking behaviour is performed. The influences of the boundaries have to be determined to quantify the degree of restraint on the *S.o.G.*. Research into the concrete technology aspect, regarding the time-dependent and transient properties, has to give insight into the stress development. Proper models have to be found for the calculation of the non-linear stress development in the statically undetermined concrete structure loaded by shrinkage. Recommendations have to be found to reduce the crack risk and crack width. After the analyses of the stresses, the research will focus on the cracking behaviour in the slab. The aim is to give insight into the effect of cracking on the stresses. Also, information on the crack width development, due to sustained loading, has to be found. The aim is to find the best crack width calculation method for cracks in the *N.F.D.C.P.* loaded by shrinkage. With a special focus on steel fibre reinforcement, the research aims to contribute to the development and understanding of *S.F.R.C.* design. Also, explanations have to be found for the reason that less than the theoretically required reinforcement ratio is sufficient to control cracks according to the experienced-based slab design. The research also aims to combine the standard design procedure with *N.L.F.E.A.* and give information about *F.E.M.* to make the calculation more accurate and practical. Finally, external loading is briefly addressed. First, the linear elastic calculation is examined to check whether these are conservative. Secondly, the external load, in combination with shrinkage, is analysed.

With this research, the goal is to meet the following objectives for industrial floors:

1. To create a better understanding of the stress behaviour in *S.o.G.* by imposed deformation and external loading.
2. To get insight into the cracking behaviour of restrained jointless *S.o.G.*.
3. To create a better understanding of steel fibre and hybrid reinforcement.
4. To implement (non) linear finite element modelling into the design method.
5. To find an explanation of the gap between the theoretical and experience-based slab design.
6. To advise about crack width control for dominant shrinkage problems combined with external loading.

1.4 Research methodology

The research methodology is to downgrade the topic into four subjects: degree of restraint, concrete technology, stress behaviour and cracking behaviour. For every subject, the relevant theoretical models are determined and elaborated. Next to the analytical approach based on proven theoretical models, non-linear finite element modelling is performed to analyse the complex behaviour in the slab due to the transient effects in Restraint tensile member (*R.T.M.*). With the use of the found analytical models, a sensitivity analysis is performed to investigate the effect of every parameter. The results found in the sensitivity analysis are compared with the data from the literature review and the *N.L.F.E.A.*. Recommendations are made based on comparative analysis. The analysis focus on the general research question formulated in the problem statements. Every parameter per subject is analysed to realise a complete view of the stress behaviour. By analysing the slab behaviour of the experience-based slabs, the reason behind this design method can be brought to light. The relevant parameters are addressed and clear recommendations are made regarding the design and calculation method of *S.o.G.*.

1.5 Outline of the thesis

The thesis is separated into eleven chapters. The content per chapter is briefly mentioned.

Chapter 1: Introduction
An introduction of the research is given with respect to the topic, problems and aim of the research. The research approach is explained.

Chapter 2: General information on *I.F.*
The general information is given for all the relevant elements of the *I.F.*. For a good understanding of industrial floors, the elements like the structural parts, foundation, construction methods and design principle are elaborated.

Chapter 3: Failure analysis
In the failure analysis, the literature survey of cracking issues in *S.o.G.* is given. The governing cracking problem is determined to delimit the research.

Chapter 4: General information on materials
Extensive information on the concrete and reinforcement properties is given. First, the concrete behaviour is described with special attention to the time-dependent properties. The shrinkage and creep behaviour is discussed and the theoretical models regarding these subjects are explained and compared. The mathematical models of concrete relaxation due to creep are elaborated. Secondly, the reinforcement models and time-dependent behaviour for the conventional and hybrid reinforcement are shown. The bond-slip behaviour of the reinforcement is also addressed. Because of the generally unknown behaviour of steel fibre reinforcement, additional information on the behaviour and time-dependent properties is given. The influence of fibre on the stress-strain behaviour in hybrid reinforced concrete is also addressed. Finally, vertical and horizontal soil support and their properties are discussed. The relevant findings based on all the information and models are elaborated at the end of the chapter.

Chapter 5: General information on stress behaviour
First, the global behaviour of *S.o.G.* is described. From the global behaviour, the *S.o.G.* is translated into a *R.T.M.*. The parameters which influence the restraints and determines the dimensions of the *R.T.M.* are elaborated. Both axial and flexural restraints are shown. Secondly, the stress and cracking principle of a *R.T.M.* is described. The behaviour in the linear stage, *N.F.D.C.P.* and the *F.D.C.P.* are given. The sensitivity analysis will focus on the first two stages.

- Stage 1: Linear stress behaviour: Stress development: $\sigma_c < \sigma_{cr}$
- Stage 2: Non-linear stress behaviour: Cracking behaviour: $\sigma_c \geqq \sigma_{cr}$

Chapter 6: Theoretical calculation models
Based on the stress development and the described models, the theoretical models for the calculations of the relevant parameters are given. The theoretical models to calculate the degree of restraint, stress development in restrained concrete structures. Also, the theoretical and experienced-based crack width methods in reinforced and hybrid concrete are elaborated.

Chapter 7: General information on the *F.E.M.*
The set-up considerations for the *F.E.M.* are elaborated. The material models used for the *N.L.F.E.A.* are given and the analysis method of the *R.T.M.* model is given. Special attention is given regarding the random field application. Finally, some notes are given on the risks of using advanced (non-linear) finite element calculation.

Chapter 8: Sensitivity analysis - Stress development
With the use of the failure analysis and the *R.T.M.* behaviour, multiple subjects are formulated, which are calculated and analysed. Parallel to the calculations, the *F.E.M.* is used to verify and compare the results and calculation methods. To get more insight into the behaviour, a sensitivity analysis is performed to investigate the effects of the relevant parameters. The following subjects are analysed for the stress development stage.

- degree of restraint
- Stress development due to *I.D.* in a *R.T.M.*
- Crack risk

Chapter 9: Sensitivity analysis - Cracking behaviour
The same approach, as in chapter 8, is used for the analysis of cracking in *R.T.M.*. The influences of the slab dimensions, concrete mixture and conventional and hybrid reinforcement on the cracking behaviour are analysed. The stress development at cracking and the effect of the parameters on the crack pattern and crack width are visualised. The analytical models are compared with the results from the *N.L.F.E.A.* for the following situations:

- Stress development:
  - Stress state at first crack
  - Stress state at cracking
- Crack width calculations:
  - Conventional reinforced concrete
  - Hybrid reinforced concrete

Chapter 10: External loads
The effect of the point loads on the stress behaviour is elaborated. First, the linear elastic approach of *Westergaard* is explained and the relevant parameters are analysed. With the use of the *F.E.M.*, the effect of cracking on the stress behaviour of point loads and combined loading is shown. Various situations are compared to give insight into the behaviour of jointless *S.o.G.* loaded by external and shrinkage.

Chapter 11: Conclusion
Conclusions from the complete research are summarised in this chapter. The research questions are elaborated and answered with the use of the findings in this research.

Chapter 12: Recommendations
At last, the recommendation is given. Besides the theoretical design recommendations, there are also practical recommendations given for the concrete mixture and execution to increase the final quality of industrial floors.

2. Industrial floor

To realise a high quality and durable floor, a good understanding of all the structural elements and basic principles is essential. In this chapter, the general information regarding industrial floor design is given. The structural elements, construction method and design principle of an *I.F.* are described. The main elements are the foundation, (reinforced) concrete slab and the detailing. The general loads and design principles are briefly discussed. Finally, the relevant provisions are mentioned.

2.1 Structure

The components of the industrial floors are separated into the foundation, concrete slab and the joints. In Fig: 2.1 the cross-section of a standard structural *S.o.G.* is shown. The foundation is a combination of the subgrade and the sub-base. Sometimes a slip membrane is added beneath the concrete slab to reduce the friction.

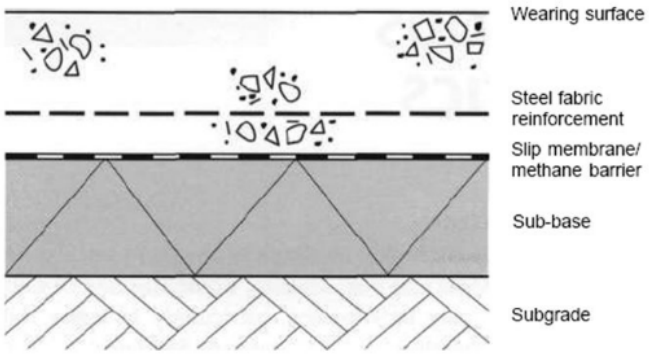

Figure 2.1: Structural components

Foundation

For ground supported industrial floors, the foundation is a critical part of the structural integrity. The bearing capacity and serviceability of the *IF's* depends greatly on the capacity of the foundation. An experienced floor designer often quoted: *"the floor is as good as the grade below"*[4]. To create a high-quality foundation, a good understanding of all the elements is required. Therefore, the elements are discussed below.

Support system

Two foundation types are applicable to *IF's*. The support system greatly determines the structural behaviour and design of the *I.F.*. The type of support system depends on the soil type at the location. In Holland, the type of support system can relatively easy be determined based on the geological map of the country. In Fig: 2.2 the red circle indicates clay and loam which requires *S.o.P.*. The green circle shows the area of sandy soil were *S.o.G.* are often realised. This area is also the logistic hotspot in Europe with many *D.C.*. As mentioned 70% of all the *IF's* are *S.o.G.*.

Figure 2.2: Geological map of Holland [16]

Slab on Piles *S.o.P.*

Pile-supported slabs are recommended when the bearing capacity of the deeper soil-layers is low. Enhancement of the deep soil layers is often assumed expensive, and therefore, piles are used in these situations. During construction, the slab is supported by the sub-base, but in time due to settlement, this support will fade away and the slab become suspended over the pile foundation. The suspended concrete slab has to be able to resist hogging and sagging moments and punching forces. Thicker slabs are required for pile-supported slabs compared to *S.o.G.*. The minimum recommended slab thickness for *S.o.P.* is 200 mm according to Technical Report 34 – Concrete Industrial Ground Floors (*TR-34*) [17].*S.o.P.* are not taken into account in this research but some theories and conclusion can be relevant for *S.o.P.*.

Slab on Grade *S.o.G.*

A *S.o.G.* is continuous elastic supported by the sub-base. The support of the ground has to be sufficient to distribute the loads on the floor without excessive deformation. The slab is generally in full contact with the ground support in its lifetime. The slab distributes the external force over an area directly into the ground. This results in lower stresses in the slab compared with *S.o.P.*. Therefore slender slabs with less reinforcement are possible[16]. A drawback is the possible settlement difference in the soil which can influence the structural integrity. The minimum recommended slab thickness for *S.o.G.* is 150 mm according to *TR-34* [17].

Foundation elements

The foundation is a combination of the subgrade, sub-base and optional a slip membrane.

Subgrade

The subgrade is the underlying ground or imported fill material, which provides the continuous elastic support for the concrete slab. The subgrade can consist of multiple soil types. Therefore, the quality of the subgrade can vary a lot in both vertical and horizontal directions. To determine the quality of the subgrade, it is important to do preliminary research. A cone penetration test gives information on the soil quality. When a sensitive settlement layer is present, it has to be determined if the settlement would be within the design limits. Otherwise, the soil stiffness has to be enhanced. This can be done by replacing the top-layer or by compaction techniques. A very efficient method is the Cofra Dynamic Compaction (*C.D.C.*), which compacts the soil till depths of five to eight meters. Beneficial to this technique is that the weak spots can be extra compacted to create a uniform soil stiffness and that detailed measuring data over the area is available after compaction. When compacting is not sufficient, local pre-loading can reduce the risk of differential settlement even more [16]. Long-term uniform loading can result in a large settlement when there are weak layers present. When large uniform or differential settlements are expected, the floor should be built on piles.

Figure 2.3: *C.D.C.* in progress

Sub-base

Often a sub-base is realised on top of the subgrade even when the subgrade is of excellent quality. Multiple recommendations advise constructing a well-graded and compacted sub-base with a minimum height of 0.2 m[18][17] below the slab. Applying a high-quality sub-base will enhance the effective subgrade k_{mod}. Another important property of the sub-base is that it acts as a working surface during the construction of the building. A good working platform improves the final building quality and reduce the construction time [4].

Lastly, the sub-base layer is essential to provide a flat surface for casting the concrete slab. Height differences in the sub-base can result in locally not achieving the nominal design thickness. Also, extra restraints can come from an unequal surface of the sub-base. The surfaces should be within +0 to -25 mm of the datum for the bottom of the slab[17]. Traffic can damage the already prepared sub-base layer with rutting as a result. It is advised to have a heavy roller standby to repair defects if they occur during the casting process. The quality of the sub-base is directly linked to the quality of the floor. Therefore it is important to pay enough attention to it[10]. The sub-base should be drained to decrease the risk of exposure of the concrete slab to moisture. *Bishop* found an increase of 39% in vertical edge deflection when the bottom of a dried slab is exposed to moisture from the sub-base. Therefore, *Bishop* advised to place the concrete slab on a drained sub-base[19].

Slip membrane

A membrane can be placed below the concrete slab to reduce the friction between the slab and the sub-base. The lower friction will enable the slab to adjust to shrinkage strains without restraints from the sub-base. Therefore no high stresses are formed in the slab. The membrane also avoids the loss of cement-fines into the sub-base. The membrane can also have negative effects on the slab performance. The plastic slip membrane is likely to act as a moisture barrier and therefore increases the initial plastic and drying shrinkage. This can result in a non-uniform drying of the slab, which may result in curling, Fig.2.4. Another downside is that the sheets can come into the concrete during casting, which can create a weak spot on the floor. It is advised to tape the end-laps and place the sheet without any folds.

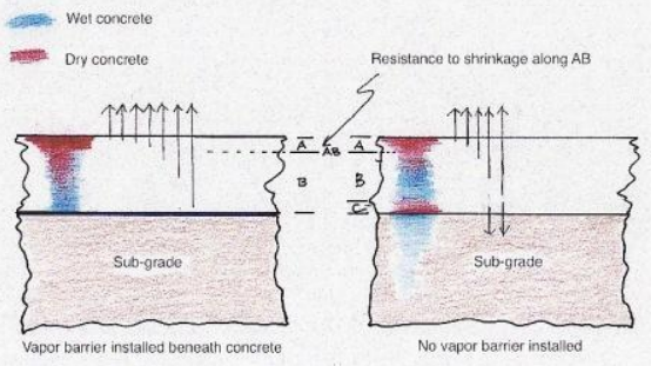

Figure 2.4: Drying of slab with and without slip membrane

Concrete slab

The concrete slab is the main structural element of the industrial floor. The function of the slab is to resist the impacts and transfer the load to the foundation during its lifetime. Reinforcement is used to compensate for the low tensile strength of concrete. Nowadays, steel fibre reinforcement is often used to reduce or replace the conventional reinforcement. For reinforced concrete *S.o.G.* the slab thickness is typically between 150 and 250 mm. Serviceability is of great importance, so do not thin the slab [4]. Over the years, different types of concrete slab are realised. The concrete slab can be classified according to the type of reinforcement. The types are briefly elaborated.

Plain-concrete slabs

Only applied for warehouses with light loadings systems. Because no reinforcement is present, the stresses in the slab should be lower than the tensile capacity of the concrete. Therefore, it is often realised in combination with a ground supported foundation system. The slab is always in combination with saw-cut joints to relief the shrinkage stresses. The joint spacing should be limited to 6 m for saw-cut slabs. The research focus on jointless slabs, and therefore, plain slabs are outside the scope.

Continues reinforced concrete slab

The reinforcement is applied to realize a post-cracking capacity in the slab. Therefore, cracks can be controlled and the slab can take up larger bending moments. With the use of reinforcement, the thickness of the concrete slab can be reduced significantly compared to plain concrete slabs. Fabric mesh is mostly used as reinforcement due to the large area's. The location of the reinforcement determines its effectiveness for certain situations. To control cracks, the cover should be as small as possible. For negative and positive bending moments, the reinforcement should be placed respectively in the most extreme top and bottom fibre of the cross-section. The design method of a jointless reinforced slab is based on the highway engineering. The continues reinforced rebar method is designed to created cracks to relieve shrinkage stresses with a large amount of small cracks. This method is transferred to the design of indoor floors to eliminate the number of joints. Over the years, concrete slabs have been constructed with top, middle, bottom and top-bottom reinforcement. The typical concrete slab based on experience is constructed with C30-37 in combination with an upper reinforcement grid of 8-100 mm for slab length up to 50 meter [20].

Steel fibre-reinforced concrete slab

A recent development is to use steel fibres as reinforcement in concrete ground slabs. Using steel fibres can be very cost-effective because the workload of placing reinforcement is avoided[10]. The steel fibres increase the residual capacity of plain concrete. The fibre amount should be at least 80 $kg\,m^{-3}$ to realise a strain hardening effect[6]. To ensure structural integrity, the *S.F.R.C.* slab always needs reinforcement in edges, corners and around columns[21]. In Holland, one of the first *S.F.R.C.* slabs was realised. The steel fibres eliminated the conventional reinforcement and reduced the slab thickness from 200 mm to 180 mm, which reduced the cost of the slab[22]. This research focuses on strain softening *S.F.R.C.* and crack control in jointless slabs.

Hybrid reinforced concrete slab

Hybrid reinforcement is the combination of conventional rebar with steel fibres. The two types of reinforcement are complementary to each other. Hybrid reinforcement results in a more efficient crack control and can reduce the total amount of reinforcement[23]. The steel fibres increase the bonding capacity of concrete, and therefore, the reinforcement is more efficient in controlling cracks. Hybrid slabs are mostly used for piles supported slabs or for heavily loaded ground floor slabs. The exact behaviour, especially during shrinkage, is not widely known. The available design methods for theUltimate Limit State (*U.L.S.*) can be cumbersome, and for the Serviceability Limit State (*S.L.S.*), no acceptable calculations methods are present[17]. In this thesis, the behaviour of hybrid slabs will be elaborated.

Joints and edge detailing

Joints are always a critical element in structures. Joints have to transfer the forces between the structural elements, which results in high local stresses. Dowels are required in the joints to transfer the shear forces and to limit the high difference induced, for example, by curling. At the same time, the joint must meet the design requirements and often ensure free movement in a specific direction. Joints are always needed, even in large jointless floors. A frequently applied method in the last 20 century is to reduce the joint spacing in such a way that imposed deformation is negligible. This is often done with saw-cut or movement joints, which resulted in many joints in large *D.C.*. These joints give problems to the usability of the floor. Besides shrinkage relieving joints, construction joints are also required. Finally, joints are used to isolate the slab from restraints such as a column. Perimeter strips can also be used along the edges of the slab. In Fig: 2.5 the advantages and disadvantages of local thickening of the slab are given.

Advantages	Disadvantages
The edge lifting will be reduced. The larger weight reduces the edge lifting along the thicker edge.	There is a risk of cracking perpendicular to the perimeter strip in case of shrinkage and thermal strain, due to the larger horizontal stiffness in the perimeter strip in relation to the slab.
The slab will have a stiff edge with a large effective depth that is able to transfer and carry concentrated loads.	There will be restraints in one or two directions that often lead to severe through cracking.
The deformations will be less.	The loading of the perimeter strip leads to forces in the same direction as the shrinkage forces.
There is a possibility to make excavations underneath the slab-on-ground even after the construction is finished.	The joint openings will be larger with the risk of crushed joint edges, due to increased restraints.
	There will be a local increase in drying time that reduces the rate of drying. This creates a moisture gradient and a length difference between the inner parts of the slab-on-ground and the perimeter strip. This can lead to cracking.
	There can be a "stationary" moisture condition in the core of the perimeter strip that can emit moisture at cracking.

Figure 2.5: Effects of local thickening the slab

Construction joints

The area of the slab, which can be realised in a day, is limited. Therefore construction joints are needed to act as vertical form-work to put a stop end to a single day cast. After construction, the floor has to work as one uniform slab and construction joints have to transfer all the forces into the slab. A typical construction joint sometimes called a tied- or day-joint, is shown in Fig:2.6a.

Movement joints

Depending on the design principles, explained later on, movement joints are used to manage the imposed deformation of the slab. For jointless floors, movement joints may open up 20-35 mm. *M.H.E.* driving over large joint openings results in problems like degradation and wear of joint edges, resulting in damaged *M.H.E.* and injured employers[21]. These serviceability problems have to be prevented. Sinusoidal shaped movement joints are designed to have a shock and vibrating free transfer over the opened joints. They are very often used in traffic areas near the loading docks. Movement joints are also used as construction joints.

Isolation joints

Isolation joints are important to reduce the crack risk at slab details. The isolation joint is often made of a compressible material of minimal 20 mm thick, depending on the amount of slab movement, and should be applied over the full height of the slab. The primary function is to avoid any restraints to the slab by fixed elements. An internal column detail with an isolation joint is shown in Fig: 2.6c. Sensitive areas like re-entrant corners, restrained joints and internal columns act as crack inducers. It is advised to add extra conventional bar reinforcement at points where peak stresses can be expected.

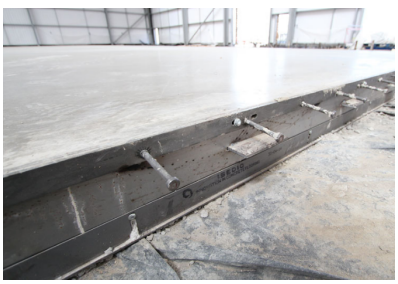

(a) Construction joint

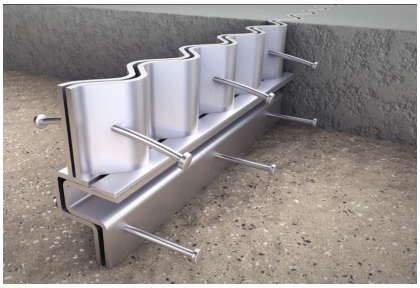

(b) Movement joint

(c) Isolation joint

Figure 2.6: Typical joints industrial floor

2.2 Construction

A good floor seldom appears by accident and is a combination of multiple disciplines. The concrete quality, construction method and execution/finishing have a large influence on the final quality of the floor. Execution errors like locally reduced slab thickness and lower concrete cover can initiate cracking. It is found that larger subdivisions of the floor result in significant quality improvement[21]. Therefore, large casting areas per day are preferred.

Construction of large jointless *S.o.G.*

It can be misleading to call this method jointless. The reason why this method is called jointless is that no additional joints are placed beside the construction joints. Because no joints are placed within the bays, there is no stress relief possible. The floor will be subjected to a combination of applied load and stresses from *I.D.*. Therefore, it is important to reduce the shrinkage load and restraint as much as possible to lower the crack risk. After placing the reinforcement and joints, the concrete can be poured on the sub-base. Most times, the concrete will be poured directly from the trucks. Attention should be paid to the final location of the reinforcement because the trucks can bend or move the mesh. There is a practical upper limit to the area of concrete, which can be cast in a single day. This limit is bonded by the site-specific details like the amount of workforce, type of reinforcement used, concrete supplier ect. Outputs of 2000 m2/day are common, but casting area's of 5000 m2/day are also reported[21]. This high production number is achievable because of laser screeding machines. These machines can distribute, vibrate and flatten the concrete in one pass. Laser screed tolerance is around +-6 mm and slump height for concrete must be targeted at 70 mm[4]. Contractors have mentioned the following benefits associated with laser screeding machines for large-area construction methods[10].

- Higher strength, denser and more durable floors
- Flatter floors
- High productivity
- Damage-prone construction joints are kept to minimum
- Choice of mesh or fibre reinforcement

Figure 2.7: Laser screed

Finishing

After the casting of the slab, the floor has to be finished. Power floating and curing are important proceedings to achieve a flat and suitable abrasion resistance concrete surface. Ways to improve the finish-ability of the floor are:[4]

- Add water, but beware of the effect on the strength and drying shrinkage
- Use more cement
- Use finer aggregate
- Switch to round grained fine aggregate
- Protect the fresh concrete from drying winds and sunshine
- Stop the floor surface drying out by applying curing methods

2.3 Loads

Loads on industrial floor can be divided into external loading and internal loading. The external loads can be defined as the design loads. The internal loads are induced by the environmental influence and the chemical behaviour of the concrete material referred to as *I.D.*. The external loads on industrial floor are briefly summarised with typical values. The *I.D.* can be separated in thermal and shrinkage effects.

External Loads

Point loads

Point loads can come from racking legs or mezzanine columns supported by the slab. Point loads are often spread by a thick steel footplate to reduce the peak stresses. Slabs in *D.C.* are often loaded by multiple point loads. A single racking load can be up to 120 kN.

Distributed loads

Often for design calculations, the Unifromly Distributed Load (*U.D.L.*) is assumed as the governing load. In theory, the *U.D.L.* will not generate differential stresses in a slab on grade. The load will directly be transferred into the foundation. Only a difference in the support stiffness will lead to stresses in the slab when its loaded by a *U.D.L.*. For design checks, block loading is taken into account for the *U.D.L.*. The *U.D.L.* are generally taken between 25 and 50 $\mathrm{kN\,m^{-2}}$.

Line-loads

Line-loads can come from different situations like separation walls, rails for transport systems and beam supported racking.

Imposed deformations

If a concrete member can move freely without any restraints, shrinkage of concrete would not be a major concern when designing a structure. Free movement of concrete due to shrinkage will not result in stresses. Often concrete members such as slabs are restrained by its support or surrounding. Therefore, the *I.D.* result in stresses in the concrete member. The *I.D.* appears to be quite complicated to take into account in the design of concrete structures. The term *I.D.*, which is often used in practice, give rise to confusion and misunderstanding. The principle is that the movement of a concrete structure is restrained and that the imposed deformation results in stresses in the structure. The term restrained deformation would, therefore, be a better name to describe the load. The *I.D.* can come from changes in temperature, shrinkage or settlement of the support. A common situation that results in imposed stresses is casting new to old concrete.

In Fig: 2.8, an example is given for a concrete bar fixed at both ends subjected to a uniform temperature drop. The required force P to make the structure compatible with its boundary conditions introduces tensile stresses in the concrete element. Imposed deformations can result in significant large stresses were from the outside no indications of these stresses could be seen. *I.D.* often has a long-term loading effect. Therefore, the complex time-dependent properties of all the materials have to be taken into account. For concrete, effects like creep have to be considered during the design. It is stated that the creep behaviour is beneficial because it can significantly reduce the stresses in statically undetermined structures loaded by *I.D.*[10][24]. The general approach to determine the response of a structure undergoing imposed deformations can be divided into three steps:

1. Divide the system into sub-systems such that the structure can freely move by the imposed deformation.
2. Apply forces (moments, axial forces, shear forces) at the ends of the sub-systems in order to restore compatibility with its original boundary condition.
3. Determine the distribution of forces in the structure caused by the applied forces.

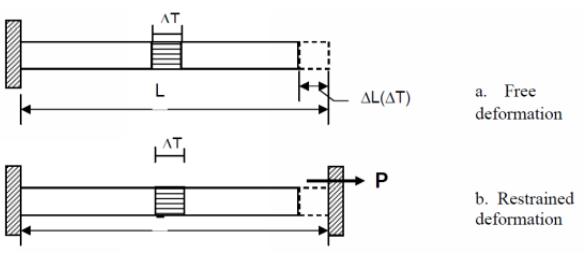

Figure 2.8: Concept of *I.D.*

Moisture related stresses are potentially greater than temperature-related stresses for indoor ground slab were environmental effects are minimised by the building[10]. The temperature change in indoor slabs due to

seasonal effects remains nearly constant during its lifetime[8]. In the sensitivity analysis, all the thermal effects below are investigated to get insight on the relevance of the thermal loads on indoor *S.o.G.*. The *I.D.* loads which are investigated in this research are then:

- Concrete shrinkage
  - Drying shrinkage
  - Autogenous shrinkage
- Thermal effects
  - Hardening temperature
  - Annual temperature
  - Daily temperature

2.4 Design

The design principle greatly determines the stress state in an *I.F.*. The engineer has to make the decision which method is the best for the situation. For the design, the engineer also has to check the structure in the *U.L.S.* and *S.L.S.*. For the *U.L.S.* design, the *I.D.* are often ignored because the stresses are reduced significantly due to cracking in the ultimate state. The load-bearing capacity of a structure is hardly affected by the *I.D.*. *I.D.* is almost never the reason for the failure of a structure[24]. On the contrary, in the *S.L.S.* design, the *I.D.* can be of great importance. The designer has to be aware of the stresses that can be present due to the *I.D.* in statically undetermined structures. The design principle greatly determines if the structure is statically determined or undetermined. *I.D.* can result in uncontrolled cracking due to a tensile force or bending moment. The stress behaviour can be described with respectively a *R.T.M.* and a flexural member both elaborated in App:A. Information about the design principle and the design check are given below.

Principle

Two design principles are described as upper and lower bound for the stress behaviour in the *I.F.* with respect to the *I.D.*. The two design principles are:

'Stress' free

The stress-free principle is based on a statically determined structure. This means free movement of the slab, e.g., the degree of restraint R is 0.0. For shrinkage, the slab has to be kept free from any restraints, such as friction and connections. When the slab is exposed to a temperature difference or shrinkage gradient, the slab will deform accordingly. Due to self-weight and friction, there will always be restrained stresses in large slabs. In practice, it is not possible to design a large jointless slab without any restraints. Therefore, a stress-free slab from imposed deformation can not be assumed and the contribution of imposed stresses should always be taken into account.

'Strain' free

The strain-free principle is relevant for statically undetermined structures. The slab is assumed to be fully restrained, e.g. the degree of restraint R is 1.0 for the imposed strain or curvature. The imposed deformations will result in stresses. These stresses can be significantly high and can result in cracking of the structure. Imposed stresses can lead to higher forces than external design loads. The additional stresses have significant influences on the slab performance and have to be taken into account during the design.

In practice, the slab will not always be fully restrained. The true degree of restraint of *I.F.* has to be investigated to get a better insight into the stress behaviour. Final design of a slab can be based on a combination of the design principles. A combination can be minimizing the restraint on the slab and use reinforcement to control the cracks. Most important is that *I.D.* are taken into account when there is some form of restraint and that proper measures are taken for the detailing.

Design Check

The design checks can be separated into two stages. A concrete structure always has to full-fill the requirements of both states.

Ultimate Limit State

The *U.L.S.* check is based on the maximum capacity of the structure. The structure has to be able to withstand the forces, including in safety factors. For industrial floor, the forces are often calculated with the elastic approach proposed by*Westergaard* and the plastic (yield-line) approach developed by *Meyerhof*. Another important design check is punching due to the high point loads from the racking. Very important to keep in mind is that when a structure has a low rotational or axial strain capacity, *I.D.* can lead to brittle failure of the structure[24].

Serviceability Limit State

In the *S.L.S.*, the crack width and deflection have to be checked. The structure has to full-fill the durability and serviceability requirements. The effect of *I.D.* has to be considered when present because it can lead to the governing stress state in the structure. The focus of this research is mainly on crack width criteria in the *S.L.S.* of the *I.F.*.

Provisions

The structural principle of an *I.F.* has a large overlap with continues reinforced pavements. The calculation methods are often based on the same design principles. Many recommendations are drafted from pavement design provisions. For this research, the focus will be on the recommendations *TR-34* [17] and CUR 36 – Design of Concrete Floors and Pavements on Elastic Foundations (*CUR-36*) [18] from respectively the United Kingdom and the Netherlands. The provision *TR-34* is based on the stress-free principle. The recommendation advises to lower the restraints as much as possible and to relive the imposed stresses with the use of joints. The provision also states that a realistic assessment of combined loading is problematical and could produce conservative designs without significantly reducing the risk of cracking. Therefore, calculations of imposed deformations are not addressed in the document. *TR-34* suggest to use the Eurocode 2 (*E.C. 2*) for crack width calculation for hybrid and conventional reinforced slabs. For *S.F.R.C.*, no standard theoretical model for crack width calculations is given in provisions.

According to *CUR-36*, the temperature and shrinkage effects have to be taken into account. According to the provision, the *I.D.* can be reduced with a relaxation factor ψ to take into account the beneficial creep behaviour of concrete. In the *CUR-36*, no crack width calculation is given. The recommendation assumes an uncracked concrete member. The *CUR-36* recommends taking into account the relaxed axial force and bending moment from imposed deformations based on the advised uniform and gradient strain profile. Superposition of these forces and bending moments to the design forces is allowed[18].

All the recommendations do not include calculation methods for deflections. Linear Finite Element Analysis (*L.F.E.A.*) is recommended for checking deflections. Besides the special recommendations, the general provisions for concrete structures *E.C. 2* and fib Model Code 2010 (*M.C. 2010*) is used.

2.5 Conclusion

The stress behaviour of an *I.F.* depends greatly on the design. The type of foundation and concrete slab have a large influence. Also, the design principle is of great importance. When the design is such that there are no significant restraints, then the *I.D.* is not relevant for the stress behaviour. For large jointless slabs, this leads to large joint openings, which leads to serviceability issues. Therefore the design method of *S.o.G.* is changed over the last years to jointless slabs. The restraints become more relevant in jointless slab, and therefore, also the *I.D.*. When the *I.D.* are neglected, which some provisions do, uncontrolled cracking can occur, which also leads to serviceability issues. With the use of a failure analysis, the governing failure type can be determined to delimit the research. Also, research into the degree of restraint is required to determine whether the *I.D.* contributes to the governing stress state. The stress behaviour due to the *I.D.* has to be analysed to get more insight to control or prevent cracking in jointless *S.o.G.*. Therefore, the materials and its time-dependent properties are analysed after the failure analysis. From thereon, the stress behaviour of the slab is analysed.

3. Failure Analysis

Cracking in concrete structures is common and can be initiated for many reasons. Various cracking types can occur in concrete structures. To prevent or control cracking it is important to understand the cause and type. Cracking is not per definition failure of the structure. Only cracks larger than the crack criteria can be defined as structural or performance failure. A failure analysis is performed to analyse the cracking behaviour in industrial floor and to find the governing cracking type. Despite the available technology and all the hard work of engineers and contractors, there are still many reports of imperfections in *S.o.G.*. It is widely known among engineers that concrete cracks, but the amount of uncontrolled cracks raise serious concerns. Not cracking types result in failure of the floor. Therefore all the issues found in the survey are categorised in three types of failures.

-Structural failure
Structural failure is when the structural integrity is lost of the slab. The structure is not able to withstand the design load anymore and fracture or excessive deformation occurs. The structure is not safe and cannot be used anymore.

-Performance failure
Performance failure is when the structure is damaged but is still structurally intact. Only the serviceability of the floor is harmed to such extent that the floor can not be used anymore according to the design requirements. The efficiency of the structure is affected by cracking. The design requirement is not fulfilled any more. Often expensive reparations are required to restore the serviceability.

-Aesthetic failure
Aesthetic failure is when the structure is cracked and results in imperfections, which does not affect the performance nor the integrity of the structure. The structure still fulfils all the design requirements. Only the look of the structure is not perfect any more, which is often undesired or unexpected by the owner. It should always be made very clear that small cracks can occur and that these cracks are not a structural or performance issue.

A lot can be learned by looking at the damages which often occurs in practice. Therefore, to specify the different types and cause, the following question is investigated:

What are the most common failures for concrete slab on grade?

In the literature review, many surveys of concrete industrial floors have been reviewed. The damages are quantified with the use of risk assessment. The consequences versus likelihood are quantified based on the findings in the survey. A short explanation is given for all the found damages. The complete surveys can be found in App: B. An overview of the analysis is given in Tab: 3.1.

Table 3.1: Failure analysis of *S.o.G.*

Problem	Failure type	Consequence	Likelihood	Cause
1. Shrinkage cracking	Structural/Performance	High	Very High	Drying and Autogenous shrinkage. Temperature changes. Execution errors.
2. Settlement differences cracking	Structural/Performance	High	High	Local soil settlement. Foundation stiffness difference.
3. Joint deterioration	Performance	Very High	Medium	Large joint opening. Bad joint execution. High dynamic loading.
4. Plastic shrinkage and settlement cracking	Performance	High	Medium	Low cover. High consistency class. Too much plasticizers.
5. Surfaces imperfections	Aesthetic	Low	High	Delamination. Low concrete quality. Steel fibres in surface. Bad finishing. Crazing.
6. Levelness issues	Performance	Medium	Low	Bad execution, weak soil support, low quality floor.
7. Overloading	Structural/Performance	Very High	Very low	Punching, *M.H.E.*, More load than designed.

3.1 Failure types

1.**Restrained shrinkage cracking**
Structural and performance issues occurred when restrained shrinkage stresses are not taken into account in the design process. Large crack openings can appear all over the slab. Crack widths of 3 mm are reported [19]. In time, the edges of the crack are likely to deteriorate by *M.H.E.*. When taken into account during the design, the cracks can be controlled with reinforcement. Restrained shrinkage cracking was by far the most reported damage type in other survey[25]. Causes are bad joint lay-out, bad isolation joints, no sufficient crack controlling reinforcement at sensitive areas and unforeseen restraints.

2.**Settlement differences cracking**
Structural and performance issues occurred when stresses from settlement differences are not taken into account in the design process. Large crack widths, up to 2 mm, were found. In most cases, the stiffness difference between the foundation structure for the building and slab is the cause of settlement cracking. The slab tends to settlement but is restricted by the surrounding foundation. A common cause is a piled foundation pad beneath a *S.o.G.*. This results in cracking around the foundation pad. Also, local settlement of the *S.o.G.* due to variation in the soil properties is found as a cause of settlement cracking. The slab should be realised on a subgrade with uniform stiffness over the area[8].

3.**Joint deterioration**
Performance is seriously affected by damaged joints. Over time, due to the use of the floor, the deterioration increases. Reparations are expensive and often only a short-time solution. The likelihood of appearance depends on the type and quality of the joints. Joints are always sensitive to traffic due to peak stresses. By reducing the number of joints and placing the joint in low traffic area's the likelihood can be reduced. The cause of damaged joints is height differences between slabs due to curling and settlement and large opening of the (movement)joints. The curling effect is a result of shrinkage and is a major issue for saw-cut joints[25]. Movement joints can open up 20-35 mm [26].

4.**Plastic shrinkage cracks**
In one case, random plastic shrinkage cracks were found up to 2 mm wide. These cracks seriously affect the performance of the slab. Normally, plastic shrinkage cracks are small and can be easily repaired during finishing. The plastic cracks are located above internal restraints like reinforcement and occur due to plastic settlement and segregation of the concrete. Too many plasticizers and high consistency class are causes of plastic shrinkage. High quality and well-composed concrete should be used to prevent plastic shrinkage cracks.

5. **Surface imperfections**
Small local areas are damaged and the performance requirement can be obtained after small reparations. Only one case has reported of a single aggregate exposure. Low-quality concrete in combination with drying of the surface in the early age are the found causes. Delamination of the surface also occurs often in *S.o.G.*.

6. **Levelness issues**
The consequence of the levelness issues depends on the type of storage and distribution system. High-racking systems can tumble or displacement of the racking at the top can result in distribution problems. For automated distribution systems, the tolerances are low and complete systems can be jammed or taken out of business. Only one minor levelness problem is reported. Also, one case of bad flatness is reported. This was for a very low-quality *S.o.G.*.

7. **Overloading cracks**
Structural failure like punching and corner breaks can occur due to heavy loading. Overloading is found to be an unusual case. In one case, cracking in the yield lines is reported where the load was seven to sixteen times higher than the design load. The cause was that changes in the final design were made without controlling the structure. Heavy loading by *M.H.E.* also resulted in local overloading cracks.

3.2 Conclusion
From the survey, it can be concluded that the two damage types: restrained shrinkage cracking and settlement cracking are the most common in industrial floor. These damages contribute to the joint deterioration problems. This research focus on the large jointless slabs, and therefore, joint failure will not be addressed. For analysing the settlement cracking, soil-structure interaction and geotechnical expertise are required. An investigation into settlement cracking is a different field of engineering, and therefore, not be addressed in this research. Further research into settlement cracks can be helpful increasing the quality of *S.o.G.* design. Many of the problems which occur in regular pavements were not found in *I.F.*. The reason is that the exposure to weather condition is significantly less on *I.F.* compared to pavements. The curling stresses and joint movement for *I.F.* are thus less [22].

The primary defect in jointless *S.o.G.* is uncontrolled restrained shrinkage cracking. The research focus from now on restrained shrinkage cracking to get insight into the structural behaviour. Furthermore, to reduce the appearance and consequences of uncontrolled restrained shrinkage cracking.

4. Material properties

The properties for all the materials within the range of the research are discussed. Also, the time-dependent behaviour of the concrete material is explained. Besides the concrete material, conventional and steel fibre reinforcement are addressed. Finally, some information is given on the soil properties.

4.1 Concrete

Concrete is a material that contains extraordinary properties. It is strong, durable, constructible in any shape and it is cheap. First used around 5000 before Christ and today by far the most used construction material in the world. Because concrete is a combination of selected components, the mechanical properties can be chosen by the engineer. The downside is that mistakes can easily be made and that expertise is required.

Concrete is an isotropic ageing material, which means that the mechanical properties change in time with variation in space. The properties of concrete are affected by environmental effects such as temperature and moisture. Besides the property change in time, the concrete behaves non-linear under specific loads. These factors make an exact calculation of concrete structures very complicated.

Extensive research has led to the translation of the variable material properties of concrete to standardise material properties. The standardise properties are given in provisions like *E.C. 2* and *M.C. 2010*. The standard values presented in the provisions are only valid for ordinary concrete subjected to stresses less than 40% of f_{cm}, with the Relative Humidity (*R.H.*) in the range of 40-100% and at a mean temperature between 5 and 30 °C. In this assumed range, the concrete can be considered as an ageing visco-elastic material. Many concrete properties are within this range linearly related to the stress. For the calculation of the properties outside this range, additional formulae are given in the provisions. The concrete properties in this research are assumed to be within the standard range. All the formulae for the calculation of these standard properties are given in App:E.

For structural design purposes, the properties of concrete are assumed to be isotropic. When analysed in detail, the concrete properties are not constant in all directions and thus anisotropic. Two reasons can be given for anisotropy of concrete. First, the stress history on the concrete results in micro-cracking. Cracking results in a degradation of the elastic stiffness and a local change of properties. This phenomenon is called damaged induced anisotropy. The second reason is that concrete is a mixture of different components. The properties of the components, such as aggregates, can be variable. After mixing and casting, the properties are likely to be variable in space. The spatial variation due to mixing the components results in an anisotropic material. The spatial variation is taken into account by an upper and lower bound value for the tensile strength in the provisions. For the compression strength, the characteristic value (5% fractile/lower bound) is taken as standard. For this research, only the spatial variation with respect to the tensile strength is taken into account.

Stages

First, the stage in which concrete is develops is elaborated. Concrete is an ageing material, which means that during its structural lifetime, the performance changes. The stages of concrete, the formation from liquid to solid form, can be separated into three stages. Directly after mixing, the concrete is in the green stage or so-called dormant period. The mixture can flow but still have some stability due to cohesion and internal friction. Due to its stability, the composition remains intact, but it can still be poured into the form-work. During casting, the un-hydrated cement particles are coming in contact with water and the hydration process starts. Volume changes and temperature development are the most important effects in the green stage with respect to durability because it can initiate cracking.

After the green stage, the concrete enters the young stage. When the hydration starts, ±2-4 hours after casting, the concrete properties are starting to develop. The concrete becomes stiffer and hydration heat increases. In the young stage the primary bindings between the Calcium Silicate Hydrate are being formed and the concrete rapidly hardens in a period of two to ten days. There is a smooth transition between the stages of young and hardened stage. During the transition, the concrete cools down and shrinks. When the concrete is restrained,

the shrinkage can lead to cracks. The moment of cracking depends mainly on the environmental effects and concrete mixture. In concrete pavement cast in the open air, the first crack appears in the first or second night due to cooling and rapid drying. For indoor *S.o.G.*, the environmental influences are lower and cracking can be initiated in a later concrete stage. Therefore, it is essential to reduce the environmental influences. Also, the hydration temperature must be kept low and the cooling of the concrete gradual to reduce the risk of cracking. The green and young stage, referred to as the early age behaviour, is not explicitly examined in this research.

After a couple of days, the major parts of the hydration is developed. The residual capillary water starts to evaporate, which results in drying shrinkage. The capillary water in the cement paste greatly determines the time-dependent properties of concrete, such as creep and relaxation. The aggregate in hardened concrete is mainly responsible for the stiffness. The strength, porosity and durability are governed by the hardened cement paste, especially by the pores in the cement paste. Over its lifetime, the concrete is continuously in motion on micro and nanoscale. Micro-cracking along the cement grains, movement of the cement paste and continuous hydration are examples of the behaviour inside the ageing concrete.

The complex behaviour of concrete is translated into multiple parameters. Theoretical models are used to quantify the parameters in the provisions. In the provisions, the standard properties are determined at the concrete age of 28 days. The important parameters related to the research are elaborated: Young's modulus, tensile strength, shrinkage, creep, relaxation, thermal behaviour.

Young's modulus E_{cm}

The Young's modulus E_{cm} is the elastic stiffness of the concrete material and is related to characteristic cylinder compressive strength f_{ck} concrete. The Young's modulus describes the relation between the stresses and strains in the linear elastic state based on Hooke's law. In general, the physical properties of concrete are governed by the micro-structure of the cement paste, which is 20 to 35 % of the volume. In contrary, the Young's moludus is mostly determined by the amount and type of aggregate. Variation of E_{cm} is possible by changing the aggregate in the mixture [27]. This effect is taken into account in the provision by an aggregate factor $\alpha_{E_{cm}}$. Compared to the standard quartzite aggregate, E_{cm} can be increased by taking basalt/dense limestone or decreased with limestone and sandstone as aggregate type. When the elastic analysis is performed often an effective Young's modulus is used to take into account the initial plastic strain, creep and cracking.

Tensile strength f_{ctm}

The tensile strength is an important parameter for the crack width analysis. The tensile strength determines the cracking force or bending moment in the concrete structure. The determination of the correct tensile strength for the calculation can be confusion. Different tensile strength values like splitting, uniaxial and flexural are given in the provisions. Next to the different types, there is also a difference between the short-, long-term and cyclic loading. In addition, some provisions obtain different formulae to calculated the tensile strength. And then, there is also a difference between mean and characteristic values. Therefore, choosing the correct tensile strength is not that straight forward.

For cracking of *S.o.G.*, it is advised to use the long-term mean tensile strength f_{ctm} [28]. For this research, the mean tensile strength f_{ctm} given by the *E.C. 2* is used. For short term loading, the f_{ctm} can be enhance by dividing it by 0.7[18]. The flexural stresses can be determined by the multiplying f_{ctm} with the factor $\left(\frac{1600-h}{1000}\right) \not< 1$ with h in mm. In the *E.C. 2*, the variation of the tensile strength is defined by the 5% and 95% characteristic values which can be calculated by multiplying the f_{ctm} with respectively 0.7 and 1.3. The different calculation method from different provisions are given in App: E. Values for the long-term tensile strength of C30/37 varied between 2.5 to 3.0 MPa which can lead to significant difference in design results. In reality, there is also a multi-axial stress situation present in the concrete structures. Fortunately, it is found that the multi-axial stresses have no influence on the tensile capacity of concrete[27]. Therefore, the principal stress is taken as the cracking stress. Research has shown that when a load is applied very slowly, cracking occurs at a lower tensile strength of concrete. To take this effect into account, a sustained loading factor α_{cr} has to be used for the calculation of the tensile cracking strength of the concrete σ_{cr}. In general, the mean tensile strength f_{ctm} of the 28-day property have to be reduced by the cracking factor α_{cr} of 0.5, 0.6 or 0.75 for respectively very slow, slow and normal applied long-term loading[24].

Fracture energy G_{f_c}

After cracking, the concrete still has some residual strength, which is taken into account by the fracture energy in *N.L.F.E.A.*. For the *F.E.M.*, the tensile behaviour of concrete is described with a softening curve. The softening curve is often based on the fracture energy G_{f_c}. The fracture energy G_{f_c} describes the resistance of the concrete subjected to tensile stresses after cracking. It is based on the fracture mechanics concepts and is defined as the energy which is needed to propagate a tensile crack in the concrete. The higher the fracture energy, the more resistance the concrete can give after cracking. The fracture energy primarily depends on the w/c ratio, maximum aggregate size, the age of the concrete and curing conditions. The fracture energy should be determined by tests when accurate calculations are required. In practice, G_{f_c} is determined with a formula based on the mean compressive strength provided in the *M.C. 2010*. Typical amount of fracture energy for plain concrete is 0.1-0.15 N mm. The fracture energy of *S.F.R.C.* is typically 4 N mm for 35 $\frac{kg}{m^3}$ hooked end-high yield fibres which is ± 25 times higher than plain concrete [20].

Time-dependent concrete behaviour

The long-term behaviour of concrete has to be considered when analysing *I.D.*. The time-dependent behaviour of concrete structures can be defined by shrinkage, creep and relaxation. The strain changes in a structure can be positive(expansion) and negative(shrinkage). The drying and autogenous strain changes are related to the concrete material and are always negative. Therefore it is defined as concrete shrinkage. The relaxation is closely related to creep. Therefore, the creep behaviour is also extensively discussed. First, the shrinkage behaviour is elaborated.

Shrinkage, the shortening of concrete without the influence of any load(Fig:4.1a).
Creep, the increase of deformation with time under a sustained constant load(Fig:4.1b).
Relaxation, the decrease of stresses when the deformation of the concrete structure is kept constant(Fig:4.1c).

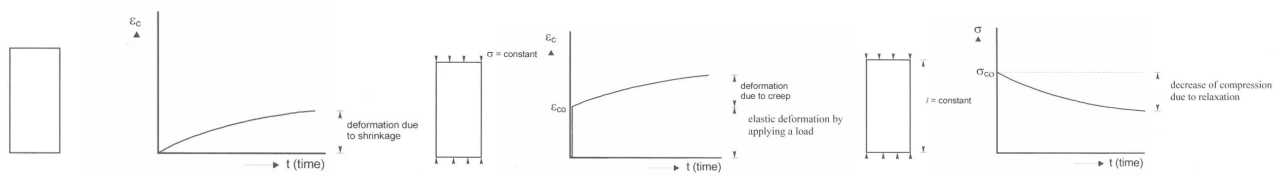

(a) shrinkage strain **(b)** Creep **(c)** relaxation effect

Figure 4.1: Time-dependent behaviour of concrete

Shrinkage

Shrinkage is a stress independent volume change and when restrained, the deformation can lead to stresses. Different types of shrinkage are known for concrete. This research only focus on the relevant concrete shrinkages types: *drying* and *autogenous*. Shrinkage types like *plastic* and *carbonation* do not have a large influence on the long-term stress behaviour and are therefore not addressed in the research. A typical concrete shrinkage profile is given in Fig: 4.2. The drying shrinkage starts at the end of the curing period.

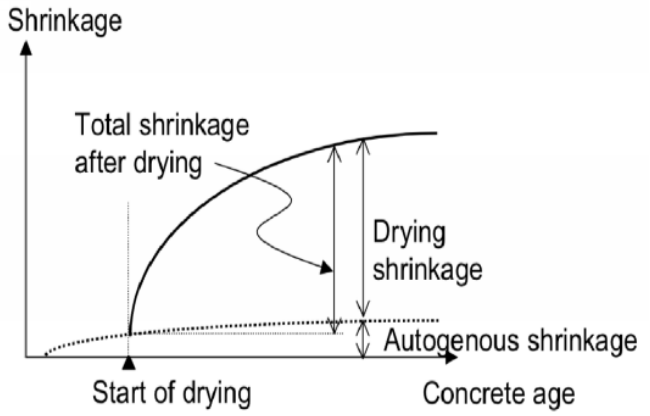

Figure 4.2: Concrete shrinkage profile

Drying shrinkage

Many factors influence the drying shrinkage of concrete. The properties of the concrete components, environmental conditions and structural dimensions determine the amount of shrinkage. Thinner slabs are more sensitive to a change in climate conditions and result in faster development of the shrinkage strain[19]. Drying shrinkage is mainly caused by a change of the moisture content in the concrete. The loss of moisture to the environment results in a volume reduction of the concrete. For the calculation of the total drying shrinkage, the formulae in the *E.C. 2* are used. The total amount depends on the cement type, concrete class, notional thickness h_0 and relative humidity *R.H.*. The development depends on the notional thickness h_0 and the curing time. The development of the drying shrinkage in *S.F.R.C.* is faster due to the additional air voids in *S.F.R.C.* [29]. In practice, the drying shrinkage in concrete can be reduced with the use of Shrinkage Reduction Admixtures (*S.R.A.*) and/or counteracted with expansion additives in the concrete mixture. *S.R.A.* can result in a reduction of 20% of the total drying shrinkage.

Drying shrinkage profile

For *S.o.G.*, the drying of the slab occurs mainly at the top surface. The drying at the bottom depends on the construction method and if the sub-base is dry or not. When a slip membrane is used, the slab will not dry at the bottom surface. When the slab is poured on dry sand/gravel, the moisture in the slab will rapidly flow into the soil beneath. In Fig: 4.3, the shrinkage profile after one year of drying as a function of the *R.H.* is shown for a slab with only the top surface exposed to drying. From practice, it can be assumed that there is always a shrinkage gradient in the slab with the largest value at the top surface. In the *CUR-36*, two shrinkage profiles are advised to take into account, which is assumed in this research. The shrinkage gradient can be assumed with a profile of 60% at the bottom and 90% at the top of the total shrinkage.

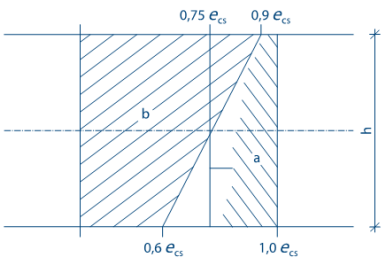

(a) Strain profile *CUR-36*

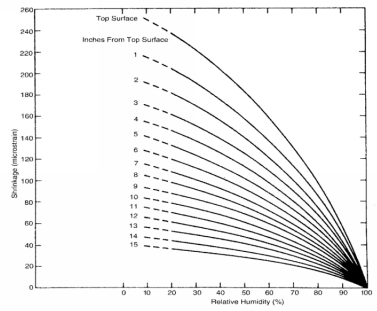

(b) Shrinkage after one year of a 380 mm thick slab depending on the *R.H.*

Figure 4.3: Shrinkage profile

Autogenous shrinkage

Autogenous shrinkage is the loss of moisture due to the chemical bonding of the water and the cement particles. The total amount depends only on the concrete class and is calculated with the characteristic compressive strength f_{ck}. The autogenous shrinkage becomes more relevant for higher concrete classes. The autogenous shrinkage profile can be assumed uniform over the height. For the calculation of the total autogenous shrinkage, the formulae in the *E.C. 2* are used. The development profile is always the same.

Creep φ

As shown in Fig: 4.1b, creep is the additional deformation under a stress. The mechanism of creep is based on the hypothesis of viscous flow. Due to stresses in the concrete, deformation of the gel in the micro-structure occurs. Creep is also caused by the capillary stress of the chemically non-bonded water. Creep can be separated into short and long-term behaviour. The short-term creep is the reversible part. The long-term creep is the permanent creep, which is more important in practice. The long-term model behaviour is as follows. When the material is in rest (unloaded), the concrete micro-structure is in balance. When the concrete is loaded, the stresses on the gel particles are not evenly distributed. The gel particles slowly start to moves to find a new stress balance. This movement in the micro-structure result in deformation in statically determined structures. Influences like temperature, moisture and salt concentrations are important factors regarding the creep behaviour. Also, factors like the w/c ratio, type of aggregate, cement content, additives and type of loading influence the creep. The many factors make creep a complex mechanism that is almost impossible to describe and calculate accurately. To have a better understanding of the creep behaviour some relevant factors and their influences are given in Tab: 4.1[27].

Table 4.1: Effect on creep

factor	Effect on creep behaviour
Slag content	More slag will results in a reduction of the creep factor (Portland cement creeps, up too factor 2, more than Blast furnace cement)
Hydration grade	Faster hardening concrete creep less
Cement content	More cement leads to more creep
W/C ratio	More water in the mixture leads to more creep
Aggregate type	A high E-modulus (stiffer concrete) leads to less creep.
Aggregate size	A higher maximum diameter leads to less creep
Silica fume	Addition of silica fume can reduce the creep with 30%.
Moisture content	A low moisture content in the concrete creeps less.
Concrete age at loading	newly cast concrete loaded leads to higher creep
Relative thickness	A thinner structure dries easier and enhances the creep.
Temperature	A higher temperature leads to more (long-term)creep
Loading	Tensile loading can leads to 5-20% more creep

The moisture content has a considerable influence on the creep behaviour. The relation of moisture content in the concrete to the relative humidity of the environment greatly determines the creep behaviour. If the concrete structure is saturated with water, the creep deformation will be higher compared to a dry concrete structure. On the other hand, when the relative humidity of the surrounding is low, the creep effect will increase. The creep increases in a dry surrounding environment because of the additional drying creep principle. The maximum creep occurs when the concrete structure is completely saturated in an arid environment [27].

In practice, the complex non-linear creep behaviour is calculated with a creep coefficient. The calculation of creep is based on the relation between the creep deformation and the elastic deformation. The magnitude of the creep deformation is directly proportional to the elastic deformation and can, therefore, be quantified by the creep coefficient φ. In the provisions, the theoretical creep coefficient φ_0 determines the final creep value. Both the magnitude and the development of creep are based on the relative humidity, concrete strength, cement type, concrete age at loadingt_0 and the relative thicknessh_0. In reality the creep behaviour becomes

non-linear for ($\sigma_c > 0.45 f_{ck}$). In this research, the linear creep effect, according to the Davis-Granville law, is assumed for all stress stages.

Several approximation methods are available for the calculation of the creep deformation. The most common method is the Age Adjusted Effective Modulus (*A.A.E.M*) method. The creep effect is then taken into account with a reduced Young's modulus based on the creep coefficient. This approach makes the calculations much easier. The downside is that it assumes that the creep deformation is completely reversible. Also, the ageing of concrete is not taken into account. For loads applied to older concretes, the creep coefficient is lower. Therefore, the *A.A.E.M* method is overestimating the creep. For the method of *Dischinger*, a basic creep function is used, which takes into account the ageing of concrete by adjusting the creep function for loads applied at a later point in time. The downside is that the standard creep function does not result in a reliable estimation of concrete ageing. Contrary to the *A.A.E.M* method, *Dischinger's* method underestimate the creep deformation[30]. A more precise method which does not have the drawbacks of the two presented methods is the method of *Trost* and *Bazant*. The method is based on the superposition principle of *Boltzmann*. The principle of superposition gives accurate result when the following conditions are met:

- The stresses during the service life are not higher than 40% of f_{ck}
- Total strain should not decrease due to a decrease of the load.
- Variation in *R.H.* should not be too large
- No large stress increments at a late point of time

Trost and *Bazant* introduced the ageing coefficient χ_{age} in order to obtain a simple equation. The ageing coefficient takes into account the creep and concrete development with respect to the creep effect and the non-uniformity of the stresses over time. The coefficient is found to be in the range of 0.5 and 1. χ_{age} is the smallest for young concrete. For hardened concrete, the value increases close to 1. *Reinhardt* states that in case of creep relaxation, the age coefficient is between 0.8-0.9 [27]. The *M.C. 2010* states that the coefficient is in the range of 0.6-0.9 for long-term effects[31]. These values are also found in the thesis of *Bishop* [19]. It is often adequate to take the value 0.8 for conceptual and preliminary design stages. For this research, the average value of 0.8 is assumed to be satisfying.

The provision *M.C. 2010* provides a creep function, also referred to as a compliance function, J_{t,t_0}, which is used to calculate the stress-dependent strain at time t loaded at time t_0. This method is also based on the superposition principle. The reciprocate value of the compliance function is equal to the effective Young's modulus. Due to the actual non-linear behaviour of concrete and time-dependent properties, it is inevitable that the compliance function has some prediction errors under variable stresses. Particularly for unloading or decreasing strains. These errors are mainly caused because of the hygral effects, interaction of stresses and because material damages are neglected[31].

It is concluded that precise prediction of creep is difficult. The linear creep prediction models for a constant load in time can be over or under-estimate the creep effect. Moreover, errors with calculations methods based on the superposition principle for varying stresses are inevitable because of the actual non-linear behaviour of concrete. The age of concrete at loading is for all methods an important parameter but is difficult to determine correctly for *I.D.*. For the continually increasing shrinkage loads and the ageing concrete, the creep effect can only be estimated. The environmental influences are often not predictable and can cause substantial creep changes. Therefore, the estimation of the creep behaviour based on simplified methods is accepted in practice[27].

Relaxation ψ

As mentioned, the relaxation effect is based on the same physical mechanism as creep. The mathematical models to described relaxation are therefore also the based on the same mechanisms. The difference between creep deformation and concrete relaxation is state of the structure. Concrete relaxation occurs in statically undetermined structure were the creep mechanism results in a reduction of the applied strain and thus the stress. When an initial strain is imposed in a fully restrained structure, the initial stresses will decrease in time due to creep behaviour. In this research, this effect is referred to as ***concrete relaxation***. The relation between the initial and the resulting stresses is the defined by the relaxation factor ψ. The concrete relaxation is often taken into account by reducing the Young's modulus resulting in the relaxation modulus R_{rel}[32]. The same downside mentioned earlier for the *A.A.E.M* are relevant for the relaxation modulus method. The relaxation modulus is expressed with the use of a relaxation factor ψ. ψ is strongly related to the creep coefficient and depends on the loading type.

$$\psi_{(t)} = \frac{\sigma_{c,bazant(t)}}{\sigma_{c,el(t)}} \tag{4.1}$$

$$R_{rel(t,t0)} = E_{cm(t_0)}\psi_{(t,t_0)} \tag{4.2}$$

$$\tag{4.3}$$

Multiple functions are developed for the calculation of ψ for different loading types. Two types of loading are considered: gradually increasing load and instantly applied load. The relaxation factor for the gradually increasing stress for example an *I.D.* is:

$$\psi_{grad(t)} = \frac{1}{1+\chi_{age}\varphi_{(t,t_0)}} \tag{4.4}$$

The relaxation factor at t for a load applied at to is given by:

$$\psi_{instant(t)} = 1 - \frac{\varphi_{(t,t_0)}}{1+\chi_{age}\varphi_{(t,t_0)}} \tag{4.5}$$

The *CUR-36* also provides a relaxation function which can be used for *I.D.*. The *CUR-36* advises to take into account the creep coefficient over the loading period.

$$\psi_{CUR36(t)} = \frac{\left(1-\exp(-\varphi(t,t_o))\right)}{\varphi(t,t_o)} \tag{4.6}$$

Especially for young concrete, the creep coefficient and thus the relaxation effect is high. In Fig: 4.4 the relaxation effect of the first three hours is given for concrete ages at loading up to 28 days. For eight hour old concrete, the imposed stresses are already dissipated for 40% after three hours. For 28-day old concrete, the relaxation is less, but still, 15% of the stresses are dissipated after three hours. For accurate relaxation calculations, the effect after minutes of loading should be taken into account. In general, time steps of days are taken instead of hours for time-dependent calculations in the provisions. It is assumed that the provisions have taken into account the short term effects of relaxation in the formulae for the estimation of the long-term relaxation behaviour. In the sensitivity analysis, the influences of the functions and the age of concrete at loading on the relaxation effect are analysed.

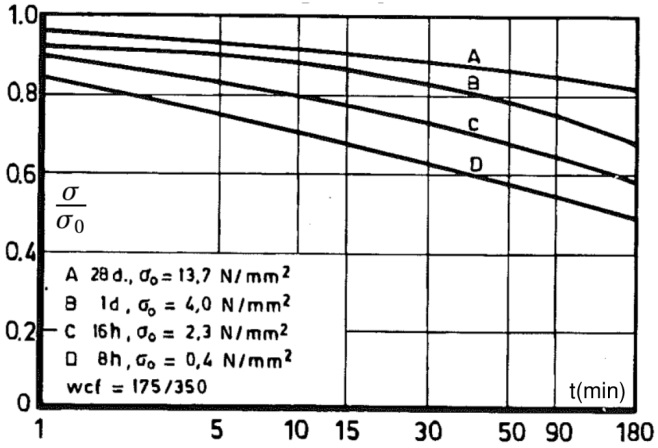

Figure 4.4: Relaxation effect after minutes

Thermal effects

The changes in the temperature in the concrete structure can result in strain changes and concrete property changes. The properties of concrete behave differently under extreme temperatures. It is assumed that thermal changes of the concrete structure are not significant for indoor *S.o.G.*, and therefore, the properties are taken according to the provisions without thermal effects.

On the other hand, the thermal deformation of concrete due to temperature changes can have large influences on the structural behaviour of the slab. The thermal changes can result in expansion or shrinkage of the concrete material depending on the temperature load. The thermal expansion coefficient for concrete is assumed as $10 \cdot 10^{-}6°C^{-1}$. Three temperature effects are relevant for *S.o.G.*. The hardening, seasonal and daily temperature changes are investigated. The hardening temperature change is due to the chemical reaction of the concrete and occurs in the young stage of concrete. In Fig:4.5, the stress development principle of hardening concrete is restrained concrete is shown. When the contraction due to cooling is too high, the concrete can crack after days. In the dormant period, the heat-loss to the environment is higher at the bottom-fibre than at the surface to the air. Research showed that there is no large difference found in the calculation of uniform and gradient temperature difference for indoor slabs[19]. Therefore, the hardening temperature can be taken as a uniform stain load, e.g., constant over the height over the cross-section.

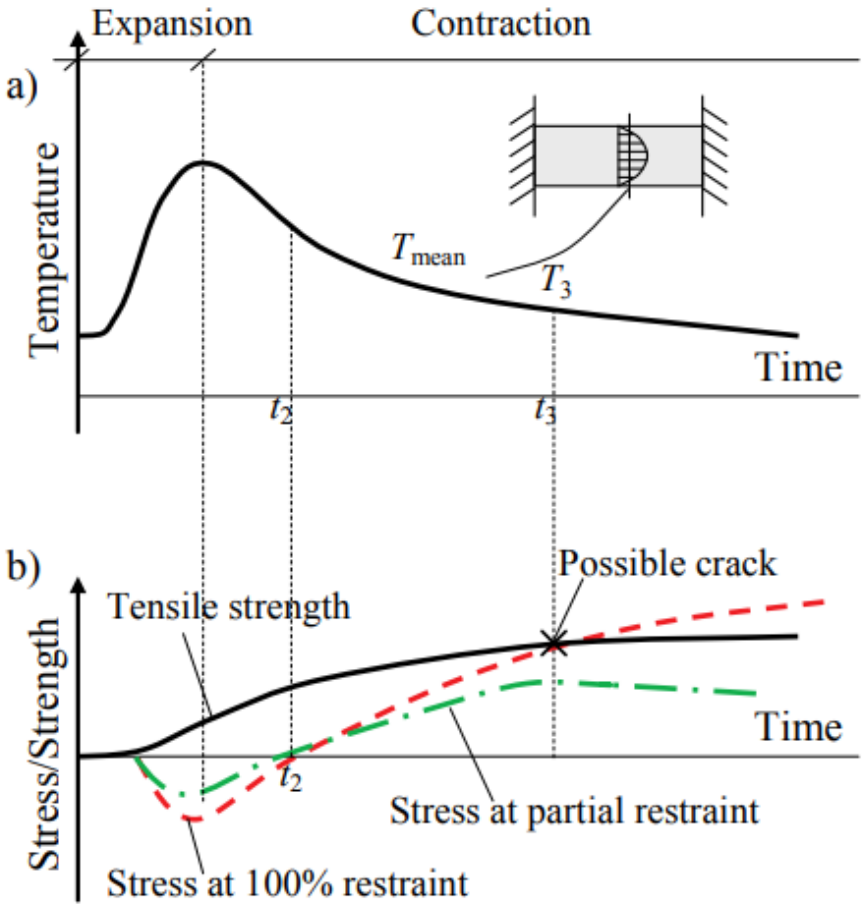

Figure 4.5: Stress development during hardening

The seasonal temperature change is the yearly temperature variation of the slab. When, for example, the slab is cast in the winter, the slab will warm up in the next six months. The seasonal temperature increases or counteracts the shrinkage of the slab and has, therefore, influence on the stress behaviour in the restrained slab. In the literature, it was found that the seasonal temperature does not have a significant influence on the behaviour of indoor *S.o.G.*. All the temperature effects are analysed in the sensitivity analysis to determine if the thermal effects can be neglected for indoor slab design.

4.2 Reinforcement

Cracking behaviour

Cracking of the concrete is assumed to occur when the stresses are higher than the tensile strength. In reality, cracking starts sooner, but this normally happens inside the concrete and at a scale that can not be seen with the human eye. Cracking of concrete can be separated into micro cracking and macro cracking. When the tensile stresses are increasing in the concrete, micro-cracks are formed in the cement matrix. Often the micro-cracks start on the interface of the aggregate with the cement paste. The type of initial cracking depends on the composition of the concrete mixture. The weakest element in the matrix will crack first. The crack will propagate through the matrix until a stress balance is found within the structure, which can result in macro cracks. When no balance can be found within the structure, (brittle) failure occurs. Therefore reinforcement is required to keep the structural integrity of the concrete structure after cracking. The reinforcement becomes "active" after cracking and the tensile forces in the crack can then be transferred back into the concrete by the bonding between the concrete and the reinforcement. The properties of conventional and steel fibre reinforcement are elaborated.

Conventional reinforcement

Conventional reinforcement is used as continuous reinforcement in the slab often by single rebars or fabric meshes. The reinforcement is made out of steel and has an elastic-plastic stress-strain relation. Standard *B500* reinforcement, according to the provisions, is taken into account in this research. The reinforcement has to be placed in the location where the tensile stresses are assumed to be higher than the concrete tensile capacity. In the top layer, the reinforcement is effective against surface cracking. In the middle of the slab, the reinforcement takes over the high axial forces. Near the bottom fibre, the reinforcement is most effective for increasing the positive bending moment capacity. To make sure that yielding of the reinforcement does not occur, a minimum reinforcement ratio ω_{min} is required. The advised minimum reinforcement ratio in the tensile area of the cross-section is given by Eq:4.7. For indoor concrete slabs, the minimum reinforcement ratio ω_{min} can be reduced with 15% because the environmental influences are relatively low[33]. This result in ω_{min} of 0.29%, 0.35% and 0.40% for respectively C20/25, C30/35 and C35/45 for indoor concrete floors. The American provision *ACI 360* recommend a minimum steel ratio of 0.5% in the direction of the restraint placed with a typical cover height of 50 mm.

$$\omega_{min} = \frac{100}{\left(\frac{f_{yd}}{\sigma_{cr}}\right) - \alpha_e} \cdot 0.85 \tag{4.7}$$

Bond-slip behaviour

The interaction between the reinforcement and the concrete is described by the bond-slip behaviour. In analytical models, often a maximum bond stress is assumed based on the concrete strength or a factor that represents the bonding quality is used. The *E.C. 2* uses the factor k_1 to take into account the bonding quality. The bonding quality influences the transfer length in the cracked zone and larger crack spacing in the *F.D.C.P.*. Larger crack spacing commonly results in larger crack widths. Therefore good bonding is often required in reinforced concrete structure to reduce the crack width. Smaller reinforcement diameter also increases the contact area and thus the bonding when the ρ_s is taken as a constant value.

In *N.L.F.E.A.*, the behaviour can be described in more detail and different bond-slip relations can be modelled. In this research, the bond-slip model for monotonic loading, according to the *M.C. 2010* is used. In the model, two failure types are defined; pull-out failure and splitting failure. Because reinforcement is often placed at the outer layers of the concrete structure to make it efficient, the splitting failure type is more likely to occur. The splitting failure type results also in the lower bound bond-slip capacity. The model separates confined and unconfined bond-slip behaviour. Confined bond-slip behaviour is present when shear reinforcement is applied. *S.o.G.* are generally not reinforced with stirrups. Therefore, the unconfined splitting bond-slip type is taken into account in the *F.E.M.*.

The long-term bond-slip properties changes under sustained loading. In the crack width calculation method of the *E.C. 2*, the factor kt takes into account the loading time. kt is advised as 0.6 and 0.4 for respectively short-term and long-term loading. In the *M.C. 2010*, the bond shear strength factor is reduced from 1.8 to 1.35. The bond-slip capacity reduces with 33% and 25 % according to the *E.C. 2* and *M.C. 2010* from short to long-term loading. The *M.C. 2010* also advised increasing the slip for cracks with 50% and 100% for sustained loading of respectively one year and ten years. From experimental studies reduction factors for the maximum bond-shear stress and the shear stiffness are determined[34]. The obtained shear stiffness reduction parameter K_{red} depends on the loading time t_l. The maximum bond stress τ_{bm} is reduced with 25 % to take into account the reducing bonding capacity due to sustained loading.

$$t_l = t - t_0 \tag{4.8}$$

$$K_{red} = \frac{\left(0.25 + 0.5 t_l^{0.2}\right)}{t^{0.2}} \tag{4.9}$$

4.3 Steel fibre reinforcement

Improving the performance of brittle material has been done by the ancient Egyptians. They used straws to improve the cracking behaviour of sundried mud bricks. Nowadays fibres are becoming more common in the construction industry, especially in industrial floor. As mentioned, 65% of the produced steel fibres are used

in concrete slabs. The main benefit of adding steel fibres to the concrete is that the concrete structure has some residual tensile strength. The undesirable brittle behaviour of concrete changes into a more ductile one. Adding steel fibres to the mixture improves the concrete toughness, ductility and fatique endurance [22]. In addition, studies have shown that steel fibre reinforcement can reduce the required conventional reinforcement significantly. In some cases, the conventional reinforcement can even be eliminated. The punching shear resistance also increases significantly for *S.F.R.C.* when conventional reinforcement is present. Many studies have been performed to investigate the behaviour of *S.F.R.C.* and hybrid reinforcement. Despite the ongoing research, there are still no general design formulae to predict all the effects of the steel fibre reinforcement[35]. Especially more knowledge is required on the cracking behaviour in the *S.L.S.*[36]. The general behaviour is explained to have a good understanding of steel fibre reinforcement.

Contrary to conventional reinforcement, steel fibres are randomly distributed in the concrete structure. The steel fibre reinforcement can be seen as a change in the concrete properties. By adding steel fibres, the crack in the concrete can be bridged. Fibre bridging is the transfer of stresses from the concrete matrix at a crack through the steel fibre into the concrete matrix at the other side of the crack. The principle is equal to that of conventional reinforcement only on a smaller scale and randomly distributed in the mixture.

The residual tensile behaviour of *S.F.R.C.* can be separated into strain softening and strain-hardening. Strain softening is defined by that the residual tensile strength is lower than the cracking stress, $\sigma_{cr} > \sigma_{R1}$. For strain-softening *S.F.R.C.*, the force in the crack can not be redistributed and one dominant crack will be formed. Strain hardening is defined by that residual stress is higher than the cracking capacity of concrete, $\sigma_{cr} < \sigma_{R1}$. In theory, one large cracking zone will be formed and the axial force in the tensile member can increase beyond the concrete cracking force N_{cr}. Due to the randomly distributed fibres, there will be weak zones in the member and crack localisation will appear when the maximum residual tensile stress is locally reached. In practice, a large amount of steel fibres, up to 80 kg m^{-3}, is required to realise a strain hardening behaviour in *S.F.R.C.*[37]. This amount of steel fibres is not often applied in *S.o.G.*. Therefore, only the strain-softening *S.F.R.C.* is taken into account in this research. According to CUR 111 - Design of Steel Fibre Reinforced Concrete Industrial Floors on Piles (*CUR-111*), Steel fibres can be used as structural reinforcement when there are sufficient fibres in the concrete mixture. A minimum of 35 kg m^{-3} of fibres with a minimum length of 60mm is demanded to realise structural reinforced concrete with fibres [38].

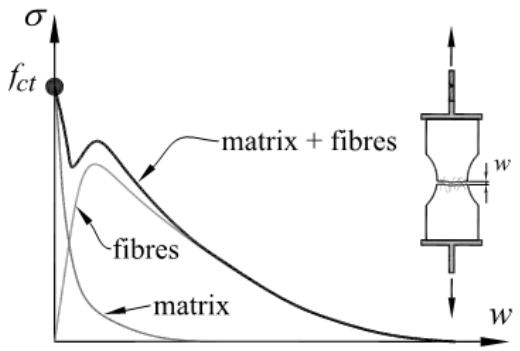

(a) Principle of *S.F.R.C.* behaviour [39]

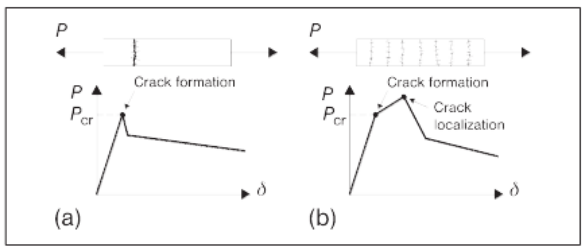

Figure 5.6-2: Softening (a) and hardening (b) behaviour in axial tension

(b) a: Strain softening b:Strain hardening

Figure 4.6: stress strain behaviour of *S.F.R.C.*

Failure mechanism

The failure mechanism of the fibre determines the behaviour of *S.F.R.C.*. A steel fibre can fail by two mechanisms: Fibre rupture or fibre pull-out. Rupture occurs when the tensile stress in the steel fibre reaches the failure stress of the fibre. The fibres are made of steel with a high tensile strength of 1345 N mm^{-2} to reduces the risk of this failure type. The risk of rupture is higher at large strains, e.g. in the *U.L.S.*.

The pull-out mechanism greatly determines the *S.F.R.C.* behaviour in the *S.L.S.*. The pull-out behaviour can be separated into four stages with failure at the end shown in Fig:4.7. First, the bond-slip has to be broken the initiate elongation of the fibre. Secondly, the debonding continuous along the straight part of the fibre. In this stage, the maximum residual strength is reached. Then the anchorage of the hook-end fibre has to be broken.

Finally, to pull-out the fibre, a large displacement is required to let the *S.FR.C.* fail. The stages A and B are relevant for the investigation on the crack behaviour in the *S.L.S.* and are mainly determined by the fibre type. For normal strength concrete and single hooked fibres, fibre pull-out is not likely to occur[37].

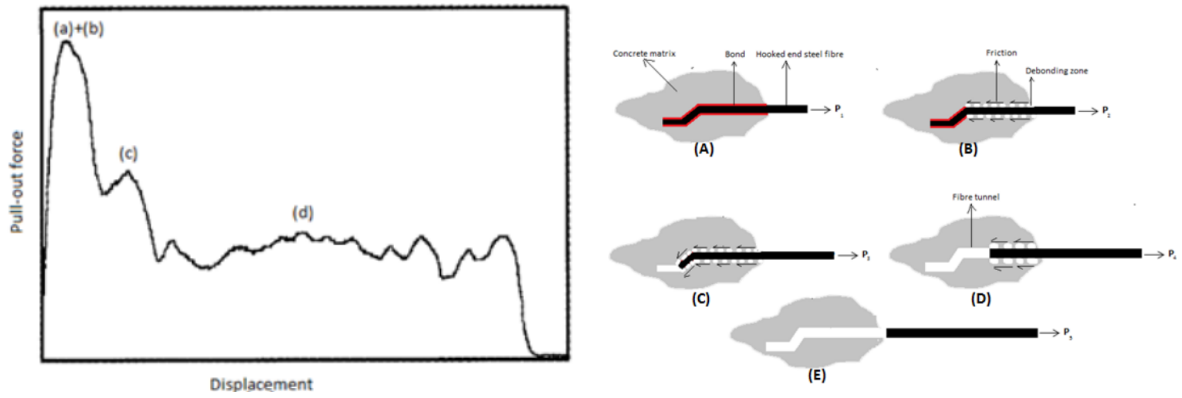

(a) Stress-displacement behaviour **(b)** Pull-out stages

Figure 4.7: fibre pull-out behaviour

Many different fibre types are available in the market. The effect of fibre dosage V_f, fibre aspect ratioλ_f, fibre length l_f and fibre types (hooked end and undulated) on the residual strength is shown in Fig:4.8.

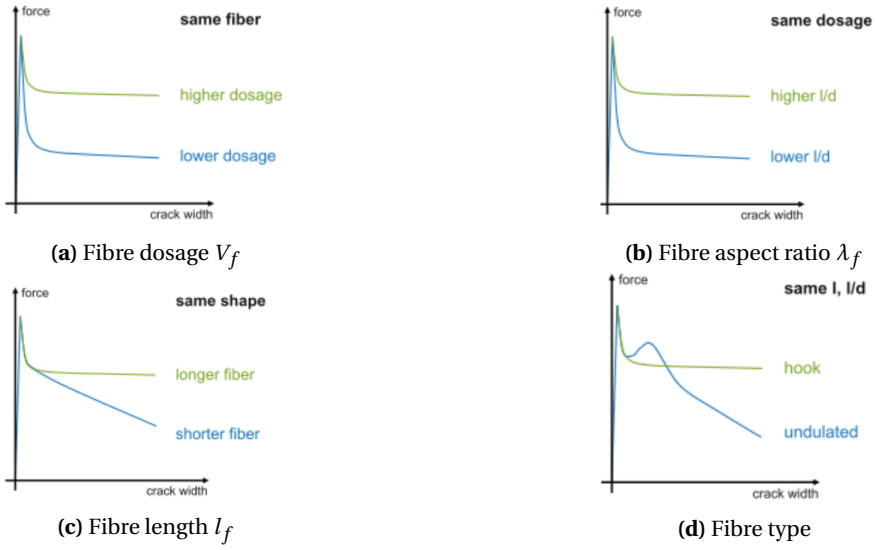

(a) Fibre dosage V_f **(b)** Fibre aspect ratio λ_f

(c) Fibre length l_f **(d)** Fibre type

Figure 4.8: Influence fibres on residual strength

More fibres and fibres with a higher aspect ratio increases the residual strength. Long and good anchored fibres increase the residual capacity at large crack widths. In this research DRAMIX 3D and 4D fibre types are examined. The behaviour of these fibre types is shown in Fig: 4.9. The 3D fibre type is used to improve the performance of standard industrial floors, where 4D can be used for heavy-duty outdoor pavements. The 5D fibres are designed for liquid thigh floors, which are outside the scoop. 4D fibres are specially designed to improve the serviceability of *I.F.* The 4D fibres are the most efficient to control cracks between 0.1 and 0.3 mm and are perfect for hybrid reinforced concrete.

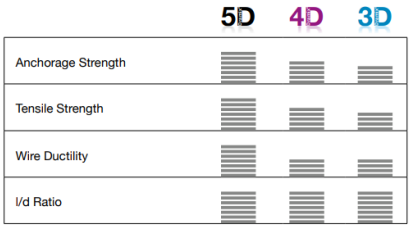

(a) Properties per fibre type

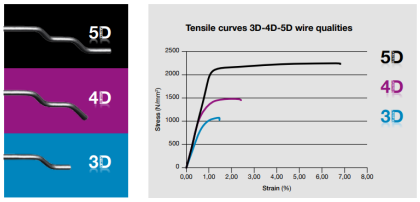

(b) Stress-strain

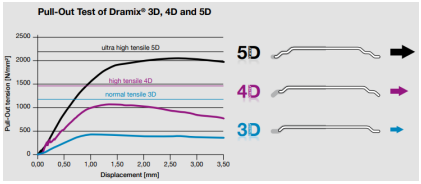

(c) Pull-out

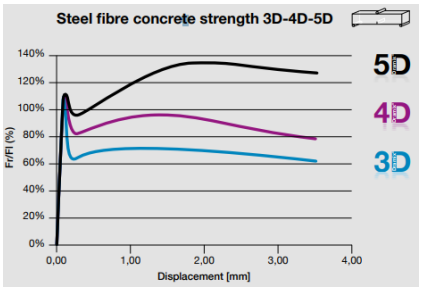

(d) Stress-displacement

Figure 4.9: Behaviour of fibres type

For the determination of the *S.F.R.C.* properties, standard notched beam test according to *EN 14651* have to be performed. Specimens are tested under a vertical point load which result in a force-displacement diagram[17]. A common method is to determine the force in relation with the crack mouth opening displacement (*C.M.O.D.*). The loads are recorded at crack openings of respectively 0.5,1.5,2.5 and 3.5 mm. In Fig:4.10 a diagram of a typical strain softening *S.F.R.C.* is shown. From these force-*C.M.O.D.* relationship, the residual flexural tensile stress $f_{R,i}$ can be derived. These flexural stresses are then translated to the mean uniaxial tensile strength σ_{R1} and σ_{R4} corresponding to *C.M.O.D.* of 0.5 and 3.5 mm. For *U.L.S.* calculations σ_{R4} should be used and for *S.L.S.* the σ_{R1} is advised according to *RELIM*[17].

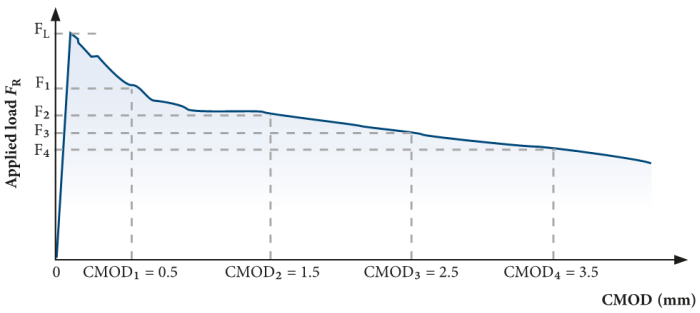

$$f_{Ri} = \frac{3 \cdot F_{Ri} \cdot l}{2 \cdot b \cdot h_{sp}^2} \tag{4.10}$$

$$\sigma_{R1} = 0.45 \cdot f_{r1} \tag{4.11}$$

$$\sigma_{R3} = 0.37 \cdot f_{r3} \tag{4.12}$$

Figure 4.10: Typical beam test

Contrary to the general thought, steel fibres do not increase the cracking strength of concrete. No significant cracking strength enhancement is found for strain softening *S.F.R.C.*. Other research reported no significant increase of σ_{cr} for normal strength concrete up to C35/45. But for high strength concrete and/or fibre volume of 1% or higher, an increase in cracking stress were observed[37][36].

For linear elastic calculation, an enhanced equivalent tensile strength $f_{fctd.f_{eq}}$ is used to take into account the beneficial residual strength property of *S.F.R.C.*. The enhancement of the steel fibres is determined with the bending toughness value $R_{1,5}$ with a three-point bending test according to the *NEN EN 14651*[38]. Research has shown that the bending toughness $R_{1.5}$ can be assumed with good accuracy with the following equation[40].

$$f_{fctm,f_{eq}} = f_{ctm}\left(1 + \frac{(R_{1.5} - 0.3)}{0.7}\right) \quad \text{for} \quad 0.3 < R_{1.5} < 1.0 \tag{4.13}$$

$$R_{1.5} = \rho + 20 \quad [\%] \quad \text{for} \quad \rho > 15[\text{kg m}^{-3}] \tag{4.14}$$

Sustained loading on *S.F.R.C.* reduces the residual capacity found in a time-dependent crack width analysis. The experiment showed that the creep behaviour of cracked *S.F.R.C.* increases the crack width. Bond creep on the fibres is the driving mechanism for the time-dependent crack widening[41]. Other research showed that due to restrained shrinkage, micro-cracking occurs in the *S.F.R.C.*, which results in a reduction of 40% of the residual tensile strength[29].

For concrete, the cracking factor α_{cr} is used to take into account the sustained loading on the tensile strength. The residual tensile strength is also affected by sustained loading. Therefore, the residual tensile strength should also be reduced for long term calculations. As mentioned earlier, the residual tensile strength of *S.F.R.C.* reduces under sustained loading up to 40%. Therefore, a factor of 0.6 is assumed for long-term cracking factor of *S.F.R.C.* equal to the cracking factor of plain concrete α_{cr}. When the sustained loading effect is not taken into account on the residual tensile strength, strain softening *S.F.R.C.* becomes, in some cases, strain hardening shown in Fig:4.11 with the black dotted line.

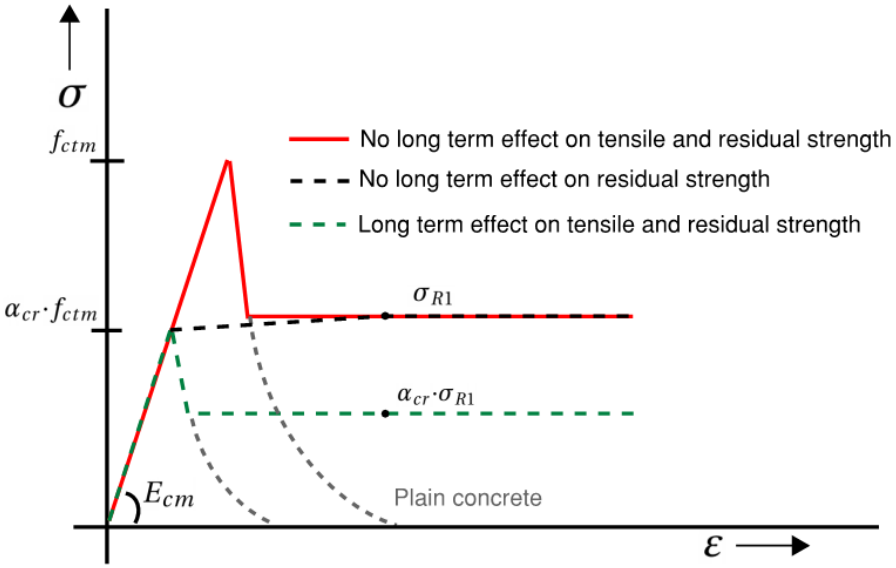

Figure 4.11: Possible stress-strain diagram of *S.F.R.C.*

Directly after cracking, this would be correct. For example, the concrete starts to crack after 50 days of loading and cracks. The force on the *S.F.R.C.* after cracking is instantly applied. The short term residual strength properties can then be used. After some time, the residual strength is reducing and crack localisation starts to form. A gradual crack formation occurs instead due to the residual strength reduction in time. Research also showed that cracking in *S.F.R.C.* is more gradual[36]. So just after cracking, the steel fibres can take over all or major parts of the cracking force depending on the *S.F.R.C.* properties. In Tab: 4.2 and 4.3 the residual strength directly after cracking and for sustained loading are shown and compared with the cracking stress of plain concrete. The short term residual strength ratio can be obtained by $\alpha_{sfrc_{t0}} = \frac{\sigma_{R1}}{\sigma_{cr}}$. The long-term residual strength ratio can be obtained by $\alpha_{sfrc_{\infty}} = \frac{\alpha_{cr} \cdot \sigma_{R1}}{\sigma_{cr}}$. Some *S.F.R.C.* mixtures result in strain hardening directly after cracking, $\alpha_{sfrc_{t0}} > 1.0$, which is not realistic for long-term crack width calculation method. Therefore, the sustained loaded residual strength properties have to be used when the tensile stress of the concrete is also reduced due to sustained loading. In this research the residual tensile strength is assumed constant from σ_{R1}, e.g. σ_{R1}=σ_{R4}. For crack widths up to 1.0 mm, this assumption has no significant influence.

Table 4.2: 3D 65/60BG *S.F.R.C.*

	V_f	σ_{cr}	σ_{r1}	$\alpha_{sfrc_{t0}}$	$\alpha_{sfrc_{\infty}}$
C20/25	30	1.32	1.32	**1.00**	0.60
	40	1.32	1.76	**1.33**	0.80
C25/30	30	1.56	1.43	0.92	0.55
	40	1.56	1.95	**1.25**	0.75
C30/37	30	1.74	1.45	0.83	0.50
	40	1.74	2.03	**1.17**	0.70
C35/45	30	1.92	1.44	0.75	0.45
	40	1.92	2.08	**1.08**	0.65

Table 4.3: 4D 65/60BG *S.F.R.C.*

	V_f	σ_{cr}	σ_{r1}	$\alpha_{sfrc_{t0}}$	$\alpha_{sfrc_{\infty}}$
C20/25	30	1.32	1.54	**1.17**	0.70
	40	1.32	1.98	**1.50**	0.90
C25/30	30	1.56	1.69	**1.08**	0.65
	40	1.56	2.21	**1.42**	0.85
C30/37	30	1.74	1.74	**1.00**	0.60
	40	1.74	2.32	**1.33**	0.80
C35/45	30	1.92	1.76	0.92	0.55
	40	1.92	2.40	**1.25**	0.75

Pullout fibre properties

For the developed crack width model based on the pull-out stiffness of the fibres the properties are required. The pull-out fibre stiffness K_{fibre} is largely determined by the anchoring type of the fibre. Multiple hooked-end fibres have a significantly higher pull-out stiffness than straight plane fibres. The fibre pull-out properties, which are mainly influenced by the anchorage and bonding quality, are determined from several experiments found in the literature. A large variation is found for the pull-out properties of fibres. In Fig: 4.12 the results are shown from different experiments with different fibre type, pull-out angles and concrete properties[42] [43][44][45].

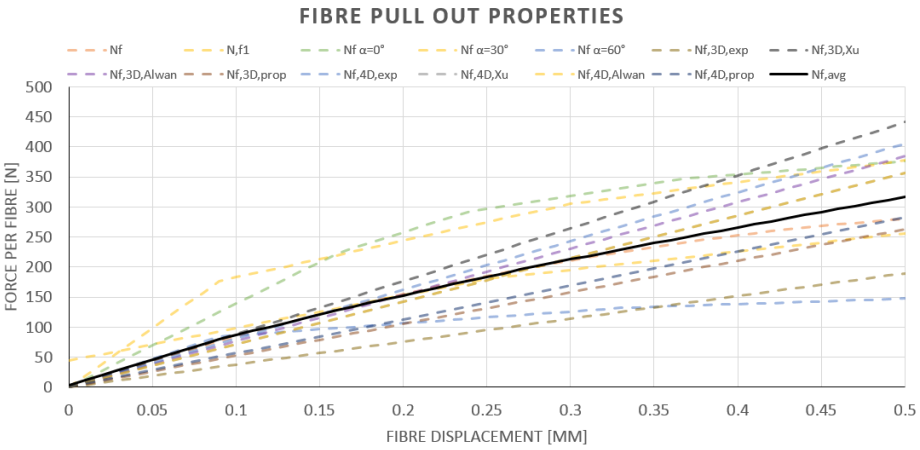

Figure 4.12: Experimental values of fibre pull-out stiffness

For this research, an average value is assumed to take into account all the different effects. The fibre stiffness variates between 1000 N/mm and 600 N/mm for respectively high and low stiffness. The influence of the fibre stiffness on the cracking behaviour is analysed in the sensitivity analysis.

Number of fibres

For the *S.F.R.C.* crack width calculation, the number of fibres in the cross-section is required. The number of fibres in a cross-section is the relation between the fibre volume V_f, fibre diameter and fibre orientation factor O_f. The fibre orientation factor depends on the type of structure, pouring method and vibration method. For slabs, it can be assumed that almost all fibres are oriented horizontally. In the case of a 2D random fibre orientation, the factor for any sectional plane perpendicular to the cross-section is 0.64 [46]. Other research shows that an orientation factor between 0.60 and 0.80 is common, depending on the dimensions of the concrete element[47]. An orientation factor of 0.64 is assumed in the research.

$$n_f = \frac{A_c O_f V_f}{0.25\pi d_f^2} \qquad V_f = \frac{W_f}{\rho_{fibre}} \tag{4.15}$$

It should be kept in mind that there is always a large scatter of fibres inside the *S.F.R.C.* structure. Therefore, during casting, tests have to be performed to check the fibre content in the mixture. The scatter in fibre dis-

tribution decreases with an increasing fibre volume. A matrix with lower fibre volume is more likely to show larger variation than one with higher fibre volume. Low volume *S.F.R.C.* results therefore in lower characteristic values[36].

4.4 Hybrid reinforcement

Hybrid reinforcement is the combination of steel fibres with conventional reinforcement. In this research strain softening *S.F.R.C.* is examined. Therefore to ensure structural integrity, additional conventional reinforcement is required. By adding steel fibres to the reinforced concrete, the behaviour slightly changes. The main benefit of the hybrid reinforcement is that steel stress reduces and that the bonding capacity significantly increases. The fibres aid in the transmission of load across the crack. The hybrid member acts stiffer after cracking, which results in smaller crack spacing and thus more cracks compared to conventional reinforcement. Crack width decreases with 65% for hybrid elements(V_f=1%) compared with only conventional reinforcement. The tension-stiffening effect is more present in hybrid concrete structures shown in Fig: 4.13[36].

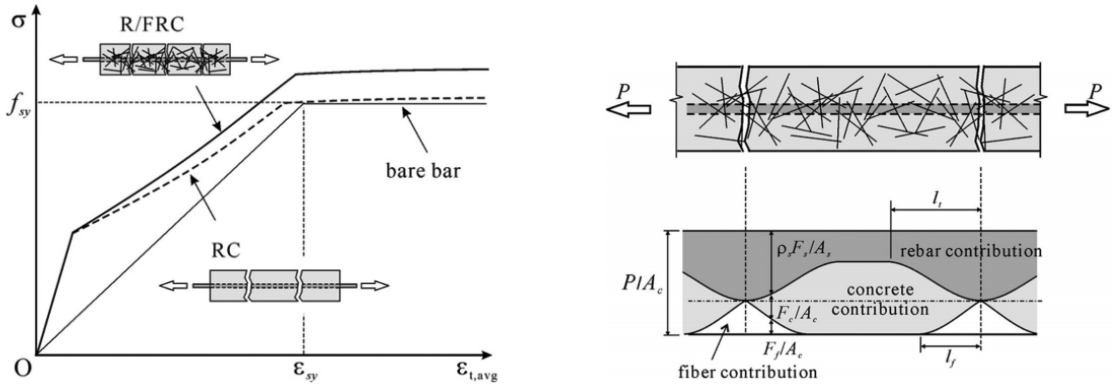

(a) Stress-strain behaviour **(b)** Cracking behaviour

Figure 4.13: Hybrid reinforced concrete

All the found effects for the *S.F.R.C.* are confirmed in the research of *Deluce*[35]. *Deluce* found that the crack spacing is significantly reduced in hybrid concrete elements. The maximum crack width of conventional reinforced concrete was significantly higher than those in the hybrid reinforced concrete. During loading, it is again stated that the cracking propagation was significantly more gradual for the hybrid specimens and that the tension stiffening behaviour is more present for the hybrid specimens. Also, higher fibre volume resulted in a decrease in the steel stress, mean crack spacing and width. The load on the reinforcement decreases and, therefore, also the crack spacing and crack width. A higher fibre aspect ratio λ_f results in a lower crack spacing and crack width. This is because smaller diameter fibres result in higher bonding capacity. An important notation in the study was that the fibres should have a high tensile strength to avoid rupture. It was stated that the fibre length has little effect on crack behaviour. Deluce also investigated the effect on the crack spacing. In an extensive "dog-bone" experiment of hybrid reinforced concrete, the crack spacings are examined and compared with crack spacing formulae developed for *S.F.R.C.*. The formulae can be found in App: F. This study showed that adding steel fibres to reinforced concrete reduces the steel stress, which translates to a shorter transfer length and, thus, shorter crack spacings. A lower steel stress also results in a lower strain at the crack and, therefore, also smaller crack widths. It was found that the theoretical formulae for the crack spacing of hybrid concrete are conservative and generally overestimate the crack spacing in the experiment. The mean ratio $\frac{s_{m,pred}}{s_{m,exp}}$ for both models were 3.26 and 2.81 for respectively *RELIM* and *Moffatt*. For crack spacings, up to 100 mm, the ratio is around 2.0. This means that the crack width was, in reality, 50% lower than calculated with the provided formulae. A possibility is that the formulae calculate the mean crack spacing in the *F.D.C.P.*. The cracking in the experiment is likely to be in the *N.F.D.C.P.* and, therefore, not maximal.

4.5 Soil

The soil supports the slab during its lifetime and can be divided into a vertical and horizontal support. Both the structural and geotechnical engineer has to make the correct assumptions for the support to create a representative soil boundary. Chosen the correct properties is difficult because the soil is built up out of layers with different soil types. The soil properties have to be determined by field tests and are often translated to a subgrade modulus k_{mod}. Furthermore, the soil properties are affected by the loading type. The properties of the soil greatly determine the performance of *S.o.G.*. The vertical support influences the loading resistance of the slab. In the horizontal plane, the soil develops a frictional stress when the slab slides over the sub-base. Both the vertical and horizontal support systems are elaborated.

Vertical support

The vertical support is often considered by designers with a simplified method. The simplest representation of a continuous elastic support is based on a *Winkler* model developed in 1867, Fig: 4.14a. The stiffness of the subgrade is modelled as closely spaced independent linear springs. The stiffness of the subgrade is quantified as the subgrade modulus k_{mod}. Practical design values for poor and excellent soil are respectively k_{mod}=0.014 and k_{mod}=0.082. The subgrade modulus can be enhanced by placing a high-quality subbase layer on the subgrade. In Tab:4.4 indicative values of the enhanced k_{mod} for different sub-base types and thickness are given. Important to keep in mind is that the relative thin sub-base layer is only effective for concentrated loads and not for *U.D.L.*. For long-term loading, the k_{mod} should be reduced by a factor three, according to *CUR-36*[18]. In App: H soil models are compared and investigated by *Walker* and *Holland*[48]. They also advise a long-term subgrade modulus for racking load and a short term for wheel loads with an average ration of $\frac{Long}{Short}$ of 0.3. The vertical support can also be modelled with the *Pasternak* soil model, which takes into account the shear interaction of the soil, Fig: 4.14b. The influence of the models on the *S.o.G.* are analysed in the sensitivity analysis.

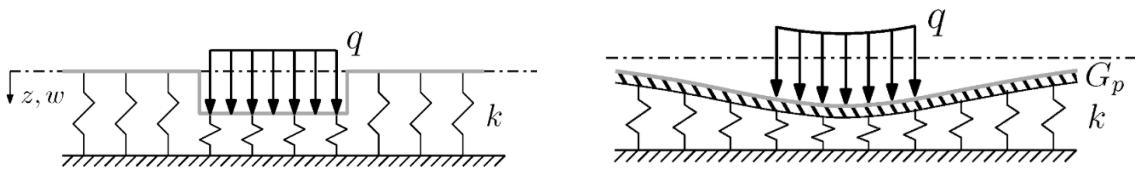

(a) Winkler model

(b) Pasternak model

Figure 4.14: Idealised soil models

Table 4.4: Indicative value for the effective subgrade modulus with sub-base enhancement[4]

k_{mod}	"standard" granular, h=[mm]				Cement-bound, h=[mm]			
[N mm^{-3}]	150	200	250	300	100	150	200	250
0.014	0.018	0.022	0.027	0.033	0.045	0.063	0.081	0.106
0.027	0.034	0.038	0.044	0.051	0.075	0.104	0.137	-
0.054	0.59	0.065	0.072	0.081	0.125	0.175	-	-
0.082	0.089	0.096	0.105	0.114	-	-	-	-

Horizontal friction

The slab behaviour under shrinkage is strongly related to the friction between the slab and the sub-base. Due to shrinkage, the slab wants to move and the horizontal friction restraints the slab movement. For accurate calculations of the frictional behaviour, the stress-slip friction relationship must be taken into account [49]. In this research, a linear and non-linear friction model is taken into account. The non-linear model is based on the Mohr-Coulomb theory. The maximum shear stress τ_{max} for the Coulomb friction model depends on the cohesion c_s, friction angle ϕ_s and the vertical load q_v. In practice, the linear shear stiffness is often taken as 10% of the subgrade modulus. The assumed stress-displacement diagram is shown in Fig:4.15 for both models

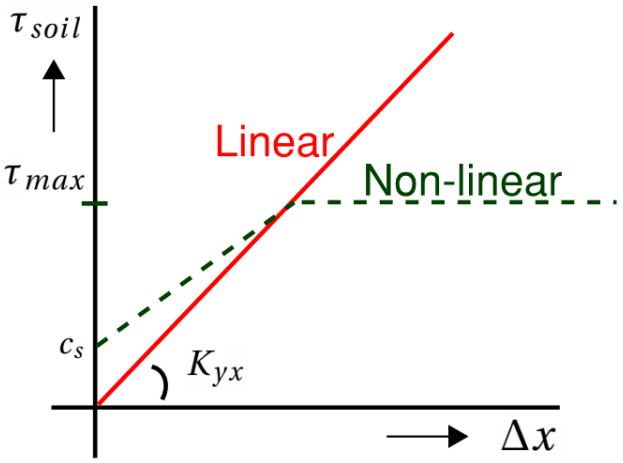

Figure 4.15: Stress displacement graph of soil models

5. Floor behaviour

The behaviour of the *S.o.G.* loaded by shrinkage has been analysed. The *S.o.G.* is translated into a theoretical model. The relevant parameters of the model are mentioned. Finally, the stress behaviour of the model is discussed. The stress behaviour is divided into two stages: uncracked and cracked. First, the general behaviour of a large jointless *S.o.G.* loaded by shrinkage is discussed.

5.1 Slab behaviour

The uniform shrinkage strains induce movement of the slab-edge towards the centre of the slab. When the slab is not restrained, there will be no stresses in the slab. In reality, the slab will always have some form of restraint. The friction from the sub-base should be regarded as negative when an uncracked slab is designed based on the "stress" free principle. When the slab is designed to control the cracks rather than preventing them, the friction has a positive effect after cracking. The friction then functions in analogy with the reinforcement, reducing the crack widths by reducing the force in the crack. It creates a system of many cracks rather than a set of a few wide cracks[8].

When assuming that the friction with the sub-base causes the only restraint on the slab. The restraint due to the friction induces a tensile stress in the slab. The frictional force works at the bottom surface and is thus an eccentric load on the cross-section. Research has shown that for slabs with a high aspect ratio, $\frac{L_{slab}}{h_s} > 150$; there are no bending moments present in the slab from the eccentric friction force[19]. Therefore, in large jointless slabs that have higher aspect ratios than 150, the frictional force can be assumed as an axial force. The stress development in a slab loaded by a uniform strain restrained by friction is shown in Fig: 5.1.

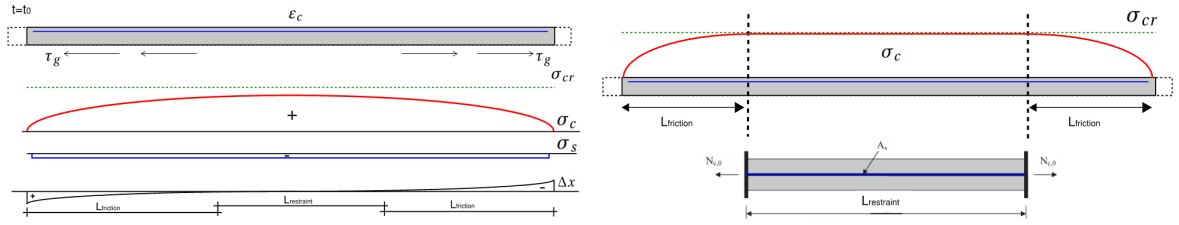

(a) Shrinkage stress development

(b) Considered fully restrained member

Figure 5.1: Stage 1: Stress development

Because of the non-linear stress-slip behaviour of the soil friction, the stresses are not linearly increasing from the edges. In practice, often, a linear stress increment is assumed. The slab can be separated into a build-up zone $L_{friction}$ and a constant zone $L_{restraint}$. Movement of the slab is still possible in the build-up zone. The length of this zone is defined by the friction length $L_{friction}$. When the total length of the slab is longer than twice the friction length, the middle zone $L_{restraint}$ cannot move and is thus fully restrained. Therefore, the fully restrained middle zone can be considered as a *R.T.M.* shown in Fig: 5.1b. The friction length is found when the axial force in the slab is equal to the imposed shrinkage force. The restrained length $L_{restraint}$ due to friction can then be obtained with: $L_{res} = L_{slab} - 2 \cdot L_{fric}$.

The slab can also be loaded by a shrinkage gradient, which results in a curvature strain in the slab. The rotation in the slab is restrained by its self-weight and the additional vertical load on the slab. The rotational restraint of the shrinkage curvature leads to positive bending moments in the slab. The maximum tensile stress will be at the top fibre of the slab. The compressive stresses at the bottom fibre increase the positive bending moment capacity of the slab. This results in a higher resistance to rack loading. The opposite will occur in the aisle where the capacity to resist the hogging moment from the point load is lower due to the restrained shrinkage gradient. The gradient will also result in the uplifting of the slab edges. This effect is defined as curling. The maximum curvature length is found when the imposed bending moment is equal to the bending moment in the concrete slab. The rotational restraint is fully present at a distance $L_{curvature}$, curvature length, from the edge. The rotational restrained length $L_{restraint}$ due to vertical loading can then be obtained with: $L_{res} = L_{slab} minus 2 \cdot L_{cur}$. For a slab with small joint spacing, smaller than ten meters, the curling stress is

significantly larger than the uniform shrinkage restrained stresses[19]. The behaviour of the slab exposed to a shrinkage gradient is shown in Fig: 5.2.

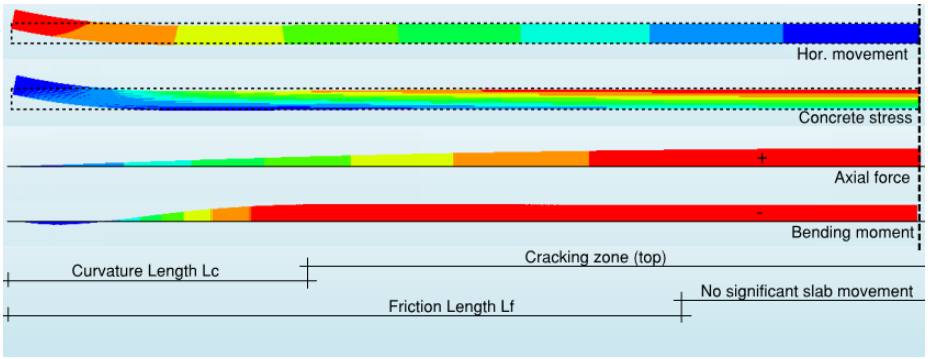

Figure 5.2: Stage 1: Linear Stress Development

The length of the considered *R.T.M.* is defined by the smallest length from the axial or rotational restraint. The non-linear behaviour of the soil friction is also investigated based on the Coulomb friction. The non-linear analysis is performed with the *F.E.M.*. The degree of restraint is extensively investigated in a sensitivity analysis given in Section 7.5.

5.2 Restrained Tensile Member

It is found that for a large *S.o.G.*, the middle section of the floor can be fully restrained. For the analysis of the stress and cracking behaviour, the slab is considered as a *R.T.M.*. The tensile member represents the fully restrained section of the *S.o.G.* per unit width. The stress and cracking behaviour of a *R.T.M.* can be described with the load-strain diagram in Fig: 5.3. The load-deformation diagram is based on the well-known TU Delft Tensile Member Model (*T.U.D.M.*). The *T.U.D.M.* is often used for the calculation of the stresses in a restrained member. In combination with other crack width models, the crack widths are determined in *R.T.M.* for the *N.F.D.C.P.* and the *F.D.C.P.*. The *T.U.D.M.* assumes a centric reinforced concrete member, which is contrary to the commonly applied reinforcement layout in *S.o.G.*. These theoretical models are addressed in Sec: 6.3.

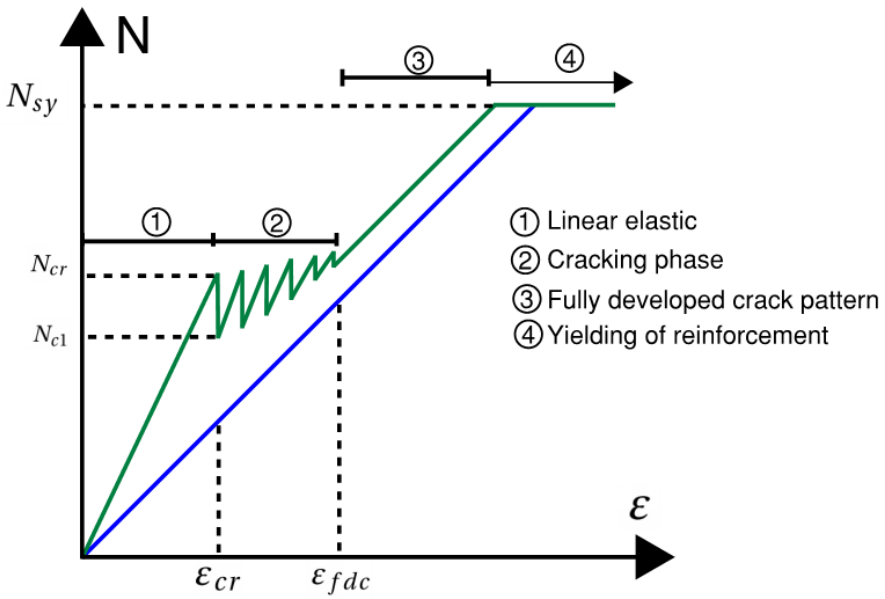

Figure 5.3: Load-deformation diagram of a tensile member

The load-deformation behaviour can be separated into four phases: uncracked, cracking, cracked and yielding phase. The type of loading greatly determines the phase of the member, especially the cracking phase. For

both loading types, the force is constant over the total length of the *R.T.M.*. When the *R.T.M.* is loaded with an increasing external tensile force, the behaviour follows the vertical axes. In the linear stage, the axial force in the member increases. When the external force $N_{(t)}$ is equal to the cracking force N_{cr}, cracking is initiated. Because the force in the member is everywhere equal to the crack force, cracking can be initiated at every location. In reality, weak zones are present in the concrete structures due to the inhomogeneous properties and local imperfections. When the reinforced member cracks, the total axial stiffness reduces, and therefore, the axial capacity of the slab decreases. The force in the member drops from N_{cr} to $N_{c(i)}$. This important effect is referred to as ***crack relaxation***. The crack relaxation effect is taken into account with a crack relaxation factor ψ_{crack} calculated with $\frac{N_{c(i)}}{N_{cr}}$. The most important aspect is that cracking does not influence the external loading. Only the *R.T.M.* is elongated due to the cracking. Therefore, the axial stress in the uncracked region remains equal to $N_{(t)}$=N_{cr}, which results in the formation of multiple cracks. In reality, N_{cr} will not be constant but slightly increasing from the minimal cracking force based on $f_{ctk_{0.05}}$ up to the maximum cracking force according to $f_{ctk_{0.95}}$. Often a simplified model is assumed by taking a constant tensile cracking force N_{cr} corresponding to a horizontal line. The simplification is regarded as accurate enough because of the large number of uncertainties, such as the real cracking stress, reinforcement position and construction quality[31]. The difference between the minimum and maximum cracking force N_{cr} is relatively low, and in practice, it is found that the external load is not in the range of the cracking force. Therefore, when cracking occurs due to an external load, it is assumed that this always results in a *F.D.C.P.*.

Contrary to the cracking behaviour due to external loading, the imposed deformation is effected by the cracking in the *R.T.M.*. The *I.D.* can be seen as an internal strain load. Moreover, when cracking occurs, the concrete moves away from the crack and reduces the *I.D.*. After the first crack, the crack relaxation effect has reduced the axial member force from N_{cr} to $N_{c,i}$. Instead of elongation of the slab due to cracking, the internal force reduces. When the imposed load continues to increase, the concrete stress in the uncracked zone increases again. A second crack will occur when the concrete stress reaches the cracking stress. Opposed to the external loading, the difference between the cracking strain and the strain at the fully developed crack pattern is large $\varepsilon_{fdc} - \varepsilon_{cr} \gg 0$. Therefore a large strain load is required to develop a *F.D.C.P.*. It is found that an imposed load almost always results in a *N.F.D.C.P.*[24]. In combination with the fact that shrinkage is a slowly increasing strain load, the crack pattern is developed over a long period of time.

The stress behaviour during cracking in the *N.F.D.C.P.* and *F.D.C.P.* for reinforced concrete is shortly elaborated. When the concrete is not reinforced, no equilibrium can be found and one dominant crack will be formed.

Phase 1: Linear elastic

In the linear elastic phase, the concrete member is un-cracked. When imposed strains increase, the stresses in the member increase accordingly, and is generally calculated with the linear stress-strain relation of Hooke's law. It is known that in restrained concrete, the generated stresses dissipate over time due to creep. The parameters which influence the stress development are investigated to get insight into the relaxation effect and crack risk in *S.o.G.*.

Phase 2: Not fully developed crack pattern

Cracking will occur in the weakest zone in the concrete. In the crack, the concrete stresses will drop to zero and the local axial stiffness of the member decreases. The reinforcement will find a new equilibrium and takes over the tensile force in the crack. The steel stress σ_{sr} after cracking is equal to the stress in the cracking phase. The tensile force is transferred by the bond of the reinforcement to the concrete. Because the total strain in the reinforcement has to be zero in the *R.T.M.*, there should be a compressive stress in the reinforcement in the uncracked zone. In Fig: 5.4, the stress behaviour in the cracking zone is given. An indication of the crack pattern in the *N.F.D.C.P.* for *S.o.G.* is given in Fig: 5.5. The crack pattern found in actual projects has a crack width between 0.2 and 0.3 mm with a crack spacing ranging between 0.5 and 3 m[20].

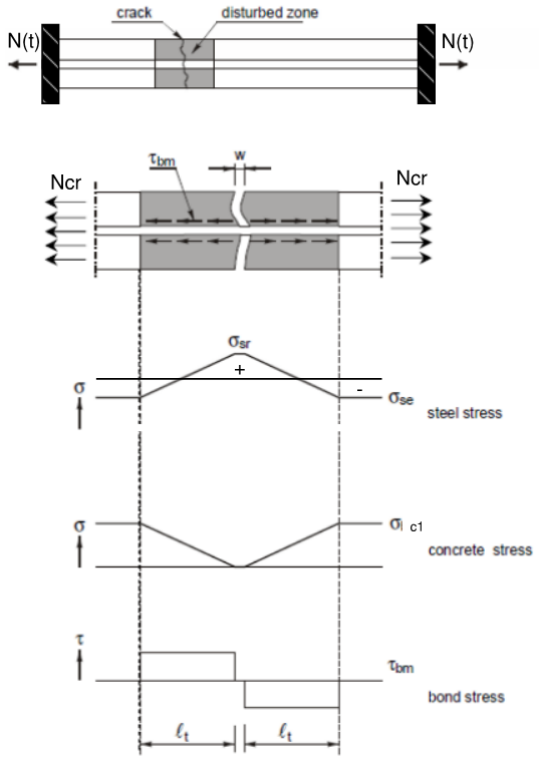

Figure 5.4: *R.T.M.* loaded by *I.D.*

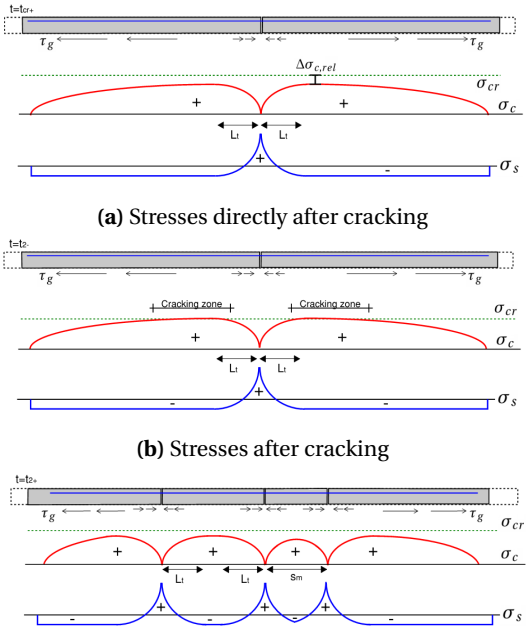

(a) Stresses directly after cracking

(b) Stresses after cracking

(c) Stresses directly after multiple cracks

Figure 5.5: Stage 2: Stress development after first cracking

Phase 3: Fully developed crack pattern

The *F.D.C.P.* is reached when an external load higher than N_{cr} or an imposed load higher than ε_{fdc} is applied on the concrete structure. The *F.D.C.P.* is characterized by the constant and minimum distance between cracks. The minimum crack spacing indicates that the maximum number of cracks is reached in the structure, as shown in Fig: 5.6. Only cracked zones are left in the tensile member. The transfer zones of the cracks are overlapping, and therefore, the smallest crack spacing is l_t and the largest $2l_t$. Additional loading in the *F.D.C.P.* has to be taken by the reinforcement and increases the steel stress after cracking σ_{sr} with $\delta\sigma_s$ and increases the crack width instead of creating more cracks.

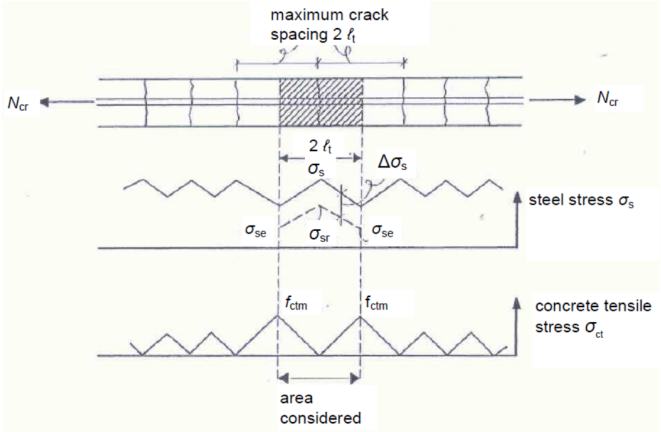

Figure 5.6: Fully developed crack pattern

When the steel stress is reaching the yielding capacity, the forces can not be redistributed any more, which results in large crack widths or failure of the structure. In this research, the focus is on the development of the stresses in the linear phase and on the *N.F.D.C.P.* due to imposed deformation.

5.3 Conclusion

A *S.o.G.* is restrained, and when full, a constant stress zone is present in the slab. The restrained section of the slab can be modelled as a *R.T.M.* to describe the behaviour inside the slab. The length of the restrained zone is influenced by the soil friction and has to be investigated. The stress development in the *R.T.M.* is affected by creep. When the stress reaches the cracking strength of the concrete, cracking is initiated. Cracking occurs in the weakest zone of the concrete structure. When the *S.o.G.* cracks the stiffness reduces and the *I.D.* decreases. Therefore, the axial force in the uncracked zone reduces after cracking. The same principle of the *R.T.M.* is applicable for the shrinkage gradient. The shrinkage gradient results in a combination of a tensile force and a negative bending moment. The behaviour in a tensile member loaded by an external force is different than in a *R.T.M.* loaded by *I.D.*. The cracking behaviour affects the stress behaviour in the *R.T.M.*. The influence of this crack relaxation effect has to be analysed. Also, it has to be investigated if the *T.U.D.M.* is applicable for the calculation of the stresses in a *R.T.M.* loaded by *I.D.*. The theoretical models to analyse the stress and cracking behaviour are given in the next chapter.

6. Calculation methods

6.1 Uncracked phase

The calculation of the stress development due to *I.D.* in the *R.T.M.* can be done with various methods. Most methods do not take into account the time-dependent properties of concrete, which have a large influence on the structural behaviour. For that reason, the stress development in the *R.T.M.* is calculated with the use of the superposition method of *Bazant* and *Trost*, referred to the Bazant Model (*Bazant*).

6.1.1 *Bazant* model

The *Bazant* model is based on the superposition model of the creep mechanism of ageing linear viscoelastic concrete. For the calculation of the stress development in concrete, the *I.D.* is divided into small strain increments per day. The strain increment results in a stress increment linear related to the Young's modulus of the concrete directly at loading. In time, the stress increments dissipate due to creep, as shown in Fig:6.1 for the early-age behaviour in concrete.

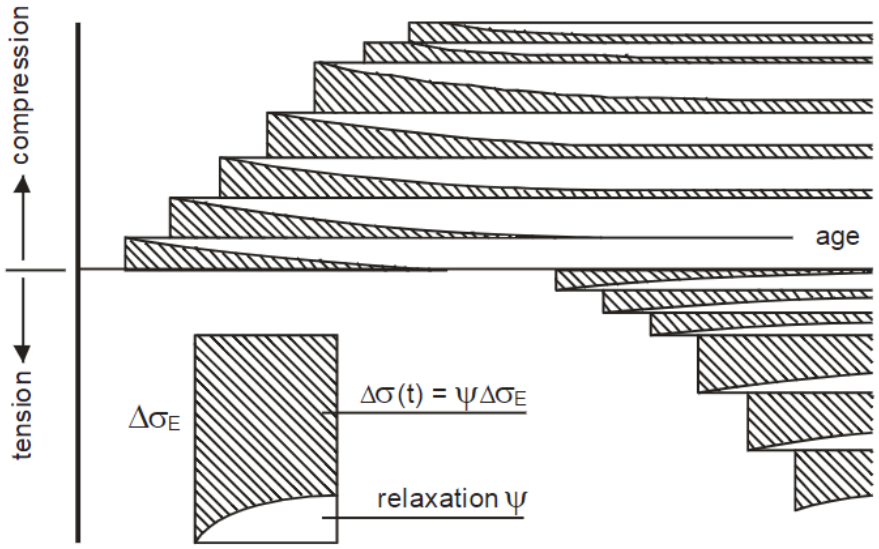

Figure 6.1: *Bazant* model

The concrete stress at a certain moment in time can be calculated by the summation of all the residual stresses from the increments. The residual stress from a strain increment is calculated by multiplying the initial stress times the relaxation factor ψ. Due to the ageing of the concrete, the relaxation factor changes in time. Based on the relaxation function $\psi_{instant(t,t_i)}$ for instantly applied loads, the relaxation factor $\psi_{(t,t_i)}$ is determined for every time step. In Eq: 6.16, the formula is given for the calculation of the relaxed concrete stress at a certain moment in time. In the formula, t_i is the concrete age at loading for the determination of the properties. The concrete properties are based on the time-dependent properties formulae provided in the *E.C. 2* given in App: E. With the model, a more accurate stress development can be estimated compared to the simplified approach of the *A.A.E.M* method.

$$\sigma_{(t)} = R \cdot \int_{t_i}^{t} \cdot \psi_{(t,t_i)} \cdot \Delta\varepsilon_{c(t_i)} \cdot E_{cm(t_i)} \tag{6.16}$$

$$\sigma_{(t)} = R \cdot \int_{t_i}^{t} \cdot \left(1 - \frac{\varphi_{RH}\beta_{(f_{cm})}\beta_{(t_i)} \cdot \beta_{c(t,t_i)}}{\left(1 + \chi_{age}\varphi_{RH}\beta_{(f_{cm})}\beta_{(t_i)} \cdot \beta_{c(t,t_i)}\right)} \right) \cdot \Delta\varepsilon_{c(t_i)} \cdot E_{cm(t_i)} \tag{6.17}$$

6.2 Cracking phase

The stresses in the concrete and steel are constantly changing due to the formation of cracks. It was found that the *T.U.D.M.* based on the external loading is not perfect for the calculation of the stresses by *I.D.* in the cracking phase. Therefore, for the calculation of the stresses in the uncracked and cracked zone, the approach of *R. Gilbert*, referred to as the Gilbert Model (*Gilbert*), is used. In practice, the reinforcement is often placed in the top layer. Therefore, the theoretical model of *VENCON 2.0* is considered, which takes into account the eccentricity of the reinforcement. For the determination of the contribution of the soil friction, the spring model of *ABT* is used.

For the calculation of the crack width in the *N.F.D.C.P.*, three theoretical models are used. First, the *Gilbert* model based on strain equilibrium is given. Secondly, the Breugel Crack Width Model (*Van Breugel*) based on the steel stress directly after cracking is taken into account. Finally, the crack width model in the *M.C. 2010* which specifically addresses the crack width due to *I.D.* in the *N.F.D.C.P.* The provision also gives additional information for the crack width if hybrid reinforced concrete is used. Furthermore, two practical based crack width models are elaborated and analysed.

All the crack width models are adopted to take into account the steel fibres. First, the stress-related calculation methods are elaborated, then the crack widths models are given.

6.2.1 *Gilbert* model

Gilbert's model considers the stress and cracking behaviour in direct tension reinforced members loaded by uniform shrinkage[50]. The member is fully restrained by its support. When the concrete shrinks an axial tensile stress σ_c develops in time. Over time, the stresses in the concrete exceeds tensile concrete capacity σ_{cr} and cracking occurs. A full depth, direct tension crack occurs in the member and the stress in the uncracked zone decreases. The sustained loading increases in time and the concrete stress increases again. In Fig: 6.2 a common stress-time flow is shown in a cracking *R.T.M.*. After every formation of a crack, the stress reduces again.

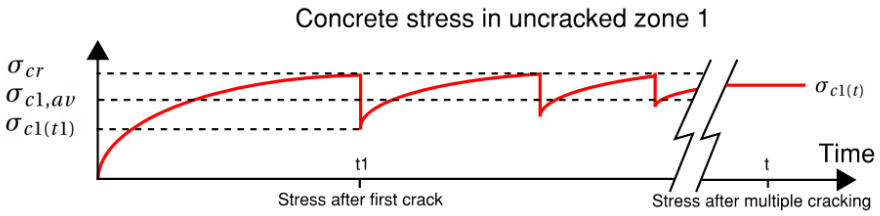

Figure 6.2: Development of concrete stress development in cracking member

For the calculation of the forces, the ageing of concrete is taken into account conform the time-dependent properties in *E.C. 2*. The behaviour is calculated at the first crack t_{cr} and at a certain moment in time t.

Behaviour after first crack at t_{cr}

Gilbert developed a model to calculate the concrete and steel stresses in the uncracked zone (*zone 1*) and the steel stress in the crack (*zone 2*). In Fig: 6.3, the stresses after the first crack is shown. For the calculation of these stresses, the transfer length (l_t) of the reinforced concrete member is required. In this research, the transfer length is based on the simplified method in the *E.C. 2*. The steel stress is also schematized to calculate the relation between the uncracked and cracked zone expressed in the stress relation c_1. Based on this relation and the cracking force of the slab, the axial force after cracking ($N_{cr_{(t_{cr})}}$) is determined. Also, the steel stresses in zone 1 and 2 can be calculated. The force in the crack ($N_{cr_{(t_{cr})}}$) depends mainly on the reinforcement ratio (ρ_s), the cracking strength of concrete (σ_{cr}) and the area of the slab (A_c). More reinforcement reduces the transfer length and c_1, which results in an increase of $N_{cr_{(t_{cr})}}$. A_c and σ_{cr} are directly related to the axial force in after cracking. With an increase of $N_{cr_{(t_{cr})}}$, the steel stress in the crack and concrete stress ($\sigma_{c1_{(t_{cr})}}$) in zone 1 is also increased. Due to the higher concrete stress($\sigma_{c1_{(t_{cr})}}$), the crack risk of secondary cracking is higher. According to Gilbert, more reinforcement results in smaller but more cracks which is also found in other research. The

crack width is calculated by taking the total free shrinkage movement in the restrained member minus the shrinkage movement in the uncracked zone. From the formula, it can be concluded that a smaller transfer length, higher concrete stress and lower effective Young's modulus reduces the crack width. The concrete relaxation effect reduces the effective Young's modulus and thus, the width of the first crack.

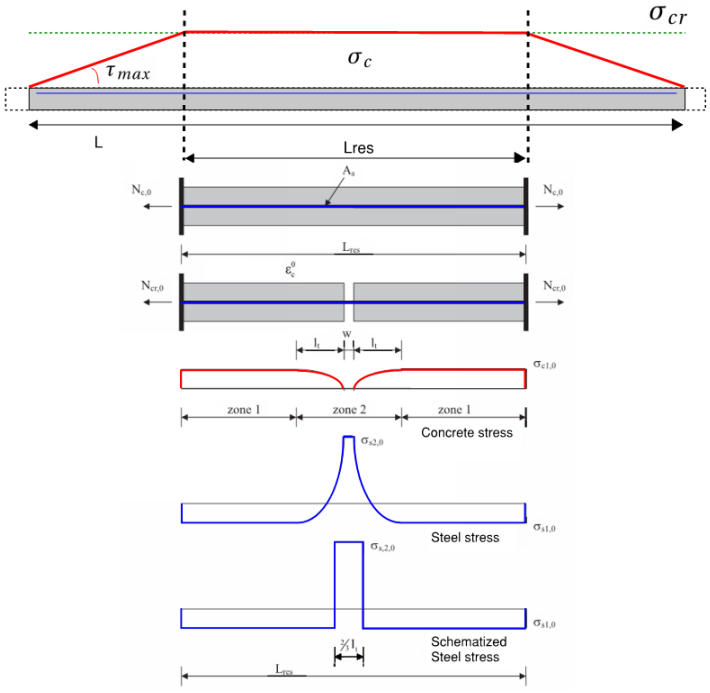

Figure 6.3: Shrinkage behaviour at first crack

$$L_{min} = \frac{2 \cdot Ncr}{\tau_g \cdot b} \tag{6.18}$$

$$L_{restraint} = L - L_{min} \tag{6.19}$$

$$l_t = \frac{f_{ctm} \cdot \varnothing}{4 \cdot \tau_{bm} \cdot \rho_s} = \frac{\varnothing}{8 \cdot \rho_s} \tag{6.20}$$

$$c_1 = \frac{\frac{2}{3} \cdot l_t}{L_{restraint} - \frac{2}{3} \cdot l_t} \tag{6.21}$$

$$N_{cr_{(t_{cr})}} = \frac{\alpha_e \cdot \rho_s \cdot \sigma_{cr_{(t_{cr})}} \cdot A_c}{c_1 + \alpha_e \cdot \rho_s \cdot (1 + c_1)} \tag{6.22}$$

$$\sigma_{s1_{(t_{cr})}} = -\frac{c_1 \cdot N_{cr_{(t_{cr})}}}{A_s} \tag{6.23}$$

$$\sigma_{c1_{(t_{cr})}} = \frac{N_{cr_{(t_{cr})}} - \sigma_{s1_{(t_{cr})}} \cdot A_s}{A_c} = \frac{N_{cr_{(t_{cr})}} (1 + c_1)}{A_c} \tag{6.24}$$

$$\sigma_{s2_{(t_{cr})}} = \frac{N_{cr_{(t_{cr})}}}{A_s} \tag{6.25}$$

$$w_{(t_{cr})} = -\left(\frac{\sigma_{c1_{(t_{cr})}}}{E_{cm_{eff_{(t_{cr})}}}} (L_{res} - \frac{2}{3} l_t) + \varepsilon_{(t_{cr})} \cdot L_{res} \right) \tag{6.26}$$

Behaviour after cracking at t

Gilbert also provided formulae to determine the stresses and crack width at a certain chosen moment in time t. In Fig: 6.4 the stresses after formation of multiple cracks at t are shown. First, the average concrete stress in the uncracked zone is assumed equal to the mean value of the cracking strength and the concrete stress after the first crack. Based on the average stress, the axial force is determined. For the calculation of the axial force, the concrete relaxation effect is taken into account with ψ. First, the stress relation (β_s) is determined. Then, the crack spacing (s_c) is calculated, and finally, the relation c_2 between the crack spacing and the cracked zone is determined. The theory is based on the fact that the overall shortening of the concrete is the sum of the crack widths. It should be noted that the applied strain $\varepsilon_{(t)}$ must initiate a second crack for the calculation of the stresses e.g. $(\sigma_{c1(av)} + \varepsilon_{(t)} \cdot \psi \cdot E_{cm}) < 0$. With the use of c_2 the axial force and the steel stress, the precise concrete stress in zone 1 is determined. The same approach as for the first crack is taken for the calculation of the average crack width. Only this time, the restrained length is replaced by the crack spacing. When analysing the formulae, it can be concluded that smaller crack spacing(more cracks) reduces the average crack width in the *R.T.M.*. The effect of concrete relaxation is difficult to determine because it reduces the axial force, which increases the crack width. On the other hand, concrete relaxation reduces the effective Young's modulus and thus the crack width. Therefore, the influences of each parameter have to be analysed in the sensitivity analysis.

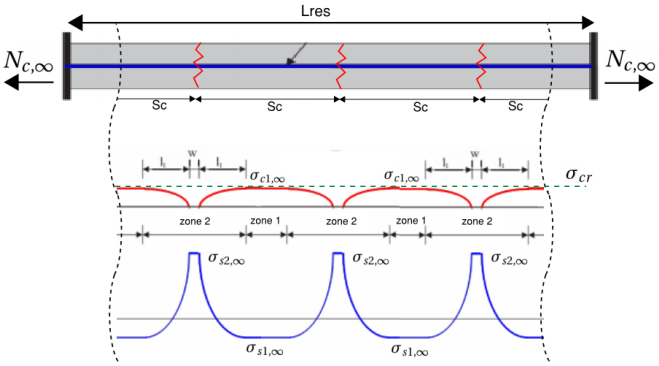

Figure 6.4: Shrinkage behaviour at t

$$\sigma_{c1_{av}} = \frac{\sigma_{c1_{(t_{cr})}} + \sigma_{cr_{(t)}}}{2} \tag{6.27}$$

$$\beta_s = -\frac{\left(\frac{\alpha_e \cdot \rho_s}{\psi}\right)\left(\sigma_{c1_{av}} + \varepsilon_{(t)} \cdot \psi \cdot E_{cm_{(t)}}\right)}{\left(\frac{\alpha_e \cdot \rho_s}{\psi}\right)\left(\sigma_{c1_{av}} + \varepsilon_{(t)} \cdot \psi \cdot E_{cm_{(t)}}\right) + \sigma_{cr_{(t)}}} \tag{6.28}$$

$$s_c = \frac{\frac{2}{3} \cdot l_t (1 + \beta_s)}{\beta_s} \tag{6.29}$$

$$n_{crack} = round(\frac{L_{res}}{s_c}) \tag{6.30}$$

$$c_2 = \frac{\frac{2}{3} \cdot l_t}{s_c - \frac{2}{3} \cdot l_t} \tag{6.31}$$

$$N_{c_{(t)}} = -\frac{\alpha_e \cdot A_s}{\psi \cdot c_2}\left(\sigma_{c1_{av}} + \varepsilon_{(t)} \cdot \psi \cdot E_{cm_{(t)}}\right) \tag{6.32}$$

$$\sigma_{c1_{(t)}} = \frac{N_{c_{(t)}}\left(1 + c_2\right)}{A_c} \tag{6.33}$$

$$\sigma_{s1_{(t)}} = -\frac{c_2 \cdot N_{c_{(t)}}}{A_s} \tag{6.34}$$

$$\sigma_{s2_{(t)}} = \frac{N_{c_{(t)}}}{A_s} \tag{6.35}$$

$$w_{(t)} = -\left(\frac{\sigma_{c1_{(t)}}}{E_{cm_{eff_{(t)}}}}(s_c - \frac{2}{3}l_t) + \varepsilon_{(t)} \cdot s_c\right) \tag{6.36}$$

6.2.2 Frictional force after cracking

As mentioned before, the friction of the sub-base is beneficial after cracking for the crack width[8]. After cracking, the concrete in the cracked zone will undergo a small horizontal movement. This movement results in a frictional force which is in the opposite direction to the cracking force and in analogy with the reinforcement. For the calculation of the frictional force after cracking N_{soil}, the theory of the spring model *Vloerstaal 1.0* proposed by *ABT* is used. In Fig: 6.5, a schematization of the movement and shear stresses is shown. When there is no force-transfer in the crack (α=0), e.g., no reinforcement, the crack length is unrestrained and given by L_2. L_2 is taken from a report by the Dutch consultancy agency *Hageman B.V.*. The reinforcement restraint degree α is the relation between the cracking force (N_{cr}) and the (hybrid) reinforcement force ($N_s + N_{fibre}$). The force in the reinforcement after cracking is determined with the *Gilbert* model. When α is known, the crack influence length L_s can be calculated. Based on the crack length, the average displacement of the slab in the cracked zone is determined. A linear shear stiffness (K_{yx}) is assumed for the calculation of the frictional force. The frictional force N_{soil} is calculated by multiplying the shear stiffness of the soil with the assumed average displacement of the slab times the length of the cracked zone. The blue line in Fig: 6.5 represents the displacement at one side of the crack. The formulae are given below. The influence of this frictional force after cracking is analysed in the sensitivity analysis in Chapter: 8.4.

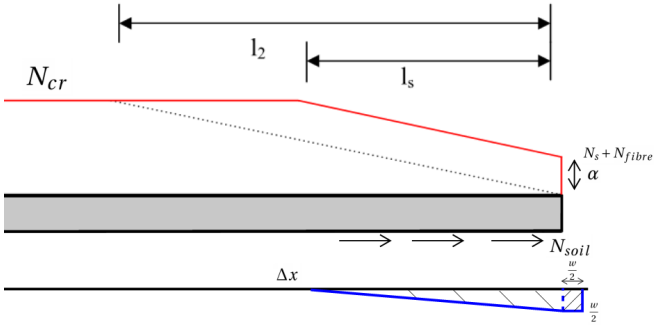

Figure 6.5: Schematisation of friction behaviour after cracking

$$L_2 = \sqrt{\frac{E_{cm} \cdot h}{K_{yx}}} \tag{6.37}$$

$$\alpha = \frac{N_s + N_{fibre}}{N_{cr}} \tag{6.38}$$

$$L_s = L_2\left(1 - \alpha\right) \tag{6.39}$$

$$N_{soil} = K_{yx} \cdot \left(\left(L_s \cdot \frac{w}{4}\right) + \frac{w^2}{4}\right) \tag{6.40}$$

6.2.3 Eccentric reinforcement

Reinforcement is often placed in the top layer of the slab. Therefore the influence of the eccentricity of the reinforcement on the behaviour was analysed. When the reinforcement is placed centric, the steel stress is directly related to the force in the crack. According to the design philosophy of *VENCON 2.0*, eccentric reinforcement results in a lower reinforcement force when the member is fully restrained by the soil friction[51]. The *VENCON 2.0* model takes the eccentricity of the reinforcement into account by an eccentricity factor, α_{ecc}. When taking the moment around the reinforcement steel and the horizontal force equilibrium, the steel force (N_s) can be determined and the eccentricity reduction factor (α_{ecc}) can be derived. The force equilibrium in the cross-section is shown Fig: 6.6. According to this model, the steel stress can be reduced with 20%, 33% and 43% for eccentricities of 25, 50 and 75 mm in a slab of 200 mm thick. It should be noted that the model is only validated up to an eccentricity of 25 mm. Research showed that higher eccentricity resulted in an overestimation of the effect. The effect of higher eccentricity values should be investigated with *F.E.M.*.

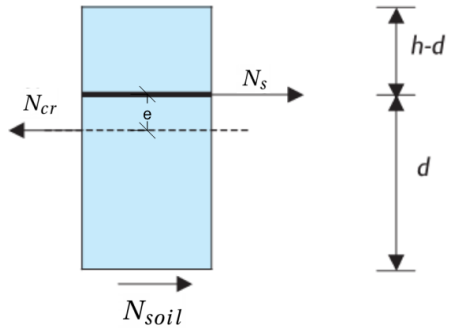

Figure 6.6: Force balance

$$N_{cr} \cdot \left(d - \frac{h}{2}\right) - N_{friction} \cdot d = 0 \tag{6.41}$$

$$N_s + N_{friction} - N_{cr} = 0 \tag{6.42}$$

$$N_s = \left(N_{cr} - N_{friction}\right) \cdot \alpha_{ecc} \tag{6.43}$$

$$\alpha_{ecc} = \frac{h}{2d} \tag{6.44}$$

6.3 Theoretical crack width models

Multiple models were developed for the calculation of the crack width in reinforced concrete structures. The downside is that not all models can be used in the *N.F.D.C.P.*. Also, sustained loading results in a different behaviour of the concrete-reinforcement interaction. In practice, this result in a large scatter of design values when crack width calculation is performed for *I.D.*. For this research, the theoretical models of *M.C. 2010*, *Van Breugel* and the earlier explained model of Gilbert were compared. Also, two practical based models according STUFIB-11 - Controlled Cracking in Jointless Elastic Supported Concrete Floors (Stu*fib*-11) and CUR 65 – Design Execution and Repair of Liquid Tide Concrete Structures (*CUR-65*) were elaborated. All the models were altered to take into account the effect of *S.F.R.C.*.

Effective tension area in the cross-section

For thick or single reinforced slab, the effective area surrounding the reinforcement is smaller than the total cross-sectional area. This results in a higher reinforcement ratio ρ_s. Therefore, an effective tension area of the concrete $A_{c_{eff}}$ has to be taken into account and can be determined by taken the smallest value of Eq:6.45. For direct tension cracks, the concrete compression height (x) is assumed 0. The effective area is used in the models were the $\rho_{s_{eff}}$ is specifically defined, such as in the *M.C. 2010*.

$$h_{c_{eff}} = MIN\left[2.5 \cdot \left(c + \frac{\varnothing}{2}\right), \frac{(h-x)}{3}, \frac{h}{2}\right] \text{(For overall tension)} \tag{6.45}$$

$$\rho_{eff} = \frac{A_s}{b \cdot h_{c_{eff}}} \tag{6.46}$$

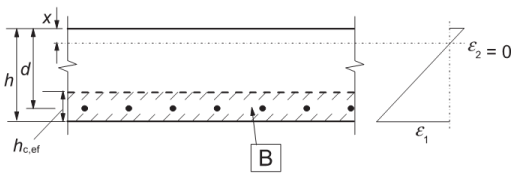

Figure 6.7: Effective area of the cross-section

6.3.1 *Breugel* model

For the calculation of the crack width in the *N.F.D.C.P.*, the *TU-Delft* tensile member model loaded by an axial force is often used. This *TU-Delft* crack width model is referred to as the *Van Breugel* model in this research. *Noakowski* and *van der Veen proposed the Van Breugel model* and is based on the bond stress-slip relationship of reinforcement and concrete which were determined by pull-out tests. The model determines the mean crack width in the member based on the steel stress σ_s in the crack due to the load. The advantage of the model is that the crack width can be determined in both crack patterns. First, the cracking force is calculated, then the steel stress directly after cracking $\sigma_{s,cr}$ is determined. The mean crack width in the *N.F.D.C.P.* directly after cracking is w_{mo} and in the *F.D.C.P.* this is w_{mv}. The behaviour and the formulae are given below.

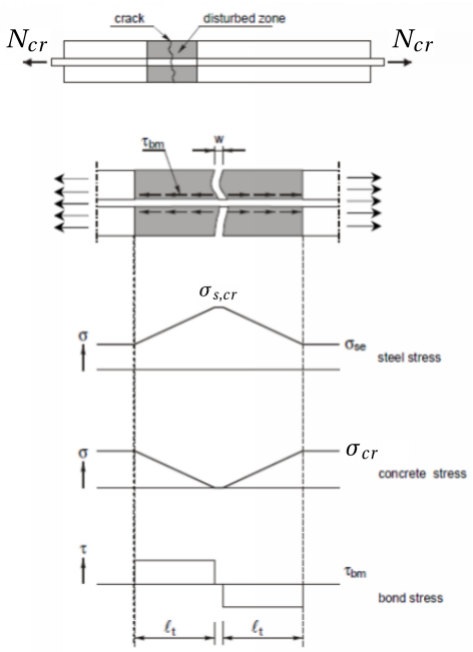

$$N_{cr} = \sigma_{cr} A_c \left(1 + \alpha_e \rho_s\right) \tag{6.47}$$

$$\sigma_{s,cr} = \frac{N_{cr}}{A_s} \tag{6.48}$$

$$w_{mo} = 2\left(\frac{0.4\varnothing}{f_{ccm} E_s} \sigma_{s,cr}\left(\sigma_{s,cr} - n\sigma_{cr}\right)\right)^{0.85} \tag{6.49}$$

$$\sigma_{s,cr} = \frac{n\sigma_{cr}}{2} + \sqrt{\left(\frac{n\sigma_{cr}}{2}\right)^2 + \frac{f_{ccm} E_s (0.5 w_{mo})^{1.18}}{0.4\varnothing}} \tag{6.50}$$

$$\varepsilon_{fdc} = \left(60 + 2.4\sigma_{s,cr}\right) \cdot 10^{-6} \tag{6.51}$$

$$w_{mv} = w_{mo} 1.8\left(\frac{\sigma_s}{\sigma_{s,cr}} - 0.5\right) \tag{6.52}$$

Figure 6.8: Cracking behaviour of a classic reinforced concrete tensile member

The bonding quality has a considerable influence on the determination of the crack width and is considered by the mean compressive stress, f_{ccm}. A higher concrete class increases the bonding quality, and thus, a smaller crack width is observed. The downside is that a higher concrete class also leads to a higher cracking stress and, thus a higher steel stress after cracking. A higher steel stress results in larger crack widths. From the formula, it can also be concluded that a smaller reinforcement diameter results in smaller crack widths. The phase of the crack pattern has also influence on the crack width. Therefore, it should be checked in which stage the crack pattern is. This can be done by checking the applied strain. When the applied strain is larger than ε_{fdc}, the crack pattern is in the *F.D.C.P.*. When the crack pattern is fully developed, the crack width w_{mv} can be calculated by taking into account the steel stress ratio between σ_s and $\sigma_{s,cr}$.

In reality, there is always a certain scatter, and therefore, the mean crack width should be enhanced. From experiments, the ratio between the mean and maximum was determined for different situations. The enhancement factor γ_s is used for the possible crack width variation. Besides the variation, the creep phenomenon also results in enhancement of the mean crack width when loaded by a sustained load. The bond between steel and concrete is affected by the constant load, which results in an increase of crack width and transfer length up to 40 %[24]. The same effect occurs when the member is loaded by an alternating load. Because a combination of sustained and alternating loading is in practice rather an exception than a rule, only one enhancement factor which takes both effects into account is used. The research resulted in the enhancement factors γ_∞ for sustained/alternating loading depending on the steel stress. In Fig:6.9, the increase of the enhancement factor is shown for the steel stress exceeding 295 MPa. The factor significantly increases for the steel stresses for higher than 295 MPa. Therefore, it is advised to design the concrete structure in a way that the steel stress is not higher than 295 MPa.

$$w_m \cdot \gamma_s \cdot \gamma_\infty \leq w_{design} \tag{6.53}$$

$$\text{for} \quad N.F.D.C.P. \quad \gamma_s = 1.3 \tag{6.54}$$

$$\text{for} \quad F.D.C.P. \text{ tension} \quad \gamma_s = 1.5 \tag{6.55}$$

$$\text{for} \quad F.D.C.P. \text{ flexure} \quad \gamma_s = 1.7 \tag{6.56}$$

$$\text{for} \quad \sigma_s \quad \leq 295 \text{N mm}^{-2} \quad \gamma_\infty = 1.3 \tag{6.57}$$

$$\text{for} \quad \sigma_s \quad \geq 295 \text{N mm}^{-2} \quad \gamma_\infty = \frac{1}{1 - 9 \cdot \sigma_s^3 \cdot 10^{-9}} \tag{6.58}$$

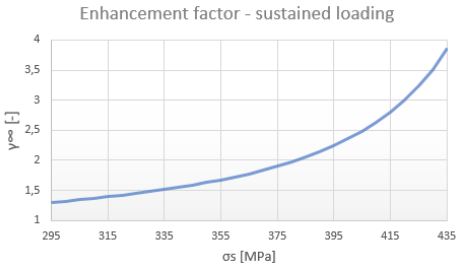

Figure 6.9: Enhancement factor γ_∞

Hybrid reinforcement

As discussed, the steel fibres act as a bridge in the cracked cross-section. Over the total cross-section, tensile stresses are transferred in the crack through the fibres. Less tensile stress has to be transferred by the reinforcement. For the calculation of the crack width in hybrid reinforced concrete, this effect is taken into account by reducing the steel stress in the crack. The stress reduction by the steel fibres is based on the residual tensile stress, σ_{R1}. An equivalent steel stress, $\sigma_{eq,s,R1}$, representing the contribution of the fibres is used in the crack width calculation given in the research of *Dooren*[23]. The crack width calculation methods for hybrid reinforcement based on the *Van Breugel* model results in the following behaviour and formulae:

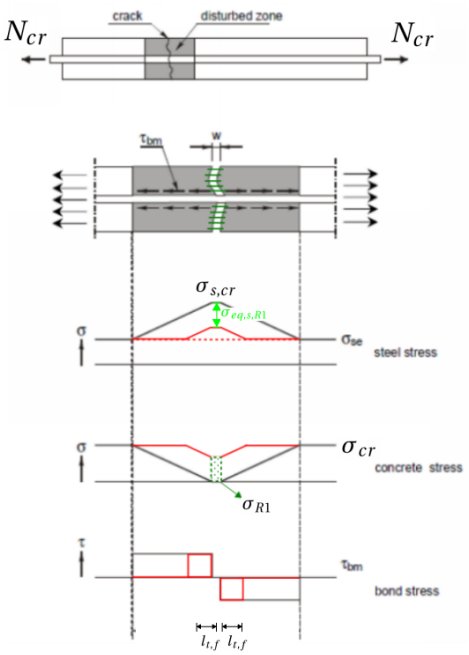

Figure 6.10: Cracking behaviour of hybrid concrete member

$$l_{t,f} = 1.2 w_{mo,f} \frac{E_s}{(\sigma_{s,cr} - \sigma_{eq,s,R1})} \tag{6.59}$$

$$w_{mo,f} = 2 \left(\frac{0.4 \varnothing}{f_{cm,cube} E_s} (\sigma_{s,cr} - \sigma_{eq,s,R1}) \left((\sigma_{s,cr} - \sigma_{eq,s,R1}) - \alpha_e \sigma_{cr} \right) \right)^{0.85} \tag{6.60}$$

$$l_{m,f} = 1.8 w_{mo,f} \frac{E_s}{(\sigma_{s,cr} - \sigma_{eq,s,R1})} \tag{6.61}$$

$$w_{mv,f} = 1.8 w_{mo,f} \left(\frac{(\sigma_s - \sigma_{eq,s,R1})}{(\sigma_{s,cr} - \sigma_{eq,s,R1})} - 0.5 \right) \tag{6.62}$$

With (6.63)

$$\sigma_{eq,s,R1} = \frac{\sigma_{R1}}{\rho_s} \tag{6.64}$$

$$\sigma_{R1} = 0.45 \cdot f_{R,1} \tag{6.65}$$

6.3.2 *M.C.2010* model

The provisions *M.C. 2010* provide a general design crack width formula for all cracking phases and loading types. The crack width method of *M.C. 2010* for the *N.F.D.C.P.* by long-term loading was used in this research. The crack width is based on the maximum transfer length and the strain in the cracked zone. The *M.C. 2010* provide a different formula for the ε_{fdc} compared to the *Van Breugel* model. The general formula is given with the coefficient per loading and cracking stage, as shown in Tab: 6.1. The model predicts the crack width at the reinforcement. In order to calculate the crack width at the extreme fibre, the crack width should be multiplied with the factor $\left(\frac{h-x_u}{d-x_u}\right)$. The provision *M.C. 2010* also provides a formula to calculate the design crack width in hybrid concrete structures. The method is also based on the residual tensile strength of *S.F.R.C.*. For the determination of the stress in the steel σ_s, the contribution of the steel fibres needs to be taken into account. The calculation of the transfer length is only valid for covers up to 75 mm, according to *M.C. 2010*. This limitation for the analysis of centric reinforced concrete, where covers of 150 mm were present, is neglected in this thesis.

$$\varepsilon_{fdc} = \frac{\sigma_{cr}\left(1-\beta\right)}{E_s} \tag{6.66}$$

$$w_d = 2 \cdot l_{t,max} \cdot \left(\varepsilon_{sm} - \varepsilon_{cm} - \varepsilon_{cs}\right) \cdot \frac{h-x_u}{d-x_u} \tag{6.67}$$

$$l_{tmax} = c + \frac{1}{4}\frac{\varnothing}{\omega_{eff}}\frac{f_{ctm}}{\tau_{bm}} \tag{6.68}$$

$$l_{tmax_f} = c + \frac{1}{4}\frac{\varnothing}{\omega_{eff}}\frac{f_{ctm}-\sigma_{r1}}{\tau_{bm}} \tag{6.69}$$

$$\varepsilon_{sm} - \varepsilon_{cm} - \varepsilon_{cs} = \frac{\sigma_s - \beta \cdot \sigma_{s,cr}}{E_s} - \eta_r \cdot \varepsilon_{sh} \tag{6.70}$$

$$\sigma_{s,cr} = \frac{f_{ctm}}{\omega_{eff}}\left(1 + \alpha_e \omega_{eff}\right) \tag{6.71}$$

$$\sigma_{s,cr_f} = \frac{\left(f_{ctm}-\sigma_{r1}\right)}{\omega_{eff}}\left(1 + \alpha_e \omega_{eff}\right)\omega_{eff} \tag{6.72}$$

Table 6.1: Crack width coefficient *M.C. 2010*

	N.F.D.C.P.	*F.D.C.P.*
Short-term	$\tau_{bm} = 1.8 \cdot f_{ctm(t)}$ $\beta = 0.6$ $\eta_r = 0$	$\tau_{bm} = 1.8 \cdot f_{ctm(t)}$ $\beta = 0.6$ $\eta_r = 0$
Long-term	$\tau_{bm} = 1.35 \cdot f_{ctm(t)}$ $\beta = 0.6$ $\eta_r = 0$	$\tau_{bm} = 1.8 \cdot f_{ctm(t)}$ $\beta = 0.4$ $\eta_r = 1$

6.4 Practical crack width models

The models given in the *CUR-65* and Stu*fib*-11 are based on theoretical models in the *E.C. 2* and the *Van Breugel* and are adapted to practical design methods.

6.4.1 CUR-65

For the calculation of the crack width in *S.o.G.*, the *CUR-65* comity advises to take into account an enhanced cracking bending moment. The cracking bending moment is calculated with the 28-day flexural tensile strength $f_{ctm_{fl}}$ in combination with the cracking factor α_{cr}. The cracking bending moment is enhanced with a factor 1.4 to agree with the practical findings. It can be assumed that this factor 1.4 considers the ageing of the concrete and the compensation of the tensile force, which is also present in the structure. Therefore, no axial and bending moment interactions have to be taken into account. For the crack width calculation, the steel stress resulting from the enhanced bending moment should be determined. The formulae for the calculation of the crack width are shown below and are based per unit width of the slab [33]. The estimation of the transfer length is based on the provision *M.C. 2010*. The *CUR-65* method is also altered to take into account the *S.F.R.C.*. This method is assumed to analyse the influence of the steel fibre contribution. The hybrid method is not based on research or validated with experiments and can not be used for design purposes. For the calculation of the maximum crack width, a fixed enhancement factor of 1.7 was advised instead of the enhancement factors γ_s and γ_∞. The factor 1.7 is in good agreement with the results found in practice [8].

$$\sigma_{cr_{fl}} = \alpha_{cr} f_{ctm} \left(\frac{1600 - h}{1000} \right) \qquad \text{with} \qquad h \not> 600\text{mm} \tag{6.73}$$

$$M_{cr} = 1.4 \cdot \sigma_{cr_{fl}} \cdot \frac{h^2}{6} \tag{6.74}$$

$$M_{cr_f} = 1.4 \cdot (\sigma_{cr_{fl}} - \sigma_{r1}) \cdot \frac{h^2}{6} \tag{6.75}$$

$$x_u = \frac{A_s f_{yd}}{0.75 \cdot f_{cd} \cdot b} \tag{6.76}$$

$$z = h - cover - \frac{\varnothing}{2} - 0.39 x_u \tag{6.77}$$

$$M_u = A_s f_{yd} z \tag{6.78}$$

$$\sigma_s = \frac{f_{yd} M_{cr}}{M_u} \tag{6.79}$$

$$l_t = c + \frac{1}{4} \frac{\varnothing}{\omega_{eff}} \frac{f_{ctm}}{\tau_{bm}} \cdot \frac{M_{cr}}{M_u} \tag{6.80}$$

$$l_{t_f} = c + \frac{1}{4} \frac{\varnothing}{\omega_{eff}} \frac{f_{ctm} - \sigma_{r1}}{\tau_{bm}} \cdot \frac{M_{cr_f}}{M_u} \tag{6.81}$$

$$w_{mo} = 0.6 \cdot 2 l_t \frac{\sigma_s}{E_s} \tag{6.82}$$

$$w_{max} = 1.7 \cdot w_{mo} \tag{6.83}$$

6.4.2 Stu*fib*-11

Stu*fib*-11 provides a model based on the 28-day concrete properties in combination with the *Van Breugel* model. The eccentricity effect is also taken into account. The crack width is based on the final steel stress in the crack at time t. The steel stress directly after cracking is determined by the cracking force. After cracking, the steel stress in the crack will continue to increase due to shrinkage. The additional steel stress in the crack $\Delta\sigma_s$ depends on the strain load at t ($\varepsilon_{sh(t)}$), cracking strain of concrete (ε_{cr}), tension stiffening effect ($\Delta\varepsilon_{ts}$), steel yield strain (ε_{sy}) and the strain limit (ε_{fdc}) for the *F.D.C.P.* The final steel stress σ_s in the crack is used to calculate the mean crack width according to *Van Breugel* for the *N.F.D.C.P.*. The maximum crack width is not based on the enhancement factors according to *Van Breugel* but with the constant enhancement factor of 1.7. In practice, when no time-dependent calculations are performed, the cracking strength (σ_{cr}) is taken as $\alpha_{cr} \cdot f_{ctm,28}$ with α_{cr}=0.6 . The cracking factor of 0.6 in combination with the 28-day mean tensile strength is in good agreement with the results found for the crack width calculation.

$$\sigma_{cr} = 0.6 \cdot f_{ctm(28)} \tag{6.84}$$

$$\sigma_{s,cr} = \frac{\sigma_{cr}}{\omega}\left(1+\alpha_e\omega\right)\cdot\frac{h}{2d} \tag{6.85}$$

$$\sigma_{s,crf} = \frac{(\sigma_{cr}-\sigma_{r1})}{\omega}\left(1+\alpha_e\omega\right)\cdot\frac{h}{2d} \tag{6.86}$$

$$\Delta\sigma_s = \frac{E_s\left(\varepsilon_{sh(t)}-\varepsilon_{cr}\right)^2}{2\cdot\left(\varepsilon_{sy}-\varepsilon_{cr}-\Delta\varepsilon_{ts}\right)} \tag{6.87}$$

$$\varepsilon_{sy} = \frac{f_{yd}}{E_s} \tag{6.88}$$

$$\Delta\varepsilon_{ts} = \frac{\sigma_{s,cr}}{E_s} - \varepsilon_{fdc} \tag{6.89}$$

$$\sigma_s = \Delta\sigma_s + \sigma_{s,cr} \tag{6.90}$$

$$w_{mo} = 2\left(\frac{0.4\varnothing}{f_{ccm}E_s}\sigma_s\left(\sigma_s - n\sigma_{cr}\right)\right)^{0.85} \tag{6.91}$$

$$w_{max} = 1.7 \cdot w_{mo} \tag{6.92}$$

6.4.3 Pull-out stiffness model

All the crack width models of hybrid reinforcement are based on the fixed residual tensile stress, σ_{R1}, at a *C.M.O.D.* of 0.5 mm. In reality, the fibres have to be activated before they can transfer stresses. Therefore, the residual stress is assumed to be increasing per crack width with a maximum of the σ_{R1} based on the pull-out stiffness of one fibre. The force taken by the fibres is calculated by multiplying the fibre pull-out stiffness times the number of fibres in the cracked cross-section times the crack width, $N_{fibre} = K_{fibre} \cdot n_f \cdot w_{mo}$. The maximum fibre force is given by the residual tensile stress (σ_{R1}) times the cross-sectional area of the concrete (A_c). Both the crack width directly after cracking and at time t are determined in the analytical model. The eccentricity effect and the contribution of the soil friction after cracking are also taken into account. With the use of the *Gilbert* model the cracking force at moment t_{cr} and at time t are calculated. The steel stress of the reinforcement per crack width is determined according to *Van Breugel* (Eq:6.50). The cracking force has to be taken by the reinforcement, N_s and N_{fibre} and the soil friction force $N_{friction}$. The crack width can be calculated for the situation when there is equilibrium in the crack shown in Fig: 6.11a. All these forces can be determined per crack width shown in Fig: 6.11b.

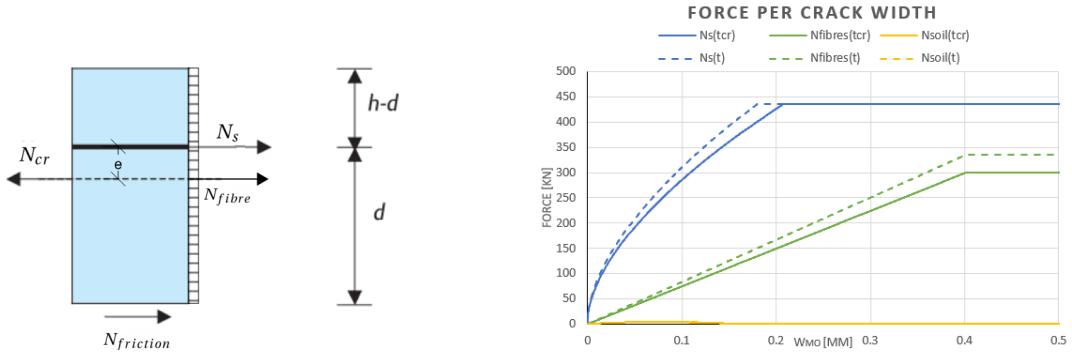

(a) Force equilibrium in crack

(b) Forces per crack width

Figure 6.11: Combined crack width model

An example for both the centric, eccentric and hybrid reinforcement is given in Fig: 6.12. Ageing concrete properties are considered, and therefore, the forces N_s and N_{fibre} are different at time t_{cr} and at time t. The cracking force is determined without the crack relaxation effect and with the 28-days properties. The crack relaxation effect is clearly visible between $N_{cr(tcr)}$, $N_{cr(t)}$ and $N_{cr,breugel(28)}$. The force directly after the first crack $N_{cr_{(t_{cr})}}$ is in all cases significantly lower than $N_{cr_{breugel}}$. For the hybrid model the cracking force is reduced with the steel fibre force N_{fribre} which results in a lower crack width and lower reinforcement force N_s.

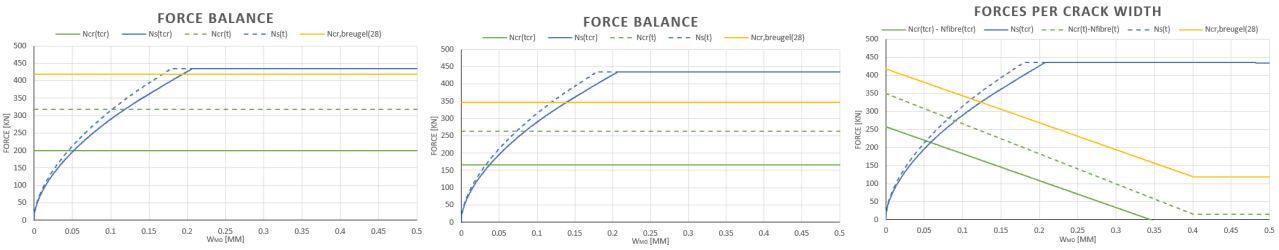

(a) Centric reinforcement

(b) Eccentric reinforcement

(c) Hybrid reinforcement

Figure 6.12: Model examples

7. Finite Element Model

In this chapter, the model set-up is elaborated. Many different settings can be chosen for a non-linear model. With the use of the guideline *RTD* for non-linear finite element analysis provided by the *Rijkswaterstaat* [15] and with the *DIANA FEA* manual the model is developed. The chosen methods are discussed in detail. Extra information is given on the analysis method for a better understanding of non-linear finite element analysis. Special attention is given on the random field application. Finally, a short notation about the awareness, which is required for designing with non-linear finite element models, is given. The finite element program DIsplacement ANAlyser Finite Element Analysis (*DIANA FEA*) is used for the analysis. In App:C, all additional information on the *F.E.M.* and the analyses can be found.

7.1 Model set-up

The finite element is developed to analyse the behaviour inside a *S.o.G.* in detail. A cross-section of the slab is taken to investigate aspects like stress development, crack propagation and influence of reinforcement. By creating a 2D model of the slab, the size of the *F.E.M.* can be kept small. Non-linear transient analysis is computationally intensive, and therefore, a relatively small model is preferred. The cross-section will give a detailed view of the internal behaviour of the slab. The model can be interpreted as the critical cross-section perpendicular to the crack in an *I.F.*, Fig: 7.1. Because the focus of the research is more on the crack width than the total crack pattern in the slab, it is chosen not to model the slab in 3D.

Two models are developed to investigate the behaviour of a restrained tensile member loaded by imposed deformation. The first model is the cross-section of the *I.F.* Because of the constant stress zone, a random field has to be applied for crack localisation. Otherwise, the total cross-section will crack at the same time. The random field takes into account the anisotropy of the concrete properties. With the random field, the *F.E.M.* can find a single solution instead of an infinite amount, which is impossible to solve. The random field will be explained later on. In Fig:7.2a, the general model of the cross-section is shown.

The second model is a Notched tensile member (*N.T.M.*) created to investigate the behaviour of one single crack. By making a notch, the crack location is predetermined. Therefore, the tensile strength can be kept constant and the effect such as bond-slip can be adequately investigated. An overview of the notched tensile model is shown in Fig: 7.2b.

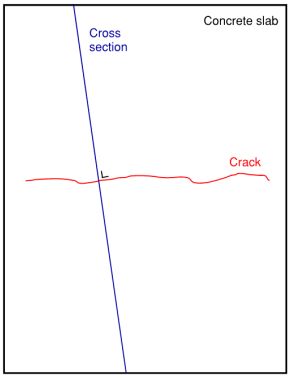

Figure 7.1: Top view *I.F.*

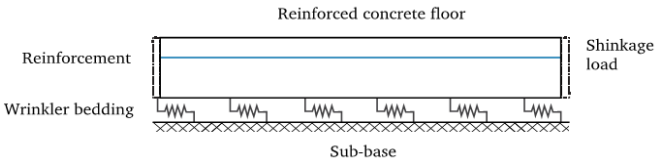

(a) Mechanical scheme *F.E.M.*

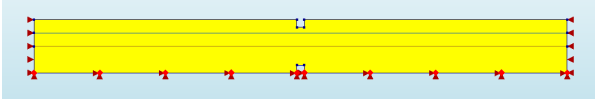

(b) Notched tensile member

Figure 7.2: *F.E.M.* of *I.F.*

To analyse the complex shrinkage behaviour of *S.o.G.*, the following (non-linear) problems have to be taken into account.

- Analysis method
- Creep/relaxation
- Cracking
- Bond-slip of reinforcement
- Soil-structure interaction

The non-linear aspects are elaborated per material model. First, the analysis method is explained.

Analysis method

A finite element analysis can be separated into three parts. The preprocessing, the analysis and the post-processing. The preprocessing step is modelling the structure, applying boundary conditions and material properties, generate a mesh and set-up the analysis method. In the analysis, the system has to be solved. The first step of the calculation method of a *F.E.M.* is to determine the stiffness of the model. The right-hand side equations are formed according to the boundary conditions, displacement and loading. The total system has to be solved based on equilibrium. For *N.L.F.E.A.*, the solution vector can not be calculated right away. To determine the state of equilibrium, the problem is made discrete in space(with finite elements) and in time(with increments). To solve the system, an iterative solution algorithm is used. The solution procedure is therefore called an *incremental-iteration* method. For *N.L.F.E.A.* a standard work-flow of an analysis is shown in Fig: 7.3. A defined load increment is applied to the model. The strain and stresses are calculated based on the stiffness. For different norms, the equilibrium is determined and the ratio between the internal and external force is calculated. If this ratio for one norm is within the convergence criteria, the iteration is accepted and the analysis continues. The ratio is called the Out of Balance (*O.o.B.*) of an iteration.

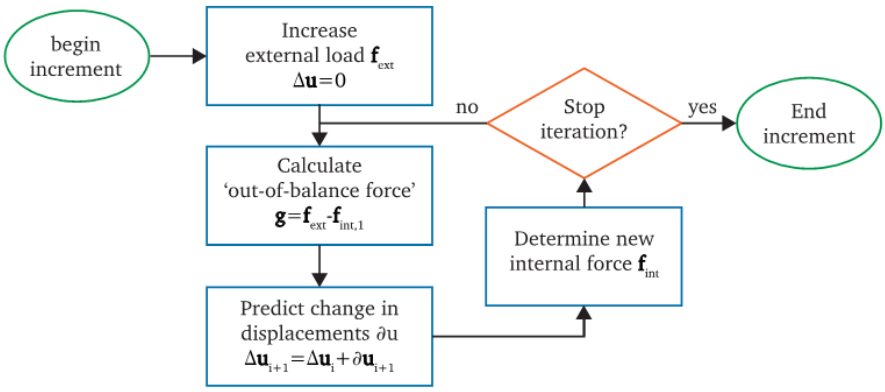

Figure 7.3: Analysis scheme of *F.E.M.*

Looking at crack width analysis for sustained loaded structures, the *N.L.F.E.A.* becomes more complicated. The convergence of the analysis is difficult to reach, especially during the formation of dominant cracks. Cracking of concrete leads to the loss of energy within the structure. Therefore it is difficult to find an equilibrium. In this research, the equilibrium norms are based on the force and energy. The displacement norm is generally less useful when a prescribed displacement is used, especially for a *R.T.M.* with no free movement. Experience shows that for a softening type behaviour, the convergence criterion should be more strict because the difference in result can be substantial. In this study, the convergence criterion of 0.01 and 0.001 for force and energy norms are used. These convergence criteria are also advised in the *RTD*[15]. From practice, it can be stated that when crack localisation occurs, convergence is often not reached. Especially for direct tensile cracks. When the *O.o.B.* is approximately 0.10-0.20, for some analysis steps during excessive cracking, the solution can be assumed acceptable.

Besides the convergence norm, an additional method called *linesearch* can be used to enhance the likelihood of convergence in the *N.L.F.E.A.*. *Linesearch* can stabilize the convergence behaviour or increase the convergence speed. The linesearch algorithm scales the incremental displacement in the iteration process automatically based on the minimum energy potential. The effect of linesearch on the convergence behaviour is analysed for the *N.T.M.* and the *R.T.M.* shown in Fig: 7.4. The linesearch method has some positive influence on the analysis in the more "stable" periods when no extreme cracking occurs. Linesearch helps when the analysis is close to its convergence criteria but is not converging. The *O.o.B.* after 50 iterations is close to the convergence criteria, but no convergence occurs. With the use of linesearch, the analysis convergence eventually. This effect is visible in Fig: 7.4c. In the cracking period, linesearch does not help with the convergence. On the contrary, linesearch increases the *O.o.B.* significantly during cracking. A maximum of 50 iterations is assumed due to the difficulty of convergence of the analysis.

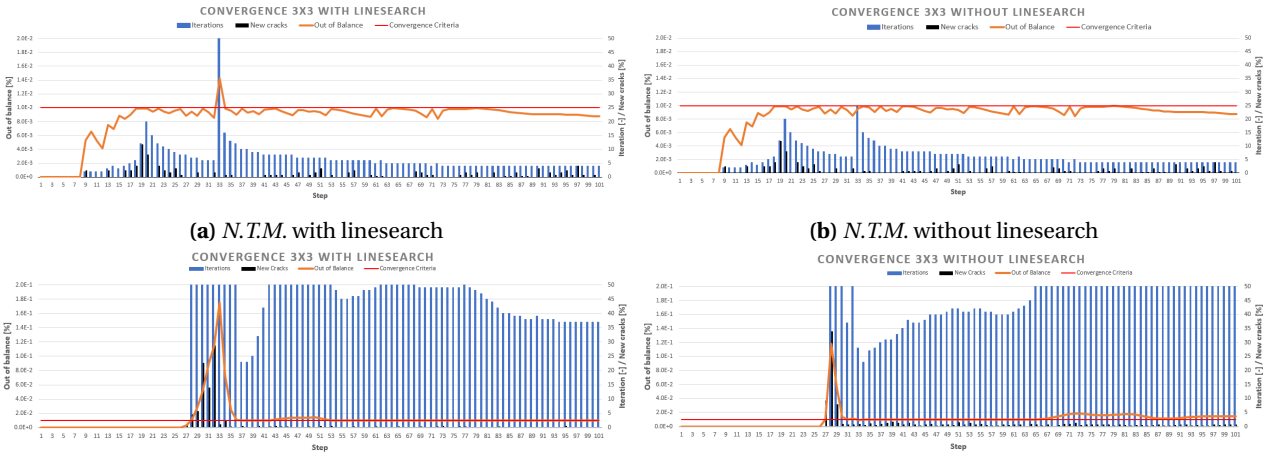

(a) *N.T.M.* with linesearch

(b) *N.T.M.* without linesearch

(c) *R.T.M.* with linesearch

(d) *R.T.M.* without linesearch

Figure 7.4: Comparison of analysis method

Elements

The concrete is modelled with plane elements. Eight-node quadrilateral isoparametric elements are used. Because bond-slip is not applicable in plane strain elements, the model is also developed with plane stress elements. A high *Gauss* integration scheme of 3x3 is applied based on the suggested by in the *RTD*.

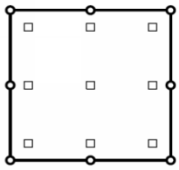

Quadratic quadrilateral: *3x3-point Gauss*

Figure 7.5: Continuum element

Plane strain

Plane strain elements are characterized by the fact that the strain, displacement and shear stress perpendicular to its plane is zero. The element requires that every cross-section is a plane of symmetry for the structure, load and stresses. This means that the stresses and strains are independent of the coordinate along the out-of-plane axis. The elements are applied for the analysis of the cross-section in infinite long structures. The thickness is per unit width. The plane strain element used is CQ16E.

Plane stress

Plane stress elements are characterized by the fact that the stress components to the face are zero. The elements must be *thin*. This means that the thickness must be small in relation to the height. The applied load on the element must be in the plane. The plane stress elements are used to investigate the bond-slip behaviour of the reinforcement. The thickness of the *R.T.M.* and the *N.T.M.* is defined by the spacing between the longitudinal reinforcement bars. The models represent a slice of the concrete slab with one reinforcement bar. The plane stress element used is CQ16M.

Composed line

For calculation of the cross-section forces and bending moments, a composed line is used. A composed line sums up all the forces of the structural elements within the defined thickness of the line. The composed line only required a thickness to set a bandwidth for the location of the structural nodes, which includes the composition of the forces. No other material data have to be defined. The CL3CM three-node curved line base element is applied.

Interface

For the soil-structure interaction, an interface is applied. The interface element which is used is the CL12I line element based on quadratic interpolation with 3x3 nodes for two-dimensional configuration. The properties of the interface have to be defined and multiple models can be chosen. The linear and Morh-Coulomb friction models are assumed in this research.

Mesh size

The mesh size can have a large influence on the result. Therefore the effect of the mesh size on the stresses behaviour is important to analysis. For *N.L.F.E.A.*, the mesh size is limited for two reasons. First, to ensure that the post-peak response for softening materials does not exhibit a "snap back" in the stress-strain relationship. Therefore, the mesh edge should be smaller than h_{eq} which is based on the E_{cm},G_{f_c} and f_{ctm}. Secondly, the finite element discretization may not be too coarse else the stress field is not continuous. The element size should result in a relatively smooth stress field. The *RTD* gives values of the maximum element size based on the height and length of the 2D model shown below.

$$h_{eq} = Min\left(\frac{E_{cm} \cdot G_f}{f_{ctm}^2}, \frac{h}{6}, \frac{l}{50}\right)$$

7.2 Material models

For *S.L.S.* calculations, the characteristic values should be used. The material properties are based on the provision *M.C. 2010* and the *E.C. 2*. For some models, the manual of *DIANA FEA* is consulted. The constitutive models used in the *F.E.M.* specifies the stress-strain behaviour of the material. The material models can be seen as a lower bound simplified abstraction of the true behaviour.

Soil

The properties of the soil are represented as the spring stiffness known as the subgrade modulus k_{mod} of the soil. Contact loss, e.g., no tensile capacity of the interface, is taken into account. The vertical springs can only take up compressive stresses. When the total (long-term) settlements have to be analysed, the soil can best be modelled with volume elements over a certain depth. The friction behaviour is modelled with vertical springs. The linear and non-linear friction are analysed. The non-linear behaviour is modelled according to the Coulomb friction model. Input parameters are the shear stiffness K_{yx}, cohesion c_s and friction angle ϕ_s. The *F.E.M.* takes into account the increase of shear stress capacity when the vertical load on the slab increases.

Concrete

The behaviour of concrete can be modelled with many different models. In this research, the compressive behaviour is linear elastic (Fig:7.6a) because the compressive stresses are likely to be lower than f_{cm}. The tensile behaviour is represented with a total strain-based rotating crack model, known as the smeared cracking model. A rotating crack model is taken because it provides less stress locking and is preferred for analyses with localised cracking. Multiple softening curves are available to model the softening behaviour (Fig:7.6b). In this study, the exponential softening diagram of *Hordijk* is chosen. The model determines the softening curve on the fracture energy G_{f_c} and crack bandwidth h per element. *DIANA FEA* automatically calculates the crack bandwidth of the model. When progressive cracking occurs, it is advised to include a Poisson ratio reduction after cracking, which is also taken into account.

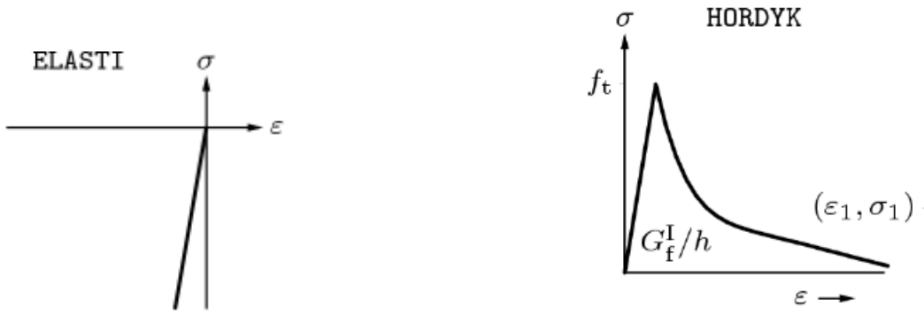

(a) Compression **(b)** Tension

Figure 7.6: Concrete material models

The ageing of concrete is not taken into account in the *F.E.M.*. To investigate the cracking behaviour, the concrete properties are taken constant with the 28-days value. The stress development at the early age is investigated in the stress development phase of the research. The *F.E.M.* is made to examine the cracking behaviour in time. By assuming a constant Young's modulus, the stresses and the cracking force after 28 days are slightly underestimated but the same hold for the bonding properties. On the other hand, the stresses before 28 days will be lower. The goal with the *F.E.M.* is to get insight into the cracking behaviour, and therefore the differences are assumed acceptable.

Shrinkage & creep

The concrete properties for shrinkage and creep are calculated according to the *E.C. 2*. Both properties are time-dependent and related to the visco-elasticity of concrete. The shrinkage load is applied to the concrete as a pre-described strain, which changes in time. The development and final value are calculated for the autogenous and drying shrinkage. A shrinkage gradient is applied by creating multiple sheets over the height. The autogenous shrinkage is assumed constant over the height of the cross-section.

The modelling of creep is complex. The numerical solution based on the Kelvin chain model is applied in the model. In the *F.E.M.*, the kelvin creep chain uses the creep compliance $J_{(t,\tau)}$ as an input parameter to model the creep behaviour [52]. The compliance function is based on an instantaneous part and creep part, which changes in time. The first instantaneous part describes the elastic stiffness by a single spring. The creep part is predefined by curve fitting the given creep compliance shown in Fig:7.7. The *A.A.E.M* is also used in the research to investigate which model can best be used for design purposes. The creep behaviour is taken into account by reducing the Young's modulus. Both methods are not taken into account ageing of concrete and can, therefore, over- or under-estimate the stresses. The creep effect depends on concrete properties for the calculation of the creep compliance of the applied concrete relaxation coefficient ψ.

$$J_{(t)} = \frac{1}{E_{cm(28)}} + \frac{\varphi_{t_0,t}}{E_{cm(28)}} \tag{7.93}$$

$$E_{cm,eff} = E_{cm} \cdot \psi \tag{7.94}$$

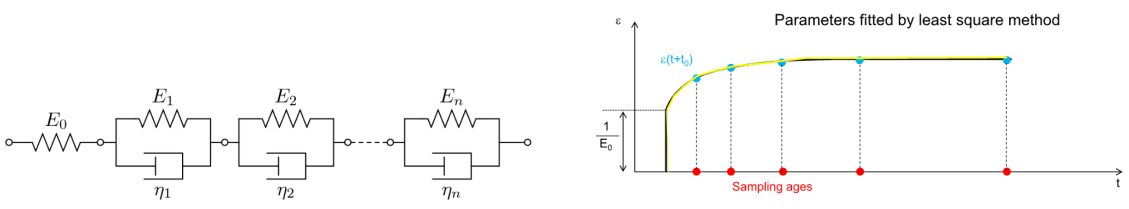

(a) Kelvin chain model **(b)** Fitted creep compliance

Figure 7.7: Modelling of creep

Conventional reinforcement

In the plane strain elements, the reinforcement is fully bonded(embedded) and modelled with grid reinforcement elements. In plane-strain elements, it is not possible to model the bond-slip behaviour. To take into account the bond-slip behaviour, plane-stress elements are used. The properties depend on the bond quality, failure type and the reinforcement type. For reinforced *S.o.G.*, the failure type will most likely be splitting because the reinforcement is placed in the outer layer of the slab. The stress-slip behaviour of the bond-slip model can be seen in Fig: 7.8a. The bond-slip model provided in the *M.C. 2010* is used. The shear reinforcement is often not necessary in *S.o.G.*. Therefore unconfined reinforcement is assumed in this research. All models take into account the yielding of the reinforcement. The non-linear effect of the reinforcement is based on Von Mises. The strain hardening is modelled with a hardening plasticity model.

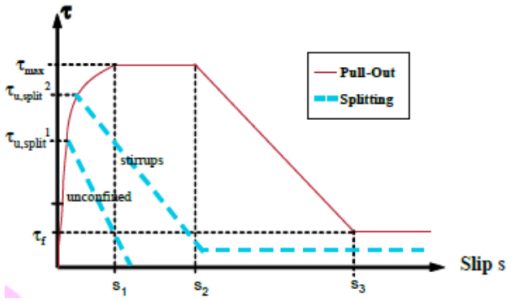

(a) Bond-slip properties

	1	2	3	4	5	6
	Pull-out (PO)		Splitting (SP)			
	$\varepsilon_s < \varepsilon_{s,y}$		$\varepsilon_s < \varepsilon_{s,y}$			
	Good bond cond.	All other bond cond.	Good bond cond.		All other bond cond.	
			Unconfined	Stirrups	Unconfined	Stirrups
τ_{bmax}	$2.5\sqrt{f_{cm}}$	$1.25\sqrt{f_{cm}}$	$2.5\sqrt{f_{cm}}$	$2.5\sqrt{f_{cm}}$	$1.25\sqrt{f_{cm}}$	$1.25\sqrt{f_{cm}}$
$\tau_{bu,split}$	–	–	$7.0\cdot\left(\frac{f_{cm}}{25}\right)^{0.25}$	$8.0\cdot\left(\frac{f_{cm}}{25}\right)^{0.25}$	$5.0\cdot\left(\frac{f_{cm}}{25}\right)^{0.25}$	$5.5\cdot\left(\frac{f_{cm}}{25}\right)^{0.25}$
s_1	1.0 mm	1.8 mm	$s(\tau_{bu,split})$	$s(\tau_{bu,split})$	$s(\tau_{bu,split})$	$s(\tau_{bu,split})$
s_2	2.0 mm	3.6 mm	s_1	s_1	s_1	s_1
s_3	c_{clear} 1)	c_{clear} 1)	$1.2s_1$	$0.5c_{clear}$ 1)	$1.2s_1$	$0.5c_{clear}$ 1)
a	0.4	0.4	0.4	0.4	0.4	0.4
τ_{bf}	$0.40\tau_{max}$	$0.40\tau_{max}$	0	$0.4\tau_{bu,split}$	0	$0.4\tau_{bu,split}$

(b) Bond-slip

Figure 7.8: Behaviour of reinforcement

Steel fibre reinforced concrete

The steel fibre reinforced concrete properties are based on the *M.C. 2010*. The behaviour depends on the type of fibre reinforced concrete. In this research, the *S.F.R.C.* is characterised by that the residual tensile stress σ_{R1} is lower than the cracking stress σ_{cr} of concrete. This softening behaviour is shown in Fig:7.9a. In *DIANA FEA*, the predefined tension softening function for fibre reinforced concrete based on crack opening *FRCCON* is used to implement the softening model according to *M.C. 2010*. Input values are the cracking stress and the residual stresses per *C.M.O.D.*.

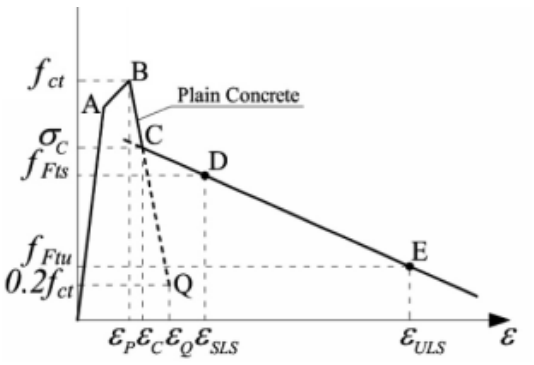

(a) *M.C. 2010*

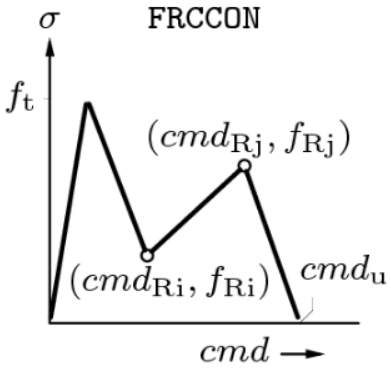

(b) Diana model

Figure 7.9: Modelling of *S.F.R.C.*

7.3 Random field

As discussed, crack localisation does not occur when a constant tensile strength is applied on a *R.T.M.*. A crack analysis with such a model results in cracking in all the elements. To localise cracking, the material properties are varied over the model to create local imperfections were cracking can start by applying a random field over the tensile strength of concrete. Multiple methods can be used in *DIANA FEA* to generate the random field. The construction of the random field is based on the following input parameters: correlation length L_{cor}, coefficient of variation α_{var}, number of variation points in the length n_{var_l} and height n_{var_h} and the threshold value α_{th}. In Fig: 7.10, the visualisation of the random field models is shown.

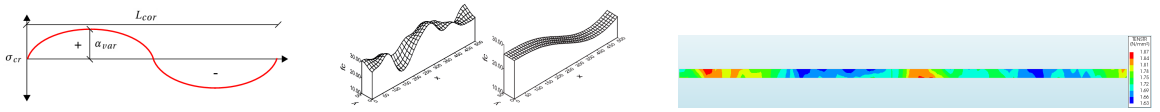

(a) Schematisation of parameters **(b)** Example of random field **(c)** Random field of the cracking stress σ_{cr} in *F.E.M.*

Figure 7.10: Random field visualisation

The assumptions made in this research are based on the extensive research by *R. ten Have* on random fields [53]. The *covariation matrix decomposition method* is used for the generation of the correlated spatial variables. The method for the decomposition of the correlation matrix is the Cholesky method. This method is easy to implement, and it is the most accurate method in creating a random field, according to *R. ten Have*. Downside is that it becomes computational intensive when the number of nodes increases. In this research, the number of nodes is relatively low and generating the random field is not too intensive. The exponential method is applied for the correlation function. For the variation coefficient α_{var}, it is suggested to use values between 0.1-0.3 and 0.18 for respectively plain concrete and *S.F.R.C.*. Looking at the lower and upper bound tensile strength properties in the *E.C. 2*, the 5% and 95% fractile values are calculated by multiplying the mean value with $\cdot \pm 0.3$. Therefore the α_{var} for plain concrete is taken as 0.3. The correlation length of the random field L_{cor} is advised to be taken between 0.5 and 5 meters. In Fig: 7.11, the influence of the random field parameters are visualised for the upper and lower bound values. The parameters are analysed and the results are given in App: C.

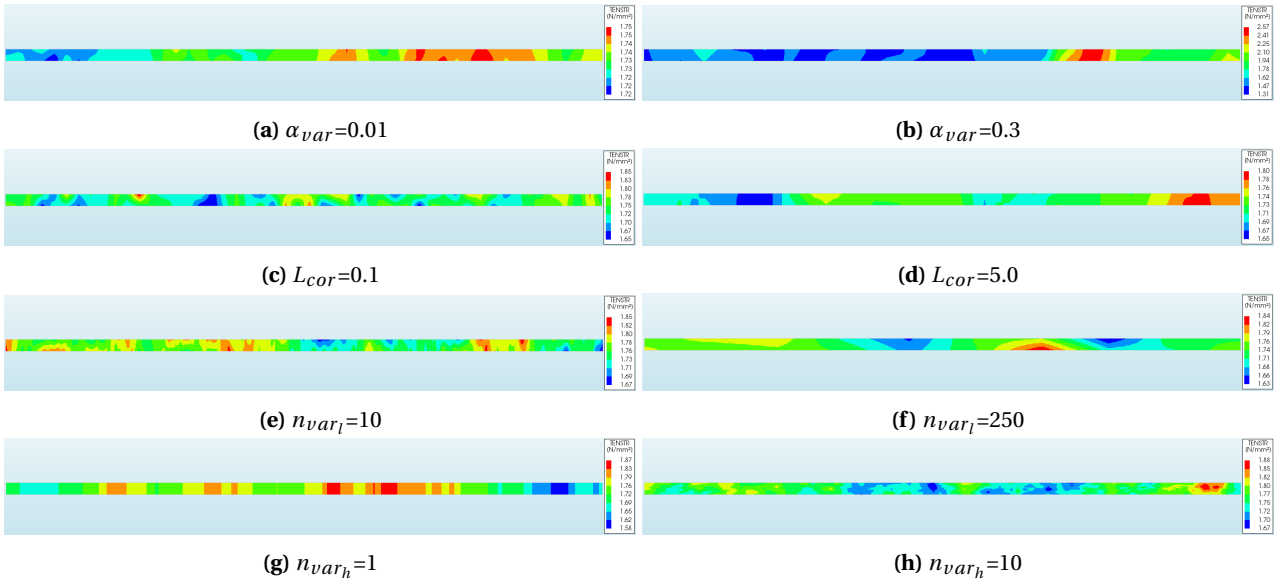

(a) α_{var}=0.01 **(b)** α_{var}=0.3

(c) L_{cor}=0.1 **(d)** L_{cor}=5.0

(e) n_{var_l}=10 **(f)** n_{var_l}=250

(g) n_{var_h}=1 **(h)** n_{var_h}=10

Figure 7.11: Random field parameter analysis

The following can be concluded regarding the random field parameters:

- The proposed α_{var} of 0.3 results in high variation of the material property ± 30-40%. The values match the 5% and 95% fractile values of the *E.C. 2*.
- The correlation length L_{cor} has a significant influence on the crack pattern. An increase of L_{cor} result in a larger crack spacing. The crack spacing is almost linked directly with the correlation length. The crack spacing can, therefore, be predetermined by the L_{cor}. *F.E.M.* will always generate output based on the input parameters. An engineer should always be aware of this fact when modelling a structure. In this research, the L_{cor} is taken as 1.0 meter, which results in a crack spacing of 1.0-3.0 meters. These crack spacings are equivalent to spacing found in practice.
- The variation point per slab length n_{var_l} also has a significant influence on the crack pattern. The variation point per slab height n_{var_h} influence the crack type in the weak zones. When n_{var_h} is one, a crack over the full depth will occur. A high n_{var_h} result in a local weak spot in the cross-section and full depth crack localisation is not likely to happen. For the investigation, is it suggested to use one variation point each 100 mm.
- The threshold value has no significant influence on the crack behaviour and pattern in this model. Therefore, this value is taken as zero.
- In the literature, no advised random field parameters were found, which represents the true spatial variation of the concrete properties. Most parameters are based on engineering sense and practice. Further research should be performed on the random field parameters for concrete.

Another important aspect is that the generated random field varies per analysis. Also, when the same random field parameters are taken. In Fig: 7.12, an overview of four generated random fields with the same parameters is shown. It is likely that each field will result in a different crack pattern in the tensile member. The variation in space and in property value per analysis makes a comparison analysis of the crack pattern difficult. The lower bound tensile strength in the four random fields varies between 1.55 to 1.93. In practice, it was found that cracking was initiated around $0.5/0.6 \cdot f_{ctm}$, which is in the range of 1.45-1.74 MPa. The assumed α_{var} is in good agreement to model the concrete property variation.

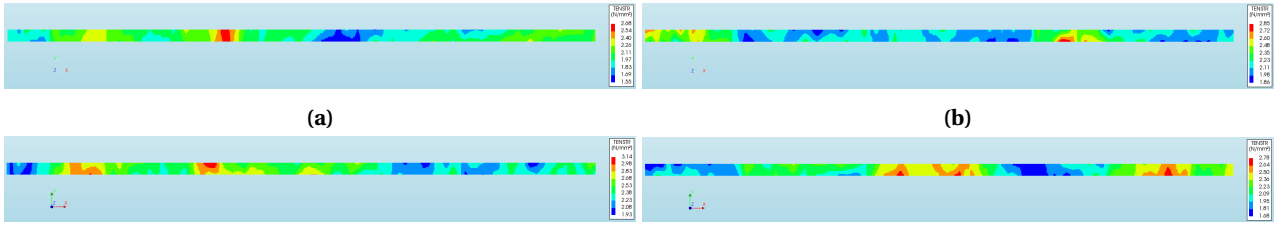

Figure 7.12: Random field with constant parameters

7.4 Post-processing of crack width

The *M.C. 2010* and *RTD* requests that the crack width verification are performed as post-analysis checks. The stress state and deflection control can be read directly from the *N.L.F.E.A.*. The results can then be compared with the limit values imposed by the codes. For the crack width control, an extra step has to be taken to calculate the crack opening. Multiple models are available to determine the crack width in the *F.E.M.*. Three common methods are compared in this research.

- Average steel strain method
- Maximum steel stress method
- Average element crack width

Average steel strain method

The average steel strain method calculates the crack width by multiplying the average strain value of the longitudinal reinforcement in the cracked zone times the maximum crack spacing. The crack spacing depends on the number of forces in the tensile member and the bond-slip properties. The crack spacing and the average steel strain can be directly be determined from the nodes in the *F.E.M.*. The crack spacing is the distance where the steel strain is positive, e.g., the tensile strain shown in Fig:7.13. The average steel strain over the crack spacing is determined by the summation of the strain per node divided by the total amount of nodes present in the crack spacing. The crack width is calculated at the location of the reinforcement.

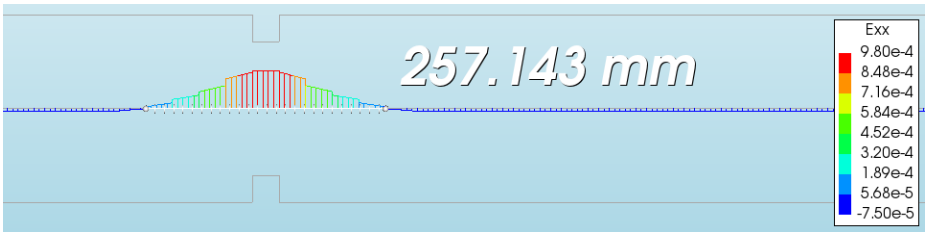

Figure 7.13: Average steel strain method

Maximum steel stress method

The maximum steel stress method calculates the crack width according to the *Van Breugel* based on the maximum steel stress in the crack found in the *F.E.M.*. The crack width can be determined for the not fully developed crack pattern. The calculated crack width is the mean value. The maximum crack width should be used as the design crack width, which has to be less than the design limits. This method also calculated the crack width at the location of the reinforcement.

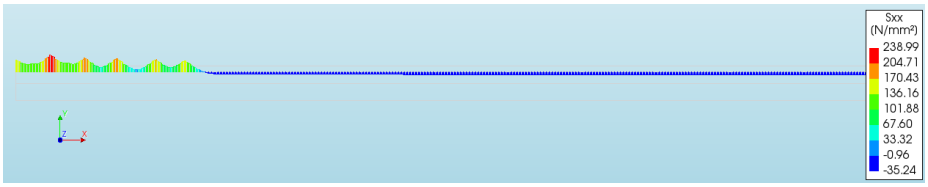

Figure 7.14: Steel stress method

Average element crack width

The average element crack width method determines the crack width in the elements. In the *F.E.M.*, the crack width over the element can be selected as the output. Important for this method is that the crack must be localised in one element. The program can output the maximum crack width in the integration points and the average crack width over the element. The maximum crack width value is calculated by multiplying the cracking strain in the integration point times the crack bandwidth of the total element. This means that the cracking strain in the integration point is assumed to be over the total element. When the crack is localised in one element, the cracking strain is only maximum at one side of the element shown in Fig:7.15a. Therefore the maximum crack width values are significantly overestimated when calculated with the maximum strain in the integration point. By taking the average cracking strain in the element times the crack bandwidth, the realistic crack width is calculated shown, see Fig:7.15b. The average crack width in the element should be taken for the post-analysis of the crack width in the member. With this method, the crack width can be determined at every location. No extra calculation step has to be performed to determine the crack width at the surface.

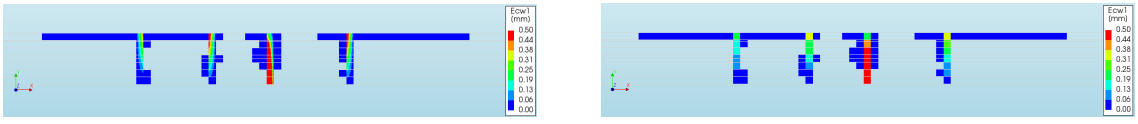

(a) Maximum crack width in element

(b) Average crack width in element

Figure 7.15: Element crack width

Analysis of model set-up

The effect of the mesh size on the behaviour is analysed. The stress and crack behaviour depending on the mesh-size, is shown in Fig: 7.16. The following is concluded from the analysis. The crack relaxation effect is more present for the coarse mesh. The cracking is more gradual in the finer mesh model. The contribution of the concrete in the cracked zone ($N_{c(min)}$) is slightly smaller for the fine mesh after crack localisation. Therefore, the steel stress in the crack is higher. The stress behaviour inside the crack can be calculated more precise shown in Fig: 7.16c and 7.16d. The advised mesh and fine mesh of respectively $\frac{h}{7}$ and $\frac{h}{14}$ have no significant influence on the crack width development. Therefore, the advised mesh sizes in the *RTD* are adopted. Similar research has been performed by *Prakash* on the non-linear behaviour of reinforced *S.o.G.*[54]. He concluded that a smaller mesh size results in more accurate results and a change in crack pattern. Finer mesh sizes result in more finer cracks shown in Fig: 7.16b.

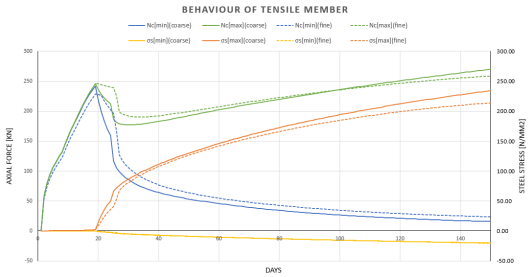

(a) Stress behaviour

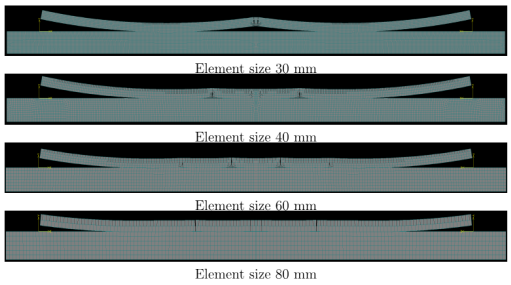

(b) Crack pattern

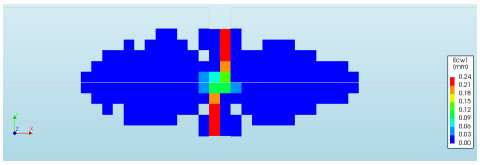

(c) Crack width in fine mesh

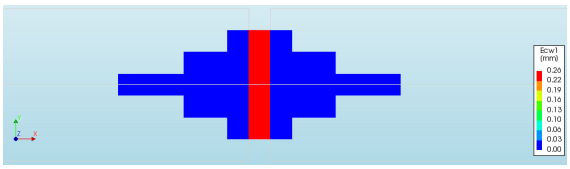

(d) Crack width in coarse mesh

Figure 7.16: Influence of mesh size on:

The location of the reinforcement with respect to the mesh can also have influence when a coarse mesh is taken. For embedded reinforcement, the stiffness of the mother element is enhancement takes into account the reinforcement. It is found that when an even number of meshes in combination with centric reinforcement is used, the mother elements beneath the reinforcement line is enhanced. This results in an eccentric stiffness enhancement of the model, which influence the stress behaviour. Especially for coarse meshes, stress variation of 10% was found between even and uneven meshes for centric reinforced concrete. Therefore, an uneven amount of fine meshes is assumed.

The number of integration point in the element also has an influence on accuracy and the computational time. The elements with 2x2-point *Gauss* integration are compared with 3x3-point *Gauss* integration. More integration points result in higher concrete stresses in the uncracked zone. The crack relaxation effect is more present for a lower number of integration points. The stresses can be calculated more precise in the element for smaller elements and higher integration points. More integration points also affect the convergence of the analysis. In Fig: 7.17 it can be seen that 3x3-point result in a much lower *O.o.B.* during crack localisation in the *N.T.M.*. For more precise calculations, a high number of integration points and small element size is required. The downside is that a higher number of integration points and smaller mesh sizes increase in computational time.

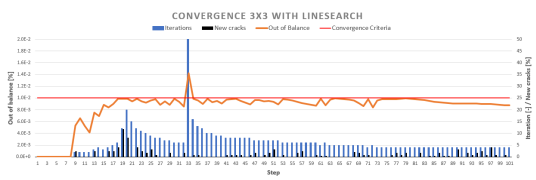

(a) Convergence of analysis 3X3-point

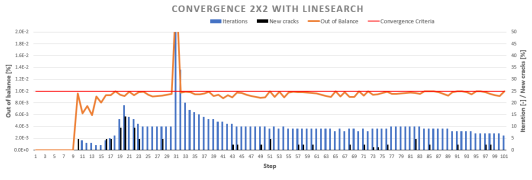

(b) Convergence of analysis 2X2-point

Figure 7.17: Effect of mesh size and integration points

The linesearch methods also significantly increase the computational time. The required calculation "force" is determined by the total CPU time per analysis. In Tab: 7.1 the effect of linesearch and element integration are shown. Because a random field is used in the *R.T.M.*, the number of cracked integration points is not constant for the models. Therefore, the computational time can not be compared one on one. It can be concluded that the use of linesearch and a higher number of integration points result in less diverged steps in the *R.T.M.*. A high number of integration points also reduces the maximum *O.o.B.* in both models. The downside is that the computational time increases when linesearch is used. Because linesearch also decreases the accuracy of the analysis, it is not advised to use linesearch for this type of analysis.

Table 7.1: Effect of analysis settings

Analysis	CPU-time	Total iterations	max. *O.o.B.*	Total diverged steps	Cracked points
NTM-2X2-LS	204	921	2.68E-02	1	84
NTM-3X3-LS	223	613	1.42E-02	1	246
NTM-2X2	194	891	9.99E-03	0	84
NTM-3X3	208	587	9.97E-02	0	246
RTM-2X2-LS	1734	2788	4.19E-01	35	407
RTM-3X3-LS	3238	3320	1.75E-01	21	1412
RTM-2X2	1834	3302	3.28E-01	66	427
RTM-3X3	2930	3287	1.18E-01	40	762

Based on the analysis of the model set-up, a mesh size of $\frac{h}{7}$ with elements with high *Gauss* integration points are used. Linesearch is not applied in this thesis due to the negative effect on the accuracy and computational time.

Validation of *F.E.M.*

Every *F.E.M.* has to be validated or checked. In this research, the model is compared with an experiment of the stress behaviour of concrete in the uncracked region after cracking under restrained drying shrinkage in a notched tensile member[55]. The comparison is elaborated in App: C. The behaviour of the *F.E.M.* is in good agreement with the stress behaviour of the experiment. In the experiment, concrete relaxation factors of 0.22 were found. The *F.E.M.* resulted in concrete relaxation factors of 0.31 when a significant high creep coefficient was used. The crack relaxation effect was also less present in the *F.E.M.*. In the experiment, the crack relaxation effect was in the order of 0.22-0.27 were the *F.E.M.* resulted in crack relaxation factors of 0.77-0.86. It is assumed that the difference can come from the fact that the degree of restraint in the experiment was not fully in the complete analysis. Also, the concrete relaxation effect can be more present in the experiment because the *F.E.M.* uses time steps of days. The short term creep effect is neglected in the *F.E.M.*. The bond-slip quality difference can also be a reason for the different behaviour between the experiment and the *F.E.M.*. Not all boundary conditions and material properties were given in the paper, which makes validation of the model difficult. The stresses can therefore not be compared one on one. On the other hand, The global behaviour was in good agreement.

7.5 Precision, Safety and reliability

With the use of *N.L.F.E.A.*, a new dimension can be given to structural engineering. More complex and sophisticated problems can be analysed with the use of powerful computational modelling if the correct approaches are used. To ensure the outcome of the model, the engineer has to be aware of the shortcomings of numerical modelling. Structural modelling will always follow the *input is output* rule, and *'Black box'* models should always be prevented. It is very important that the engineer known what happens in the analysis and that the model is set-up by a user with advanced structural and FE modelling knowledge. Also, the model has to be validated and post-analysed. Especially for concrete structure, which can have a large variation in properties within the structure, a sensitivity analysis on the relevant parameters is advised to get a better insight on the outcome. In the *N.L.F.E.A.* state-of-the-art of 2007 made by *fib*, the following issues and potential dangers are given on which the user should be mindful about [56]:

- Diversity of theoretical approach
- Diversity of behaviour (cracked) models
- Incompatibility of models and approaches
- Experience is required
- Too much information
- Incomplete knowledge
- Research philosophy

In the last half-century, remarkable progress has been seen regarding the development of non-linear analysis. Non-linear computer analysis are now close to being an every-day tool for the structural engineer. The models are becoming more reliable but only if the correct steps are taken and the knowledge of the user is sufficient.

8. Sensitivity Analysis - Stage 1: Stress development

To investigate the concrete stress development in the linear stage, the influences of the parameters are analysed. The stress development is determined with the *Bazant* model explained earlier. The degree of restraint and the concrete relaxation effect, which both influence the stress development, are also analysed in detail. For the sensitivity analysis, the standard parameters in Tab:8.1 are used unless specified otherwise. The most important findings are presented in this chapter. More detailed information, such as the formulae and the sensitivity results, can be found in App: E.

Table 8.1: Standard parameters

Parameter	Value	Unit
Concrete strength F_{ck}	30	MPa
Relative Humidity	60	%
Slab height	200	mm
Cement type	N	-
Aggregate type	Quartz	-
Curing day's	7	day
degree of restraint R	1	-
Temperature change (Spring) ΔT	5	°C
Cracking factor α_{cr}	0.6	-

8.1 Concrete mixture

The influence of the concrete can be separated into the strength, strain and relaxation effect.

Strength

The most relevant strength parameters for this research are the Young's modulus E_{cm} and the tensile strength f_{ctm}. As mentioned, the Young's modulus greatly depends on the aggregate type. E_{cm} can be reduced by 30% or increased with 20% for respectively sandstone and basalt aggregate. The cement type and concrete class have a small influence on the Young's modulus. A change in one concrete class results in a 5% difference of the Young's modulus. A lower concrete class gives a lower Young's modulus.

The cement type has some influence on the development rate. For slow-developing concrete (type S), 60% of the stiffness is developed after one day. Rapidly developing concrete (type R) has 77% of its stiffness developed after one day. The 28-days stiffness property is regarded to be 100%. The long-term influence of the cement type Young's modulus is low, only ±2%. For regular concrete the development is 72%, 93% and 104% for respectively one day, seven days and one year.

The tensile strength f_{ctm} is related to the compression strength of the concrete. Multiple calculation methods are given in the provisions and recommendation, which result in a range of f_{ctm} for the same concrete class. The long-term tensile strength f_{ctm} for C30/37 can vary between 2.1 and 3.0 MPa according to the different calculation methods. A change in one concrete class result in ± 10% difference of f_{ctm}. A lower concrete class gives a lower tensile strength.

The development of the tensile strength is significantly slower, and the increase after 28 days is more present compared to the Young's modulus. The tensile strength after one day, seven days and one year is respectively 34%, 78% and 113% of the 28-days property for cement type N. The tensile strength development is significantly influenced by the cement type. For cement type S and R, the development after one day is 20% and 42%. After one year, the tensile strength for cement type S and R is respectively 120% and 110% of the 28-day property. In Fig: 8.1 the relative development of cement type N with respect to the 28-day value is shown for E_{cm} and f_{ctm}.

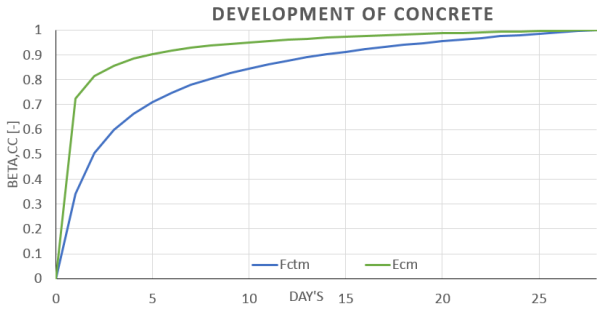

Figure 8.1: Development of E_{cm} and f_{ctm}

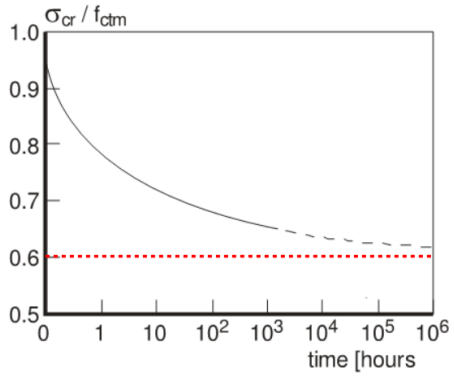

Figure 8.2: Long-term behaviour of tensile strength

Cracking strength σ_{cr}

Because the focus is on very slowly applied imposed deformation on concrete floors, more investigation is done into the cracking strength of concrete. Surveys of concrete *S.o.G.* have indicated that the first crack due to imposed deformation appears at 50% of f_{ctm}. It is stated that cracks that occur after three months are in good agreement with the tensile strength of approximately $0.6 \cdot f_{ctm,28}$ [8]. It should be noticed that the survey is only up to the first three months and that the ageing of the concrete can be more present after years. The same cracking factor α_{cr} of 0.6 is found in other research. In Fig:8.2, the outcome of the research is shown. It can be seen that after one hour, the tensile capacity of concrete is reduced by 20%. Finally the cracking strength σ_{cr} stabilises around 60% of the mean term tensile strength f_{ctm}[24]. In restrained shrinkage experiments of normal and high-performance concrete, a strength reduction factor of 0.8 was typically obtained[57]. It is known that the cracking stress σ_{cr} has a large influence on the crack width calculation. Assuming a low cracking factor can result in an underestimation of the cracking force and, thus, the crack width. The effect of the cracking factor on the crack width is analysed in the next chapter.

Creep φ

The quantification of the non-linear viscous mechanism is done according to the provision *E.C. 2*. In the provision, formulas are given for the estimation of the theoretical creep coefficient φ_0 at t=∞. The final creep coefficient of concrete is related to the following parameters: cement type, concrete class, relative slab thickness h_0, age of concrete at first loading t_0 and the relative humidity *R.H.*. The development of the creep depends on the cement type, slab thickness and relative humidity. φ_0 is mainly influenced by the concrete age at loading t_0. Especially during the young stage of concrete, the creep value is high, shown in Fig: 8.3a. Loading the concrete at the age of one day results in a significantly high theoretical creep value of 7.37 compared to 3.69 for 28-day old normal concrete. After one year, the effect of the concrete age at loading reduces and becomes less relevant. The *R.H.* and h_0 influence ±2% the development of the creep coefficient. The final creep φ_0 increases ±10% per higher concrete class, significantly decreases for cement type R (-23%) and reduces with 17% when the relative humidity increases with 20%. h_0 have no significant influence on φ_0.

In Fig: 8.3b the influence of the parameter on the creep development is shown. After one year ≈70% of the theoretical creep is developed. It can be concluded that the influence of the parameters on the creep behaviour is significant. The determination of the concrete age at loading is difficult for imposed deformation. Also the climate influences, which can be significant because creep mainly depends on the moisture in and around the concrete structure, are difficult to quantify. Therefore it is important that the designer is aware of the fact that creep calculations are only a estimation of the true behaviour. An average creep value of approximately 2.5 at t=365 is found in the sensitivity analysis.

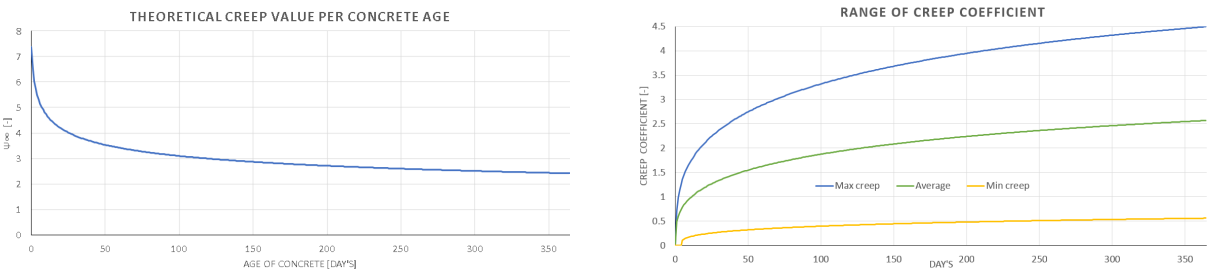

(a) φ_0 per concrete age at loading

(b) Upper and lower bound of φ_0

Figure 8.3: Creep behaviour

Concrete relaxation ψ

The relaxation factor ψ quantifies the concrete relaxation effect which depends on the type of loading, ageing coefficient χ_{age} and creep coefficient φ_0. Many experiments were performed to determine the relaxation factor in restrained concrete structures. In this research, a sensitivity analysis of the relaxation effect is performed. The results from the experiments are compared with the results of the analysis.

Multiple studies showed that a relaxation factor of 0.5 is in good agreement with the tensile creep behaviour before cracking [55]. In 1982 *P.B. Bamforth* suggested that stresses due to early age thermal cycles are reduced with 35% (ψ=0.65). *R. I. Gilbert* recommends a relaxation factor of 0.6 due to creep at in early age of concrete. For cracked concrete, where cracking occurred after approximately one month, *R. I. Gilbert* advises a relaxation factor not smaller than 0.36[58].

A study by *T. Seo* and *J. Kim* on the concrete relaxation effect in the uncracked region in a *R.T.M.* found relaxation factors of 0.22-0.26 after cracking. The amount of reinforcement also affected the stress development. A higher ρ_s (from 1 % to 1.6%) resulted in an increase of 27% of the relaxation factor from 0.26 to 0.33. This suggests that the uncracked zone after cracking is not fully restrained. More reinforcement increases the degree of restraint and, thus, the amount of tensile stress from shrinkage. The reason for the low relaxation factor after cracking can be that cracking results in a partly restrained member instead of the assumed fully restrained tensile member. Therefore, the suggestion made by *R.I. Gilbert*, to take a minimum value for the relaxation factor after cracking, seems accurate.

In the *F.E.M.* the experiments of *Seo et al.* the *F.E.M.* is validated. Even with a high creep coefficient, the relaxation factors of 0.22 and 0.26 were not obtained. Maximum relaxation factors of 0.31 and 0.36 are found in the analysis. The global behaviour of the *F.E.M.* is in good agreement with the stress behaviour in the experiment shown in Fig: 8.4.

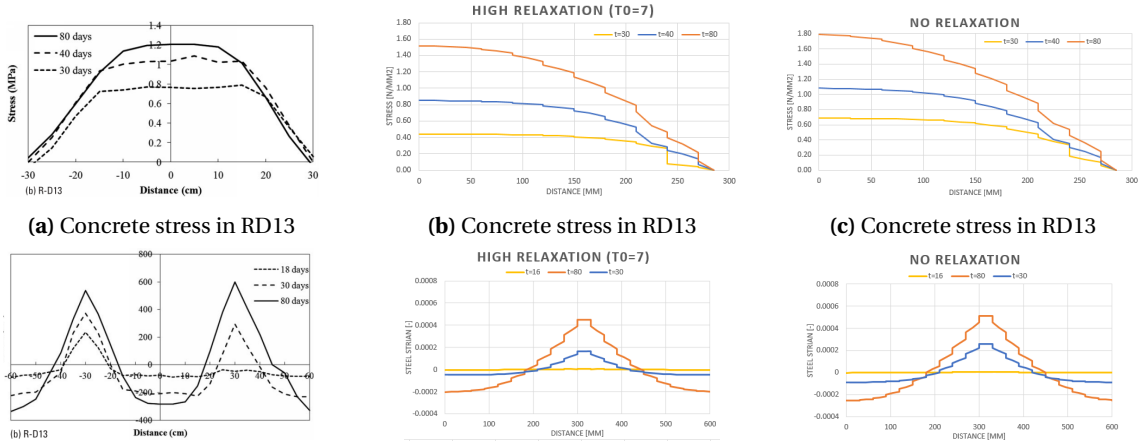

(a) Concrete stress in RD13

(b) Concrete stress in RD13

(c) Concrete stress in RD13

(d) Steel strain in RD13

(e) Steel strain in RD13

(f) Steel strain in RD13

Figure 8.4: Behaviour in member experiment and *F.E.M.*

In other papers, suggestions were made of higher relaxation factors ψ between 0.5 and 0.8 [34]. *Breugel* stated in his reader that stress reduction up to 83% is possible for fully restrained concrete structures loaded by shrinkage[24]. The *M.C. 2010* states that, from practice, it is known that for normal-weight ordinary structural concrete, the relaxation factor lies in the range of 0.1 and 0.3 at the end of the service life of 100 years due to imposed deformation [31].

A large range of concrete relaxation values is found in the literature. The same large range is found during the sensitivity analysis. Relaxation factors in the range of 0.25-0.54 were found after a loading period t_l of 365 days for standard concrete properties. The large range comes from the large variation of the creep coefficient. When looking at the extreme lower and upper-bound values from the analysis in Fig: 8.5a, it can be seen that the stresses reduce for both values. Also, for the lower bound value, all the stresses by the applied load are dissipated in time. The lower bound value is for early aged loaded concrete with an extremely high creep coefficient. The upper bound is for old loaded concrete, low creep and an ageing coefficient of 1.0.

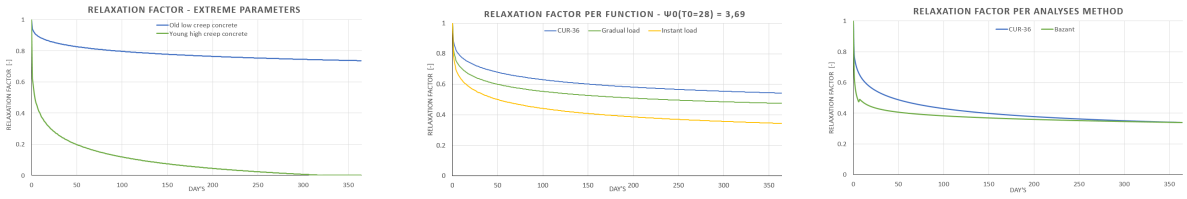

(a) Upper and lower bound of ψ **(b)** ψ for constant creep **(c)** ψ per calculation method

Figure 8.5: Relaxation effect

Relaxation function

The relaxation formulae, given in section 4.1, are compared in the analysis. In Fig:8.5b the relaxation effect is shown per relaxation function calculated with the same parameters. The instant loading type results in a larger concrete relaxation effect. The *CUR-36* formula results in a more conservative relaxation effect compared with the gradually applied load function. The relaxation factor ψ_{CUR36} is ±10% higher than $\psi_{gradual}$. For the instantly applied load, the concrete age at loading t_0 is often known or can be estimated with a certain precision. For gradually applied loading, such as shrinkage, only the starting point of the load can be determined. In theory, the concrete age at loading can be minutes or hours for imposed loads such as hardening temperature and shrinkage. In the *CUR-36* it is stated that the creep coefficient should be taken over the period of loading t_l=t-t_0. For example, t_0 would be for drying shrinkage at the end of the curing period. Autogenous shrinkage starts during hardening, which results in $t_0 \approx 1$. These low concrete ages at loading result in large creep coefficients and thus large relaxation effects. The higher creep effect at the early age is taken into account with the superposition method of *Bazant*. In Fig: 8.5c the *CUR-36* and *Bazant* method are compared. The creep coefficient after one year of loading based on the 28-day concrete properties is 2.76, which is used for the *CUR-36* function. It can be seen that the *CUR-36* method overestimates the early age stresses because it does not take into account the high early age creep effect. After one year, the relaxation factor is equal to the superposition method. The *CUR-36* relaxation function is in good agreement with the more precise superposition method of *Bazant* when 28-day properties are used. The same conclusion is found in the relaxation comparison analysis of the *F.E.M.* given in App: C. The *Bazant* method is compared with the creep compliance function and the standard creep models of the program *DIANA FEA* based on the provisions *E.C. 2* and *M.C. 2010*. All models are in good agreement when the creep function is calculated with the 28-day properties.

It can be concluded that concrete relaxation substantially lowers the stresses in statically undetermined concrete structures. Common values between 0.4 and 0.8 are found for the relaxation factor. The concrete relaxation effect can only be approached with a relaxation factor. Accurate calculations are complicated due to the many influences. For design purposes, the *CUR-36* method in combination with the creep coefficient over the loading period based on the 28-day concrete properties is advised for taking into account the concrete relaxation effect in fully restrained tensile member loaded by shrinkage.

8.2 Imposed deformations

The strain loads on the concrete structures are a result of environmental influences and material behaviour of concrete. The strain changes due to drying shrinkage, autogenous shrinkage, hardening temperature, seasonal temperature and daily temperature are analysed. The shrinkage is analysed according to the *E.C. 2* formulae. The temperature effect has been analysed with the use of the measurements from the survey of *Bishop* [19]. The results of the analysis are presented in App: E. The thermal expansion coefficient α_{cT} for concrete is assumed to be $10 * 10^{-6}$ °C^{-1}.

Drying shrinkage ε_{cd}

For the drying shrinkage the following can be concluded:

- The drying shrinkage strain for the standard concrete properties is 0.43 mm m^{-1} for t=∞ and 0.17 mm m^{-1} for t=365.
- A higher concrete class leads to a lower drying shrinkage. ±6% per concrete class.
- A higher *R.H.* leads to a significantly lower drying shrinkage. *R.H.* of 40% and 80% respectively increases and decreases the drying shrinkage with 20% and 40% compared with a *R.H.* of 60%
- The slab thickness does not affect the total drying shrinkage.
- A more slender slab results in a faster development of the drying shrinkage. ±24% per 50 mm after one year.
- The curing time only delays the shrinkage development and does not affect the final nor the development of the shrinkage strain.
- The cement type S and R respectively decreases and increases the drying shrinkage with 20% and 38 % compared with type N.
- On average, 38% of the drying shrinkage is developed after 365 days.

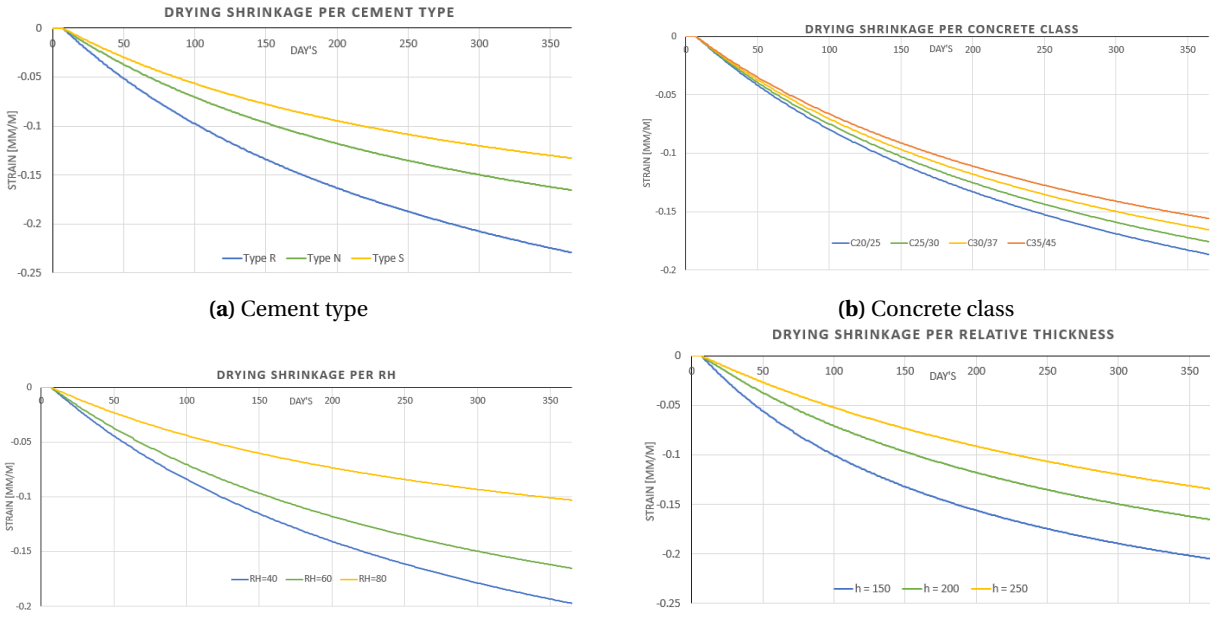

(a) Cement type

(b) Concrete class

(c) Relative humidity

(d) Slab thickness

Figure 8.6: Drying shrinkage

Autogenous shrinkage ε_{ca}

For the autogenous shrinkage the following can be concluded:

- The autogenous shrinkage strain for the standard concrete properties is 0.050 mm m^{-1} for t=∞ and 0.049 mm m^{-1} for t=365.
- A higher concrete class leads to a significant increase of autogenous shrinkage. ±25% per concrete class.
- 98% of the autogenous shrinkage is developed after 365 days.
- Autogenous shrinkage begins to develop directly after casting.
- Autogenous shrinkage is 5, 8, 11 and 14% of the drying shrinkage for respectively C20/25, C25/30, C30/37 and C35/45 at t=∞.

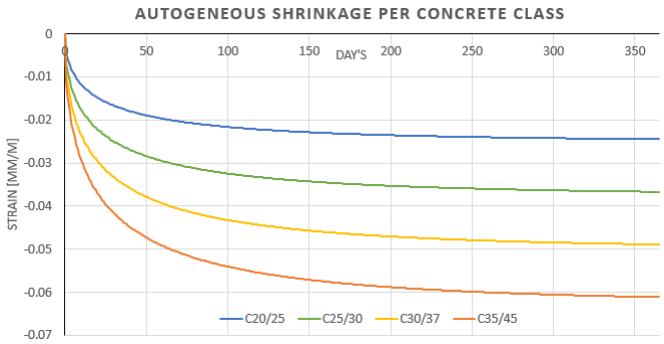

Figure 8.7: Autogenous shrinkage per concrete class

Table 8.2: Total shrinkage per concrete class

Parameter		$\varepsilon_{cd,0,t=\infty}$	[%]	$\varepsilon_{ca,\infty}$	[%]	$\varepsilon_{cs,tot}$	$\varepsilon_{cd,0,t=365}$	[%]	$\varepsilon_{ca,t=365}$	[%]	$\varepsilon_{cs,tot,t=365}$
F_{ck}	20	0.49	95	0.025	5	0.512	0.19	88	0.024	12	0.211
[MPa]	25	0.46	92	0.038	8	0.497	0.18	83	0.037	17	0.212
	30	0.43	90	0.050	10	0.482	0.17	77	0.049	23	0.214
	35	0.41	87	0.065	14	0.472	0.16	72	0.061	28	0.217

A higher concrete class reduces the final amount of shrinkage but increases the amount of shrinkage after one year. This is due to the larger autogenous shrinkage contribution, which is almost fully developed after one year.

Thermal strains

The thermal changes are separated into an annual, daily and hydration heat during hardening. In Fig: 8.8 the results of the survey are shown for a common *I.F.* The effects are investigated with the use of the *Bazant* model given in section 6.1.1.

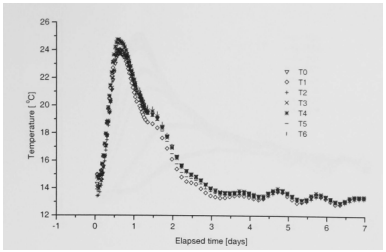

(a) Hardening temperature profile

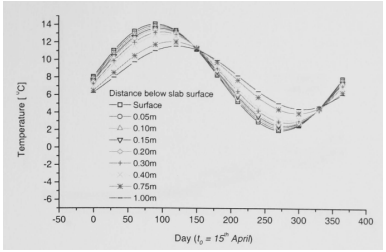

(b) Seasonal temperature change

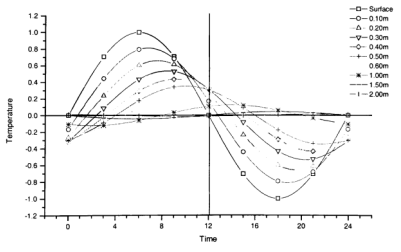

(c) Daily temperature change

Figure 8.8: Temperature measurements

Hardening temperature

Many studies have been performed for different types of structures on the investigation of early age stress development. The linear and relaxed stresses are shown in Fig: 8.9a for a temperature drop of 15 °C in three days. The temperature change of 15 °C can be assumed as the upper bound value. In practice, the measured temperature changes were not bigger than 12 °C. The temperature drop due to hardening results in a maximum stress of 50% of the cracking stress σ_{cr}. In Fig:8.9b, the results from a study that measured the early age stress development in a 140 meter long *S.o.G.* are shown. A maximum stress of 18% of σ_{cr} was found. The temperature rise due to the chemical reaction is relatively low because of the slender concrete structure. Therefore, the risk of early age cracking in *S.o.G.* due to hardening temperature is low. The effect of rapid cooling is also analysed. It is found that rapid cooling increases the crack risk at early age, but these stresses are more relaxed after one year. Slower cooling leads to ≈ 1.5 times more long-term stresses in the slab compared to rapid cooling. Stresses from hardening temperature will not likely result in early age cracking. From the analysis, it is concluded that the hardening temperature is not significant and can be neglected.

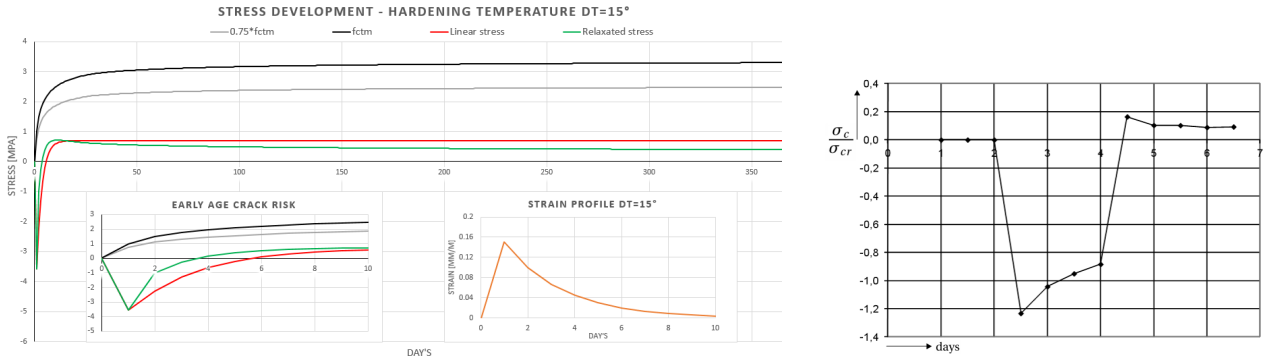

(a) Hardening stresses in *R.T.M.*

(b) Stress development in 140 m long *S.o.G.*

Figure 8.9: Early age stress behaviour

Seasonal temperature

The seasonal temperature change is analysed for the first year after casting. From measurements, it is found that the seasonal temperature change is low for indoor slabs. *I.F.* are often casted inside where environmental effects are minimised by the building. Therefore the seasonal temperature change does not have a large influence on the stresses in a industrial floor[10]. The temperature in the slab remains, after the change due to hardening, nearly constant[8]. Contrary statements are made by *Bishop* in his survey. An extensive survey was performed on two large jointless floors (50x50 m) in unheated buildings. The seasonal temperature significantly affected the measured strains in the floors. Annual temperature variations of 15 °C were recorded[19].

Several researchers performed model calculations to illustrate the effect of the surrounding temperature per joint spacing. In the research, the surrounding temperature T_{sur} during casting and the cooling temperature gradient dT are changed. The crack risk is plotted for joint spacing from 10 to 100 meter. In Fig: 8.10a and Fig: 8.10b the upper and lower bound situations are shown. Cracking is likely to occur for joint spacing larger than 50 meter casted in the summer with temperature changes of ±15°C. According to the research, there is no crack risk for 100 meter long slab casted in the winter with a small temperature difference (dt=5°C).

The same conclusions are found in the sensitivity analysis in this research[59]. In Fig: 8.10c and 8.10d the results are shown for the situation that the casting period results in additional shrinkage strain or additional expansion strain for respectively summer and winter casting. The casting period determines the temperature difference between the concrete and the average year temperature. It can be concluded that the concrete temperature during casting should be equal or lower than the average year temperature to make sure no extra strain load is applied to the concrete structure. When the concrete temperature at casting is equal to the average year temperature, then only the seasonal temperature change dT affects the strain load. Otherwise an additional temperature load of $T_{season} = T_{conc} - T_{ave}$ has to be taken into account.

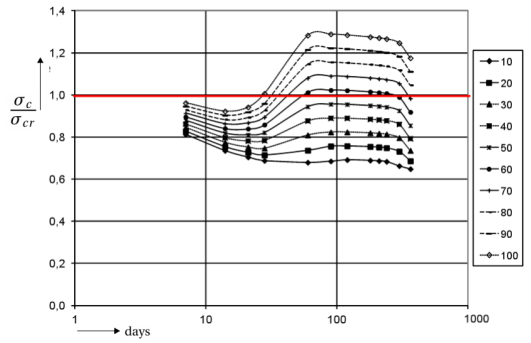

(a) Summer $T_{sur} = 30, dT = 15$

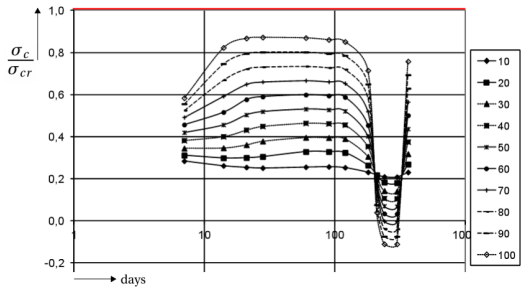

(b) Winter $T_{sur} = 10, dT = 5$

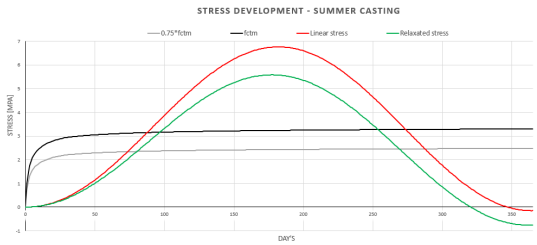

(c) Summer casting:dT= -10 °C +10 °C with T_{season}=-5

(d) Winter casting:dT= +10 °C -10 °C with T_{season}=+5

Figure 8.10: Stress development due to seasonal temperature change

Daily temperature

The daily temperature changes are low and constant during the year. Focussing only on the daily temperature change, the stresses fluctuate around zero. When a concrete slab has a daily temperature change of 1 °C, the daily unrelaxed stress deviation is ≈ 0.3 MPa. The daily temperature only influences the moment of cracking per day and is likely the reason that cracking is often noticed in the morning after cooling of the concrete slab. Because the concrete floors are assumed to be indoor, the daily temperature effects like solar radiation and snow are not relevant and thus not taken into account.

8.3 Degree of restraint

The degree of restraint depends on multiple factors. For large industrial floor on grade the most important is the external restrained by soil friction. Other aspects are the internal restraints by reinforcement and temperature differentials. External restraints by construction detail such as joints and connections can also be significant. In App:D, more information can be found about the restraint calculations.

Restraint by conventional reinforcement

The internal restraint by the reinforcement is initiated by the shrinkage of the concrete. The stiffness difference between the concrete and the embedded reinforcement results in a restrained effect on the concrete. The reinforcement can be seen as an internal spring. As the concrete shrinks, the reinforcement becomes in compression and imposes a tensile force on the concrete. Thermal loads do not result in internal restraint by the reinforcement, because the thermal expansion coefficient α_{cT} of concrete and steel are equal. The degree of restraint depends on the amount of reinforcement in the slab. A higher ρ_s results in a higher degree of restraint. In Tab:8.3 the degree of restraint per ρ_s are given for E_s=200.000 $N^2\,mm^{-1}$,E_{cm} =20.000 $N^2\,mm^{-1}$ and ψ = 0.38[9]. At joints, extra reinforcement is often added. *Bishop* investigated the presence of dowels on the stresses. Dowels in joints may result in additional restraint stresses along joints. It is found that longitudinal and transverse dowel can result in 0.17 MPa restrained stresses, which is equivalent to a degree of restraint of 0.1[19].

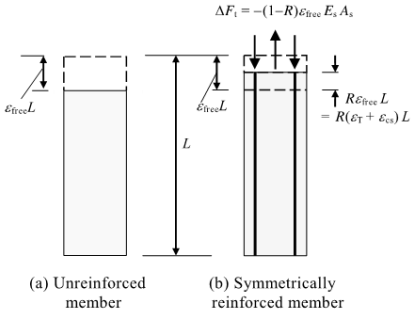

Figure 8.11: Internal restraint by reinforcement

Table 8.3: degree of restraint by reinforcement

ρ_s [%]	0.2	0.5	1	1.5	2
R [-]	0.05	0.12	0.21	0.28	0.34

$$R = \frac{\frac{n}{\psi}\omega_s}{1+\frac{n}{\psi}\omega_s} \tag{8.95}$$

Restraint by steel fibre reinforcement

Now it is known that more reinforcement increases the degree of restraint. Therefore, it is likely to assume that adding steel fibre to the concrete mixture also results in internal restraint when loaded by shrinkage. The presence of steel fibres in a concrete mixture influences the micro-structure. Adding steel fibres results in more air voids in the concrete. Extra air voids decrease the elastic stiffness of the mixture. The steel fibres increase the elastic stiffness of the concrete. Both effects counteract each other during shrinkage, and therefore, the steel fibres do not provide any significant internal restraint[29].

Restraint by temperature differentials

When a concrete structure rapidly changes in temperature, which often occurs during hardening, a temperature difference ΔT arises. The ΔT results in restrained stresses known as *eigenstresses*. Research recommends a degree of restraint of 0.42 for this effect[58]. For indoor industrial floor, this effect can be neglected because the temperature differences are significantly low.

Restraint by foundation strips

To increase the slab capacity for vertical loading along the edge, the perimeter of the slab is sometimes thickened. Slabs can also be casted on foundation strips. This local thickening restraint the slab movement. The restrained movement results in a tensile force in the slab. *Narin* and *Wiklund* derived a formula to calculate this tensile force based on the schematization shown in Fig:8.12[6]. In Tab:8.4 the degree of restraint $R = \frac{N_{strip}}{N_{cr}}$ is calculated with the standard parameters. The soil Young's modulus E_{soil} of 100 and 400 $\mathrm{N\,mm^{-2}}$ are representative values for respectively sand and dense gravel. For stiff soil and large edge movement Δ_x, it is possible that the slab is fully restrained over the complete length.

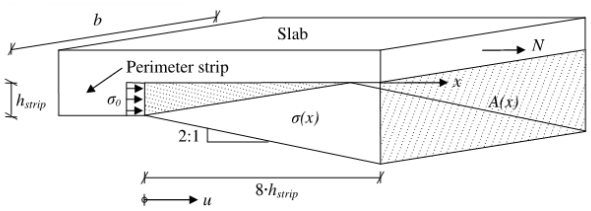

Figure 8.12: Schematisation of edge restraint

$$N_{strip} = \frac{E_{soil} \cdot b}{2 \cdot \ln(5)} \cdot \Delta_x \tag{8.96}$$

Table 8.4: degree of restraint by perimeter strip

E_{soil} [$\mathrm{N\,mm^{-2}}$]	100	400	100	400
Δ_x [%]	1	1	3	3
R [-]	0.09	0.36	0.27	1.00

Restraint by casting sequence

The most famous imposed restraint is probably casting old to new concrete. This situation also occurs in *S.o.G.*. When the slab can not be realised in one pour, the slabs have to be casted in sections over multiple days. Because of temperature and stiffness differences between the sections, restraints arise parallel to the day-joint. In the middle of the joints, the restraints are the highest. To minimise the restraint, it is advised to keep the time between the casting sequences as low as possible. The best casting sequence is with only one contact edge. In Fig: 8.13 the restraints are shown for nine casting sections for the standard concrete properties which result in a maximum degree of restraint of 0.51 from the research of *Al-Gburi* [60]. Other casting sequences can increase the degree of restraint to 0.56 and 0.65 for slabs with two contact and four contact edges. When slabs are casted with four contact edges, the degree of restraint is over the entire slab instead of locally along the day-joint.

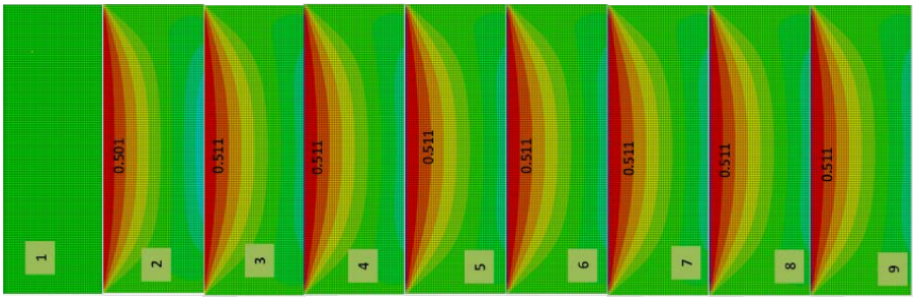

Figure 8.13: degree of restraint due to casting

Restraint by soil friction

The restraint by soil friction is assumed to be the most governing aspect regarding the restraints in jointless *S.o.G.*. As mentioned before, the slab is fully restrained when the slab length is twice the frictional length $L_{friction}$. An extensive study has been performed on the influence of the friction. Calculations are based on the recommendation of *CUR-36*(*L.F.E.A.*), studies of *F. Narin* and *O. Wiklund*(*L.F.E.A.*)[6] and *F.E.M.*(*N.L.F.E.A.*). The main difference in calculations is that the linear method assumes full friction over the total friction length. The non-linear calculations take the slip behaviour into account. The difference between the *L.F.E.A.* is the assumed soil properties. In Tab: 8.5 practical values are given for $L_{friction}$ based on the linear and non-linear models.

Table 8.5: Frictional length $L_{friction}$ [m]

Foundation type	Narin/Wiklund	Petersons	CUR-36	F.E.M.
Sand	31.5	24.2	18.5	37.8
Gravel	27.6	16.1	12.0	34.9

In Fig: 8.14 the linear and non-linear calculation methods are compared. It can be seen that the non-linear slip effect significantly increases the edge movement of the slag. The degree of restraint profile along the slab is also changed. The slip effect significantly reduces the fully restrained length of the slab. Only a small zone is fully restrained compared to the linear methods. When the required force to initiate slipping N_{slip} is equal to the cracking force N_{cr} of the slab, only the midpoint of the slab will be fully restrained, as shown in Fig:8.14b. If $N_{slip} > N_{cr}$, the degree of restraint profile becomes more like the linear model. If $N_{slip} < N_{cr}$, the maximum degree of restraint would never be higher than $\frac{N_{slip}}{N_{cr}}$.

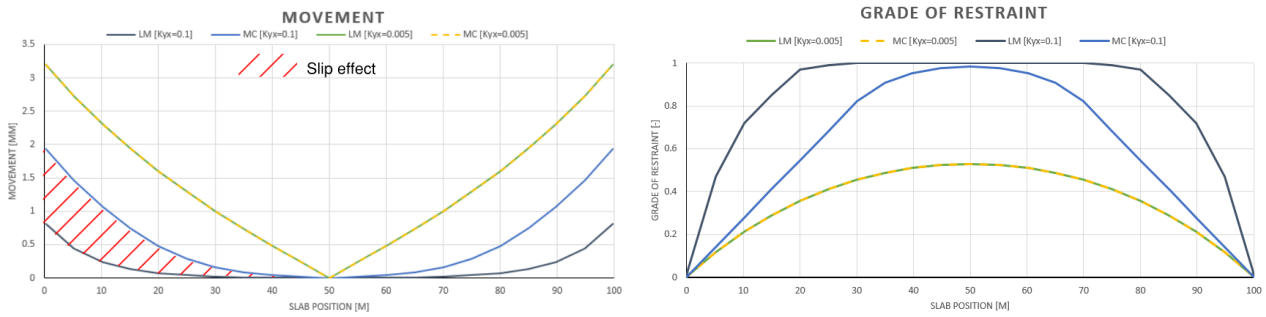

(a) slab movement

(b) degree of restraint

Figure 8.14: Comparison of models: LM vs CM

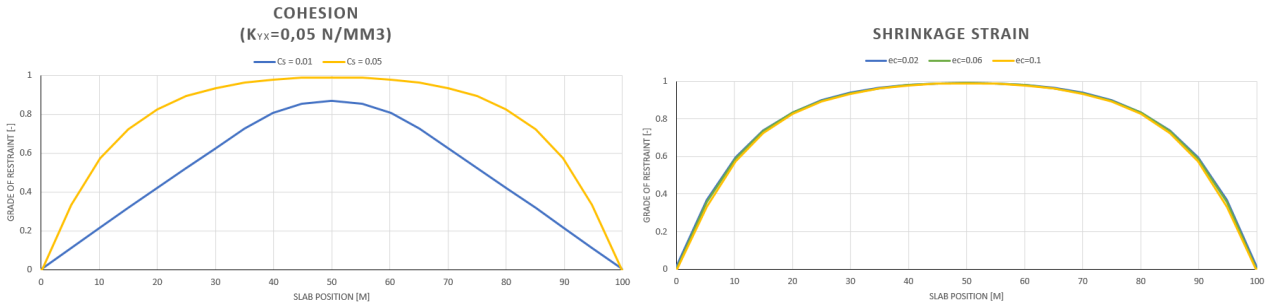

(a) Shear capacity τ_{max}/ Cohesion c_s

(b) Shrinkage strain

Figure 8.15: Effect on degree of restraint

The following can be concluded from the analysis:

- Slip behaviour significantly increases the friction length . $L_{friction}$ increases with a factor 2 to 4 when slip is taken into account.
- The sub-base properties greatly determines the degree of restraint in the slab.
- A higher shear stiffness modulus K_{yx} result in a significantly lower $L_{friction}$. It is advised to use the relation: $K_{yx} = \frac{k_{mod}}{2}$ instead of the commonly used $K_{yx} = \frac{k_{mod}}{10}$.
- Linear calculation methods like *CUR-36* result in underestimation of the frictional length.
- Averages values for $L_{friction}$ are in the range of 23 and 28 meters for gravel and sand sub-base .
- In the *N.L.F.E.A.* a higher vertical load decreases the edge movement Δ_x of the slab. Δ_x slightly decreases by $\pm$4% when the vertical load is doubled.
- The amount of shrinkage does not affect the friction length and degree of restraint. It only affects the axial force.
- Concrete relaxation has no effect on the degree of restraint and friction length when $N_{c_{(t)}}$=N_{cr}.
- The shear capacity τ_{max} of the soil significantly influences the degree of restraint profile.

Restraint by vertical load

The curvature length $L_{curvature}$ at the slab edge is investigated. A strain gradient results in a rotation in the slab. Due to its self-weight and vertical load, the curvature will be restrained. The slab is fully restrained by this effect when the bending moment from the restraint $M_{restriant}$ is equal to the maximum bending moment in the slab M_{slab}. The $L_{curvature}$ can be derived from this equilibrium situation and is given in Eq:8.97.

$$L_{curvature} = \sqrt{\frac{\sigma_{cr_f} \psi b h^2}{3 q_v}} \tag{8.97}$$

From the analysis, it is found that $L_{curvature}$ is significantly lower than $L_{friction}$. $L_{curvature}$ is in the range of 3-10 meter mainly depending on the slab height, flexural cracking stress and relaxation factor. *Walker* states that when the joint spacing is larger than eight meters the curling stresses are constant [61]. In turn this results in $L_{curvature}$>4m. Therefore, it can be assumed that the curvature restraint is always one for loaded jointless *S.o.G.*.

8.4 Crack risk

The influences of the parameters on the stresses are now known. All these individual parameters together affect the stress behaviour in the *S.o.G.*. The combination is analysed to gain insight into the crack risk. From practice, it turns out that uncontrolled cracking occurs mostly at the beginning of the slab lifetime. From observations in practice, it is found that cracking is most likely to occur between two and twelve months after casting the concrete floor according to *Silfwerbrand* [25]. Stu*fib*-11 states that cracking often occurs in the first two months, even before the floor is taken into service. This is because approximately 50% of the shrinkage is present after two months of casting [8]. This is in contrast to the amount of shrinkage according to the *E.C. 2*, where approximately 17% is developed after two months.

In Fig:8.16a, it can be seen that for standard parameters, the risk of cracking is indeed between two and twelve months. In this case, the moment of casting determines largely whether its cracks after two months or after one year. The stresses, which develop in the first month, have a high relaxation effect. The early age stresses due to temperature are low and the floors are mostly casted in a controlled area. Therefore cracking is not likely to occur in the first two months for industrial floor. The crack risk can be quantified according to *Silfwerbrand* with the following equation[25]. Theoretically, the concrete will not crack when η_{cr}<1, but for design calculation, a lower value of 0.7 is proposed. From the equation, it can be seen that the risk of cracking can be reduced by reducing the degree of restraint, increase the cracking strength of concrete, lowering the Young's modulus, reducing the shrinkage strain or increase the creep coefficient. To realise an uncracked concrete structure, the engineer has to combine all the options.

$$\eta_{cr} = \frac{\sigma_c}{\sigma_{cr}} \quad = \quad \frac{R \cdot \varepsilon_{cs} \cdot E_{cm} \cdot \psi}{\alpha_{cr} \cdot f_{ctm}} \tag{8.98}$$

It is very effective to reduce the shrinkage in order to reduce the crack risk. The shrinkage can be reduced by taking into account certain aspects like the porosity of the aggregate. A high porosity will have more cement paste and, therefore, more shrinkage. A well-graded aggregate mixture is preferred for industrial floors. The total porosity decreases with an increase in maximum aggregate size. The aggregate can restraint the drying shrinkage in concrete when aggregates with a low shrinkage value are chosen[62]. Using less water also reduces the drying shrinkage[4]. Besides that, the aggregates can reduce the shrinkage of concrete, and also influence the Young's modulus E_{cm}. A lower E_{cm} reduces the crack risk in the concrete. Therefore, the aggregate type is an essential aspect with respect to the crack risk. *S.R.A.* can also be used to reduce the amount of shrinkage. It is found that adding *S.R.A.* can reduce the total drying shrinkage with 20%[25].

Therefore, the concrete mixture, which is chosen by the engineer, is of great importance. The effect of the concrete mixture on the crack risk is visualised in Fig:8.16b. When bad decisions are made regarding the concrete mixture, the crack risk significantly increases. In this example, the parameters f_{ck}= 20, cement type S and sandstone aggregate are chosen for the good concrete mixture. The parameters f_{ck}= 35, cement type R and basalt aggregate are chosen for the bad concrete mixture.

Besides the concrete mixture, the environment and slab dimensions also affect the crack risk. In Fig: 8.16c, the influences of slab thickness, the *R.H.* and the seasonal temperature are shown. In the figure, there is a significant difference between the upper and lower bounds, which indicates that the moment of cracking and crack risk can vary a lot for *I.F.*. The crack risk is directly related to the degree of restraint. For jointless reinforced *S.o.G.*, there is a high possibility that there is a fully restrained zone in the slab. Reducing the degree of restraint is beneficial but it is difficult to realise. If the degree of restraint is reduced to 0.5, the concrete can remain un-cracked for the assumed standard parameters shown in Fig: 8.16d. For design purposes, the degree of restraint is advised to be taken as one in jointless *S.o.G.*.

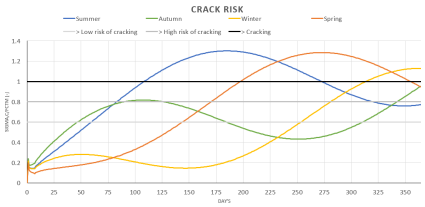

(a) Moment of cracking

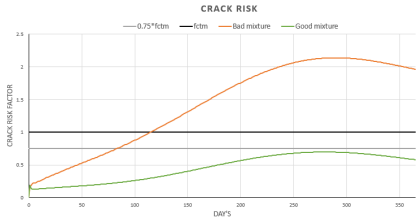

(b) Effect of concrete mixture

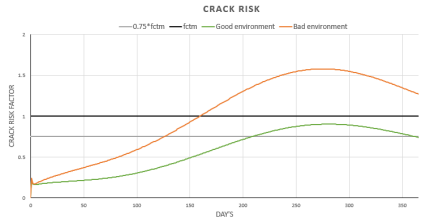

(c) Effect of environment

(d) degree of restraint $R = 0.50$

Figure 8.16: Crack risk

The concrete relaxation coefficient ψ also reduces the crack risk. From the sensitivity analysis, it is shown that the concrete relaxation effect is challenging to determine. Significant variations were found for different parameters. The best method to quantify the long-term relaxation effect for sustained loading is with the formula provided in *CUR-36* in combination with the 28-days concrete properties. Relaxation coefficient between 0.4 and 0.8 was found. Therefore, the relaxation effect significantly reduces the crack risk for *I.D.*.

From the extensive survey of *Bishop*, the true crack risk in *I.F.* can be analysed. *Bishop* looked into the stress development inside the slab due to *I.D.* [19]. In the survey, multiple floors are analysed. The floors were made out of approximately 45 by 45 meter pours with free movement joints in-between. The stresses from the survey are determined with a theoretical *A.A.E.M* and it is assumed that the strain at $t = 0$ in the slab are zero and are an indication of the stress development. Theoretical stresses due to cooling of 0.16 and 0.36 MPa after three days were calculated from the measurements. The frictional restraint across the building resulted in theoretical stresses of 0.20, 0.22, 0.35 and 0.24 MPa after respectively three, three, 28 and 28 days. These restrained stresses accounted for 13%, 14%, 9% and 6% of the tensile capacity. The same values were found in a second jointless *S.F.R.C.*, large area pour, industrial floor. Long-term measurement between seven and 140 days resulted in frictional stress of 0.51, which is approximately 20% of the tensile concrete capacity. Based on the friction models, the degree of restraint due to friction for the 45 meters long slab is around 0.67. Translating the measurements to fully restrained floors with a reduced cracking stress, the maximum crack risk is estimated at around $\frac{20}{0.67*0.6} = 50\%$. From the survey, it can be concluded that the stresses in the slab from imposed deformation did not initiate cracking. The crack risk was very low, not higher than 0.2 for all the floors, in the first 140 days.

Other research developed a crack risk graph depending on friction length, soil friction and cracking stress. In Fig:8.17, the crack risk is given to quickly check if the likelihood of cracking is high in the slab. Concrete on compacted fill has a friction coefficient of 1-2 [63]. The same range of the friction length is found in the graph for normal strength concrete on gravel as in the research. Both methods result is friction length between 20 to 40 meters.

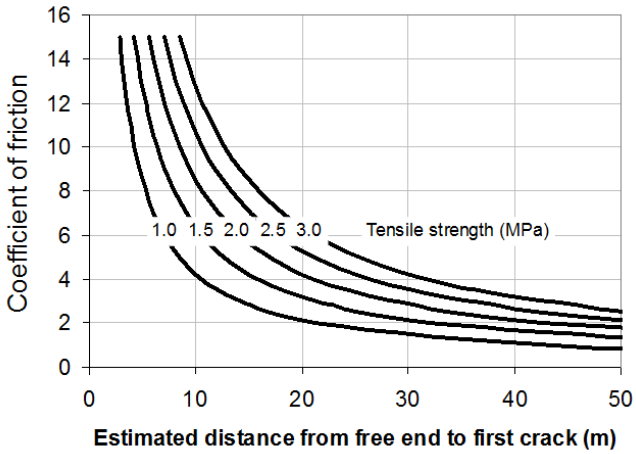

Figure 8.17: Likelihood of cracking due to friction

9. Sensitivity Analysis - Stage 2: Cracking

From the stress analysis, it is concluded that for large *S.o.G.*, the stresses can exceed the tensile strength capacity of the concrete, which results in cracking. Earlier it was found that the fully restrained mid-zone of the slab with the constant stress zone can be modelled with the *R.T.M.*. For this constant stress zone, the cracking behaviour for reinforced and hybrid concrete elements are analysed. For the stress analysis in the crack and uncracked zone, the theoretical models of *Gilbert* is used. The crack width are determined with the models of *Van Breugel*, *Gilbert*, *M.C. 2010*, Stu*fib*-11, *CUR-65* and the *F.E.M.*. According to the *Gilbert*, the behaviour after the first crack and after ten years is analysed. For both situations, the stresses and crack widths are determined. The ageing of the concrete is taken into account according to the formulae in the *E.C. 2*. The moment of the first crack is determined by the intersection of the applied shrinkage load $\epsilon_{sh(t)}$ with the cracking strain of the concrete $\epsilon_{cr(t)}$. The crack width analysis is first performed in centric reinforced *R.T.M.*.

$$\epsilon_{cr(t)} = \frac{\alpha_{cr} \cdot f_{ctm(t)}}{E_{cm(t)} \cdot \psi} \tag{9.99}$$

$$\epsilon_{sh(t)} = \epsilon_{d(t)} \cdot \alpha_{sra} + \epsilon_{d(t)} + \epsilon_{temp(t)} \tag{9.100}$$

All the relevant parameters are analysed per aspect. The following aspects are discussed: slab structure, reinforcement and concrete mixture. The effect of steel fibre reinforcement and the influence of the soil friction on the crack width is also analysed. The analysis is performed with the standard parameters shown in Tab:9.1. The most important findings are elaborated per aspect. Unfortunately, the results from the analysis are not compared with crack widths found in practice. No comprehensive documentation of the concrete properties and reinforcement in the cracked slabs were found. Only general damages reports with uncontrolled crack widths are found. Comparison of the practical and analytical crack widths without knowing all the parameters of the slab is not accurate and, therefore, not performed.

Table 9.1: Standard parameters

Parameter	**Value**	**Unit**
Slab height	200	mm
Restrained length	50	m
Sub-base	Granular	-
Concrete strength F_{ck}	30	MPa
Cement type	N	-
Aggregate type	Quartz	-
Crack factor α_{cr}	0.6	-
Relaxation factor ψ	0.75	-
Relative Humidity *R.H.*	60	-
Temperature change ΔT	0	°C
Reinforcement ratio ρ_s	0.5	%
Diameter $\varnothing$	9	mm
Eccentricity	0	mm

9.1 Slab structure

The parameters of the slab structure, which influence the behaviour are the thickness, length, soil friction and the environmental effects such as *R.H.* and temperature changes. First, the slab thickness is discussed.

Slab thickness

With an increase in slab height, the cracking forces increase significantly. Because the reinforcement ratio ρ_s is constant, the steel stress is not increased and the crack width is not substantially influenced according to *Van Breugel*. The small difference is because the slab thickness influences the shrinkage development. Therefore, the first crack is delayed and the number of cracks after one year is slightly lower for the thicker slabs. The first crack is wider for the thicker slab, according to *Gilbert*, because of the more developed concrete properties. This is also found for the *CUR-65* method. The *M.C. 2010* calculates the transfer length based on the cover. Thicker slabs increase the cover resulting in longer transfer length and thus wider cracks. It should be kept in mind that the *M.C. 2010* states that the transfer length formula is only valid up to a cover of 75 mm. The centric reinforced slab exceeds this limit. Therefore, the transfer length can be overestimated. The bonding strength also increases between the first and the final crack due to the ageing of the concrete. Therefore, the crack width is not always wider for a higher cracking force. The results are shown in Tab: 9.2 and the relevant effects are highlighted.

Table 9.2: Analysis of stresses and crack width

		Breugel	Gilbert					Breugel		Gilbert			*M.C. 2010*		CUR-65	Stufib-11
Parameter	t	N_{cr}	$N_{c_{(t)}}$	ψ_{crack}	$\sigma_{c1_{(t)}}$	$\sigma_{s1_{(t)}}$	$\sigma_{s,cr}$	w_{mo}	w_{max}	Cracks	s_m	w_{max}	l_t	w_{max}	w_{max}	w_{max}
h=150	**34**	271	239	0.88	1.6	-1.0	315.2	0.12	0.22	1	-	0.28	**182**	**0.35**	0.29	0.27
	3650	311	**257**	0.83	2.0	-57.5	340.7	0.12	0.24	48	1.0	0.30	182	0.34	0.32	
h=200	**49**	371	326	0.88	1.6	-1.0	323.4	0.13	0.23	1	-	0.35	**207**	**0.41**	0.32	0.27
	3650	414	**344**	0.83	2.0	-53.7	342.3	0.12	0.24	45	1.1	0.30	207	0.39	0.35	
h=250	**65**	471	415	0.88	1.7	-1.0	328.9	0.13	0.24	1	-	0.36	**231**	**0.46**	0.35	0.27
	3650	518	**432**	0.83	2.0	-49.9	343.9	0.12	0.25	42	1.2	0.30	231	0.45	0.38	

Restrained length

The restrained length $L_{restraint}$ significantly affect the crack relaxation effect. A longer $L_{restraint}$ result in a higher crack relaxation coefficient ψ_{crack}. After the first crack, ψ_{crack} of 0.48 and 0.92 for respectively $L_{restraint}$=5 and $L_{restraint}$=100 meter are calculated. The difference is smaller for cracking after one year, ψ_{crack} is 0.69 and 0.88 for respectively $L_{restraint}$=5 and $L_{restraint}$=100 meter. For small restrained lengths, the cracking zone is relatively large to the total length, which results is a higher axial stiffness reduction and thus a lower ψ_{crack}. A higher ψ_{crack} result in higher axial forces and, thus, higher steel stress in the crack. The higher steel stress results in significantly larger crack width according to *Van Breugel*, from 0.06 mm to 0.21 mm for $L_{restraint}$ of 5 and 100 m. A large difference of 0.06 mm to 0.28 mm is found between the first crack width of the 5 m and 100 m restrained slab according to the *M.C. 2010*. The restrained length does not influence the crack spacing due to the assumed constant transfer length. Only the number of cracks increases significantly. The restrained length does not affect the crack width calculation provided by *CUR-65* and Stu*fib*-11. In Tab:9.3, the design crack widths are shown per method and restrained length based on the same parameters of the *N.L.F.E.A.*. The analytical calculations are compared with two *F.E.M.* with a restrained length of 5 and 25 m shown in Fig: 9.1.

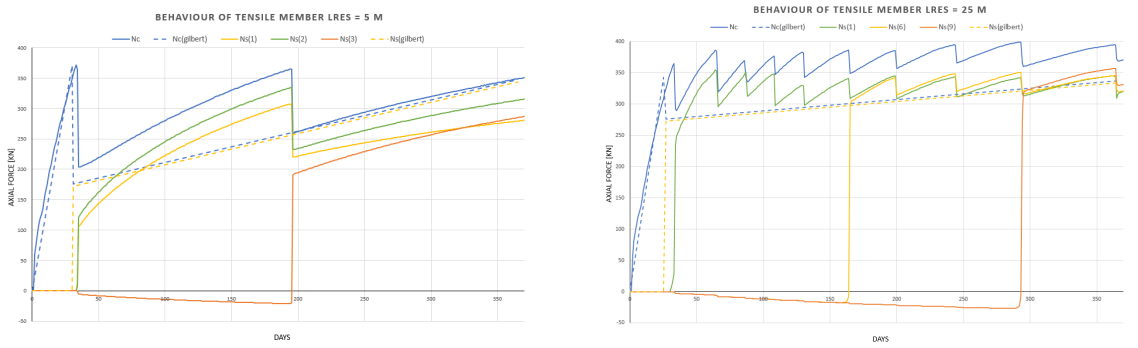

(a) $L_{restraint}$= 5 m, 1.81 <f_{ctm}< 2.59

(b) $L_{restraint}$=25m, 1.68 <f_{ctm}< 2.89

Figure 9.1: Stress behaviour tensile member

Table 9.3: Analysis of crack width

Model:		Gilbert	*F.E.M.*	Breugel	Gilbert			*M.C. 2010*	CUR-65	Stufib-11	*N.L.F.E.A.*	
Parameter	t	ψ_{crack}	ψ_{crack}	w_{max}	Cracks	s_m	w_{max}	w_{max}	w_{max}	w_{max}	w_{mo}	w_{max}
$L_{restraint}$=5	26	0.48	0.56	0.06	1	-	0.13	0.06	0.29	0.24	0.08	0.08
	365	0.69	0.96	0.13	4	1.25	0.22	0.23	0.32	-	0.30	0.32
$L_{restraint}$=25	26	0.81	0.79	0.16	1	-	0.22	0.28	0.29	0.24	0.13	0.16
	365	0.85	1.02	0.19	16	1.56	0.26	0.26	0.32	-	0.32	0.38
$L_{restraint}$=50	26	0.88	-	0.18	1	-	0.25	0.34	0.29	0.24	-	-
	365	0.87	-	0.21	31	1.61	0.27	0.37	0.32	-	-	-
$L_{restraint}$=100	26	0.92	-	0.21	1	-	0.28	0.37	0.29	0.24	-	-
	365	0.88	-	0.22	61	1.64	0.27	0.38	0.32	-	-	-

For proper comparison, the analytical results are calculated with the lowest f_{ctm} in the *F.E.M.*. Because of the long length, multiple weak zones are present in the member. After cracking, the uncracked zones will eventually exist of higher quality concrete with a higher cracking stress. This results in a higher axial force in the member if the reinforcement can transfer the forces. In Fig: 9.1b this is clearly visible. Due to the large variation of σ_{cr} in the *F.E.M.*, the axial force $N_{c_{(t)}}$ exceeds the cracking force N_{cr}. The *Gilbert* gives a good estimation of the stress behaviour and crack relaxation effect. The downside is that a fixed cracking stress and transfer length have to be assumed for the calculation. In reality, the cracking stress increases after every crack. The transfer length also increases when the steel stress increases. The steel stress in the crack at t_{cr} and at t=365 is in good agreement with the *F.E.M.* for $L_{restraint}$=5m. For $L_{restraint}$ = 25 m, the maximum steel stress in the first year is slightly underestimated by the *Gilbert* due to the increasing cracking stress compared to the *F.E.M.*. For safe design calculation, the upper bound of the cracking stress and transfer length should be taken into account.

Soil friction

As determined previously, the sub-base parameters greatly determine the restrained length, but it is also found that the friction has an influence on the cracking behaviour. It is stated that after cracking, a high sub-base friction is positive regarding crack width[8]. From the analysis, it can be concluded that the influence of the friction after cracking is very low. For controlled cracking, the soil friction force after cracking N_{soil} is between 1.0 and 5.6 kN, which is 0.3 and 1.3% of the cracking force for respectively sand+foil and a massive loaded slab on granular sub-base. Even smaller values of 0.12 kN were found in the *N.L.F.E.A.*. The soil friction can, therefore, be neglected for crack width calculations and is only a relevant parameter for the restrained length of the slab.

Environmental effects

A higher relative humidity decreases the amount and development speed of drying shrinkage. With an increase in *R.H.*, the first cracking moment is delayed. The first crack is initiated after 42 49 and 76 days for respectively *R.H.* of 40%, 60% and 80%. Due to the lower total shrinkage strain, the total number of cracks decreases from 54 to 27 after ten years in a 50 meter long restrained slab. Therefore the crack relaxation effect is slightly lower, resulting in higher steel stresses in the crack, this results in a small increase of cracks width.

The *CUR-65* and Stu*fib*-11 methods do not depend on the strain load, only on the cracking strength. Due to the later cracking, the concrete property slightly changes but do not have any substantial effect.

The temperature change fluctuates around the average environmental temperature. When the concrete mixture is the same temperature as the average environmental temperature during casting, no additional strain will be applied to the concrete structure in the long-term. Therefore it is advised to keep the temperature of the concrete mixture before casting below the average and environmental casting temperature. In the analytical model, the effect of concrete mixture warmer than the average temperature is analysed. A constant decreasing temperature (cooling) load is taken into account. Applying a temperature load ΔT results in earlier cracking of the concrete and more cracks. According to the *Van Breugel* and *M.C. 2010*, higher strain loads result in a lower crack width because they are based on the steel stress calculated according to the *Gilbert*. This model gives a lower steel stress for higher strain loads due to the more present crack relaxation effect from the high amount of cracks. The crack width calculation method provided by *Gilbert* does not result in a smaller crack width when more strain load is applied, only more cracks. The influence of the *R.H.* and a higher temperature difference e.g., more strain load, is shown in Tab: 9.4.

Table 9.4: Analysis of stresses and crack width

		Breugel	Gilbert					Breugel		Gilbert			*M.C. 2010*		CUR-65	Stufib-11
Parameter	t	N_{cr}	$N_{c_{(t)}}$	ψ_{crack}	$\sigma_{c1_{(t)}}$	$\sigma_{s1_{(t)}}$	$\sigma_{s,cr}$	w_{mo}	w_{max}	Cracks	s_m	w_{max}	l_t	w_{max}	w_{max}	w_{max}
ΔT=10	**37**	364	321	0.88	1.6	-1.0	317.5	0.12	0.23	1	-	0.29	207	0.40	0.31	0.28
	3650	414	330	**0.80**	2.0	-73.8	**327.4**	0.11	**0.21**	61	0.8	**0.31**	207	0.36	0.35	
ΔT=20	**30**	358	316	0.88	1.6	-0.9	312.6	0.12	0.22	1	-	0.25	207	0.39	0.31	0.29
	3650	414	307	**0.74**	2.0	-93.9	**304.7**	0.10	**0.17**	78	0.6	**0.31**	207	0.31	0.35	
R.H.=40	**42**	367	323	0.88	1.6	-1.0	320.2	0.12	0.23	1	-	0.33	207	0.40	0.32	0.28
	3650	414	336	0.81	2.0	-64.9	**333.9**	0.11	0.22	**54**	0.9	**0.31**	207	0.37	0.35	
R.H.=60	**49**	371	326	0.88	1.6	-1.0	323.4	0.13	0.23	1	-	0.35	207	0.41	0.32	0.27
	3650	414	344	0.83	2.0	-53.7	**342.3**	0.12	0.24	**45**	1.1	**0.30**	207	0.39	0.35	
R.H.=80	**76**	380	334	0.88	1.7	-1.0	331.2	0.13	0.24	1	-	0.40	207	0.42	0.33	0.27
	3650	414	361	0.87	2.0	-31.8	**359.3**	0.13	0.29	**27**	1.9	**0.30**	207	0.42	0.35	

In the *F.E.M.*, the effects of a seasonal temperature change of 10 °C is analysed. The seasonal temperature profile represents the effect of a slab casted in the winter. The effect of the temperature on the stress behaviour is shown in Fig:9.2. It can be concluded that seasonal temperature can result in earlier cracking and that cooling of the slab during its lifetime can initiate cracking. Therefore, cracking is most likely in the period after the summer when the concrete starts to cool down. The seasonal temperature change also influence the crack width behaviour. The crack widths follows the seasonal changes shown in Fig: 9.2b. Warming up of the floor reduces temporarily the crack widths.

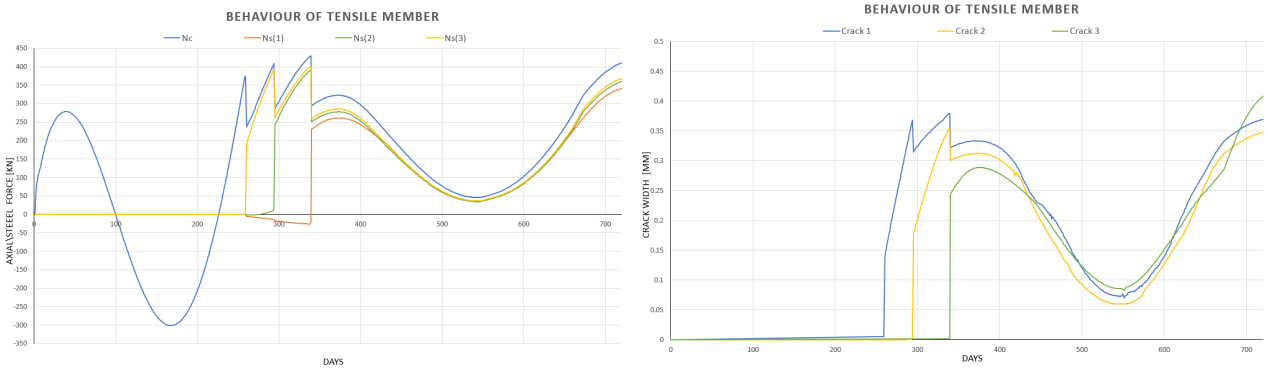

(a) Stress behaviour

(b) Crack width behaviour

Figure 9.2: Seasonal temperature influence casted in the winter

Shrinkage profile

The shrinkage profile does influence the stress behaviour. The uniform strain load of the gradient shrinkage profile is 25% less than the uniform shrinkage profile for the assumed profiles. It is just concluded that less strain load result in a small increase in crack width because the cracks are initiate later and less crack will be formed. Also, the shrinkage gradient results in an axial force combined with a positive bending moment. The shrinkage gradient will induce flexural cracking. Therefore, the axial cracking stress σ_{cr} should be enhanced to the flexural cracking stress $\sigma_{cr,fl}$. When cracking occurs, the bending moment in the crack is assumed to be no longer present [33]. Only the axial force can be transferred in a direct tensile crack with centric or single layer reinforcement. The tensile force after cracking due to a shrinkage gradient is 75% of the cracking force based on the flexural cracking stress. For a 200 mm thick slab, the cracking stress is enhanced with 1.4 and then reduced with 25%. Therefore, the force in the crack due to the uniform and gradient shrinkage profile is almost equal because 1.4 times 0.75 is 1.05. The profile also results in a different moment of cracking. The moment of cracking will be later because the cracking stress is higher with the shrinkage gradient. The *Gilbert* is developed for a uniform shrinkage profile. Therefore, the calculations of the stresses, taking into account the bending moments, can not be performed with the model. The model can be used when an equivalent cracking stress is used, which takes into account the enhancement due to flexure and the reduction due to the lower uniform strain load present in the crack after cracking.

In Fig: 9.3a and 9.3b the influence of the shrinkage profiles is shown in the *F.E.M.*. The axial force after cracking is almost the same and cracking occurs slightly later in the member with the shrinkage gradient. The crack widths at the surface in the uniform loaded model are found to be slightly higher compared to the gradient shrinkage load. This can come from the fact that less strain load is applied to the member, which is contrary to the findings from the analytical model.

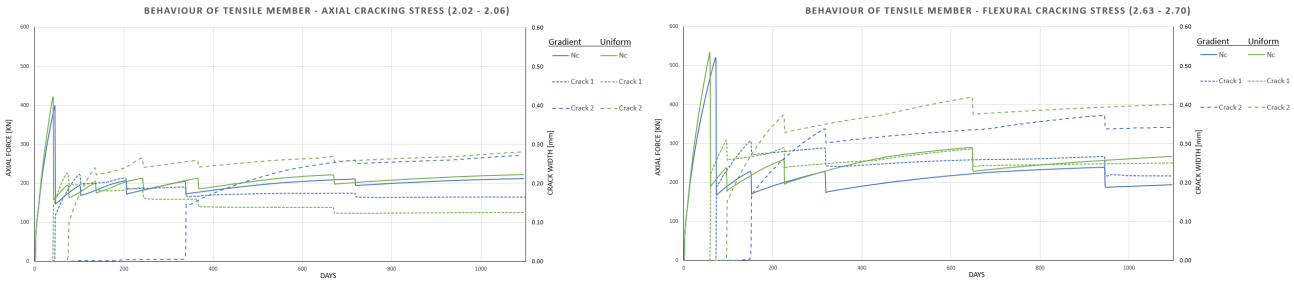

(a) Axial cracking stress

(b) Flexural cracking stress

Figure 9.3: Comparison shrinkage profile on behaviour

9.2 Reinforcement

In the design process, the amount and position of reinforcement of the reinforcement is often a discussion. On the one hand, the minimum reinforcement is desired to reduce the construction cost. The amount, layout and type of reinforcement affect the stress and cracking behaviour of the *S.o.G.*. The bonding quality is also essential to realise an effective reinforced concrete structure. The influences of these aspects are analysed with respect to *S.o.G.*.

Position

The position of the reinforcement is generally in the tensile zone of the concrete structure. For rack loading on *S.o.G.*, this means in the bottom layer under the point load and in the top layer between the legs of the rack. For serviceability crack width control, which is only at the surface of the slab, the reinforcement should be placed in the top layer for the most efficient result. When large positive and negative bending moments are expected, the reinforcement is placed in both the top and bottom of the slab. This results in four possible reinforcement layouts. Top, bottom, centric and top plus bottom. In Fig: 9.4, the effect of the reinforcement position on the crack pattern is shown for a uniform shrinkage load after three years. The reinforcement ratio ρ_s is constant for all models. Eccentric top reinforcement results in one large uncontrolled crack at the bottom fibre followed by multiple controlled cracks in the top surface. The most effective layout to reduced the cracks at the surface is to place the reinforcement as close as possible to the surface. The same crack pattern is

found for the bottom reinforcement with one large uncontrolled crack in the top surface, which is undesired. Therefore reinforcement is wanted near the surface of the slab. Top and bottom reinforcement better control the cracks compared to only centric reinforcement. Nevertheless, the crack width at the surface is still wider than the common limit of 0.3 mm. Top reinforcement is the best method to control the cracks at the surface.

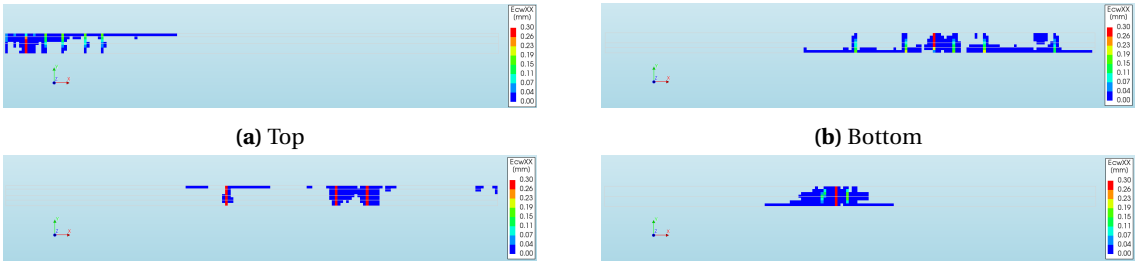

(a) Top

(b) Bottom

(c) Top and bottom

(d) Centric

Figure 9.4: Reinforcement lay-out

It is found that eccentrically placed reinforcement results in a bending moment in the uncracked zone after the first crack. The bending moment results in flexural stresses in the slab. Therefore, the flexural cracking stress should be taken for the secondary cracks that occur. So the first crack is initiated when the stress is equal to the σ_{cr} and the secondary cracks at the top will be formed when the stress is equal to $\sigma_{cr,fl}$ in eccentric reinforced members. This is almost impossible to take into account in the analysis. In Fig: 9.5, the stress and cracking behaviour is shown for the *F.E.M.* with an axial cracking stress and a flexural cracking stress. The actual behaviour will be more like a combination of the σ_{cr} up to the first crack with the behaviour of $\sigma_{cr,fl}$ after the first crack.

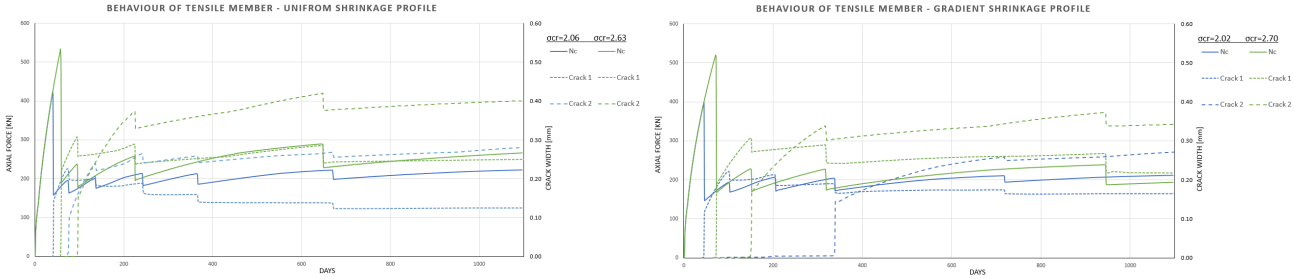

(a) Effect of cracking stress with uniform profile

(b) Effect of cracking stress with gradient profile

Figure 9.5: Influence of cracking stress

The bending moment depends on the force and the eccentricity of the reinforcement. In Fig: 9.6, the development of a bending moment in the uncracked zone is shown for a uniform shrinkage loaded top reinforced *R.T.M.*. The bending moment is also determined analytically with the steel stress in the first crack. The bending moment is calculated by multiplying the steel stress $\sigma_{s,cr}$ times the eccentricity of the reinforcement. The amount and the development of the bending moments are in good agreement. Eccentrically placed reinforcement changes the forces from an axial force to a combination of axial force and bending moment after cracking. For top reinforcement, the bending moment in the uncracked zone is negative after the first crack. The negative bending moment initiates secondary cracking in the top surface. The secondary cracking reduces the negative bending moment.

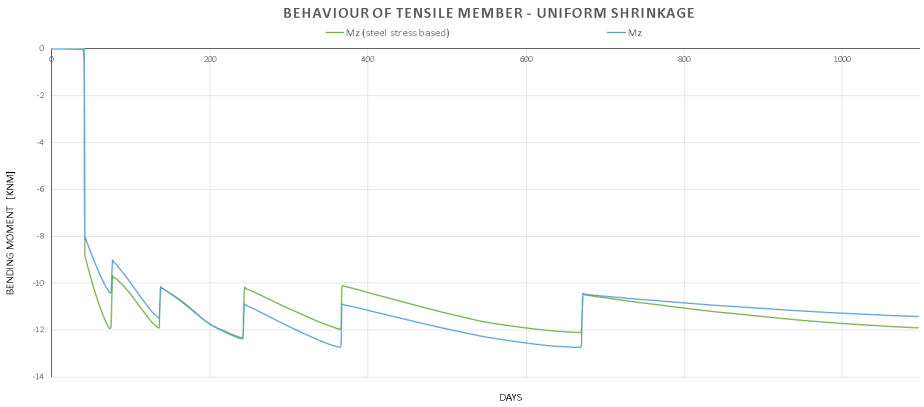

Figure 9.6: Development of bending moment in top reinforced *R.T.M.* due to cracking

The eccentricity effect is analysed in the notched and restrained tensile member and compared with the analytical model. An relaxation factor ψ_{crack} in the *R.T.M.* of 0.95, 0.84 and 0.63 for an eccentricity of respectively 25, 50 and 75 mm were found. The *N.T.M.* resulted in ψ_{crack} of 0.88, 0.75 and 0.62 for respectively 25, 50 and 75 mm eccentricity. The analysis showed that the eccentricity of the reinforcement increases the crack relaxation effect and therefore reduces the steel stress in the tensile member.

The eccentricity factor α_{cr} according to the *Vencon* model for a 200 mm thick slab are 0.8, 0.67 and 0.57 for respectively 25, 50 and 75 mm of eccentricity. The effect of the eccentrically placed reinforcement on the stress and cracking behaviour in the analytical model can be seen in Tab: 9.5. The reduction of $\sigma_{s,cr}$ result in smaller crack widths according to all models. Relaxation factors ψ_{crack} of 0.70-0.66 and 0.59-0.56 are calculated for eccentricities of 25 and 50 mm depending on the moment in time. These relaxation factors are larger compared to the *F.E.M.*. It is stated that for eccentricities larger than 25 mm, the *VENCON2.0* model is not applicable. From the analysis, it is found that the effect is still present for larger eccentricities but to a smaller extent than the model calculates. Significant larger stress reduction than 33% is not found in *N.L.F.E.A.*. Therefore, it is advised to use the eccentricity model with a maximum eccentricity of 25% of the slab height.

Table 9.5: Effect of eccentric reinforcement

		Breugel	Gilbert					Breugel		Gilbert			*M.C. 2010*		CUR-65	Stufib-11
Parameter	t	N_{cr}	$N_{c_{(t)}}$	ψ_{crack}	$\sigma_{c1_{(t)}}$	$\sigma_{s1_{(t)}}$	$\sigma_{s,cr}$	w_{mo}	w_{max}	Cracks	s_m	w_{max}	l_t	w_{max}	w_{max}	w_{max}
Eccentricity=0	49	371	326	0.88	1.6	-1.0	323.4	0.13	0.23	1	-	0.35	207	0.41	0.32	0.27
	3650	414	344	0.83	2.0	-53.7	342.3	0.12	0.24	45	1.1	0.30	207	0.39	0.35	
Eccentricity=25	49	371	261	0.70	1.6	-1.0	256.3	0.08	0.14	1	-	0.28	182	0.23	0.22	0.19
	3650	414	275	0.66	2.0	-53.7	270.1	0.08	0.13	45	1.1	0.24	182	0.22	0.24	
Eccentricity=50	49	371	219	0.59	1.6	-1.0	212.8	0.06	0.10	1	-	0.23	157	0.13	0.16	0.14
	3650	414	230	0.56	2.0	-53.7	224.4	0.06	0.10	45	1.1	0.20	157	0.12	0.17	

The *Vencon* model is also analysed by the developers with a parameter study (h=250 mm, $\varnothing$=16 mm and C35/45). In Fig:9.7, the results of the analysis are shown. It is found that a higher eccentricity reduces the required reinforcement ratio ρ_s significantly. Furthermore a smaller reinforcement diameter $\varnothing$ also reduces the required ρ_s. The *N.L.F.E.A.* confirms the findings in the parameter study that reinforcement is necessary near the top fibre of the slab to reduce the crack width.

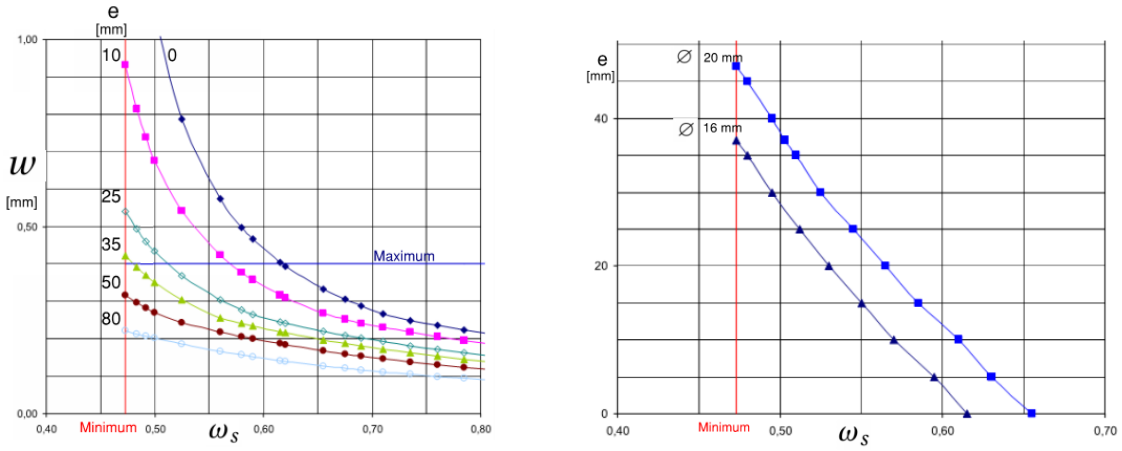

(a) Influence of eccentricity

(b) Min required ρ_s for w_{max}<0.4mm

Figure 9.7: Parameter study of VENCON 2.0

Amount of reinforcement

It is generally known that more reinforcement reduces the crack width[54]. The same conclusion is found in this thesis. The results are shown in Tab:9.6. The reinforcement ratio has a significant influence on the cracking behaviour. Significantly more cracks occur with a higher ρ_s because of a smaller transfer length l_t. The cracking force slightly increases, but the final force in the crack reduces when the ratio is increased, e.g., the crack relaxation coefficient reduces in the long-term. In Tab:9.6, the results of the analytical analysis are shown. In the final row of the table, the results are shown of an eccentric low reinforced *R.T.M.*, which is also analysed with the use of the *N.L.F.E.A.* shown in Fig: 9.8.

Table 9.6: Analysis of stresses and crack width

		Breugel	Gilbert					Breugel		Gilbert			*M.C. 2010*		CUR-65		Stufib-11	
Parameter	t	N_{cr}	$N_{c_{(t)}}$	ψ_{crack}	$\sigma_{c1_{(t)}}$	$\sigma_{s1_{(t)}}$	$\sigma_{s,cr}$	w_{mo}	w_{max}	Cracks	s_m	w_{max}	l_t	w_{max}	w_{max}	$\sigma_{s,cr}$	w_{max}	$\sigma_{s,cr}$
ρ_s=0.32	49	368	288	0.78	1.5	-2.1	435.0	0.24	1.22	1	-	0.67	270	-	0.64	393	0.57	569
	3650	411	352	0.86	1.9	-54.4	-	-	-	19	2.6	0.71	270	-	0.71	435		
ρ_s=0.50	49	371	326	0.88	1.6	-1.0	323.4	0.13	0.23	1	-	0.35	207	0.41	0.32	258	0.27	367
	3650	414	344	0.83	2.0	-53.7	342.3	0.12	0.24	45	1.1	0.30	207	0.39	0.35	285		
ρ_s=1.00	49	380	349	0.92	1.8	-0.3	174.2	0.04	0.07	1	-	0.16	151	0.15	0.13	142	0.09	191
	3650	423	297	0.70	2.0	-53.2	147.8	0.03	0.05	176	0.3	0.08	151	0.10	0.14	154		
ρ_s=0.32	37	415	112	0.27	0.6	-8.74	102.5	0.02	0.03	1	-	0.14	205	-	0.32	248	0.29	379
F.E.M.	1095	467	306	0.66	1.7	-50.1	275.7	0.08	0.14	2	2.5	0.37	205	0.11	0.36	275		

Minimum reinforcement ratio $\rho_{s_{min}}$

The reinforcement ratio in practice is often lower than the minimum value. In theory, this will result in yielding of the reinforcement, which is shown in the table for ρ_s=0.32 were steel stresses of 435 MPa and higher are found. The theoretical minimum reinforcement ratio for σ_{cr}=2.03 MPa, α_e=6.67 and taken into account the reduction for an indoor slab is 0.41%. From the *N.L.F.E.A.*, it is found that the reinforcement yield when it is evenly distributed over the height of the cross-section. When the reinforcement is applied in the top layer, the steel stress in the reinforcement remains below the yield stress. In Fig:9.8 the axial force $N_{c_{(t)}}$ and the steel stresses in crack of crack 1, 2, 3 and 6 is shown for h=200mm, cover=34.5 mm, ρ_s=0.32%, σ_{cr}=2.03 MPa. The maximum steel stress $\sigma_{s,cr}$ in the model is 300 MPa. Crack relaxation factors ψ_{crack} of 0.38 and 0.54 for respectively after the first crack and after one year were found. Due to the substantial crack relaxation effect, the steel stresses are not reaching the yield stress. After cracking, the tensile area in the cross-section is significantly lower in an eccentrically reinforced member, which results in a larger effective reinforcement ratio. The eccentric reinforcement also induces a negative bending moment in the uncracked zone after the first crack. Therefore secondary cracks are initiated at the top where the effective reinforcement is relative high. This results in a controlled crack at the top, which tends to a maximum of 0.3 mm. The *F.E.M.* is compared with the analytical models. The practical based crack width calculation method *CUR-65* and Stu*fib*-11 give the best results regarding the crack widths with maximum values of 0.36 and 0.32 mm, but the steel stress

is significantly overestimated by Stu*fib*-11. The steel stress, according to the *Gilbert* and *CUR-65* is in good agreement. The *Gilbert* underestimates the number of cracks. This is because the model is only valid for a centrally reinforced tensile member. It can be seen that the crack width reduces every time a new crack occurs. The crack width of the first crack is significantly reduced in time were the secondary cracks remain quite constant in width.

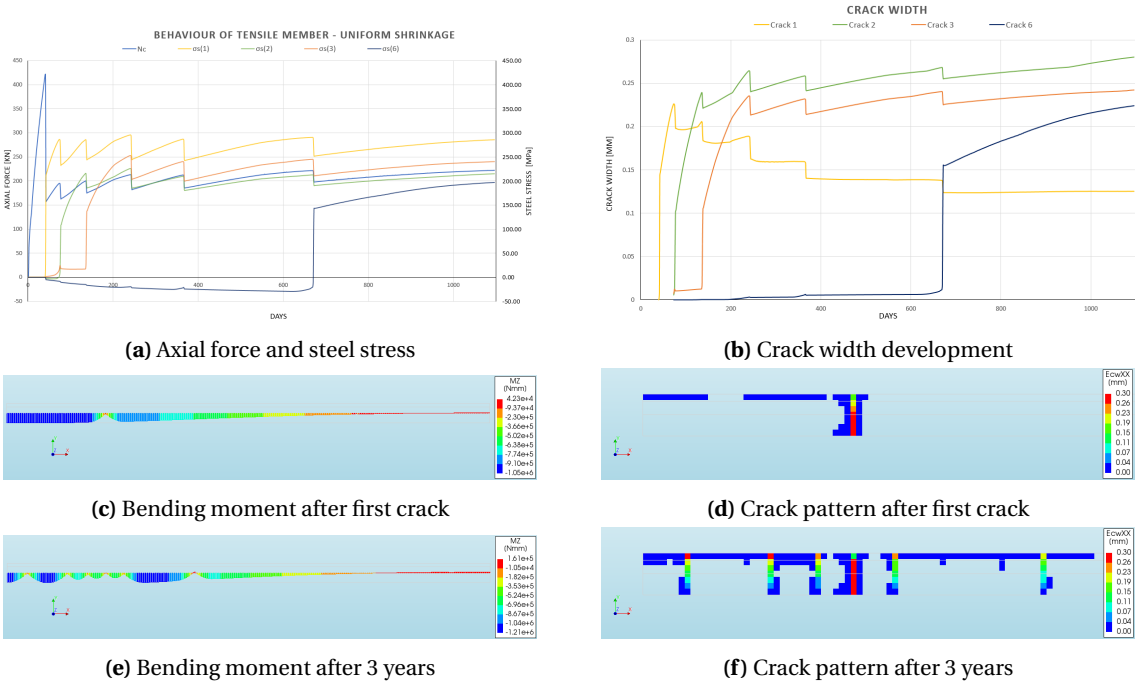

(a) Axial force and steel stress

(b) Crack width development

(c) Bending moment after first crack

(d) Crack pattern after first crack

(e) Bending moment after 3 years

(f) Crack pattern after 3 years

Figure 9.8: Stress behaviour in low reinforced tensile member

Quality of reinforcement

The quality of the reinforcement regarding cracking is based on the interaction of the rebar with the concrete specified as the bond-slip quality. It is found that the bond-slip has a considerable influence on the crack pattern and the crack width. If the bonding quality is good and sufficient reinforcement is applied and new cracks will be formed. For bad bonding quality, slipping can occur with one dominant crack as a result. In Fig: 9.9, the effect of bonded and slipping reinforcement is shown. In the *F.E.M.*, slipping occurs when the axial force is higher than the bond-interface capacity. The bond-slip capacity is based on the *M.C. 2010* parameters and mainly depends on the concrete class. In the slipping *R.T.M.*, due to a reduced bonding capacity, one dominant crack results in an undesirable crack width of 0.8 mm after 300 days.

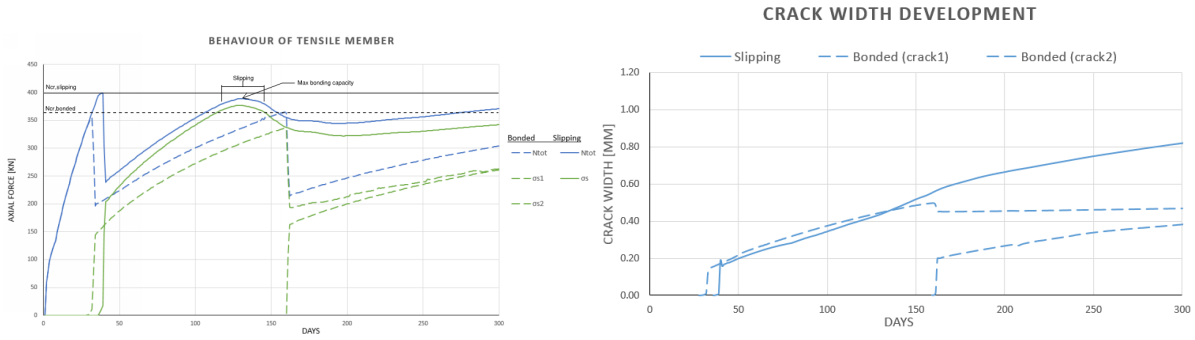

(a) Stress behaviour of slipping reinforcement

(b) Crack width development

Figure 9.9: Behaviour of dominant crack

In the bonded *R.T.M.*, the cracking stresses are reached in the uncracked zone and new cracks are formed. Due to the formation of multiple cracks, the maximum crack width in the member is 0.5 and 0.4 mm for respectively the first and second crack. The width of the two cracks together is almost equal to the width of the

dominant crack. Therefore, more cracks are favourable and dominant cracks should be avoided. The same effect occurs when the reinforcement yields. This can be done by ensuring that the reinforcement capacity and the bond-slip capacity is higher than the cracking force N_{cr}. The bonding capacity can be enhanced by, for example, reducing the reinforcement diameter, adding steel fibres or adding more fine particles to the concrete mixture.

The effect of bond-slip on the crack behaviour is also examined with the use of the *N.T.M.*. This is done to exclude the influence of the random field on the behaviour. In general, for external loads, a lower bonding capacity results in a larger crack width. A lower capacity increases the transfer length. The maximum steel stress is load dependent and is for external loading often constant during cracking. For imposed loading, the same conclusion is found. A lower bonding quality results in larger crack width. However, contrary to external loading, the steel stress significantly reduces during cracking when bad bonded reinforcement is used. The axial force reduces more when wider cracks are formed. This crack relaxation effect is more present in members with lower bond-slip capacity. This behaviour can be seen in Fig: 9.10a. For fully, good and bad bonded reinforcement crack relaxation factor ψ of respectively 0.69, 0.67 and 0.54 are found. After 100 days, the crack width of bad and good bonding is 25% and 10% higher compared to fully bonded reinforcement, Fig:9.10b.

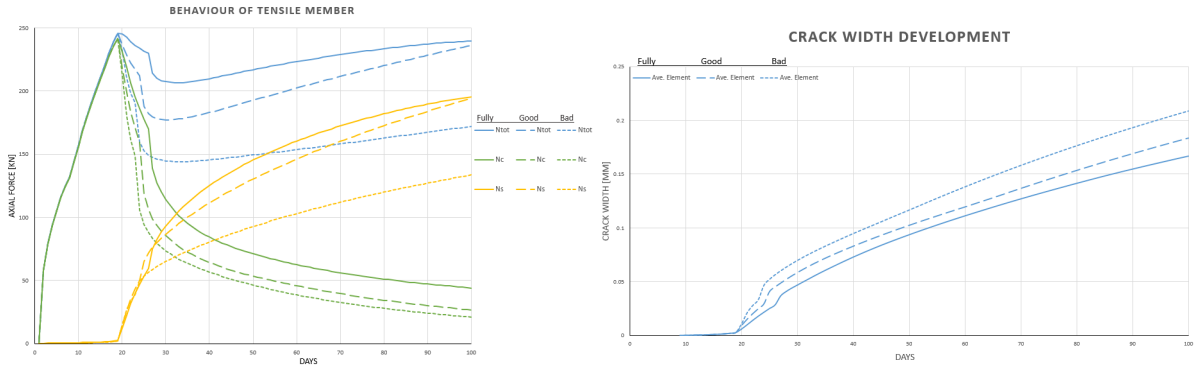

(a) Force behaviour

(b) Crack width development

Figure 9.10: Effect of bond-slip capacity

In general, the crack width depends on the transfer length and the steel stress in the crack. A smaller reinforcement diameter results in a higher bonding capacity. This results in a smaller transfer length and, thus, a smaller crack width for the same steel stress. For the analytical method, the bonding effect is investigated by changing the diameter ∅. In the mean crack width formula of *Van Breugel*, the reinforcement diameter has a considerable influence. When the diameter is twice as big, the crack width increases with approximately 80%. Smaller ∅ resulted in smaller transfer length, which resulted in a smaller cracking zone, which finally results in an overall stiffer tensile member after cracking. Therefore, the crack relaxation effect is less present for good bonded reinforcement. This results in slightly higher axial forces after cracking and thus higher steel stresses in the crack. The increased steel stress results in a small increase of the average steel strain in the cracked zone, which should lead to an increase in crack width. This effect was not found in the results. The reason is that the transfer length is significantly lower for good bonded reinforcement compared to the strain increment due to the higher steel stress in the crack. Therefore, the crack width is eventually smaller for good bonded reinforcement, even with the higher steel stress. Both the analytical model and the *F.E.M.* result in a significantly smaller crack width when bonding quality is increased.

The bond-slip behaviour significantly influences the stress and cracking behaviour in *R.T.M.* loaded by imposed deformation. Therefore, the bond-slip behaviour should be mandatory in *N.L.F.E.A.* in *R.T.M.*. This is contrary to the suggestion made in the *N.L.F.E.A.* guideline R.T.D. which advises to use embedded reinforcement. It should be mentioned that the guideline is specially set-up for the analysis of existing civil structures. Besides that, the cracking phase in this research is *N.F.D.C.P.* were general design is often in the *F.D.C.P.* due to the external load. Embedded reinforcement can be used for *U.L.S.* design checks or for analysis where fully developed crack patterns are present.

9.3 Concrete mixture

Earlier it was found that the composition of the concrete mixture has a large influence on the elastic stress behaviour. The influence of the mixture is also analysed with respect to the cracking behaviour. According to all the models, a higher concrete class significantly increases the steel stress in the crack, which increases the crack width. The higher member stiffness, due to the higher concrete class, increases the crack widths and result in lesser cracks after ten years. The higher cracking stress for higher concrete classes leads to a significant increase in the cracking force. A lower Young's modulus, taken into account by the aggregate type, result in significantly later cracking. The strain load in the first crack is, therefore, higher, which results in a large crack width. Choosing cement type S results in a delay of crack initiation and thus an increase in cracking strength σ_{cr}, which finally results in wider cracks. According to the crack width models of *Gilbert* and *Breugel*, cement type R result in a significant decrease of crack width after ten years. The number of cracks is significantly higher for cement R after ten years than cement S, 32 compared t0 65. The moment of the first crack and the total number of cracks influence the crack widths largely. When the cracking factor α_{cr} is increased from 0.6 to 0.8 and 1.0, the reinforcement yield and equilibrium in the crack can not be found according to the analytical model of *Gilbert*. The crack widths according to *CUR-65* and Stu*fib*-11 are increased from 0.32 and 0.27 mm to 0.56 and 0.65 mm for α_{cr}=0.6 and 1.0. A higher α_{cr} delays the moment of cracking from 49 days to 125 days. The same effect is found when the relaxation coefficient ψ is reduced. Cracking is initiated after approximately 102 day's for ψ=0.5 compared to 29 day's for ψ=1.0. More strain load is required to initiate cracking in the *R.T.M.* due to the concrete relaxation effect. Again the crack width models of *Gilbert* and *Breugel* are largely influenced by ψ. Concrete relaxation will result in fewer cracks. The cracking force at cracking is therefore higher. With respect to crack control it can be concluded that concrete relaxation in not beneficial for *R.T.M.* loaded by *I.D.*. The same tendency is found in the *N.L.F.E.A.*. For controlled cracking, the concrete mixture should consist of a low concrete class, cement type R, stiff aggregate such as basalt, low cracking strength and low relaxation effect.

The effect of the concrete mixture with respect to the cracking behaviour is analysed with the use of the *F.E.M.*. The stress and cracking behaviour of "good" and "bad" concrete are compared and shown in Fig:9.11a. The slab structure and reinforcement are kept constant. Good concrete according to the crack width models is cement type R, C20/25 and basalt aggregate type. Bad concrete is composed with cement type S, C35/45 and sandstone aggregate. The bad concrete mixture results in slipping of the reinforcement due to the high cracking stress. The behaviour is significantly influenced by the concrete mixture and can be the difference between acceptable controlled cracking and undesired uncontrolled cracking. The stresses and crack widths, calculated with the analytical models for the good and bad concrete mixtures, are given below in Tab:9.7. A large variation is found for different types of concrete mixtures. The complete analysis can be found in App: F.

Table 9.7: Influence of concrete mixture

		Breugel	Gilbert				Breugel		Gilbert	*M.C. 2010*			CUR-65		Stufib-11
	t	N_{cr}	ψ_{crack}	$\sigma_{c1_{(t)}}$	$\sigma_{s1_{(t)}}$	$\sigma_{s,cr}$	w_{mo}	w_{max}	Cracks	s_m	w_{max}	l_t	w_{max}	w_{max}	w_{max}
"Bad"	125	690	0.90	2.3	-76.0	435	0.45	2.28	65	2.5	0.73	207	0.47	0.59	0.65
"Good"	29	250	0.78	1.3	-0.8	248	0.09	0.15	20	0.8	0.24	207	0.27	0.25	0.23

With the use of special measurements such as *S.R.A.* and expansion additives, the shrinkage can be reduced to a certain extent that cracking does not occur. Even in fully restrained *S.o.G.*, the concrete stress does not reach the cracking stress when concrete mixtures measurement is taken and concrete relaxation is taken into account during calculations. In Fig:9.11b, the analysis of a *R.T.M.* with the concrete properties C30/37, Cement type S, Sandstone aggregate, ψ=0.5, $\sigma_{cr,fl}$=2.39 MPa and α_{sra}=0.8. The seasonal temperature effect of ΔT=2.5 °C is also taken into account to simulate the maximum strain load on the *S.o.G.*. This figure shows that cracking can be prevented in *S.o.G.*.

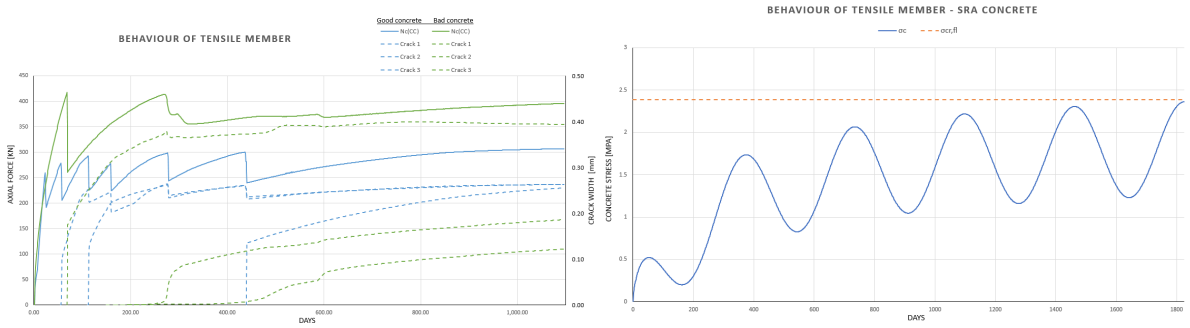

(a) Effect of concrete mixture on cracking

(b) *S.R.A.* concrete mixture result in no cracks

Figure 9.11: Effect of concrete mixture on behaviour

From the *N.L.F.E.A.*, it came forward that the combination of the creep model and cracking is not practical in the *N.L.F.E.A.*. A tendency is found that the combination of creep and bond-slip results in cracking parallel to the reinforcement. Due to the concrete relaxation effect, the concrete can undergo more strain load before it cracks. The reinforcement does not move because of the steel stress, which makes equilibrium in the crack. The strain difference between the concrete and reinforcement is, therefore, more substantial along with the reinforcement in the cracked zone. The higher strain difference results in local cracking along with the reinforcement, which results in a slipping behaviour of the reinforcement. Therefore the time-dependent effect of concrete relaxation results in larger crack widths. This can be taken into account by using the long-term bonding properties according to Section: 4.2 in *N.L.F.E.A.*. Besides the cracking behaviour, also the computational time is increased with ±10% when the creep compliance function is used compared to the *A.A.E.M*. The outcome of the creep compliance function is compared with the simplified *A.A.E.M* method given in App: C. The results of the models are in good agreement.

9.4 Stresses: Analytical model v.s. *N.L.F.E.A.*

The stress behaviour calculated with the *Gilbert* model is in good agreement for the *R.T.M.* with centric reinforcement. The analytical model only overestimates the number of cracks and the steel stress compared with the *N.L.F.E.A.*. In Fig: 9.12 the behaviour is shown in a 5 meter long *R.T.M.* with ρ_s=0.5%, h=200 and σ_{cr}=1.81 MPa. A maximum crack width at the location of the reinforcement of 0.32 mm was found. The crack width from the analytical calculations were 0.26, 0.27, 0.34, 0.28 and 0.35 mm for respectively *Van Breugel*, *Gilbert*,*M.C. 2010*, Stu*fib*-11 and *CUR-65*. The crack width model of *CUR-65* and *M.C. 2010* give the best results regarding the crack width.

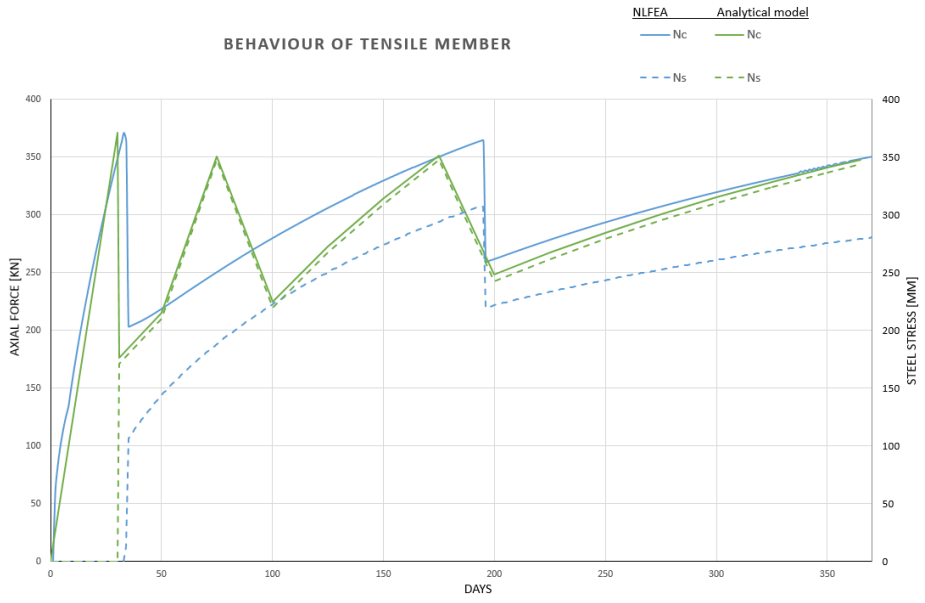

Figure 9.12: *N.L.F.E.A.* vs Analytical model for centric *R.T.M.*

In practice, the reinforcement is always placed in the top layer. Therefore the model is checked for eccentrically placed reinforcement. From the analysis, it came forward that after the first crack, an effective tensile zone is present in the member due to the bending moment in the uncracked zone. Therefore, the analytical model is adopted by using the effective reinforcement ratio for all calculation methods according to the *M.C. 2010*.

The analysis is done for a typical concrete slab of 200 mm high, C30/37, and upper reinforcement of 9-100 mm with a cover of 30 mm. The eccentric reinforcement results in flexural cracks at the top surface. Therefore, the flexural cracking stress of $f_{ctm,fl}$=2.63 is used in the analysis. The reinforcement ratio $\rho_{s_{eff}}$ in the analytical model was 0.93%. The slab is loaded with a uniform shrinkage profile. No measurements were taken to reduce the imposed stresses by creep.

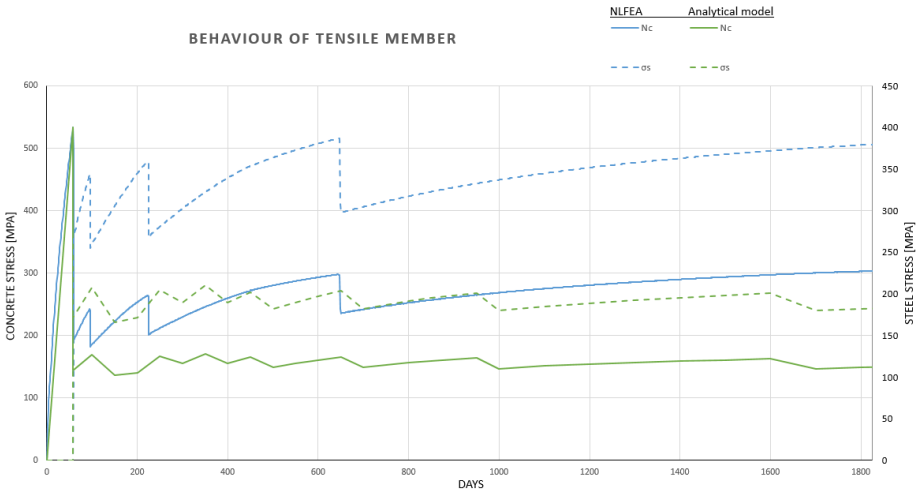

Figure 9.13: *N.L.F.E.A.* vs Analytical model for eccentric *R.T.M.*

In Fig: 9.13, the axial force calculated with the analytical model and the *N.L.F.E.A.* is shown. In App: F, the results of the crack width calculations are given. The maximum crack width at the top, according to the *N.L.F.E.A.*, was 0.43 mm after five years of shrinkage. The crack widths according to the models of *Van Breugel*, *Gilbert*, Stu*fib*-11 and *CUR-65* were respectively 0.07, 0.12, 0.12 and 0.46 mm. The crack width calculation of *M.C. 2010* do not result in crack width because the steel stress σ_s is not larger than the steel stress at cracking $\sigma_{s,cr}$ according the model with the effective ratio $\rho_{s_{eff}}$. Also, in the eccentric reinforced member, the crack width model of *CUR-65* gives the best result regarding the crack width. The models based on the steel stress in the crack significantly underestimates the crack width when the effective reinforcement ratio is applied. When the effective reinforcement ratio is not taken into account the crack widths were 0.38, 0.54, 0.33, 0.53 and 0.46 for respectively *Van Breugel*, *Gilbert*,*M.C. 2010*, Stu*fib*-11 and *CUR-65*. It should be stated that the steel stresses in the crack were 383, 540 and 372 MPa according to *Gilbert*, Stu*fib*-11 and *CUR-65* models. The crack widths and steel stress are not in good agreement with the *N.L.F.E.A.*. Theoretical yield or underestimation of the crack width is results when the analytical methods for centric reinforced concrete structures are transferred into an eccentric model. Only the *CUR-65* model result in representative crack width values because it is based on an enhanced cracking bending moment based on practical experience.

From the analysis, it can be concluded that the translation of the centric reinforced *R.T.M.* to an eccentric reinforced member is not accurate. The effective height of the tensile zone and the flexural cracking stress are assumptions that influence the stress and cracking behaviour greatly. Considerable variation is found in the crack width and steel stress because of the assumptions and changes to the models. The *CUR-65* model, which is based on the bending cracking moment of the cross-section, gives the most accurate result when compared with the *N.L.F.E.A.*.

9.4.1 Validation of *N.L.F.E.A.* with hand calculations

The stress profile in a restrained tensile member with top reinforcement loaded by a uniform shrinkage load is analysed. The stresses are analytically determined and compared with the result in the *N.L.F.E.A.*. The situations of just prior to cracking at t=31 days, directly after the first crack at t=34 days and before the localisation of the secondary flexural crack at t=69 day's are analysed. The relevant parameters of the slab on grade are: slab height h= 200 mm, Young's modulus E_{cm}= 32836.4 MPa, restrained length $L_{restraint}$= 5 meter, *F.E.M.* width b= 100 mm, reinforcement # 9-100 mm with a concrete cover of 30 mm to the top-fibre which result in a eccentricity e of 65.5 mm. The random field application generated a field with the lowest tensile strength capacity of 1.82 MPa located in the middle of the slab at the bottom fibre, Fig: 9.14.

According to the general plate theory, the stress-strain relation in the plane of the plate in the axial direction is given below. The Poisson ratio ν for concrete is taken as 0 in the model with the plain stress element to simulate the same structural behaviour of a plain strain element model.

$$\sigma_{xx,c(t)} = \frac{E_{cm}}{1-\nu^2} \cdot \left(\epsilon_{xx,(t)} + \epsilon_{yy,(t)} \cdot \nu\right) \tag{9.101}$$

$$\sigma_{xx,c(t)} = E_{cm} \cdot \epsilon_{xx,(t)} \tag{9.102}$$

$$\tag{9.103}$$

In the *F.E.M.* the strain load $\epsilon_{[x](t)}$ at t=31 depends on the % which is developed of the autogenous ϵ_{ca} and drying ϵ_{ds} shrinkage. The analytical determined stresses are equal to the axial stresses S_{xx} in the model shown in Fig:**??**.

$$\epsilon_{xx,(t)} = \frac{\%}{100} \cdot \epsilon_{ca} + \frac{\%}{100} \cdot \epsilon_{ds} \tag{9.104}$$

$$\epsilon_{xx,(31)} = 0.67 \cdot 5 \cdot 10^{-5} + 0.07 \cdot 31.3 \cdot 10^{-5} \tag{9.105}$$

$$\epsilon_{xx,(31)} = 5.54 \cdot 10^{-5} \tag{9.106}$$

$$\sigma_{xx,c(31)} = 5.54 \cdot 10^{-5} \cdot 32836.4 = 1.82 MPa \tag{9.107}$$

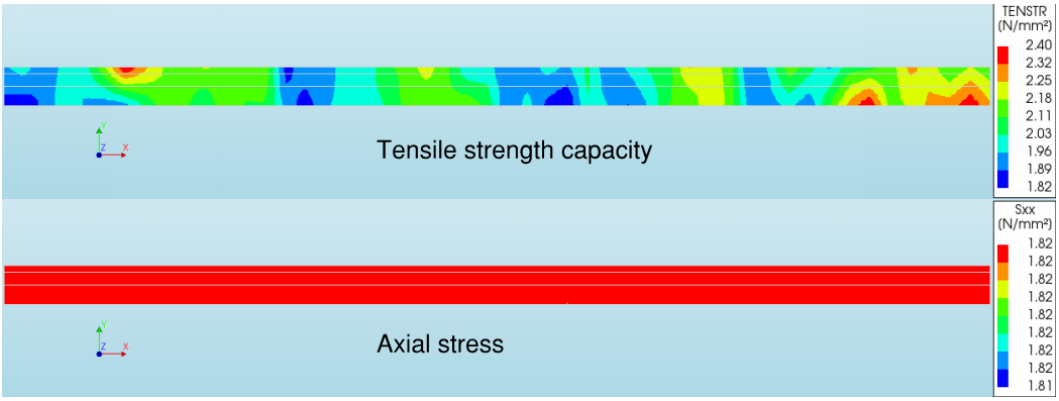

Figure 9.14: Behaviour in the *R.T.M.* at t=31 day's

Crack localisation takes three days in the model. The stress situation is determined in the uncracked zone next to the crack where the negative bending moment is the highest. Before it is stated that the crack relaxation effect is due to the reduction of the strain load by the appearance of the crack. The strain reduction $\Delta\epsilon_{crack(t)}$ in the uncracked zone by the crack is assumed to be equal to the average crack width over the cross-section divided by the total restrained slab length $L_{restraint}$. It was also stated that the negative bending moment in the uncracked zone is equal to the tensile force in the reinforcement times the eccentricity of the reinforcement. Both assumptions are checked below at t=34:

$$\Delta\epsilon_{crack(t)} = \frac{Meancrackwidth}{L_{restraint}} \tag{9.108}$$

$$\epsilon_{xx,(34)} = 0.69 \cdot 5 \cdot 10^{-5} + 0.08 \cdot 31.3 \cdot 10^{-5} - \frac{0.21}{5000} \tag{9.109}$$

$$\epsilon_{xx,(34)} = 5.88 \cdot 10^{-5} - 4.26 \cdot 10^{-5} = 1.62 \cdot 10^{-5} \tag{9.110}$$

$$\sigma_{xx,c(34)} = 1.62 \cdot 10^{-5} \cdot 32836.4 = 0.53 \qquad MPa \tag{9.111}$$

$$N_{c(34)} = A_c \cdot \sigma_{xx,c(34)} = 10.6 \qquad kN \tag{9.112}$$

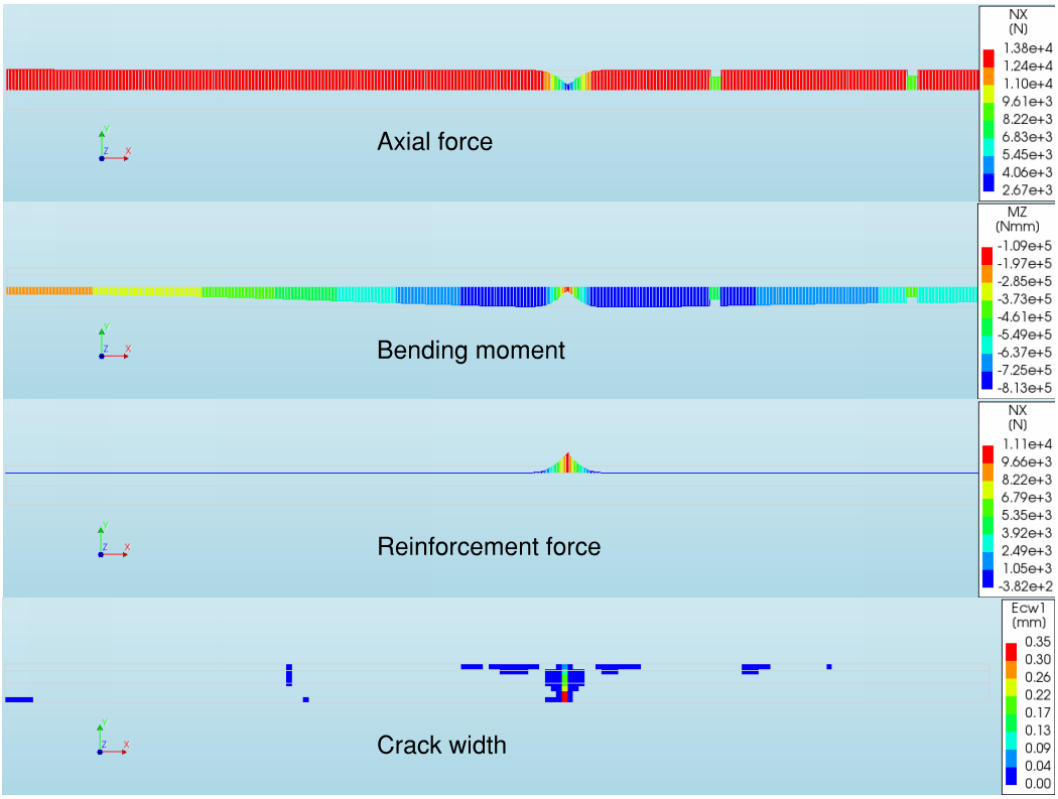

Figure 9.15: Behaviour in the *R.T.M.* at t=34 day's

The structural behaviour of the *R.T.M.* in the *F.E.M.* is shown in Fig:9.15. In the model the concrete can still transfer tensile stresses in the crack. For comparing the analytical result with the *F.E.M.* output, the axial tensile force in the uncracked zone in the model is reduced with the axial concrete tensile force in the crack, $N_{c[fem]} = 13.8 - 2.67 = 11.1$ kN. The axial force is in good agreement with the analytical calculated value. This axial force has to be transferred by the reinforcement in the crack. It can be seen that this occurs in the *F.E.M.* shown in figure below. The maximum bending moment in the uncracked zone in the *F.E.M.* is -0.81 kNm. When the negative bending moment in the crack, due to the residual tensile strength of concrete, is subtract from the maximum bending moment, the reinforcement induces a bending moment of -0.70 kNm. This is in good agreement with the assumed analytical calculation showed below.

$$M_{c(t)} = N_{c(t)} \cdot e \tag{9.113}$$

$$M_{c(34)} = 10600 \cdot -65.5 = -0.69 \qquad kNm \tag{9.114}$$

In the cross-section of the maximum negative bending moment the stress profile is compared. The analytical stresses are determined with the axial tensile force and the negative bending moment in the cross-section.

$$\sigma_{top,(t)} = \frac{N_{c(t)}}{A_c} - \frac{6 \cdot M_{c(t)}}{b \cdot h^2} \tag{9.115}$$

$$\sigma_{top,(34)} = \frac{10600}{100 \cdot 200} - \frac{6 \cdot -0.69 \cdot 10^{-6}}{100 \cdot 200^2} = 0.53 + 1.04 = 1.57 \qquad MPa \tag{9.116}$$

$$\sigma_{bottom,(t)} = \frac{N_{c(t)}}{A_c} + \frac{6 \cdot M_{c(t)}}{b \cdot h^2} \tag{9.117}$$

$$\sigma_{bottom,(34)} = \frac{10600}{100 \cdot 200} + \frac{6 \cdot -0.69 \cdot 10^{-6}}{100 \cdot 200^2} = 0.53 - 1.04 = -0.51 \qquad MPa \tag{9.118}$$

Over time, the maximum tensile stress increases due to the additional shrinkage load. At t=69, the axial stresses reaches the tensile stress capacity in the top-fibre of 1.93 MPa. The axial force and bending moment are determined according to the same assumptions as before shown in Fig: 9.16.

$$\epsilon_{xx,(69)} = 0.81 \cdot 5 \cdot 10^{-5} + 0.16 \cdot 31.3 \cdot 10^{-5} - \frac{0.36}{5000} \tag{9.119}$$

$$\epsilon_{xx,(69)} = 9.07 \cdot 10^{-5} - 7.10 \cdot 10^{-5} = 1.97 \cdot 10^{-5} \tag{9.120}$$

$$\sigma_{xx,c(69)} = 1.97 \cdot 10^{-5} \cdot 32836.4 = 0.65 \qquad MPa \tag{9.121}$$

$$N_{c(69)} = A_c \cdot \sigma_{xx,c(69)} = 12.9 \qquad kN \tag{9.122}$$

$$M_{c(69)} = 10600 \cdot -65.5 = -0.85 \qquad kNm \tag{9.123}$$

$$\sigma_{top(69)} = \frac{12900}{100 \cdot 200} - \frac{6 \cdot -0.85 \cdot 10^{-6}}{100 \cdot 200^2} = 0.65 + 1.28 = 1.93 \qquad MPa \tag{9.124}$$

$$\sigma_{top(69)} = \frac{12900}{100 \cdot 200} + \frac{6 \cdot -0.85 \cdot 10^{-6}}{100 \cdot 200^2} = 0.65 - 1.28 = -0.63 \qquad MPa \tag{9.125}$$

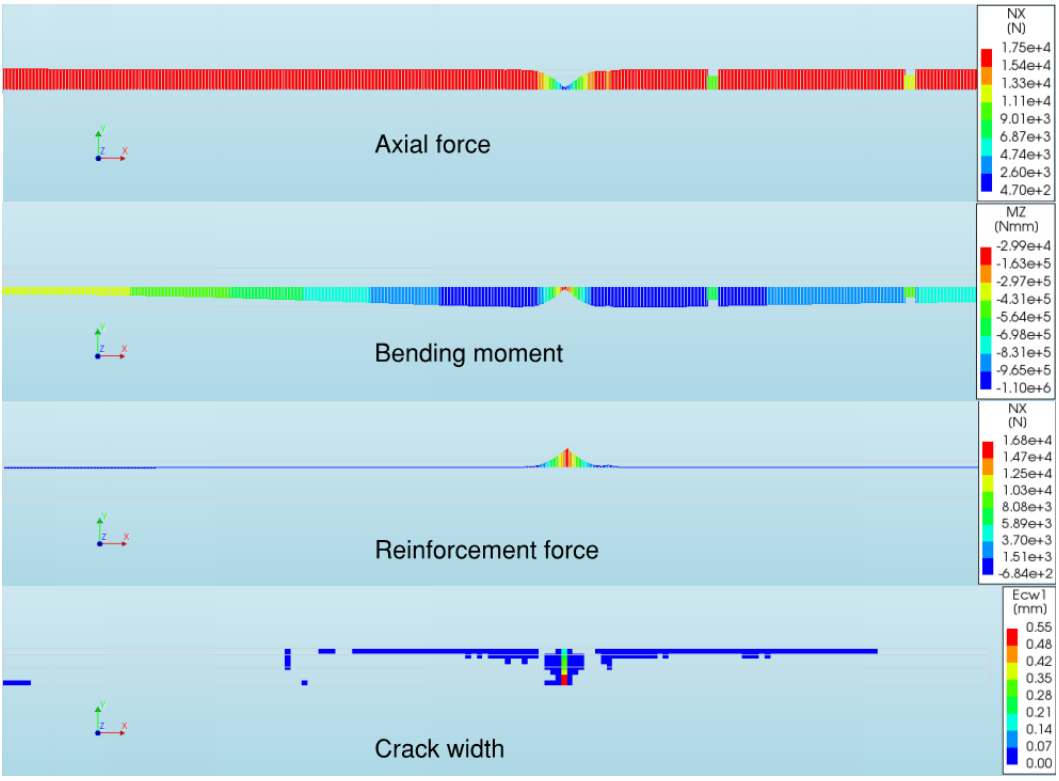

Figure 9.16: Behaviour in the *R.T.M.* at t=69 day's

Both the analytical stresses and the *F.E.M.* stresses are shown in Fig:9.17. The stress profile is in good agreement for the situation after the first crack. The stress profile, just before the second crack occurs at the top fibre, is not in line with the analytical linear stress profile. In the *N.L.F.E.A.*, a large cracking zone is present just before crack localisation is initiated. This results in a distribution of the peak stresses and a non-linear stress profile over the cross-section. On the other hand, the composed axial force and bending moment in the model are in good agreement with the analytically calculated force and bending moment. Overall, it can be concluded that the structural behaviour of *F.E.M.* is validated with hand calculations.

(a) Stresses at t=34 day's

(b) Stresses at t=69 day's

Figure 9.17: Stresses over the cross-section in *R.T.M.* loaded by shrinkage

9.5 Cracking: Analytical models v.s. *N.L.F.E.A.*

Multiple crack width models are compared in this analysis. The following is concluded from the analysis.

The two models *Van Breugel* and *M.C. 2010* are based on the steel stress in the crack. In this research, the steel stress is determined with the *Gilbert*, which takes into account the crack relaxation effect in *R.T.M.* loaded by *I.D.*. Wider cracks reduce the axial tensile force in the uncracked zone. This force has to be transferred in the crack by the reinforcement. Contrary to the general engineers' instinct, wider cracks reduce the steel stress in the crack in imposed loaded restrained structures. Therefore, steel stress-based crack width models can not be combined with the steel stress, according to *Gilbert*.

Gilbert

The *Gilbert* also provided a crack width formulae. The method is based on the strain equilibrium in the reinforcement in the uniformly distributed reinforced *R.T.M.* loaded by an *I.D.*. The method gives good results for the determination of the crack pattern and crack width. The effect of bending moment due to loading or eccentric reinforcement results in abnormal results. Therefore, the model can only be used for uniform shrinkage loading and centric reinforced *R.T.M.*. With the model, the crack spacing s_m is also estimated. The crack spacing varies between 0.5 and 2 m for cracking after 10 years and is mostly governed by the amount of shrinkage and reinforcement.

Stu*fib*-11

To overcome this problem, the Stu*fib*-11 advises to calculate the representative steel stress in the crack with the cracking force N_{cr} based on the 28-day concrete properties. In practice, the *S.o.G.* are sometimes constructed with less then the minimum required reinforcement ratio ρ_s. This will result in the yielding of the reinforcement. In the analysis, steel stresses of 540 MPa were calculated. In reality, due to the crack relaxation effect, the steel stresses in the crack will not be that high. For the calculation of the crack width, Stu*fib*-11 also uses the *Van Breugel* only with a fixed enhancement factor of 1.7 instead of the steel stress-based enhance-

ment factor γ_∞. The factor γ_∞ would be unrealistic high which results in an overestimation of the maximum crack width. The Stu*fib*-11 also takes into account the eccentricity effect of the reinforcement with α_{ecc}. This effect significantly reduces the steel stress in the crack. From the analysis, it is found that the eccentricity factor should be limited, α_{ecc} >0.67. Due to the combination of the axial force and bending moment, flexural cracks occur in the *S.o.G.*. The translation of the flexural cracks to the crack width model of *Van Breugel* for direct tensile cracks is not applicable for design purposes. An effective reinforcement ratio can be used, but the determination of the correct value is based on many effects. In the analysis, it is shown that an effective reinforcement ratio, based on the provision *M.C. 2010*, did not results is the desired outcome. The model is the most applicable for *R.T.M.* with uniformly distributed were full-depth cracks occur.

CUR-65

The *CUR-65* model based on the enhanced cracking moment of the concrete cross-section gives the best result for eccentric reinforced *S.o.G.* when compared with the *N.L.F.E.A.* outcome. The eccentric reinforcement, after the first crack, and the shrinkage gradient results in a combination of an axial force and bending moment in the uncracked zone. For the design calculation, the crack width at the surface has to be estimated. Therefore, the enhanced cracking moment is a logical method to estimate the crack width at the surface in *S.o.G.*. It is found that *I.D.* always results in flexural cracking at the surface in eccentric reinforced *R.T.M.*. Due to the increased axial force after cracking, the crack width will be larger in time than directly after cracking. Also, the ageing of the concrete affects the cracking moment. In general, the cracking moment is determined with the 28-days concrete properties. If cracking occurs later, the flexural cracking strength can be higher. This combination results in the enhancement factor of the cracking moment of 1.4, which is determined with practical findings. From the *N.L.F.E.A.* results, it can be concluded that the factor 1.4 is in good agreement with the results and give slightly conservative results. Therefore this method is advised for the design calculations of the crack width at the surface in *R.T.M.* with eccentric reinforcement loaded by *I.D.*.

Post-analysis in *N.L.F.E.A.*

Three methods were given for the determination of the crack width in the *F.E.M.*. The method based on the maximum steel stress in the crack underestimates the crack width. The same reason as for the *Gilbert* and *Van Breugel* holds here. The best method to determine the crack width is with the average crack width per element. The crack width can directly be taken from the model at every location. It is important to check whether the crack is localised in one element. The mesh size should, therefore, be according to the recommendation.

Hybrid reinforced structure

The calculation methods for the crack width in the hybrid structure are based on the reduction of the cracking stress σ_{cr} by the residual tensile strength capacity σ_{R1} of the *S.F.R.C.*. It is found that not all models are suited for the implementation of this method. Only the provision *M.C. 2010* gives comprehensive information on the crack width calculation method for hybrid reinforced concrete, which can be used in the *N.F.D.C.P.*. On the assumption that steel fibres have to be activated in the crack, the pull-out method is developed. From the analysis, it is found that this method does not result in the same results as in the *N.L.F.E.A.*. On the other hand, the model can be used to get insight in the effect of adding steel fibres to the concrete. In the App: F, the results from the analytical models can be found. It is found that a higher pull-out stiffness reduces the steel stress in the crack. The fibres can take up more stress at the same crack opening. Therefore the steel stress reduces. No large steel stress reductions were found when more or better fibres were used, $\pm 25 MPa$. Were the steel stress difference between conventional and hybrid reinforcement was $\pm 80 MPa$. When the residual tensile strength of the *S.F.R.C.* is increased, the transfer length reduces. A reduction of l_t results in significantly more cracks, according to the *Gilbert*, resulting in smaller crack widths. The crack widths variate a lot between the analytical models. Therefore it is questionable which method is the most appropriate.

When the long-term effects are not taken into account, the residual tensile strength σ_{R1} can higher than the cracking stress used in the models (strain hardening *S.F.R.C.*). This results in a negative steel stress and, therefore, no crack width value. In the literature, it was found that σ_{R1} can be reduced in time up to 40% due to the sustained loading. This should be taken into account for *R.T.M.* loaded by *I.D.*.

The effect of hybrid reinforced concrete are analysed in the *N.T.M.* to investigate the effect of the fibres on the

crack width in the *F.E.M.*. The assumed *S.F.R.C.* properties for this analysis are σ_{R1}= 1.45 MPa and 1.74 MPa for respectively C30/37-3D 30 kgm^{-3} and C30/37-4D 30 kgm^{-3}. In Fig: 9.18a, the residual axial capacity of the *S.F.R.C.* can clearly been seen after cracking. Where the contribution of the concrete in the crack reduces in time due to the increasing crack width, the contribution of the *S.F.R.C.* remains constant in the crack. The residual strength reduces only at large strains in the *S.F.R.C.*. Therefore, the reinforcement has to transfer less force in the crack. Also, the cracking is more gradual, which is in agreement with the findings in the literature. Adding steel fibres reduces the steel stress in the crack significantly. Therefore, the post-analysis crack width check in the *F.E.M.* based on the steel stress extremely underestimates the crack width for hybrid concrete and can not be used. The crack widths are reduced with approximately 17% and 23% for respectively C30/37-3D 30 kgm^{-3} and C30/37-4D 30 kgm^{-3} compared to conventional reinforcement. Adding steel fibres to the concrete with conventional reinforcement reduces the crack width in the tensile member. The best design method for the crack width in the *N.F.D.C.P.* in *R.T.M.* loaded by *I.D.* is not found.

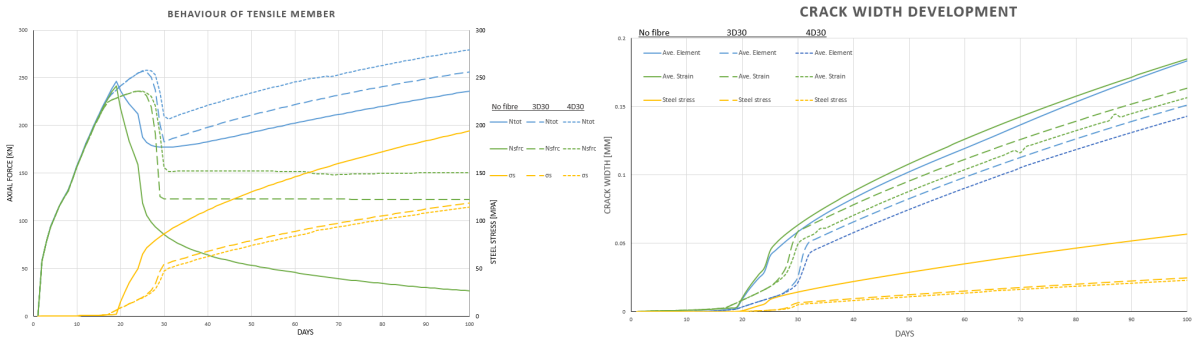

(a) Concrete force and steel stress

(b) Crack width in *N.T.M.*

Figure 9.18: Cracking behaviour of hybrid reinforcement

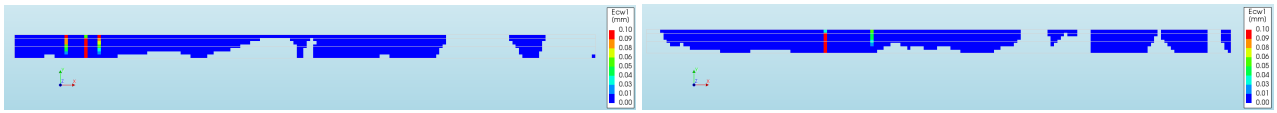

(a) Crack pattern of C30/37-3D-30kgm^{-3}in *R.T.M.*

(b) Crack pattern of C30/37-4D-30kgm^{-3} in *R.T.M.*

Figure 9.19: Cracking behaviour after one year of eccentric hybrid reinforcement ρ_s=0.32%

10. External Loading

The external loading on a *S.o.G.* is from rack loading. The common design method for the calculation of the stresses in the *S.o.G.* from point loads is still often based on the pioneering work of *Westergaard* in 1926. Westergaard developed a linear-elastic approach for the calculation of the maximum stresses in a *S.o.G.*. The design formulae give the tensile stresses in the outer fibre of the slab for an internal and edge point load. The formula for the points loads in the corner gives the maximum tensile stresses in the surface of the slab. The linear elastic approach of slabs on a continuous elastic support is comprehensively elaborated in App: G. Over the years, many engineers have made derivations and improvements on the approach of *Westergaard*. All the methods are investigated and explained in the appendix. Besides the *Westergaard* approach, a yield line approach is suggested by *Meyerhof* to calculate the upper-bound failure capacity of the slab. Still, both approaches result in a large difference between the experimental and theoretical cracking load of the slab. During experiments, the failure load of the slab was found to be four times higher than the *Westergaard* prediction model. The *Westergaard* solutions give conservative results and overestimates the deflections of the slab[64]. The reasons found in the literature for the conservative results are:

- Membrane action in the slab [65]
- Higher capacity of the soil than the design value. This can come from neglecting the shear interaction of soil in the *Winkler* soil model. *Pasternak* soil model can be used for internal loads[64].
- Failure of the slab does not happen according to the prediction models. The practical failure in the experiments is when the load capacity is no longer increasing. In the elastic approach, the failure is when stresses are equal to the concrete cracking stress.[66].

Even though it is known that these methods are conservative, the methods are still used and applicable for design purposes. Both the improved elastic approach of *Westergaard* and the plastic yield line prediction model *Meyerhof* can be found in the provisions *CUR-36* and *TR-34*. To have a better understanding of the behaviour under point loads, a sensitivity analysis is performed on the parameters of the elastic design approach of *Westergaard*. First, the stress behaviour in a slab due to a point load is given.

10.1 Stress behaviour

In Fig: 10.1 the general behaviour of *S.o.G.* loaded by a point load is shown. The point load induces a positive bending moment beneath the point load and a negative bending moment at a certain distance in the slab. The bending moment will be zero at a distance l_{rs}, which is defined as the radius of the relative stiffness. The relative stiffness takes into account the interaction of the slab and soil foundation. The positive bending moment under the point load is higher than the negative bending moment. Therefore the first crack is initiated beneath the point load. After cracking, the negative bending moment increases next to the point loads. In this zone, secondary cracking can occur due to the point loads. Cracking at the surface is undesirable, and therefore, the effect of the point loads is analysed. To investigate the behaviour in *S.o.G.* loaded by point loads, the linear approach is analysed.

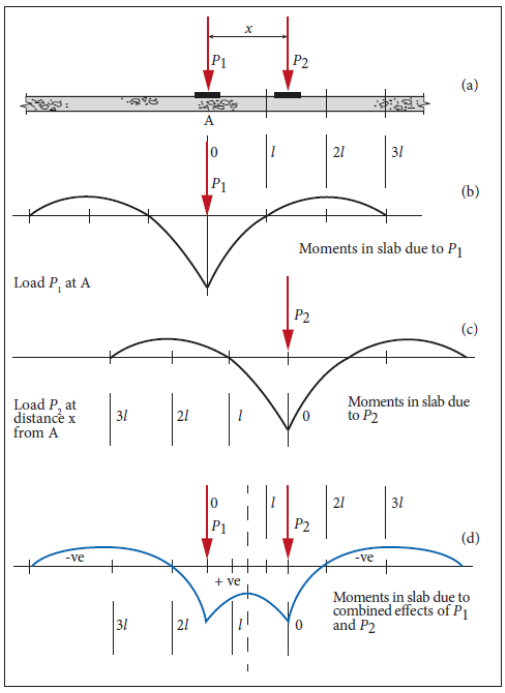

Figure 10.1: Bending moments in slab

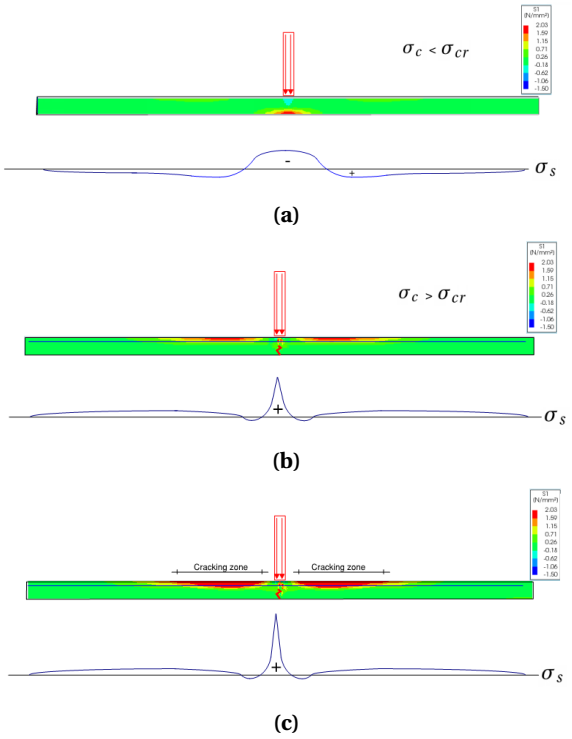

Figure 10.2: Cracking behaviour in slab

Elastic approach

The original formula of *Westergaard* is based on the relation between the point load and the slab height and on the relation between the loading area and the relative stiffness radius. First, the relative stiffness is analysed. Finally, the other parameters are investigated. For this analysis, the range of parameters given in Tab:10.1 are used.

Table 10.1: Range of parameters

Parameter	**Value**			**Unit**
Young's modulus E_{cm}	10	20	30	GPa
Slab height	120	180	240	mm
Concrete class	C20/25		C30/37	-
Subgrade modulus k_{mod}	0.01	0.05	0.10	$\mathrm{N\,mm^{-3}}$

For the calculation of the stresses in the slab the approach by *A. Abbas* is used. The general approach of *Westergaard* is conservative. Therefore, all the derivations of the approaches are analysed. The complete analysis can be found in App: G. It became apparent that the approach of *Abbas*, which is developed with the use of *L.F.E.A.*, results in lower stresses, which makes the prediction model less conservative[5]. In Fig: 10.3, the difference is shown between the methods for an equivalent load of 10 kN. The stresses calculated with the *L.F.E.A.* results in ≈ 30% lower stresses compared with the *CUR-36*. The *L.F.E.A.* method of *Abbas* is used in this thesis. The formula for the stresses in the slab due to a point load in the middle of the slab is given below.

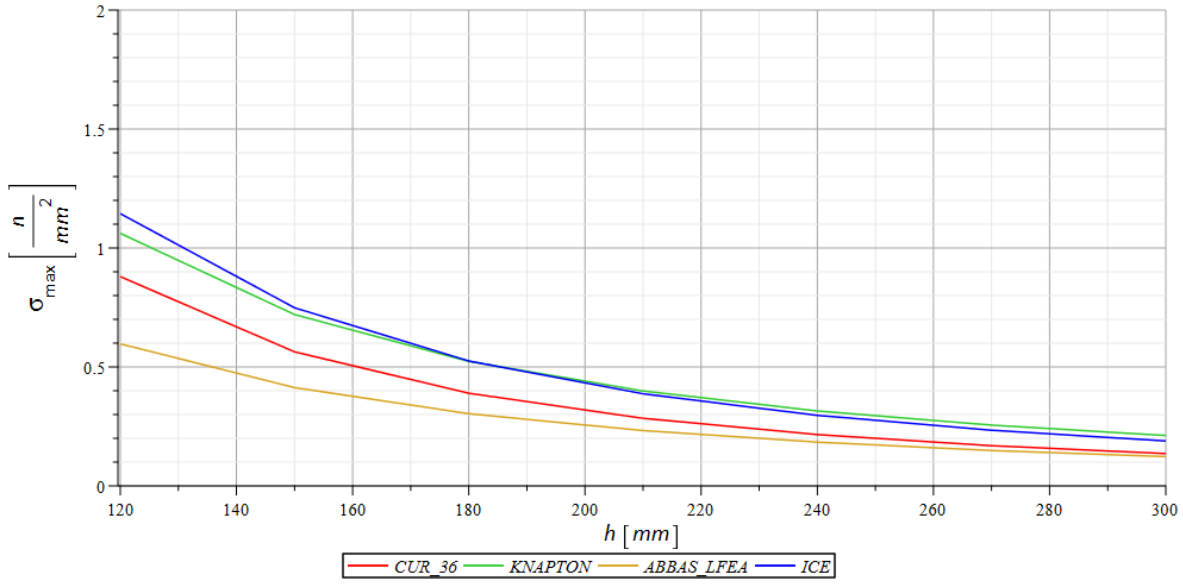

Figure 10.3: σ_{max} for interior load per method

$$\sigma_{LFEA,mid} = 1.0186 \cdot \left(1.1301 - 0.1362 \frac{L_{fp}}{b_{100}}\right) \frac{F}{h^2} \cdot \left(\log_{10}\left(\frac{l_{rs}}{b_{100}}\right)\right) \tag{10.126}$$

(10.127)

The radius of relative stiffness l_{rs} is an important parameter which relates the soil foundation to the concrete slab characteristics. The radius of relative stiffness determines the zone where the bending moments are positive or negative shown in Fig:10.1. The radius of relative stiffnes l_{rs} depends on the Young's modulus of concrete E_{cm},height of the slab h and the subgrade modulus of soil k_{mod}. The parameters are analysed within the range of practical values. The l_{rs} can be determined with the equation below. For a common concrete slab of E_{cm}=20000 MPa, h=175 mm and k_{mod}=0.05, the radius of relative stiffness is in the order of 654 mm.

$$l_{rs} = \sqrt[4]{\frac{E_c h^3}{11.73 k_{mod}}} \tag{10.128}$$

$$\sigma_{LFEA,max} \propto f\left(\log_{10}\left(\frac{l_{rs}}{b_{cone}}\right)\right) \qquad \text{with} \quad b_{cone} = 100 \tag{10.129}$$

$$\sigma_{LFEA,max} \propto f\left(1.1301 - 0.1362\left(\frac{l_{fp}}{b_{100}}\right)\right) \tag{10.130}$$

The effect of the relative stiffness radius l_{rs} on the stress is based on a log scale relation between l_{rs} and the loading area (b_{100}). In Fig:10.4a, the enhancement coefficient, based on the relation on the stress, is shown. It can be seen that a larger stiffness radius increases the stresses. For the assumed parameters, the radius is in the range of 493 to 999 mm. This results in a factor of approximately 0.65 and 1.

The width of the footplate l_{fp} is related to the fixed value b_{100}. The enhancement factor of the loading area to the maximum stress is shown in Fig: 10.4b. Using a bigger footplate beneath the point load also reduces the principal stress in the *S.o.G.*. Changing the footplate from 120x120 mm to 200x200 or 300x300 mm results in stress change from 2.36 to 2.00 or 1.68 MPa.

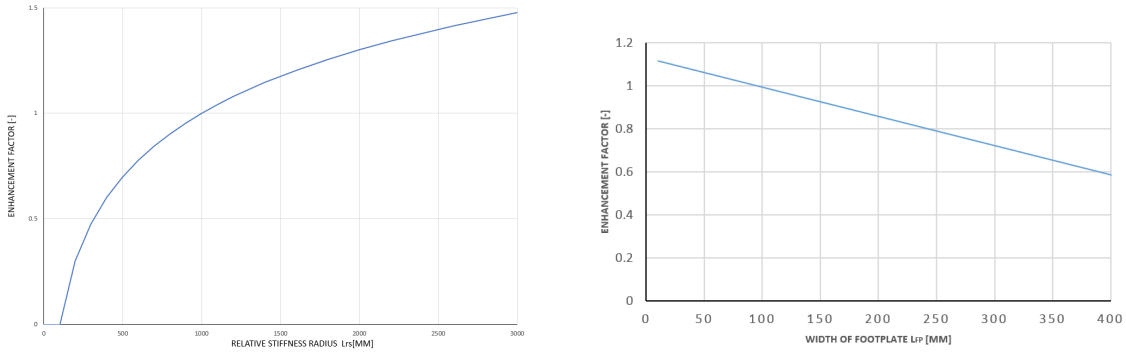

(a) Influence of l_{rs}

(b) Influence of l_{fp}

Figure 10.4: Enhancement factor on $\sigma_{LFEA,mid}$

10.2 Sensitivity analysis

The stress and cracking behaviour due to a point load are also analysed with the use of the *N.L.F.E.A.*. The downside of the 2D *F.E.M.* is that is the point load must be translated to an equivalent line load. Therefore, for all the models, an equivalent point load F_{eqv} is calculated. With the same parameters, the principal stress $\sigma_{LFEA,mid}$ due to a point load of 90 kN is determined. In the *F.E.M.*, the principal stress σ_{Sxx} is determined for a certain line load. Based on the linear relation between the stresses and the point load, the equivalent point load is determined with the following relation:

$$F_{eqv} = \frac{90}{\sigma_{LFEA,mid}} \cdot \sigma_{Sxx} \tag{10.131}$$

Equivalent point loads of 210 kN were used during the analysis for the mean parameters. For the investigation of the effect of the parameters, the outcome of the results is also scaled based on the relation between the equivalent point load and 90 kN. The translation of the point loads to line loads based on the *westergaard* theory is questionable. 3D analysis should be performed to analyse the true global behaviour due to point loads. The stresses due to a point load of 90 kN, according to the *Abbas* model, are in the range of 2.05-2.73 MPa for 180 mm thick slabs. The long-term flexural tensile stress of C30/37 is 2.47 MPa. Therefore, a point load of 90 kN on its own does not always result in cracking in the *S.o.G.*. Especially when the relaxation effect is taken into account, when the stresses are combined with the shrinkage stresses, cracking can occur. This is analysed in the next section, where shrinkage and external loads are combined.

The stress behaviour in the fully restrained slab changes after cracking. First, one large crack at the point load positions occurs. After cracking, there is a significant increase of the negative bending moment in the uncracked zone with a maximum value at 1.5-2 times the relative stiffness radius from the point load. The bending moment is larger than the cracking moment of the concrete slab; only no cracks at the top are observed. This is because there is a large axial compressive force N_{uncr} found in the slab after cracking. This axial compressive force reduces the maximum tensile stress in the uncracked zone. The steel stress in the first crack is low because no bending moment can be induced due to the small internal level arm. The crack at the position of the point load behaves like a hinge in the slab. After cracking the slab wants to move towards the sides. Because the slab is restrained, an axial compressive force is formed. In Fig:10.6, the behaviour before and after cracking is given. The local deviations in some graphs are due to the small misalignment of the nodes in the mesh with the composed line. The crack by the point load does not appear on the surface of the slab.

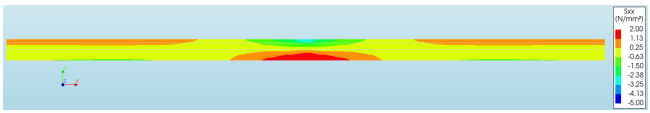

(a) Concrete stresses

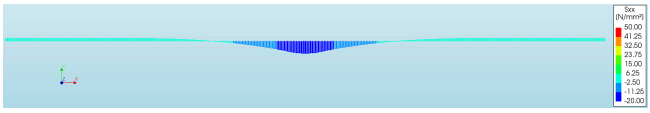

(b) Steel stresses

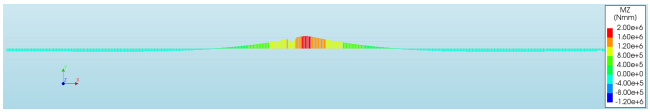

(c) Bending moment

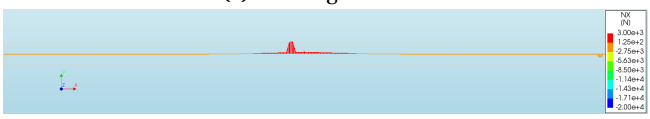

(d) Axial force

(e) Crack width

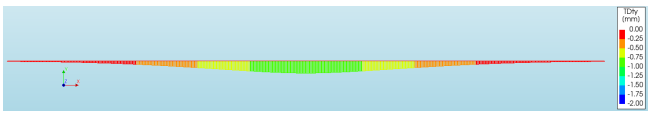

(f) Vertical displacement

Figure 10.5: Before cracking

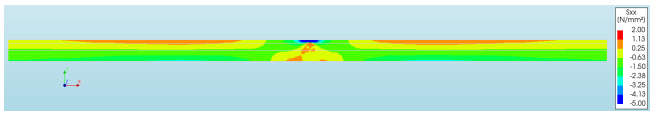

(a) Concrete stresses

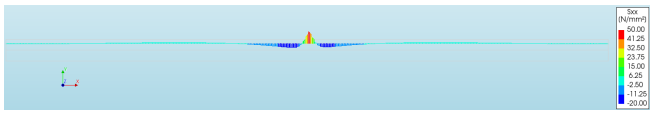

(b) Steel stresses

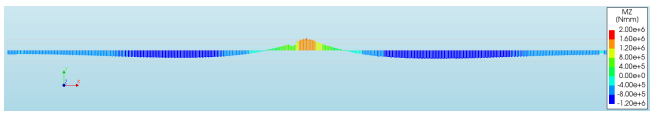

(c) Bending moment

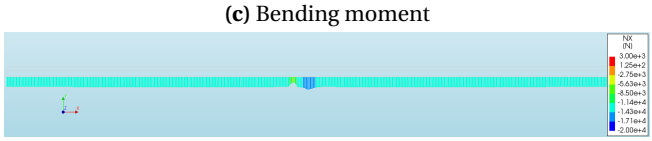

(d) Axial force

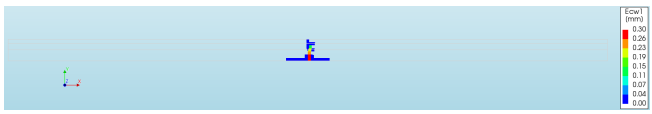

(e) Crack width

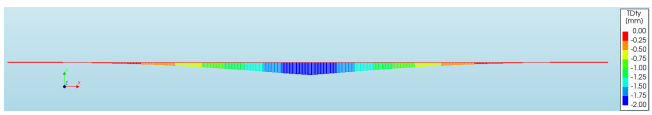

(f) Vertical displacement

Figure 10.6: After cracking

In the *N.L.F.E.A.*, the slab is reinforced with 9-100 mm and a loading area of 100x100 mm is assumed. All the scaled results are shown in Tab:10.2. The results are scaled to a point load of 90 kN with the earlier described method. The bending moment is given for the crack and uncracked zone. Also, the maximum stress based on the *L.F.E.A.* approach is given. The influence of the slab boundaries, soil foundation and concrete mixture on the relative stiffness radius and the principal stresses are elaborated for the linear and non-linear models.

Table 10.2: Analysis of parameters of *S.o.G.* loaded by a 90 kN point load

	k_{mod}=0.01	k_{mod}=0.05	k_{mod}=0.10	E_{cm}=10000	E_{cm}=20000	E_{cm}=30000	h=120	h=180	h=240	σ_{cr}=1.12	σ_{cr}=1.76	σ_c<σ_{cr}	σ_c»σ_{cr}	Unit
σ_{cr}	1.76	1.76	1.73	1.8	1.76	1.74	1.63	1.76	2.1	1.12	1.76	1.60	1.98	Mpa
M_{cr}	9.50	9.50	9.34	9.72	9.50	9.40	3.91	9.50	20.16	6.05	9.50	8.64	10.69	kNmm^{-1}
l_{rs}	999	668	562	562	668	739	493	668	829	668	668	668	668	mm
$\sigma_{LFEA,max}$	2.73	2.26	2.05	2.05	2.26	2.38	4.26	2.26	1.41	2.26	2.26	2.26	2.26	MPa
$M_{z,cr}$	23.5	16.3	13.9	13.7	16.3	17.6	14.4	16.3	31.1	17.1	16.3	28.2	16.6	kNmm^{-1}
$M_{z,uncr}$	-20.9	-11.2	-10.4	-10.7	-11.2	-12.0	-9.5	-11.2	-10.6	-10.7	-11.2	-6.4	-11.0	kNmm^{-1}
N_{uncr}	-218	-134	-109	-115	-134	-146	-142	-134	-14	-136	-134	-1	-156	kNm^{-1}
$\sigma_{s,cr}$	73.6	46.8	30.2	61.1	46.8	34.2	143.0	46.8	-21.0	41.1	46.8	-27.8	41.3	MPa
d_Y	6	2	1	3	2	2	3	2	1	2	2	2	2	mm

Influence of slab boundaries

The slab boundaries are taken as the slab height, area of the point load and the amount of loading. The radius of relative stiffness is related to the slab height according to the following relation:

$$l_{rs} \propto \sqrt[4]{h^3} \qquad \frac{h_{max}}{h_{min}} = \frac{250}{100} = 2.5 \Longrightarrow l_{rs} \propto \sqrt[4]{2.5^3} \approx 1.99 \tag{10.132}$$

An increase in slab height results in a significantly larger relative stiffness radius. The increment of h from 100 mm to 250 mm results in a 99% increase of l_{rs}. An increase of l_{rs} means an increase in stresses. The slab height also influences the stresses directly. From the *N.L.F.E.A.* formula of *Abbas*, it is found that a thicker slab reduces the principal stress in the slab. The *L.F.E.A.* model, with k_{mod}=0.027 Nmm^{-3} and E_{cm}=30000 MPa,

resulted in a stress reduction of 62% when the height changed from 140 to 220 mm. In the *L.F.E.A.* of this research, with k_{mod}=0.05 N mm^{-3} and E_{cm}=20000 MPa,the effect was more present. A change of h from 140 to 220 resulted in a stress reduction of 67% from 4.26 to 1.41 MPa. The results from the analytical formula and the *F.E.M.* are in good agreement. Only a small difference is found. In the *N.L.F.E.A.*, it is found that the steel stress in the crack is significantly higher in the slender slab. The slab undergoes more rotation en vertical displacement. This results in higher steel stresses in the crack. Also, the axial compressive force is higher in the 120 mm thick slab. This results in a significant high compressive stress. However, cracking strains in the top surface are found. This is because there is a negative bending moment of three times the cracking bending moment present. Normally this results in excessive cracking, but due to the high compressive force, no crack localisation is found. Furthermore, thinner slabs result in larger vertical displacement. To summarise, both the beneficial compressive force and the negative bending moment significantly increases when the slab hight is reduced. The height of the slab determines if the slab will crack under the point load or not.

The force of the point load is linearly related to the stress in the linear approach. In the *N.L.F.E.A.*, it is found that the amount of loading determines if the concrete slab cracks or not. When the slab is not cracked, the bending moment at the position of the point load is higher than after cracking. The axial force in the slab is negligible before cracking. The vertical displacement increases after cracking. Displacement of 0.91 mm 1.35 mm was measured just before and after crack localisation due to an increasing point load, which results in an increment of 0.44 mm. Where in the uncracked slab, an increment of 0.07 mm was found per load step. Before cracking a compressive stress is present in the reinforcement, which changes to tensile stresses after cracking. It is also found that higher point loads increased the beneficial N_{uncr} but also in a higher negative $M_{z,uncr}$.

Influence of soil

A change of the k_{mod} from 0.01 to 0.1 results in a 44% decrease of l_{rs}. A higher soil quality will have some negative effect on the influence length.

$$l_{rs} \propto \sqrt[4]{\frac{1}{k_{mod}}} \qquad \frac{k_{mod,max}}{k_{mod,min}} = \frac{0.10}{0.01} = 10 \Longrightarrow l_{rs} \propto \sqrt[4]{\frac{1}{10}} \approx 0.56 \tag{10.133}$$

According to *Robins*, changing the subgrade modulus to a lower value, the vertical differential movement increases due to curling, but the stresses in the slab are not increased significantly[67]. This is contrary to the findings with *Abbas*. With the *L.F.E.A.* formula, it is found that changing k_{mod} from 0.013 to 0.082 results in a stress reduction of 22%. *Tomasovicova* also investigated the influences of the sub-base layer on the stresses and deflection of the slab with the use of *F.E.M.*. He showed that a stiffer sub-base decreases the slab deflection and principal stresses in the slab[68]. *Walker* stated that a large change of k_{mod} only causes small changes to the principal stresses[48]. Different results are found due to the different set-ups of the experiments and researches.

As mentioned, the subgrade can be modelled according to the spring-models of Winkler, Pasternak and Kerr. When using *F.E.M.*, the soil can also be modelled with solids. In App: H, an extensive study is performed regarding the different models. Important findings are that a uniform soil pressure is located at approximately 4.5 meters deep beneath a *S.o.G.* loaded by racking. This means that the soil settlements, due to the point loads, in the 4.5 m thick soil layer below the slab are the reason for the stresses in the slab. When this layer is of good quality than the differential settlement, and thus the stresses in the slab will be lower. For the calculation of differential settlement of the slab in a *F.E.M.*, the *Winkler* model is in good agreement. For the calculation of the total settlement of the slab, the soil should be modelled with solid elements[48]. This is outside the scoop of the research. Calculations with the *Pasternak* model, which takes into account the shear interaction of the subgrade, significantly decrease the deflections of the slab up to 40%. The downside is that the model is only valid for internal point loads. The *Kerr* model can also be used for edge calculations, only the determination of the *Kerr* parameter C is very difficult[64]. Therefore, it is concluded that the *Pasternak* and *Kerr* models are not practical and *Winkler* should be used.

From the *N.L.F.E.A.*, it is concluded that the soil quality greatly determines the stress behaviour as well as the settlement of the slab. A lower quality of the soil resulted in larger settlement of 1 mm to 6 mm for respectively k_{mod} = 0.1 and 0.01 N mm^{-3}. The bending moments in the crack also increases significantly for lower k_{mod}

due to the larger displacement. In the uncracked zone, the stresses are increased significantly when one dominant crack is present beneath the point load. The axial force increases from -109 kN to -218 kN for respectively k_{mod} = 0.1 and 0.01 N mm^{-3}. This is beneficial regarding the cracking of the slab. Unfortunately, the bending moment also becomes twice as high. The principal tensile stress in the uncracked zone will, therefore, not be influenced by the soil. Only the principal compressive stress is significantly increased. The contradictory findings in the literature can, therefore, be explained. The stress behaviour changes significantly with the soil quality. Only the most relevant stress regarding cracking in the uncracked zone remains almost equal. The beneficial force and negative moment counteract each-other. The soil mostly influences the vertical displacement of the slab. The soil parameters also influence the likely-hood of cracking. A lower subgrade modulus results in lower stresses. Therefore an increasing point load will sooner initiate in a *S.o.G.* on a weak soil compared to a stiff soil. The soil quality can determine whether the slab will crack at the bottom due to a point load, or not.

Influence of concrete mixture

The influence of the concrete mixture is taken into account by changing the Young's modulus and the cracking stress σ_{cr}. The concrete relaxation effect is simulated by changing the Young's modulus. The relative stiffness radius is also influenced by the concrete stiffness. A higher concrete stiffness results in an increase in the relative stiffness radius. The aggregate type and concrete relaxation effect can influence E_{cm} and thus the l_{rs}. A maximum increment of E_{cm} results in a 32% increase of l_{rs}. The Young's modulus does not change significantly per concrete class. Therefore, the influence of the concrete class on l_{rs} is not large. A maximum increment of E_{cm} from C20/25 to C35/45 results in a 4% increase of l_{rs}.

$$l_{rs} \propto \sqrt[4]{E_c} \qquad \frac{E_{cm,max}}{E_{cm,min}} = \frac{30000}{10000} = 3.0 \Longrightarrow l_{rs} \propto \sqrt[4]{3.0} \approx 1.32 \tag{10.134}$$

The effect of the concrete mixture on the stress behaviour by a point load is relatively low. A lower cracking stress did not significantly affect the stress behaviour. The cracking strength does not influence the stress development in a cracked *S.o.G.* loaded by a point load. Only the loading capacity of the slab is affected by the cracking stress. A crack is initiated at a lower point load for a lower cracking stress. This resulted in a small increase in slab settlement in a cracked slab with a lower cracking stress. The Young's modulus does influence the slab behaviour. A lower E_{cm} results in a reduction of the axial force and bending moment. The same effect is present as for the subgrade modulus k_{mod}. The total forces do decrease for a lower E_{cm}, but the principal tensile stress in the slab is not largely affected. With respect to the principal tensile stress in the uncracked zone, it is concluded that a stiffer concrete result is lower stresses. The settlement of the slab slightly increases with a lower stiffness of the concrete. This resulted in a higher steel stress in the crack.

10.3 Analysis of combined loading

The effects of the combined loading are analysed with the use of the *F.E.M.*. Various situations are compared. The model for the analysis schematizes the cross-section of the *S.o.G.* loaded by back-2-back racking shown in Fig:10.7. Also, a transient strain load, a combination of concrete shrinkage and seasonal temperature, of five years is taken into account. Cracking can occur due to the point load or the *I.D.*. Earlier it was concluded that cracking could be prevented for both situations, but the combination of these loads will likely result in cracking in the *R.T.M.*. To gain insight into the behaviour, seven situations are analysed.

In the analysis, two concrete mixtures are compared. The *S.R.A.* concrete mixture simulates a low shrinkage (α_{sra}=0.8), high relaxing concrete ψ=0.5 and sandstone aggregate $\alpha_{E_{cm}}$=0.7. The normal concrete is without a reduction in the total shrinkage, the concrete relaxation low ψ=0.7 and the aggregate type is quartzite ($\alpha_{E_{cm}}$=1.0). Both concrete mixtures are analysed for the two situations that the racking load induces a stress higher and lower than the cracking stress. Besides the situations that the shrinkage and external load initiate cracking, the influence of a more slender slab and lower concrete class is analysed. The last analysis is the situation eight only with *S.F.R.C.*. The results from the *N.L.F.E.A.* are compared with the model of *Gilbert* for the stress behaviour and with the *CUR-65* and Stu*fib*-11 for the crack width. The results are also scaled to a point load of 100 kN based on the outcome of the linear analysis in the *F.E.M.*. The scaling of the results is also, in this

case, questionable. Therefore, the results are only used to get an insight into the influences of the parameters. 3-D analysis should be performed to validate the results and the assumed method of the translation of a single point load to a line load. The effect of a variable racking load in time is also analysed. Finally, a strain softening and hardening *S.F.R.C.* slab without conventional reinforcement is briefly discussed.

- Situation 1: *S.R.A.* concrete and no cracking by the racking load
- Situation 2: Normal concrete and no cracking by the racking load
- Situation 3: *S.R.A.* concrete and cracking by the racking load
- Situation 4: Normal concrete and cracking by the racking load
- Situation 5: C20/25 *S.R.A.* concrete and no cracking by the racking load
- Situation 6: *S.R.A.* concrete and no cracking by the racking load on slab of 120 mm thick
- Situation 7: Hybrid *S.R.A.* concrete and no cracking by the racking load

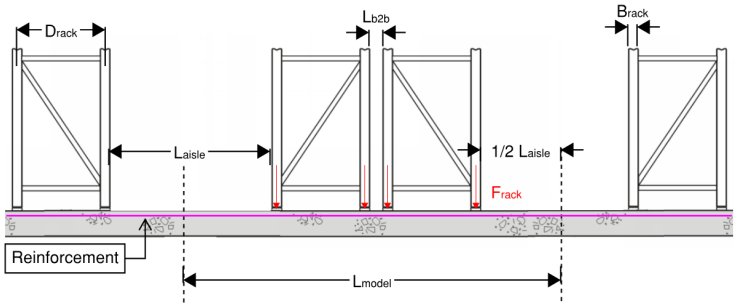

(a) Schematization of racking load

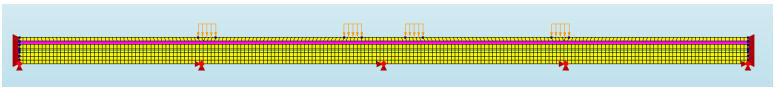

(b) *F.E.M.* of racking load

Figure 10.7: Racking loads

Table 10.3: Model parameters

Parameter	Value	Units
L_{model}	5.00	m
L_{aisle}	2.50	m
L_{b2b}	0.30	m
D_{rack}	1.00	m
B_{rack}	0.12	m
Slab height	180	mm
ρ_s	0.36	%
Cover	30	mm
Curing	7	day's
Relative Humidity	60	%
degree of restraint R	1	-
Temperature change ΔT	2.5	°C
α_{cr}	0.6	-
k_{mod}	0.05	$\mathrm{N\,mm^{-3}}$

Influence of concrete mixture

The influence of the concrete mixture is investigated by comparing situation 1 with 2 and 3 with 4. The situation 1 and 3 are with concrete mixtures which tend to reduce the crack risk of the structure, referred to as good concrete. The concrete of situations of 2 and 4 are mixtures with no special measurements, referred to as bad concrete. It is found that the negative bending moment in the uncracked zone is higher in the good concrete. On the other hand, the axial tensile force in the bad concrete mixture is higher. The numbers of cracks in the low loaded slab are 2 and 6 with a maximum surface crack of 0.15 mm and 0.25 mm for respectively, the good and bad concrete mixture. Due to the low relaxation effect and high shrinkage load, more cracks are formed in the bad concrete mixture. The many cracks in the bad concrete reduced the negative bending moment in the uncracked zone. Contrary to that, due to the higher shrinkage load and concrete stiffness, the tensile force is the member is significantly higher. This result is significantly higher crack widths in the bad concrete mixture. The steel stress in the crack was also higher in the bad concrete mixture. Because the bad concrete is modelled stiffer, the vertical displacement is slightly lower.

Influence of racking load

The influence of the amount of loading is investigated by comparing situation 1 with 3 and 2 with 4. The situations 1 and 2 are slab loaded by racking load were the linear stresses are lower than the cracking strength of the concrete. The rack loading of situations 2 and 4 does initiate stresses higher than the cracking strength. The high racking loading increased the negative bending moment in the uncracked zone but significantly reduced the axial tensile force. This is in agreement with the earlier found result that external loading results in beneficial compressive forces when the slab is crack at the bottom. The crack width was not affected by higher racking loads. Only more cracks were formed due to the increasing external loading. The maximum steel stress reduced when the loading increased in the good concrete mixture due to the lower tensile member

force. The higher load significantly affects the vertical displacement. Higher racking loads result in more settlement with the highest value in the middle of the racking. The settlement in the aisle is not influenced. Thus the slope between the aisle and middle of the racking is also increased. Which is not desired for the *M.H.E.*.

Influence of concrete class

The influence of the concrete class is investigated by comparing situation 1 with 5. Situation 1 represents a good concrete mixture with concrete class C30/37 and situation 5 with concrete class C20/25. From the earlier analysis, it was found that a lower concrete class significantly reduces the shrinkage crack widths and does not largely affect the behaviour by a point load. For the combined loading situation, the same conclusions are found. The crack width at the surface reduced from 0.15 to 0.11 mm when the concrete class is reduced. The negative bending moment and tensile force are both reduced with C20/25. The maximum steel stress in the member is also reduced. The number of cracks is significantly higher for a lower concrete class, two compared with six cracks. The vertical displacement is slightly higher for C20/25.

Influence of slab thickness

The influence of the slab height is investigated by comparing situation 1 with 6. The slab thickness is reduced from 180 mm to 120 mm for situation 6. Therefore the axial tensile stress is higher in the more slender slab. . The axial tensile stress and bending moment stress in the 180 mm slab is 0.63 and 2.69 MPa. The axial tensile stress en bending moment stress in the 120 mm slab is 0.86 and 2.63 MPa. The stresses are quite similar. The small difference can come from the phase of cracking. The thick slab has likely just cracked, were in the more slender slab, soon a new crack can be formed. It should also be noticed that the principal stresses based on the combined loading, 3.32 MPa and 3.49 MPa, for both situations are higher than the lower bound cracking stress σ_{cr}.

In theory, cracking should occur in the uncracked zone. There are two reasons why cracking does not occur. First, the cracking stress in the uncracked zone is probably higher due to the random field. Secondly, the composed line in the *F.E.M.* takes into account all the structural elements in the cross-section to compose the bending moment. This means that the reinforcement force is also used for the determination of M_{uncr}. In the model, the maximum principal tensile stress of 3.21 and 3.13 are found in the uncracked zone with a cracking strength of 3.32 and 3.16 MPa for the thick slab of respectively 120 and 180 mm. Both cross-sections have a higher cracking strength and a lower principal stress than calculated with the bending moment and axial force. The crack risk is in both sections very high.

The number of cracks is higher in the thin slab, which is logical because the stresses due to the external loading are higher. The crack width is not significantly higher. The crack width on the surface was 0.17 mm compared to 0.15 mm in the slender and thick slab. The steel stress in the first crack is higher in the slender slab, 216 to 266 MPa, because the reinforcement has a relatively large internal level arm. Therefore, the loading capacity will be lower for the more slender slab. Another downside is that the vertical displacement is increased from 7 to 10 mm. The slab thickness does influence the behaviour but is not that governing for the surface crack width.

Influence of hybrid reinforcement

The influence of *S.F.R.C.* is investigated by comparing situation one with seven. The reinforcement ratio is kept constant. Therefore the total amount of reinforcement is higher for situation seven. Adding steel fibres to the concrete mixture results in a significantly increment of the loading capacity of the slab. There was no crack localisation at the surface in the hybrid member, only a cracked zone. Because a force transfer is possible in the middle crack, due to the residual strength, the tensile force in the member is significantly higher in the hybrid member. The residual strength of the *S.F.R.C.* also reduces the steel stress. The addition of steel fibres does not influence the vertical displacement. According to the analysis, the steel fibres reduces the likely hood of surface cracking.

Global behaviour

From the sensitivity analysis, it was stated that the cracking changes the stress behaviour in the slab. A bottom crack significantly reduces the axial force and increases the negative bending moment in the uncracked zone. The secondary cracks at the surface reduce the negative bending moment in the uncracked zone. Furthermore, it was found that external loading results in an axial compressive force in the member. Both effects are found in the analysis of the combined loading. In Fig: 10.8, the stress and cracking behaviour of situation one are shown with five highlighted stages. In stage A the external loading is applied. For situation one, the external loading does not result in cracking. Due to the back-2-back racking load, the tensile force reduces and the bending moment increases significantly. From this point on, the external loading does not change anymore. Only when the shrinkage load is increased, the member cracks at the bottom. The cracking reduces the tensile force such that the uncracked zone is in compression. Also, due to the eccentrical reinforcement, an additional negative bending moment is induced. This behaviour can be seen in phase B. The *I.D.* continues to increase and after approximately two years, a surface crack appears. This surface crack has a crack relaxation effect on the bending moment in the uncracked zones. The bending moment slightly reduces due to the crack. The cracking does not significantly influence the axial force. Only a small reduction of the tensile force is found. In the next three years of loading, no new cracks were formed. In phase D and E, a small deviation in the stresses is visible. In these phases, the present cracks are slightly increased. This can clearly be seen in Fig:10.8b. In this figure, it can also be seen that due to the *I.D.*, the cracks continue to increase in time. Where in the point load analysis, it was stated that the middle crack does not appear at the surface, it is now found that, due to the combined loading, the middle crack also opens at the surface of the slab. The crack width of the middle crack is significantly smaller than the flexural cracks in the aisle.

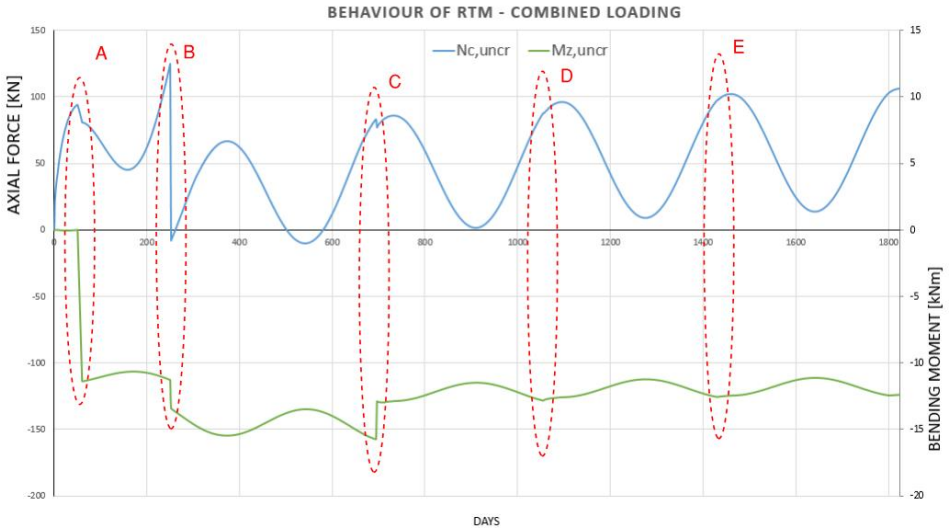

(a) Stress behaviour

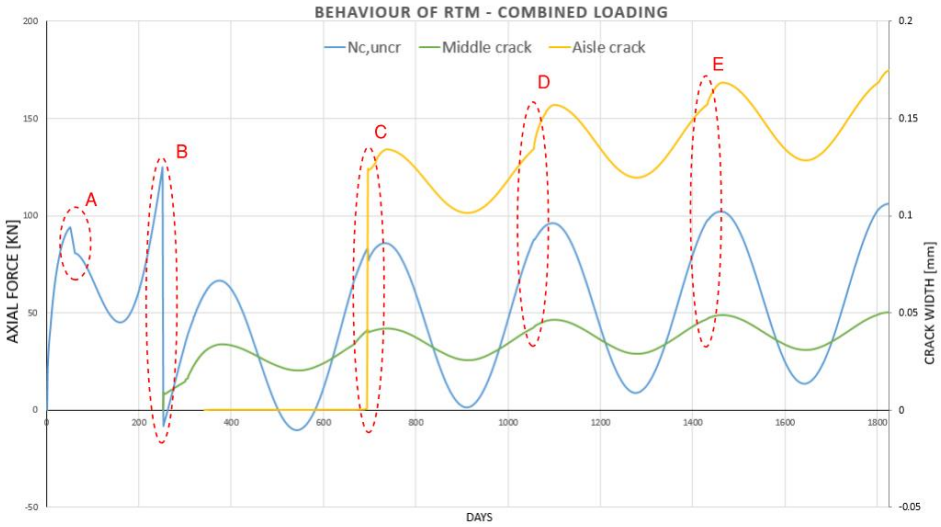

(b) Cracking behaviour

Figure 10.8: Behaviour of situation 1

Crack width behaviour

In Fig: 10.9 the crack development of the *R.T.M.* with high racking load is given for good and bad concrete. The middle crack is lower for both situations than the crack width of the surface crack in the aisle. The small crack width reduction in the aisle crack is from the adjacent crack formation. The effect of crack formation on other crack widths can, therefore, be neglected. The crack width for situation 3 with the higher *I.D.* load shows more crack growth in time. Also, the maximum crack width is significantly higher for the bad concrete mixture. The seasonal temperature change influences the crack width during the years. When measurement or repairs are planned, it should, therefore, be done when the cracks widths are the largest. This will be in the period of autumn or winter.

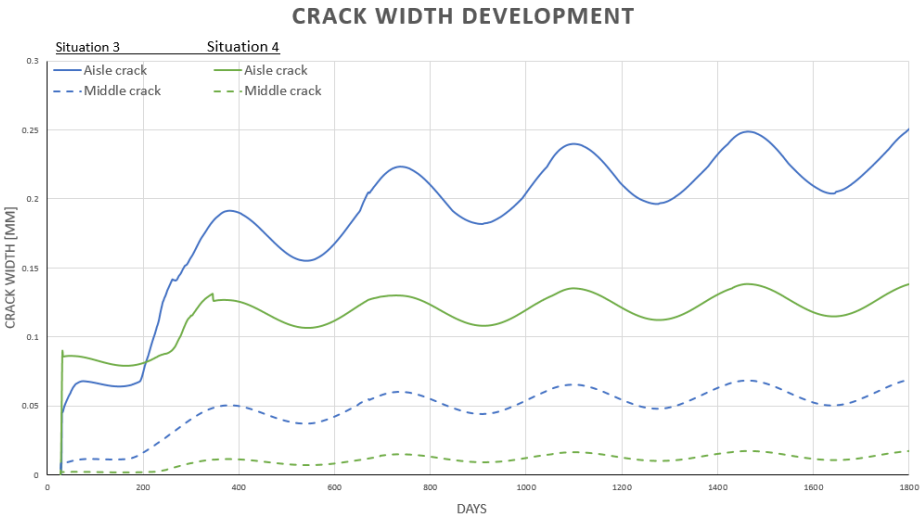

Figure 10.9: Crack width development - high racking load

The crack width from the *N.L.F.E.A.* are compared with the crack width calculation models Stu*fib*-11 and *CUR-65*. Both the methods result for all situations in higher crack width compared to the *N.L.F.E.A.* results. With the Stu*fib*-11 model the steel stress is significantly overestimated which is also found in the earlier analysis. The steel stress according to *CUR-65* is also higher than the *N.L.F.E.A.*. Only in the slender slab, situation 6, the steel stress are the same. Both methods can be used for design purposes and give safe conservative results.

Table 10.4: Analysis of crack width

	Parameter	Situation 1	Situation 2	Situation 3	Situation 4	Situation 5	Situation 6	Situation 7	Unit
N.L.F.E.A.	w_{max}	0.15	0.25	0.14	0.25	0.11	0.17	0.01	mm
	$\sigma_{s,cr}$	216	228	183	245	191	266	121	MPa
CUR-65	w_{max}	0.36	0.35	0.33	0.37	0.26	0.21	0.17	mm
	$\sigma_{s,cr}$	317	313	293	329	236	265	213	MPa
Stu*fib*-11	w_{max}	0.36	0.35	0.31	0.38	0.28	0.22	0.10	mm
	$\sigma_{s,cr}$	434	429	401	451	320	335	210	MPa

Variable racking loads

In reality, the rack loading will not be constant and maximum during the years. The racking will not always be entirely stored. Therefore, the racking load for situation one is changed in time by an assumed variation of loading following the graph in Fig: 10.11a. This situation resulted in a different stress and cracking behaviour. The racking loading, in combination with the *I.D.*, did not initiate cracking in the first two years. Also, the location of the first crack is different. This is mainly because the random field created a weak zone in the aisle and a stronger zone at the bottom in the middle of the slab shown in Fig: 10.10a. The random field resulted in a cracking factor α_{cr} of 0.86, where normally a cracking factor of 0.6 is advised. Therefore, the stresses and crack width are higher due to the higher cracking stress. A wide through crack of 0.3 mm was formed in the aisle. The axial force reduction is similar to situation one, only the tensile force in the crack is significantly higher. This is because the cracking stress in the model is high compared to the other analysis, 2.80 MPa to 2.54 MPa. This also resulted in higher steel stresses. In the variable loading situation, the maximum steel stress is 325 MPa compared to 216 MPa. The variation of the cracking strength with respect to the loading layout influence the location of the crack initiation.

When focussing on the cracking behaviour in the slab shown in Fig: 10.11c, it is found that the variable loading does not influence the crack width during it the slab lifetime. When a crack is formed and the slab is loaded, the crack width does not increase. Instead of widening of the existing crack, a new crack is formed. This is in agreement with the cracking phase of the member. In the *N.F.D.C.P.*, the existing crack widths are not increasing due to extra loading, but new cracks are formed. At approximately 1050 days, this behaviour can be seen. The load increases from 70% to 100% and a new crack are formed defined in the figure as *aisle crack 2*. The *aisle crack 1* is not significantly affected by the increasing load. Also unloading of the slab did not

influence the stress behaviour of the cracked slab. In the first year, the loading and unloading changed the bending moment. Only the *I.D.* influences the crack width in time but does not significantly increase the maximum crack width. The maximum crack width in the member was higher due to the higher cracking stress and that the racking load did not initiate the beneficial cracking beneath the point load. Therefore, the first crack in the aisle has a high tensile force in the crack. The maximum crack width after five years is 0.36 mm. The maximum crack widths and steel stresses according to Stu*fib*-11 and *CUR-65* are 0.41 mm with 473 MPa and 0.39 mm with 345 MPa. Again both models give good results regarding the crack widths. The *CUR-65* also gives a good result for the maximum steel stress in the *R.T.M.*.

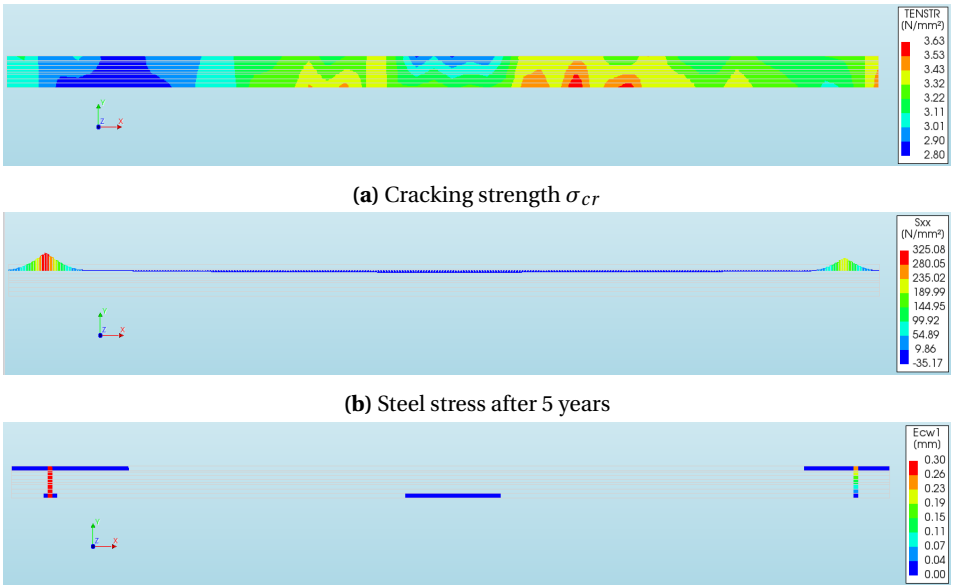

(a) Cracking strength σ_{cr}

(b) Steel stress after 5 years

(c) Crack pattern after 5 years

Figure 10.10: Behaviour in the *F.E.M.*

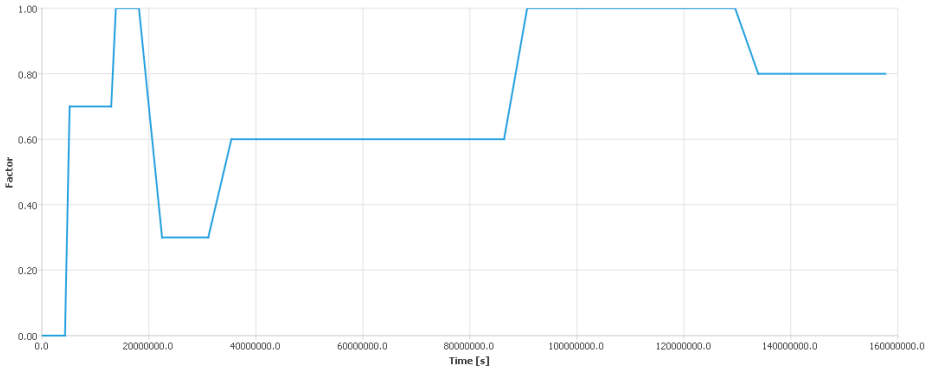

(a) Loading factor of racking load

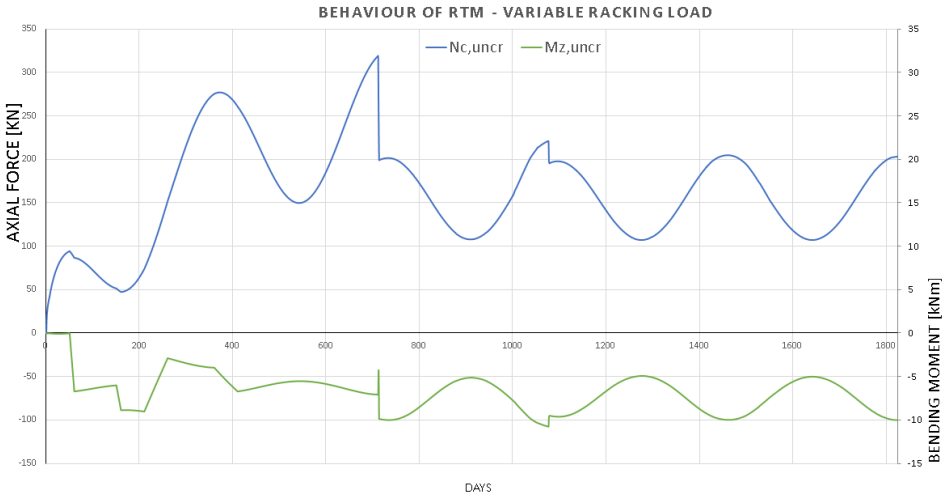

(b) Axial force and bending moment in uncracked zone

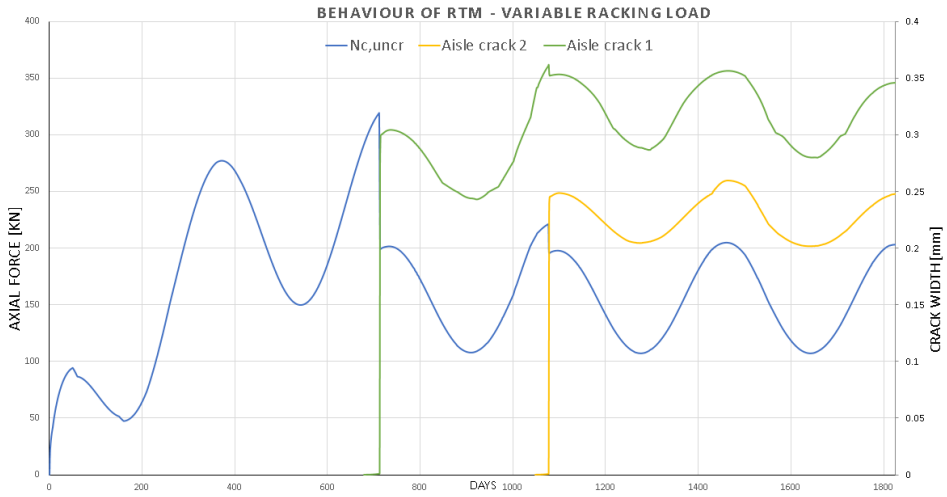

(c) Time-dependent crack width with tensile force

Figure 10.11: Time-dependent behaviour in the *F.E.M.*

S.F.R.C. only

It was stated that strain softening *S.F.R.C.* requires additional reinforcement for controlling the crack widths. The same conclusion is found in the combined loading analysis. The strain hardening *S.F.R.C.* resulted in large cracking zones with one small localised crack of 0.11 mm wide. Strain hardening *S.F.R.C.* without additional reinforcement can be used for *S.o.G.*. It has to be mentioned that the long-term behaviour on the residual tensile strength of the *S.F.R.C.* should be further investigated to ensure the crack widths.

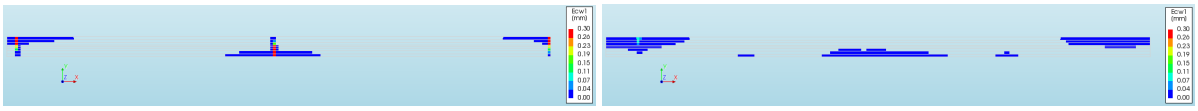

(a) Strain softening *S.F.R.C.* **(b)** Strain hardening *S.F.R.C.*

Figure 10.12: Cracking behaviour of *S.F.R.C.* due to racking loads

11. Conclusions

This research gave more insight into the behaviour and widening the knowledge of the structural design of *S.o.G.*. This is done by investigation of the questions. To answer the main research question, the multiple sub-question are answered with the use of an extensive sensitivity analysis on all the influence parameters. In the next chapter, the recommendations are given, which can be taken into account for the design of large jointless *S.o.G.*.

What is the structural behaviour of an elastic supported concrete slab loaded by an imposed deformation and point loads?

The global behaviour in a large jointless *S.o.G.* can be described with the use of a *R.T.M.* for the fully restrained section of the slab. The behaviour is complex and is based on multiple mechanisms where the parameters interact with each other. Aspects like the ageing of concrete, the environmental influences, the execution quality, the different design principles, the interaction between concrete and reinforcement and sustained loading largely influence the behaviour in the concrete slab. Therefore, the complete answer to the research question can not simply be given. The simplified global behaviour is explained in different situations. The behaviour is addressed with more detail in the sub-questions.

When a concrete structure is restrained and loaded by a shrinkage strain, an imposed stress occurs in the structure. These stresses change in time and can be significantly reduced by the concrete relaxation effect. For a fully restrained slab loaded by a uniform shrinkage strain, an axial tensile force is present. This behaviour is shown in Fig:11.1.

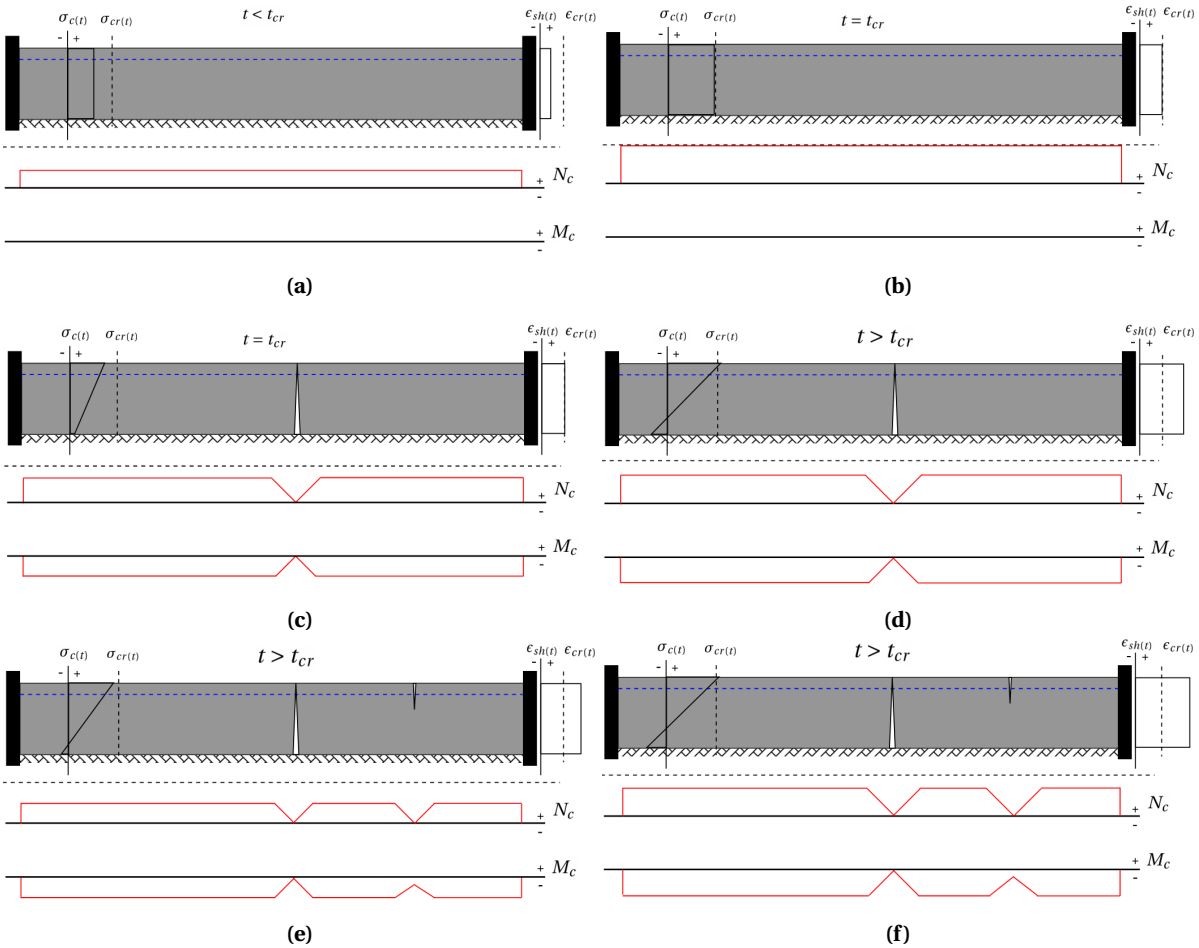

Figure 11.1: Cracking behaviour in restrained slab due to shrinkage

For a gradient shrinkage load, a bending moment is present in the slab. The force and bending moment can initiate cracking in the member. When the member cracks, the member stiffness reduces and the imposed load in the uncracked zone decreases. In time, the force in the uncracked zone increases again due to the shrinkage load and new cracks can occur. This is defined as the not fully developed cracking phase. The imposed load generally does not result in a fully developed crack pattern where the existing cracks widen instead of forming new cracks with an increasing load. The cracking force/bending moment can be significant and therefore, be governing for the crack width calculations. Therefore, in restrained concrete structures, the imposed deformation should always be taken into account. Cracking by imposed deformation is initiated at the weakest point in the concrete member.

An external point load induces a positive bending moment in the slab at the location of the point load. Next to the load, a negative bending moment is present, shown in Fig: 11.2. After cracking at the bottom, a large axial compressive force occurs in the restrained slab. This axial compressive force is beneficial regarding the crack width in the slab. The negative bending moment in the uncracked zone is not significantly affected by the bottom crack. For external loading, the location of crack initiation is often known and is most likely to occur beneath the point load.

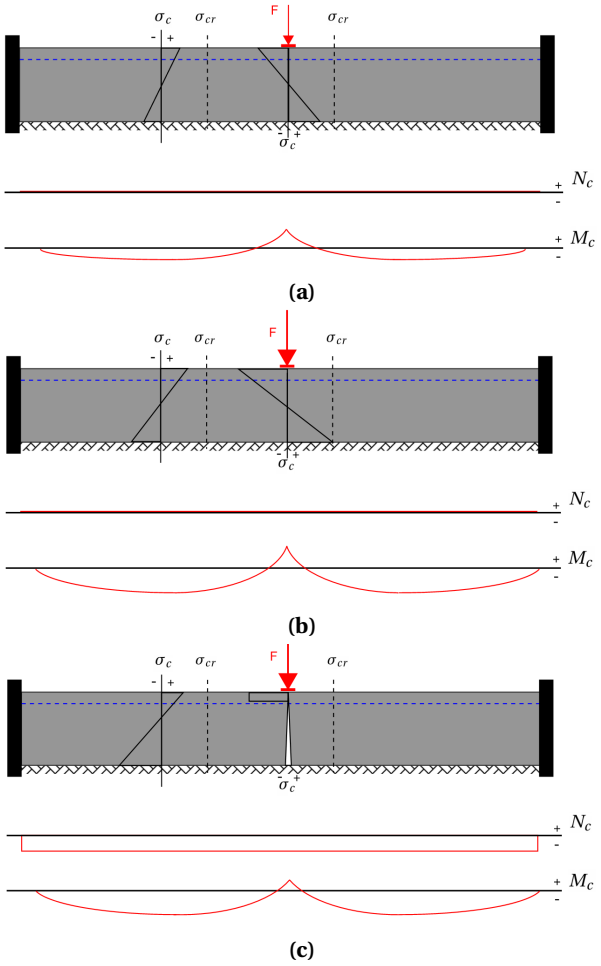

Figure 11.2: Cracking behaviour in restrained slab due to point load

For the combined loading situation, cracking is not always initiated in the weakest point of the concrete. When the external force is high enough, a bottom crack beneath the point load occurs. This results in an increase of the negative bending moment and a significant decrease of the axial tensile force in the uncracked zone. When the imposed load continues to increase, secondary cracking is initiated at the surface of the slab. These cracks slightly decrease the tensile force and negative bending moment in the nearby uncracked zones. When the slab is marginally loaded, cracking can occur at the location next to the point load where the concrete has a weak spot. This can result in a less desired crack pattern. In the research, a through crack was formed in the aisle, which was significantly larger than the situation of cracking beneath the point loads. This is because the

positive axial compressive force by the external loading was not present in the slab.

Predicting the crack pattern and crack width in large jointless *S.o.G.* loaded by shrinkage and racking remains difficult. Therefore, practical based recommendations are advised. To gain more insight into the behaviour, the conclusions per sub-questions are given below.

What is the degree of restraint of large jointless *S.o.G.*?

The degree of restraint R is the coefficient to quantify the amount of restraint on a concrete structure. When R=1.0, the structure is fully restrained and no axial or rotational movement is possible. For *S.o.G.*, multiple aspects can restrain the structure. The most relevant aspects found during the research are the reinforcement, casting sequence, edge conditions, soil friction and curvature restraint due to vertical loading.

The reinforcement has a small contribution to the degree of restraint but is always present. The casting sequence restrains the slab parallel to the contact edge. Fortunately, the restrained stresses during casting are relatively low because the degree of restraint is not fully, R=0.59, and the temperature development is low for relatively slender *S.o.G.*.

The governing degree of restraint is from the edge conditions, vertical loading and soil friction. All the aspects can fully restrain the slab. The surrounding structures of the slab can restrain the slab over its total length. The curvature restraint is fully for six to ten meter long slabs for typical parameters. The soil friction induces the largest degree of restraint in the middle section of the slab. For practical values, the slab is fully restrained at a length of 40 to 80 meters long, depending on the soil type and vertical loading. Due to the slip effect, only a small midsection is fully restrained, shown in Fig: 11.3. Because in reality, various aspects restrain the slab, the conservative design method for the calculation of the restrained length of *CUR-36* is advised. With the conservative method, it can be assumed that all other aspects are taken into account.

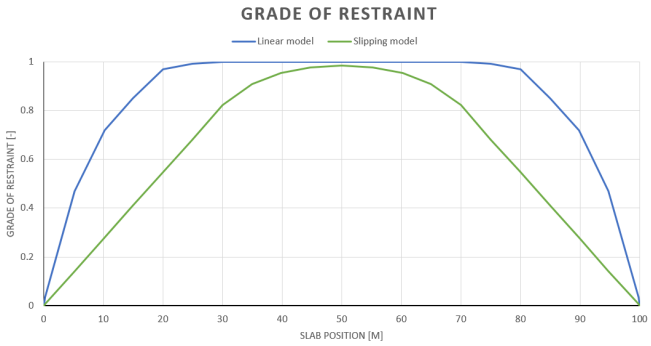

Figure 11.3: Effect of linear and non-linear interface on degree of restraint

A larger restrained length $L_{restraint}$ has a negative influence on the stress and cracking behaviour. Therefore, it is advised to reduce the restraint and to construct the *S.o.G.* loose from surrounding structures and without edge thickening.

What is the stress behaviour in restrained *S.o.G.* loaded by *I.D.* and/or point loads?

The governing stress situation is when the *S.o.G.* is fully restrained. For the stress calculation of a fully restrained *S.o.G.* it is modelled as a *R.T.M.*. From the degree of restraint, calculation of the length $L_{restraint}$ of the *R.T.M.* can be determined. A distinction can be made between the stress behaviour by *I.D.* and external loading.

The stress development in a *R.T.M.* by *I.D.* depends on the shrinkage load, concrete stiffness and the relaxation effect. For the calculation of the restrained stresses, the superposition method of *Bazant* is used to take into account the ageing and concrete relaxation effect. In a fully restrained slab, the imposed strain load results in tensile stresses, which are dissipated in time due to the concrete relaxation effect. When the curvature of the slab is also fully restrained and a shrinkage gradient is applied, a bending moment is induced in the slab. The shrinkage strain in *S.o.G.* is most likely a gradient with the maximum tensile strain present in the top of the slab. The concrete relaxation effect is strongly related to the creep behaviour. A higher creep value increases

the relaxation effect. Quantification of the relaxation effect for design is complex due to many environmental influences and parameters. Large variation is found for the upper and lower bound stress development. The best method for the calculation of the long-term concrete relaxation coefficient is the formula in the *CUR-36*. This method overestimates the stresses at early age, where the relaxation effect is the most present but is in good agreement with long-term relaxation effect for sustained loading. Practical relaxation coefficients of 0.3 to 0.6 were found in the analysis. The reduction of stresses due to concrete relaxation reduces the crack risk of the concrete member.

The relevant imposed loads for indoor *S.o.G.* are the seasonal temperature, concrete drying shrinkage and autogenous shrinkage. The restrained stresses from the hardening temperature can be neglected because of the relative thin slab and high relaxation effect at an early age. The seasonal temperature is low for indoor slabs but still determines the moment of cracking. It is advised to ensure that the concrete temperature at casting is lower than the average seasonal temperature to reduce the total shrinkage load on the concrete slab. The total drying shrinkage depends mainly on the cement type and *R.H.* in the surrounding. The development of the drying shrinkage is significantly faster in thin slabs. The autogenous shrinkage is only 5% to 14% of the drying shrinkage for low concrete classes C20/25 to C35/45 and becomes more relevant for higher concrete classes. The total amount of shrinkage is highly related to the concrete mixture, and therefore a proper mixture should be used.

Before cracking, the point loads induce a positive bending moment at the positions of the load and a negative bending moment next to the loads at approximately one to two meters. The principal stress at the bottom fibre can be determined with the less conservative *L.F.E.A.* formula of *Abbas* based on the *Westergaard* approach. The principal stress depends mainly on the slab height and soil stiffness k_{mod}. From the sensitivity analysis with the *Abbas* formula, it is found that the slab capacity can be increased by increasing the subgrade modulus k_{mod}, slab height h and lower the concrete stiffness E_{cm}. Besides reducing the stresses in the slab, a high subgrade modulus also significantly reduces the deflection of the slab. The stresses can also be reduced by increasing the footplate beneath the racking.

The stress in the slab change after cracking. After cracking, which occurs below the point load, the positive bending moment reduces. The crack at the position of the point loads acts like a hinge. The slab rotates more due to the cracking and the cross-sections want to move towards the sides. Because the *S.o.G.* is fully restrained, a large beneficial compressive force is developed in the uncracked zones. Due to additional rotation after the first crack, the negative bending moment in the uncracked zone is increased. This can lead to surface cracks. The subgrade modulus k_{mod} is the most important factor regarding the stresses and deflection of the slab. A higher subgrade modulus results in lower stresses and deflection. The statement *"the floor is as good as the grade below"* is true for *S.o.G.*.

What is the cracking behaviour in restrained *S.o.G.* loaded by *I.D.* and/or point loads?

Cracking in the slab occurs when the stresses are higher than the cracking stress σ_{cr}. The cracking stress increase over time, is variable in space and is influenced by the loading and cracking type. For an eccentric reinforced slab, the first crack occurs at the bottom. Cracking by an *I.D.* always result in a *N.F.D.C.P.* characterised by the formation of new cracks instead of widening of existing cracks when the load increases. The seasonal temperature increases and reduces the crack width in time. Cracking in the *N.F.D.C.P.* reduces the axial tensile force. Especially in short *R.T.M.*, the crack relaxation effect is large. Force reductions of 50% were found in a five meter long restrained member. The crack relaxation effect is even higher in the eccentric reinforced member,± 70%. The lower tensile force in the uncracked zone results in a lower force in the steel and thus a lower the steel stress in the crack.

The steel stress reduction due to the eccentricity can be estimated with the reduction factor α_{ecc} according to the *Vencon model*. It is found that a higher eccentricity reduces the required amount of reinforcement to control the cracks at the surface. The eccentric reinforcement also induces an additional negative bending moment in the uncracked zone. In combination with the shrinkage gradient, flexural crack at the surface will likely appear as secondary cracks. Therefore, for the calculation of the crack width, the flexural cracking stress $\sigma_{cr,fl}$ should be used. In Fig:11.4 a common crack pattern is shown. The secondary cracks at the surface also reduce the negative bending moment in the uncracked zone. Moreover, when the loading has increased, the stress in the uncracked zone can reach the flexural cracking stress again and new cracks will be formed.

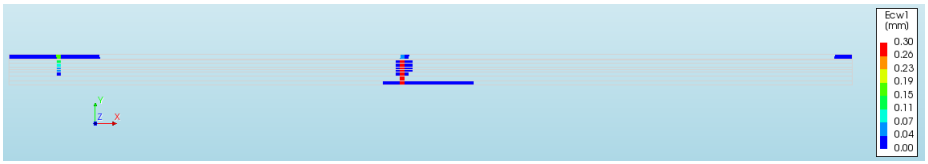

Figure 11.4: Common crack pattern in *S.o.G.*

There are many calculation methods are found in the provisions for the calculation of the crack width and the required material properties. This results in a wide variation of the results and makes it difficult to perform exact crack width calculations. Accurate crack width analyses are also not possible due to the many parameters which influence the crack width. For the design calculation, the cracking stress σ_{cr} is advised to be taken as the 28-day property with a cracking factor α_{cr} of 0.6. For flexural cracks, the higher flexural cracking stress $\sigma_{cr,fl}$ should be used.

A higher cracking stress results in larger crack widths. Therefore, to reduce the crack widths, a low concrete class is advised. To reduce the crack risk, a higher cracking stress is advised. The moment of cracking is generally between the two and twelve months, depending on the moment of casting and the amount of shrinkage and concrete relaxation. Crack spacings of 0.5 to 2.5 meters are found after ten years of *I.D.*, which is in good agreement with the findings in practice.

The reinforcement is required to control the cracks. Sufficient reinforcement, in practice determined with the minimum reinforcement ratio $\rho_{s_{min}}$, is needed. For *S.o.G.*, it is common to design the slab with less than the minimum reinforcement ratio. In theory, less reinforcement than $\rho_{s_{min}}$ will result in yielding and large crack widths. Because of the crack relaxation effect and the eccentrically placed reinforcement, the stress in the steel is significantly lower. It is found that the bond-slip behaviour greatly determines the crack width in the slab. Therefore, good bonded reinforcement should be used. By decreasing the diameter $\varnothing$ and the bar spacing, the bonding increases and the reinforcement becomes more effective to control cracks. It is also found that more reinforcement leads to more fine cracks.

In the analysis of the combined loading situation, it is found that the concrete mixture mainly determines the maximum crack width. The point loads only result in more cracks instead of wider cracks and also in larger deflections. The cracking stage in the combined loading is, therefore, still in the *N.F.D.C.P.*. A larger tensile force in the uncracked zone, due to the higher *I.D.*, results in wider cracks. Therefore, the shrinkage strain should always be kept low in *S.o.G.*. In the variable loading analysis, it was found that when the racking load does not result in bottom cracking beneath the racking, a through crack can occur in the aisle with a much greater width than the flexural cracks. Cracking by the racking load beneath the point load can, therefore, be assumed beneficial. The crack width calculated with the practical method of *CUR-65* was still in good agreement with the results from the analysis.

The addition of steel fibres to the concrete mixture increases the residual tensile strength of concrete. After cracking, the *S.F.R.C.* can still distribute tensile stresses in the crack. In a hybrid structure, with the same amount of conventional reinforcement, this results in a significant reduction of the crack width and steel stress. The reinforcement also becomes more efficient when steel fibres are added. The transfer length l_t is significantly lower compared to regular reinforced concrete. Also, the recommended formulae to calculate the transfer length l_t in hybrid reinforced concrete are found to be conservative. For strain softening *S.F.R.C.*, additional reinforcement is always required to ensure crack control.

What is the influence of concrete relaxation on the stress and cracking behaviour?

Concrete relaxation is often mentioned as a positive effect in fully restrained concrete structures. Concrete relaxation can significantly reduce the stresses in time, especially at an early age. In the analytical analyses of this thesis, it is found that the concrete relaxation effect has a negative influence on the crack width. The moment of cracking is delayed and less cracks were formed. This is contrary to the situation where the prevention of cracks is desired. Then, a high relaxing concrete mixture is beneficial to reduce the crack risk.

Can cracking be prevented in jointless *S.o.G.*? And if not, how can cracking best be controlled?

In theory, cracking can be prevented in a large jointless *S.o.G.* when measures are taken for the concrete mixture, degree of restraint and slab design. The external loading should also be relatively low. The amount of shrinkage should be reduced for reducing the crack risk in the slab. The stiffness of the concrete/aggregate should be low and the cracking stress of concrete should be increased. It is also beneficial to reduce the degree of restraint of the *S.o.G.*.

In practice, large jointless *S.o.G.* will likely have a fully restrained slab section. Therefore, restrained shrinkage stresses are always present. In combination with the stresses from the external loading, the crack risk in large jointless *S.o.G.* is very high. Preventing the large jointless *S.o.G.* from cracking is therefore not realistic and reinforcement is required to control cracks. For the best crack control design of jointless *S.o.G.*, the concrete slab should be kept slender with a low concrete tensile strength and amount of shrinkage. Also, the reinforcement should be placed near the top fibre. The subgrade modulus k_{mod} should also be realised very stiff to reduce the stresses from the external loading and to decrease the deflection.

How can *I.D.* and external loading be combined in the design procedures of jointless *S.o.G.*?

For eccentric reinforced slabs, the governing cracks are the flexural surface cracks. For combined loading, these cracks most likely occur in the aisles of the racking. The flexural crack width can best be determined with the enhanced cracking moment, according to *CUR-65*. The bending moment in the uncracked zone will never be higher than the cracking moment due to the *N.F.D.C.P.*. It was also found that the external loading does not result in a *F.D.C.P.*. Therefore, the cracking force N_{cr} and moment M_{cr} can be used as the design load for the crack width calculation. The tensile force present after cracking due to the *I.D.* is taken into account by the enhancement factor of 1.4 on the cracking bending moment M_{cr}. The ageing effect of concrete, when cracking occurs later than 28 days, is also assumed to be covered with the enhancement factor. It is found that this method is in good agreement. Also, when larger through cracks were formed in the aisle. Especially when the imposed loads are low in the concrete structure, the crack width method of the enhanced cracking bending moment can be used for design purposes.

Can *F.E.M.* be implemented in the structural design of *S.o.G.*?

F.E.M. is a powerful tool for the calculation of complex structural behaviour such as restrained shrinkage cracking. Expertise is required for accurate modelling of the situation. Also, special applications, like random fields and non-linear material models, are needed to approach the real behaviour is a *S.o.G.* and to increase the change of convergence. In this research, it is found that many aspects influence the stress and cracking behaviour of *S.o.G.*. *F.E.M.* always gives output values solely based on the engineers' input. Because the parameters of *S.o.G.* have a wide variation, it is complicated to quantify these parameters and to ensure that the outcome of the *F.E.M.* is appropriate for structural design. Besides the input parameters, it is challenging to let the *N.L.F.E.A.* converge. The criterion is often not reached during crack localisation in the member. Besides the difficulty of ensuring an accurate model, the modelling and calculation of the complex transient *N.L.F.E.A.* are also time-consuming.

The *F.E.M.* can best be used to gain insight into the structural behaviour and to perform a parametric study. Only when the modelling settings and the range of the parameters are known and the user is highly skilled with *N.L.F.E.A.*, the *F.E.M.* can be used for design purposes. Otherwise, the *F.E.M.* can best be used for an additional check next to the standard design procedures.

12. Recommendations

The recommendations found during the research are given. Finally, interesting subjects for further research are mentioned.

12.1 Design

The design principle greatly determines the behaviour of the *S.o.G.*. A stress-free design, where the *I.D.* can be neglected, is not advised for large jointless *S.o.G.*. Restrained stresses are always present and can lead to the governing cracking situation in the slab. Especially for thick or low reinforced concrete slabs, the cracking by *I.D.* can lead to uncontrolled cracks. The *I.D.* can be seen as an extra failure mechanism that should always be checked in fully restrained concrete structures. The reinforcement should always be capable of taking up the cracking force N_{cr} and cracking bending moment M_{cr} when the structure is fully restrained. This will likely result in a lower bound reinforcement ratio value in the entire structure, particularly in zones where the external loading is low.

Degree of restraint

To reduce the restrained stresses and the crack risk, the slab is advised to be kept loose from any surrounding structures like foundation strips or pads. The governing degree of restraint in the slab will then be from the soil-structure interaction. In reality, multiple aspects restrain the slab. Therefore, the determinations of the restrained length $L_{restraint}$ are advised according to the design method for *CUR-36*.

Soil quality

The subgrade beneath the slab is of great importance on the point load capacity of the *S.o.G.*. Higher k_{mod} reduces the stresses and vertical displacement in the slab. Therefore it is advised to realise a soil foundation with a high subgrade modulus. Pre-loading the area, soil enhancement techniques or applying an enhanced sub-base are examples for increasing the bearing capacity of the sub-base. For design calculation, the appropriate subgrade modulus should be taken. For wheel loading, the short-term subgrade modulus can be used and for long-term loading like racking loads, a long-term subgrade modulus (in practice $\frac{1}{3}$ of the short term) should be used.

Crack width calculation

For the crack width calculation of *S.o.G.* in the *N.F.D.C.P.* with eccentrical reinforcement, the best method is the enhanced cracking bending moment of *CUR-65*. The Stu*fib*-11 method can also be used in combination with the 28-day concrete properties, eccentricity factor α_{ecc} and the total enhancement factor of 1.7 for the calculation of the maximum crack width. Attention should be paid to the effective height of the cross-section.

A precise crack width calculation is not possible due to the many time-dependent parameters which influence the stress and cracking behaviour. With the advised methods, the crack width can only be estimated. The best method to decrease the crack width is by taking into account the recommendations for the concrete mixture and reinforcement.

Crack width methods based on the steel stress should not be used with the realistic steel stress. Cracking in the *N.F.D.C.P.* due to *I.D.* result in a reduction of the steel stress when the crack width increases. This is contrary to the principle of the crack width models based on the steel stress and the *F.D.C.P.*. Therefore, crack width models based on the steel stresses are not advised.

Stress behaviour

For centric reinforced *R.T.M.* loaded by uniform shrinkage, the behaviour can be determined accurately with the *Gilbert* model. The forces in the cracked and uncracked zone can be calculated for the moment at first cracking and for a specific moment in time. The average crack width can also be determined, which is based on the strain equilibrium of the reinforcement and the relation between the uncracked and cracked zone. The downside is that the model is not applicable for eccentrically reinforced slabs loaded by a shrinkage gradient. Both situations often occur in practice.

12.2 Concrete mixture

The best concrete mixture for a *S.o.G.* to control cracks, according to this research, is C20/25, low stiffness aggregate (sandstone), cement S and with *S.R.A.* to reduce the shrinkage as much as possible. The low concrete class can have negative effects on the durability, which is not taken into account in this research. For slabs were cracks must be prevented, the suggested concrete class should be increased to reduce the crack risk.

Concrete properties

It is found that many properties have a wide variation and it is sometimes not clear which value should be taken for the design calculation. The 28-days properties from the provisions *E.C. 2* and *M.C. 2010* are advised to be used. The creep value for the calculation of the relaxation coefficient, according to *CUR-36*, should be determined with the time-dependent properties in the *E.C. 2* throughout the sustained loading. For the cracking stress, the mean tensile strength f_{ctm}, in combination with the cracking factor α_{cr}, is advised. The cracking stress should be enhanced to the flexural cracking stress when flexural cracks are expected.

Long-term properties

For the calculation of the stress and cracking behaviour due to *I.D.*, the long-term properties are important to take into account. Sustained loading reduces the tensile strength of concrete. Therefore the factor α_{cr} of 0.6 for sustained loading is advised.

12.3 Reinforcement

To make reinforcement more efficient for controlling surface cracks, it should be applied with the smallest possible cover at the top of the slab. The reinforcement diameter $\varnothing$ and bar spacing should also be taken as small as possible to increase the bonding quality and thus a smaller transfer length l_t. A lower transfer length increases the effectiveness of the reinforcement regarding the crack control.

Long-term properties

Just like the concrete properties, the sustained loading influence the bond-slip properties. Sustained loading reduces the bonding quality, which significantly influences the crack width. Therefore, the bond-slip properties should be reduced to take into account the long-term behaviour. It is found that the residual cracking stress of *S.F.R.C.* also reduces due to sustained loading. In the literature, only one maximum value is found to quantify this effect. The residual tensile strength of *S.F.R.C.* can be reduced with 40% by sustained loading according to the literature.

12.4 Finite Element Modelling

As discussed, *F.E.M.* for structural design is complex. Therefore suggestions for modelling a transient cracking analysis are given to improve the quality of *N.L.F.E.A.*.

Elements

For crack width analysis in the *N.F.D.C.P.* in *F.E.M.*, it is found that the bond-slip behaviour is important to take into account. This is not possible in plain-strain elements, but only in plain-stress elements. Therefore, plain-stress elements are advised. Elements with a high number of integration points increase the accuracy of the model and are therefore also advised to use.

Analysis

For the accuracy of the model, it is not advised to use the linesearch method for models similar to this research. During crack localisation, the *O.o.B.* is significantly higher when the linesearch method was used. Also, the computational time is slightly higher with linesearch.

Furthermore, it is essential to check the divergence and the *O.o.B.* of the analysis. It can occur that the *O.o.B.* is very high for multiple steps. This is undesired and decreases the accuracy. During cracking, convergence of every step is unlikely. An *O.o.B.* of 10-20% during crack localisation is acceptable.

Post-analysis crack width method

The advised method for the determination of the crack width in the *N.L.F.E.A.* is the average crack width per element. The average crack width per element can directly be given as an output value in the *F.E.M.*. No additional calculation is required. The crack width can also be determined at every location of the model.

12.5 Further research

During the research, subjects came forward, which can be interesting for further investigation.

Analytical model of stress behaviour in eccentric reinforced *R.T.M.* loaded by (gradient) shrinkage

For the stress behaviour for centric reinforced *R.T.M.* loaded by a uniform shrinkage load, an analytical model is developed by *Gilbert*. Because in *S.o.G.*, the reinforcement is often placed eccentric and the shrinkage load can be a gradient, an analytical model for the calculation of the stresses in a *R.T.M.* with bending moments can be helpful for the structural design of *S.o.G.*.

Long-term cracking behaviour of *S.F.R.C.* and hybrid concrete structures

In this research, the *S.F.R.C.* properties are reduced based on assumed values from one experiment. The true long-term behaviour of cracking in *S.F.R.C.* should be investigated further for more information on the long-term behaviour. The long-term effect can be implemented into design methods for *S.F.R.C.* with respect to cracking due to sustained loading.

Failure types

Bad execution of the slab and sub-base can result in undesired cracking. Also, re-entrant corners are often the cause of uncontrolled cracking. Additional reinforcement should be placed at these critical locations. The behaviour of re-entrant corners is not investigated. Research into this subject can improve the overall quality of the floor.

From the failure analysis, it also became apparent that differential soil settlement also often results in uncontrolled cracking in *S.o.G.*. An investigation of this behaviour is advised to improve the general structural knowledge of *S.o.G.*.

The investigation of the soil-slab interaction can be expanded with an analysis of the deflection and rotation of the by external loading in combination with *I.D.*. The racking load is becoming higher and more automatic *M.H.E.* are used, which brings stricter criteria to the settlement difference in the *S.o.G.*.

Pre-loading

Based on the analysis of the variable loading situation, it is assumed that cracking beneath the point load is beneficial. The bottom crack beneath the racking introduces a compressive force in the member and initiate flexural cracking in the surface instead of large through cracks. It would be very interesting to investigate the effect of predefined bottom cracking at the known location of the racking legs to ensure only flexural cracks instead of through cracks. By pre-loading the slab, bottom cracks can be initiated and developed early-age strains are then also released. These cracks have no significant influence on the loading capacity of the slab. When the racking is placed and the load increases, only surface cracks will arise in the aisle, which can be controlled with reinforcement. The downside can be the durability and that the racking position can likely not be changed during the slab's lifetime.

Random field parameters

The random field is required in the *F.E.M.* to initiate crack localisation in the constant stress zone of the *S.o.G.*. The random field greatly determines the crack pattern of the slab. For this research, the random field parameters are assumed based on the findings in the literature. No recommended values are given in the provisions because the random field application is rather new. An investigation into the real spatial variation of the concrete properties and the translation of these properties to input parameters for the random field will increase the reality of modelling the concrete material in *F.E.M.*.

3D analysis

All *F.E.M.* analyses were performed with a 2D model, which represented the governing cross-section perpendicular to the crack. In reality, crack propagation occurs in multiple directions. The effect of cracking in a 3D *S.o.G.* should be analysed to validate the results in this research.

The translation of the point load to an equivalent line load in the model is questionable. This problem can also be solved by using a 3D model. The difference between the behaviour in the 2D and 3D models should be investigated to validate the results in this research.

Creep models in combination with bond-slip interface in *F.E.M.*

Modelling the realistic creep behaviour is complex and almost not possible due to the many different parameters which affect the behaviour. When the creep compliance model was used in the *F.E.M.* in combination with the bond-slip interface, large horizontal cracking occurred along with the reinforcement, which resulted in a slipping behaviour of the reinforcement. The cause of the effect and the correct way of modelling creep in combination with bond-slip should further be investigated. Based on this research, the most practical method to take into account the creep was by using an *A.A.E.M*.

List of Abbreviations

A.A.E.M	Age Adjusted Effective Modulus
A.M.	Analytical Model
Bazant	Bazant Model
Van Breugel	Breugel Crack Width Model
C.D.C.	Cofra Dynamic Compaction
C.F.R.	Crack Formation Stage
C.M.O.D.	Crack mouth opening displacement
CUR-111	CUR 111 - Design of Steel Fibre Reinforced Concrete Industrial Floors on Piles
CUR-36	CUR 36 – Design of Concrete Floors and Pavements on Elastic Foundations
CUR-65	CUR 65 – Design Execution and Repair of Liquid Tide Concrete Structures
D.C.	Distribution Center
DIANA FEA	DIsplacement ANAlyser Finite Element Analysis
E.C. 2	Eurocode 2
F.D.C.P.	Fully Developed Crack Pattern
F.E.M.	Finite Element Model
Gilbert	Gilbert Model
I.C.E.	The Institution of Civil Engineers
I.D.	Imposed Deformation
I.F.	Industrial floor
L.F.E.A.	Linear Finite Element Analysis
M.C. 2010	Fib Model Code 2010
M.H.E.	Material Handeling Equipement
N.F.D.C.P.	Not Fully Developed Crack Pattern
N.L.F.E.A.	Non-Linear Finite Element Analysis
N.T.M.	Notched tensile member
O.o.B.	Out of Balance
R.H.	Relative Humidity
R.T.M.	Restraint tensile member
S.C.S.	Stabilised Cracking Stage
S.F.R.C.	Steel Fibre Reinforced Concrete
S.L.S.	Serviceability Limit State
S.o.G.	Slab on Grade
S.o.P.	Slab on Piles
S.R.A.	Shrinkage Reduction Admixtures
Stu*fib*-11	STUFIB-11 - Controlled Cracking in Jointless Elastic Supported Concrete Floors
TR-34	Technical Report 34 – Concrete Industrial Ground Floors
T.U.D.M.	TU Delft Tensile Member Model
U.D.L.	Unifromly Distributed Load
U.L.S.	Ultimate Limit State

Symbols

Symbol	Description	Unit
N_{soil}	Frictional force by subbase-slab interaction	N
E_{soil}	Young's modulus of soil	$\mathrm{N\,mm^{-2}}$
k_{mod}	Normal stiffness modulus of subbase	$\mathrm{N\,mm^{-3}}$
$W_{max,soil}$	Maximum soil settlement	mm
L_{ss}	Soil settlement length	mm
$L_{friction}$	Frictional restrained length	mm
$L_{restraint}$	Fully restrained length of the slab	mm
L_{slab}	Slab length	mm
K_{yx}	Shear stiffness modulus of subbase	$\mathrm{N\,mm^{-3}}$
τ_{max}	Maximum shear stress of ubbase	$\mathrm{N\,mm^{-2}}$
τ_g	Shear stress of subbase	$\mathrm{N\,mm^{-2}}$
c_s	Cohesion of the soil	$\mathrm{N\,mm^{-2}}$
ϕ_s	Friction-angle of the soil	°
μ_0	Friction coefficient of the soil-structure interaction	-
l_{rs}	Radius of relative stiffness	mm
D	Flexural rigidity of the concrete slab	N m
h	Slab height	mm
F	Racking load	N
σ_{max}	Maximum concrete stress	$\mathrm{N\,mm^{-2}}$
b_{cone}	Cone of equivalent distribution area	$\mathrm{mm^2}$
r_{eq}	Radius of equivalent contact area	mm
a_{eq}	Radius of equivalent loading area	mm
l_{length}	Length of the loading area	mm
l_{width}	Width of the loading area	mm
$x_{max,corner}$	Distance from corner to maximum stress	mm
b_{100}	Reference cone distribution area	mm
r_{50}	Reference contact radius	mm
A_{load}	Loading area	$\mathrm{mm^2}$
κ_{cr}	Cracking curvature of concrete	$\mathrm{mm^{-1}}$
ε_{cr}	Cracking strain of concrete	$\mathrm{mm\,m^{-1}}$
ε_s	Reinforcement steel strain	$\mathrm{mm\,m^{-1}}$
κ_y	Curvature at yielding reinforcement	$\mathrm{mm^{-1}}$
κ_u	Curvature at failure concrete compresions zone	$\mathrm{mm^{-1}}$
ε_{cu3}	Strain at cracking concrete	$\mathrm{mm\,m^{-1}}$
ε_T	Strain due to temperature change	$\mathrm{mm\,m^{-1}}$
κ_{cT}	Strain due to temperature change	$\mathrm{mm^{-1}}$
ΔT	Temperature change	°C
σ_{cr}	Axial concrete cracking stress	$\mathrm{N\,mm^{-2}}$
$\sigma_{cr,fl}$	Flexural concrete cracking stress	$\mathrm{N\,mm^{-2}}$
l_t	Transfer length (cracking)	mm
τ_{bm}	Bond strength steel-concrete	$\mathrm{N\,mm^{-2}}$
V_f	Fibre dosage	%
λ_f	Fibre aspect ratio	–
l_f	Fibre length	mm
$L_{curvature}$	Curvature restraint length	mm
O_f	Orientation factor fibres	-
l_{fp}	Width/Length of loading area of rack	mm
E_{cm}	28-days secant concrete Young's modulus	$\mathrm{N\,mm^{-2}}$
β_{cc}	Time coefficient for concrete	-

Symbol	Description	Unit
ν	Possion ratio	–
α_{cT}	Thermal expansion coefficient	$°C^{-1}$
$\alpha_{E_{cm}}$	Aggregate factor	-
α_{cr}	Cracking factor	-
γ_{mt}	Material factor for concrete under tension	-
f_{cm}	Mean 28 day cylinder compression strength	$N mm^{-2}$
f_{ck}	Characteristic 28 day cylinder compression strength	$N mm^{-2}$
f_{ctm}	Mean 28 day tensile strength	$N mm^{-2}$
$f_{ctm_{fl}}$	Mean 28 day flexural tensile strength	$N mm^{-2}$
f_{cck}	Characteristic 28 day cubic compression strength	$N mm^{-2}$
f_{ccm}	Mean 28 day cubic compression strength	$N mm^{-2}$
$f_{ctd,\infty}$	Long-term design tensile strength	$N mm^{-2}$
A_c	Area of concrete cross-section	mm^2
$A_{c_{eff}}$	Effective tension area of concrete cross-section	mm^2
G_{f_c}	Fracture energy of plain concrete	N mm
η_{cr}	Crack risk	-
ε_{ca}	Autogenous shrinkage strain	$mm m^{-1}$
$\varepsilon_{ca\infty}$	Maximum autogenous shrinkage strain	$mm m^{-1}$
β_{ca}	Time coefficient for autogenous shrinkage	-
ε_{cd}	Drying shrinkage strain	$mm m^{-1}$
$\varepsilon_{cd,0}$	Basic drying shrinkage strain	$mm m^{-1}$
β_{cd}	Time coefficient for drying shrinkage	-
β_{RH}	Relative humidity coefficient for autogenous shrinkage	-
h_0	Nominal thickness of structure	mm
u	Perimeter of structure	mm
t_s	Time of curing	Day's
k_h	Thickness coefficient of structure	-
α_{sra}	Drying shrinkage reduction factor(SRA)	-
φ	Creep coefficient	-
φ_0	Theoretical creep coefficient	-
φ_{RH}	Relative humidity coefficient for creep	-
β_c	Time coefficient for creep	-
β_{t0}	Concrete age coefficient for creep	-
β_{fcm}	Concrete strength coefficient for creep	-
t_0	Concrete age at time of loading	Day's
t_l	Loading period on structure	Day's
ψ	Concrete relaxation coefficient	-
R_{rel}	Concrete relaxation modulus	$N mm^{-2}$
χ_{age}	Aging coefficient	-
J_{t,t_0}	Creep compliance	$mm^2 N^{-1}$
ψ_{crack}	Crack Relaxation coefficient	-
N_{cr}	Cracking force of concrete	N
M_{cr}	Cracking moment of concrete	N mm
$N_{cr_{(t_{cr})}}$	Axial member force directly after first crack	N
$N_{c_{(t)}}$	Axial member force at t	N
α_e	Young's modulus ratio of steel and concrete	-
σ_c	Concrete stress	$N mm^{-2}$
$\sigma_{c1_{(t_{cr})}}$	Concrete stress in uncracked zone after first crack	$N mm^{-2}$
$\sigma_{s1_{(t_{cr})}}$	Steel stress in uncracked zone after first crack	$N mm^{-2}$
$\sigma_{s2_{(t_{cr})}}$	Steel stress in cracked zone after first crack	$N mm^{-2}$
$N_{c_{(t)}}$	Force in tensile member at t	N
$\sigma_{c1_{(t)}}$	Concrete stress in uncracked zone at t	$N mm^{-2}$
$\sigma_{s1_{(t)}}$	Steel stress in uncracked zone at t	$N mm^{-2}$

Symbol	Description	Unit
$\sigma_{s2_{(t)}}$	Steel stress in cracked zone at t	$\mathrm{N\,mm^{-2}}$
s_m	Crack spacing	mm
$w_{(t_{cr})}$	Mean crack width of first crack spacing	mm
$w_{(t)}$	Mean crack width at t	mm
t_{cr}	Moment at first crack	Day's
N_s	Force of reinforcement	N
N_{sy}	Yielding force of reinforcement	N
f_{yd}	Yielding stress of reinforcement	$\mathrm{N\,mm^{-2}}$
E_s	Youngs modulus of steel	$\mathrm{N\,mm^{-2}}$
A_s	Area of reinforcement	$\mathrm{mm^2}$
ρ_s	Reinforcement ratio	%
$\rho_{s_{eff}}$	Effective reinforcement ratio	%
$\rho_{s_{min}}$	Minimum reinforcement ratio	%
σ_s	Steel stress	$\mathrm{N\,mm^{-2}}$
$\varnothing$	Diameter of reinforcement	mm
ε_{sy}	Strain at yielding reinforcement	$\mathrm{mm\,m^{-1}}$
α_{ecc}	Eccentric reduction factor for steel force	-
K_{red}	Long term reduction factor of bond slip shear stiffness	-
$\Delta\sigma_s$	Additional steel stress in crack due to shrinkage strain	$\mathrm{N\,mm^{-2}}$
N_{fibre}	Force taken by steel fibre reinforcement	N
σ_{R1}	Post-cracking residual axial concrete stress at *C.M.O.D.* 0.5 mm	$\mathrm{N\,mm^{-2}}$
σ_{R4}	Post-cracking residual axial concrete stress at *C.M.O.D.* 3.5 mm	$\mathrm{N\,mm^{-2}}$
σ_{fts}	Post-cracking residual axial concrete stress in *S.L.S.*	$\mathrm{N\,mm^{-2}}$
$\sigma_{s,eq(fts)}$	Post-cracking residual concrete stress equivalent to steel stress	$\mathrm{N\,mm^{-2}}$
K_{fibre}	Linear pull-out stiffness of fibres	$\mathrm{N\,mm^{-3}}$
n_f	Number of fibres in cross-section	-
α_{sfrc}	Ratio of the post cracking residual stress of *S.F.R.C.* to cracking stress	-
w_{mo}	Mean crack width for not fully developed crack pattern	mm
w_{mv}	Mean crack width for fully developed crack pattern	mm
w_{max}	Maximum crack width	mm
γ_s	Crack pattern coefficient for crack width calculation	-
γ_∞	Steel stress coefficient for crack width calculation	-
$\sigma_{s,cr}$	Steel stress after cracking of concrete	$\mathrm{N\,mm^{-2}}$
$G_{f_{fibre}}$	Fracture energy of SFRC	Nmm
ε_{fdc}	Strain at start of fully developed crack pattern	$\mathrm{mm\,m^{-1}}$
R	Degree of restraint	–
q_v	Vertical stress on interface	$\mathrm{N\,mm^{-2}}$
Δ_x	Edge movement of the slab	mm
L_{cor}	Correlation length of random field	mm
α_{var}	Coefficient of variation	-
n_{var_l}	Number of variation along the length	-
n_{var_h}	Number of variation along the height	-
α_{th}	Threshold value of random field	-

Figures

Tables

Bibliography

[1] J. Kleemans, "From boring warehouse to sexy product," *Savills World research*, 2017.

[2] J. Schoorl, "De verdozing van het nederlandse landschap." Paper, May 2018.

[3] W. Labib and N. Eden, "An investigation into the use of fibres in concrete industrial ground-floor slabs," *Liverpool John Moores University, Liverpool*, 2006.

[4] G. Garber, *Design and construction of concrete floors*. CRC Press, 2006.

[5] A. A. Abbas, *Analysis and design of industrial ground floor slabs using the finite element method*. PhD thesis, Imperial College London (University of London), 2002.

[6] F. Narin and O. Wiklund, *Design of slabs-on-ground regarding shrinkage cracking*. PhD thesis, 2012.

[7] R. Cajka, M. Smirakova, and P. Matečková, "Frequent failures of frc industrial floors," vol. 738, pp. 217–226, 06 2017.

[8] P. Maas, "Beheerste scheurvorming van voegloze elastisch ondersteunde betonvloeren. aandachtspunten voor ontwerp en aanleg.," tech. rep., Stufib - Stutech, 2006.

[9] R. Gilbert, "Shrinkage, cracking and deflection-the serviceability of concrete structures," *Electronic Journal of Structural Engineering*, vol. 1, no. 1, pp. 2–14, 2001.

[10] J. Knapton, *Ground bearing concrete slabs*. Thomas Telford Limited, 2003.

[11] M. Dijk, "Berekenen scheurvorming in de praktijk," *Cement*, 7-2017.

[12] M. Dijk, "Scheurwijdteberekening bij verhinderde vervorming," *Cement*, 4-2018.

[13] A. A. Abbas, M. Pavlović, and M. D. Kotsovos, "Elastic analysis of ground-floor slabs under multiple loads," *Proceedings of the Institution of Civil Engineers-Structures and Buildings*, vol. 160, no. 3, pp. 151–164, 2007.

[14] L. v. d. M. Niels Punt, "Puntlasten op vloeren vaak onderschat," *Cement*, 2017.

[15] B. B. M.A.N. Hendriks, A. de Boer, "Guidelines for nonlinear finite element analysis of concrete structures," Tech. Rep. Report RTD:1016-1:2017, Rijkswaterstaat Centre for Infrastructure, 2017.

[16] N. Loonen, "Op staal gefundeerde bedrijfsvloeren: Zettingen beheersen of voorkomen," *Civiele Techniek*, 2018.

[17] Committee, *Technical Report 34: Concrete industrial ground floors*. The Concrete Society, 4 ed., 2013.

[18] Commissie, *CUR 36: Ontwerpen van elastisch ondersteunde betonvloeren en -verhardingen*. CUR bouw & infra, 2011.

[19] J. W. Bishop, *The early age behaviour of concrete industrial ground floor slabs*. PhD thesis, © Jonathan William Bishop, 2001.

[20] A. van den Bos Diana Fea and A. Garofano, "Crack predictions using random fields," 11 2016.

[21] J. Hedebratt and J. L. Silfwerbrand, "Lessons learned: Swedish design and construction of industrial concrete floors," *Nordic Concrete Research*, vol. 45, pp. 75–91, 2012.

[22] W. A. M. H. Elsaigh *et al., Steel fiber reinforced concrete ground slabs: a comparative evaluation of plain and steel fiber reinforced concrete ground slabs*. PhD thesis, University of Pretoria, 2001.

[23] M. van Dooren, "Staalvezelbeton in keldervloeren," Master's thesis, Hogeschool Utrecht, 2014.

[24] K. v. B. C.R. Braam, *Concrete Structures under Imposed Thermal and Shrinkage Deformations*. TU Delft, 2016.

[25] J. L. Silfwerbrand and A. A. Farhang, "Reducing crack risk in industrial concrete floors," *ACI Materials Journal*, vol. 111, no. 6, 2014.

[26] K. Dare, "Concrete industrial floors - a journey of compromises.".

[27] H. Reinhardt, *Beton als constructiemateriaal eigenschappen en duurzaamheid*. Delftse Universitaire Pers, 2000.

[28] G. C. B. C.R. Braam, "De treksterkten van beton nader beschouwd," *Cement*, 2003.

[29] Z. Al-Kamyani, F. P. Figueiredo, H. Hu, M. Guadagnini, and K. Pilakoutas, "Shrinkage and flexural behaviour of free and restrained hybrid steel fibre reinforced concrete," *Construction and Building Materials*, vol. 189, pp. 1007–1018, 2018.

[30] C. B. J.C. Walraven, *Prestressed concrete*. Faculty of Civil Engineering and Geoscience, 2014.

[31] "Model code for concrete structures 2010."

[32] Commissie, "Achtergrondrapport: Floor 3.0," tech. rep., SBRCURnet, 2016.

[33] A. v. d. B. C.R. Braam, "Vloeistofdichte doorgaand-gewapend, ter plaatse gestorte betonvloeren de scheurwijdtecontrole," *Cement*, 2005.

[34] T.-S. Seo and J.-C. Kim, "Behaviour of concrete in a stress continuity region after cracking under restrained drying shrinkage," *Structural Concrete*, vol. 14, no. 2, pp. 131–137, 2013.

[35] J. R. Deluce and F. J. Vecchio, "Cracking behavior of steel fiber-reinforced concrete members containing conventional reinforcement.," *ACI Structural Journal*, vol. 110, no. 3, 2013.

[36] A. Jansson, M. Flansbjer, I. Löfgren, K. Lundgren, and K. Gylltoft, "Experimental investigation of surface crack initiation, propagation and tension stiffening in self-compacting steel–fibre-reinforced concrete," *Materials and structures*, vol. 45, no. 8, pp. 1127–1143, 2012.

[37] B. E. Barragán, *Failure and toughness of steel fiber reinforced concrete under tension and shear*. Universitat Politècnica de Catalunya, 2002.

[38] Commissie, *CUR 111: Staalvezelbeton bedrijfsvloeren op palen – Dimensionering en uitvoering*. CUR - Bouw & Infra, 2007.

[39] J. A. Barros, V. M. Cunha, A. F. Ribeiro, and J. Antunes, "Post-cracking behaviour of steel fibre reinforced concrete," *Materials and Structures*, vol. 38, no. 1, pp. 47–56, 2005.

[40] J. Silfwerbrand, "Improvements of the swedish concrete association's method for design of sfrc slabs on grade," in *Proceedings*, pp. 23–32, 2001.

[41] R. Vrijdaghs, M. Di Prisco, and L. Vandewalle, "A numerical model for the creep of fiber reinforced concrete," in *High Tech Concrete: Where Technology and Engineering Meet*, pp. 366–373, Springer, 2018.

[42] V. M. Cunha, J. A. Barros, and J. M. Sena-Cruz, "Pullout behavior of steel fibers in self-compacting concrete," *Journal of Materials in Civil Engineering*, vol. 22, no. 1, pp. 1–9, 2009.

[43] C. Mpanga-A-Kangaj, "Pull-out of hooked end steel fibres : experimental and numerical study," Master's thesis, University of Pretoria, 2014.

[44] B. Weiler and C. Grosse, "Pullout behaviour of fibers in steel fibre reinforced concrete," *Otto-Graf-Journal*, vol. 7, pp. 116–127, 1996.

[45] S. Abdallah, M. Fan, and D. W. Rees, "Predicting pull-out behaviour of 4d/5d hooked end fibres embedded in normal-high strength concrete," *Engineering Structures*, vol. 172, pp. 967–980, 2018.

[46] T. Kasper, *Design guideline for structural applications of steel fibre reinforced concrete*. SFRC Consortium, 2014.

[47] A. Mudadu, G. Tiberti, F. Germano, G. A. Plizzari, and A. Morbi, "The effect of fiber orientation on the post-cracking behavior of steel fiber reinforced concrete under bending and uniaxial tensile tests," *Cement and Concrete Composites*, vol. 93, pp. 274–288, 2018.

[48] J. H. W.W. Walker, "Modulus of subgrade reaction - which one should be used?," *Structural Service - Engineering Bulletin*, 2016.

[49] G. Tiberti, A. Mudadu, B. Barragan, and G. Plizzari, "Shrinkage cracking of concrete slabs-on-grade: A numerical parametric study," *Fibers*, vol. 6, no. 3, p. 64, 2018.

[50] R. I. Gilbert, "Shrinkage cracking in fully restrained concrete members," *Structural Journal*, vol. 89, no. 2, pp. 141–149, 1992.

[51] H. L. M. S. G.Chr. Bouquet, C.R. Braam, "Ontwikkeling vencon 2.0 levert nieuw rekenmodel," *Cement*, 2004.

[52] D. Ferreira, *DIANA FEA - User's Manual 10.3*. 2019.

[53] R. Van der Have, "Random fields for non-linear finite element analysis of reinforced concrete," 2015.

[54] S. Prakash, "Nonlinear finite element analysis of shrinking reinforced concrete slabs-on-ground," 2018.

[55] S. Sato and T. Shimomura, "Stress-effective strain curve of uniaxial specimen under restrained drying shrinkage," *Proc. of Japan Concrete Institute*, vol. 28, no. 1, 2006.

[56] S. Committee, "Practitioners guide to finite element modelling of reinforced concrete structures," tech. rep., Federation internationale du beton(fib), 2017.

[57] S. A. Altoubat and D. A. Lange, "Creep, shrinkage, and cracking of restrained concrete at early age," *ACI Materials Journal*, vol. 98, no. 4, pp. 323–331, 2001.

[58] R. I. Gilbert, "Shrinkage and early-age temperature induced cracking and crack control in concrete structures," *School of Civil and Environmental Engineering, UNSW Australia, Sydney, Australia*, 2015.

[59] R. Braam, "Studie naar dwarsvoegafstand." C.R.O.W. Betonwegendag, 2011.

[60] M. Al-Gburi, J. E. Jonasson, and M. Nilsson, "Effect of casting sequences on the restraint in slab-on-ground," in *Proceedings of the Concrete Innovation Conference, Oslo, Norge*, pp. 1–8, 2014.

[61] W. W. Walker and A. H. Jerry, "Thou shalt not curl nor crack...(hopefully)," *Concrete International, Jan*, 1999.

[62] J. Lahdensivu, J. Hietala, and K. Saastamoinen, "Practical experiences on cracking of concrete slabs on ground," *Nordic Concrete Research*, vol. 40, pp. 11–20, 2009.

[63] P. Bamforth, "Control of contraction induced cracking in concrete," tech. rep., CIRIA C660, 2007.

[64] A. J. F. van Cauweleart, M. Slet, "The general solution for a slab subjected to centre and edge loads and resting on a kerr foundation," 2001.

[65] J. R. Eyre, "Membrane action in ground-bearing concrete slabs," *Proceedings of the Institution of Civil Engineers-Structures and Buildings*, vol. 159, no. 3, pp. 153–163, 2006.

[66] A. Alani, D. Beckett, and F. Khosrowshahi, "Mechanical behaviour of a steel fibre reinforced concrete ground slab," *Magazine of Concrete Research*, vol. 64, no. 7, pp. 593–604, 2012.

[67] P. J. Robins, J. W. Bishop, and S. A. Austin, "Early-age finite element modelling of industrial ground floors," *Proceedings of the Institution of Mechanical Engineers, Part L: Journal of Materials: Design and Applications*, vol. 217, no. 4, pp. 295–308, 2003.

[68] D. Tomasovicova and N. Jendzelovsky, "Stiffness analysis of the subsoil under industrial floor," *Procedia engineering*, vol. 190, pp. 365–370, 2017.

[69] B. Chiaia, A. Fantilli, and P. Vallini, "Crack patterns in reinforced and fiber reinforced concrete structures," *The open construction and building technology Journal*, vol. 2, no. 1, 2008.

[70] H. Westergaard, "Stresses in concrete pavements computed by theoretical analysis," *Public Roads*, 1926.

[71] E. Winkler, "Die lehre von der elastizitat und festigkeit," 1867.

[72] H. Hertz, "Uber das gleichgewicht schwimmender elastischer platten"," *Wiedmann's Annalen der Physik und Chemie*, 1884.

[73] A. Foppl, "Vorlesungen uber technische mechanik," 1907.

[74] A. Goldbeck, "Thickness of concrete slabs," *Public Roads*, 1919.

[75] C. Older, "Highway research in illinois," *Transactions of the ASCE*, 1924.

[76] T. M. Ioannides, A. and E. Barenberg, "Westergaard solutions reconsidered," *Transportation Research Record 1043*, 1985.

[77] F. V. Cauwelaert, "Ontwikkeling in de dimensionering van betonverhardingen en bedrijfsvloeren," *Cement*, 1997.

[78] F. R. Neal, *ICE design and practice guides: Concrete industrial ground floors*. Thomas Telford Limited, 2002.

[79] R. Bradbury, "Reinforced concrete pavements," *Wire reinforcement Institure*, 1938.

[80] E. Kelley, "Application of the results of research to the structural design of concrete pavement: a t/m c," *Public Roads*, 1939.

[81] G. Pickett, "Concrete pavement design: A study of stresses on the corner region of pavement slabs under large corner loads," *Portland Cement Association*, 1951.

[82] J. K. C.L.D. Childs, "Tests of concrete pavements on gravel subbases," *Journal of the highway division*, 1958.

[83] J. A. Barros, "Analysis of concrete slabs supported on soil," in *IV Congreso Métodos Numéricos en Ingeniería, SEMNI*, 1999.

Appendix A

Imposed deformation

The effect of shrinkage on a concrete member is discussed. First, the principle of imposed deformations with the resulting stress profiles will be elaborated. Then the crack formation stages in a concrete member are addressed. Finally, the calculation methods for the stresses and cracks are given. The stresses in a concrete member are a result of imposed deformation. If a concrete member can move freely, without any restraint, shrinkage of concrete would not be a concern when designing a structure. The free movement of concrete due to shrinkage will not result in stresses. Often concrete members such as slabs are restraint by their support or surrounding. *I.D.* appears to be quite complicated to take into account during the design of concrete structures. Even how the term imposed deformation is used in practice gives rise to confusion and misunderstanding. The principle is that the movement of a concrete structure is restraint and that the induced movement results in stresses in the structure. The term restraint deformation would be a better name to describe the situation. The imposed deformation can come from changes in temperature, shrinkage or settlement of support. A very common situation that results in imposed stresses is casting young to old concrete.

Young to old concrete

The situation of casting an element to a previously cast part is a typical example that has to be taken into account. The left part has already a high strength and stiffness. After casting, the new part deforms more and will be restrained at the joint by the older part. The shear stresses in the joint between new and old result in tensile stresses in the new concrete element. In Fig: A.1 the situation is given.

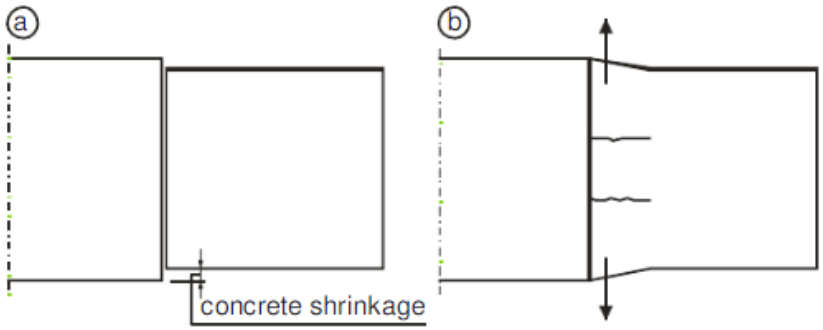

Figure A.1: Young to old concrete

The race between the developed concrete tensile strength and the generated imposed stresses has begun. Measures have to be taken to make sure that developed strength is in all-time higher then the generated tensile stresses, else cracking occurs. The bending(EI) and normal(EA) stiffness of the structural element are assumed to be constant in the calculations. The effect of cracking should be taken into account, knowing that concrete is likely to crack. When cracking occurs, the stiffness reduces, the forces also will be reduced and distributed to a nearby location.

General approach

The general approach to determine the response of a structure undergoing imposed deformations can be divided into three steps:

1. Divide the system into sub-systems such that the structure can freely move by the imposed deformation.
2. Apply forces (moments, axial forces, shear forces) at the ends of the sub-systems in order to restore compatibility with its original boundary condition.

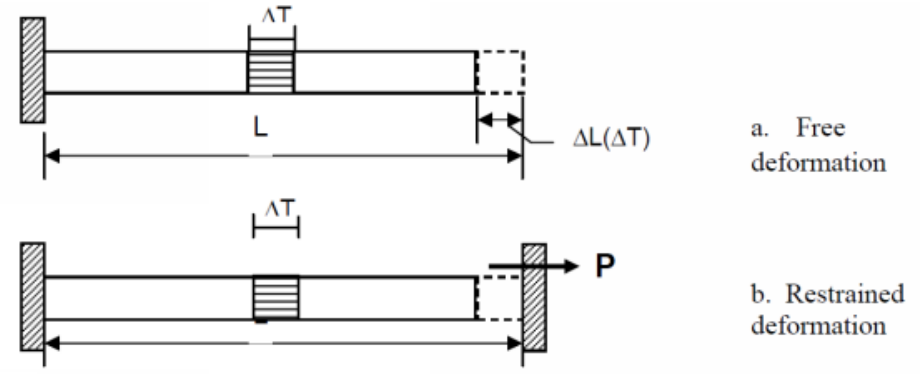

Figure A.2: Concept of imposed deformation

3. Determine the distribution of forces in the structure caused by the applied forces.

In Fig:A.2 An example is given for a concrete bar fixed at both ends subjected to a uniform temperature drop. The required force P to make the structure compatible with its boundary conditions introduces tensile stresses in the concrete element. Imposed deformations can be a risk because from the outside nothing happened but inside the element high stresses can be present.

Because imposed deformation often has a long-term loading effect, the long-term properties of concrete like creep also have to be taken into account. For the *U.L.S.* design, forces generated by *I.D.* are often ignored because the effects can be reduced significantly. The ultimate load-bearing capacity of a structure is hardly affected by it. *I.D.* are almost never the reason for the failure of a structure. *I.D.* are of great importance during the *S.L.S.* design. The designer has to be aware of the crack pattern that can develop. In the case of a structure with little rotational capacity or free axial movement, imposed deformation can cause high stresses. For *S.o.G.*, two stress profiles can occur from imposed deformations: Uniform and gradient. The stress profiles can be described with respectively a tensile and a flexural member. The behaviour of the member depends on the phase on the load-deformation diagram. The phases can be separated into a linear stage and a cracked stage. The cracked stage will be explained more in detailed.

Cracked stage

When the stresses in a concrete member reach the concrete tensile capacity, the member will crack. The kind of crack pattern depends on the type of loading. If cracking occurs, an imposed deformation results almost always in a not fully developed crack pattern and an external load a fully developed crack pattern.

Not fully developed cracking pattern

When the tensile bar is subjected to an imposed deformation and the member cracks, the axial stiffness locally decreases. The strain remains constant and therefore the tensile force will drop below the cracking force N_{cr} to $N_{cr_{(t_{cr})}}$. When the imposed deformation further increases the axial forces grows to N_{cr} were a second crack occurs. This stage were new cracks gradually are formed is denoted as the Crack Formation Stage (*C.F.R.*), Fig:A.3

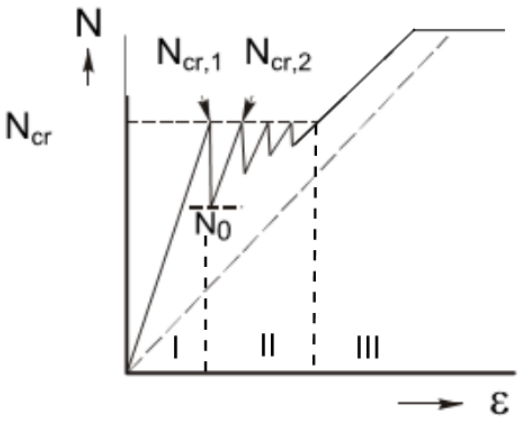

Figure A.3: The crack formation stages

The maximum stress in the reinforcement in the *C.F.R.* is $\sigma_{s,cr}$ and is related to the concrete cracking stress σ_{cr}, which depends on the type of loading. The steel stress at cracking is an important parameter for the calculation of the crack width. During the *C.F.R.* the steel stress cannot grow above $\sigma_{s,cr}$. For this reason, the crack width during the *C.F.R.* is constant.

Fully developed crack pattern

By increasing the imposed deformation further on, the number of cracks increases. Finally, a situation is reached were no more cracks can be formed. Only 'disturbed regions' are present in the tensile member. The transfer zones of the cracks are overlapping, and therefore, the smallest spacing between two cracks is l_t and the largest $2l_t$. When no new cracks can occur the *C.F.R.* will result into the Stabilised Cracking Stage (*S.C.S.*) shown in Fig: A.4. An increase in imposed deformation in the *S.C.S.* leads to an increase of the steel stress and thus an increase in crack width.

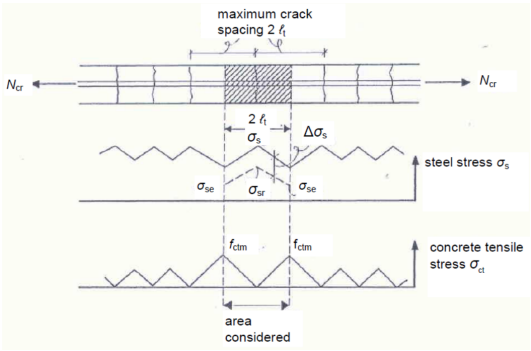

Figure A.4: The stabilised cracking stage III with the maximum crack spacing

Member behaviour

Tensile member

A relatively simple example is a tensile member. Here the element is applied with a uniform shrinkage load. The tensile member can represent a monolithic jointless slab, as shown in Fig:A.5. A structural designer wants to control the cracks. To control the cracks, it is important to have a clear understanding of the load deformations diagramA.5. Cracking behaviour can be separated into four phases. The uncracked, cracking, fully developed crack and yield phase. In practice, an *I.D.* almost always results in a not fully developed crack pattern.

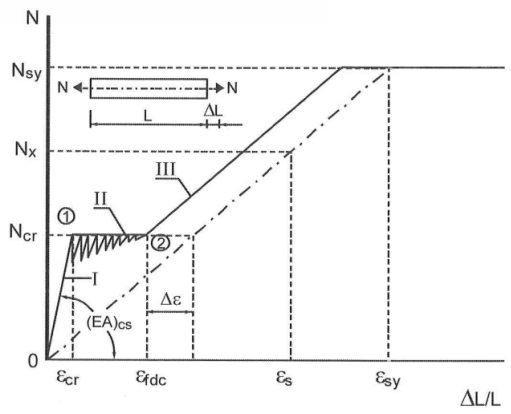

Figure A.5: Monolithic, jointless slab under imposed deformation (uniform shrinkage)

$$N_{cr} = \varepsilon_{cr} E_c A_c \left(1 + \alpha_e \rho\right) \tag{A.1}$$

$$\varepsilon_{fdc} = \left(60 + 2.4\sigma_{s,cr}\right) \cdot 10^{-6} \tag{A.2}$$

$$\sigma_{s,cr} = \frac{N_{cr}}{A_s} \tag{A.3}$$

$$\varepsilon_{s,cr} = \frac{\sigma_{s,cr}}{E_s} \tag{A.4}$$

$$\Delta\varepsilon_{ts} = \varepsilon_{s,cr} - \varepsilon_{fdc} \tag{A.5}$$

$$\varepsilon_{sy} = \frac{f_{yd}}{E_s} \tag{A.6}$$

(A.7)

Flexural member

The same principle can be applied for a flexural member but then with a moment-curvature diagram. The characteristic points on the diagram can be calculated with:

The reduced flexural stiffness and the bending moment can be derived from the Fig: A.6 for an arbitrarily imposed curvature. If the element has a lot of cracks, the stiffness will be lower, which results in smaller forces generated by imposed deformations.

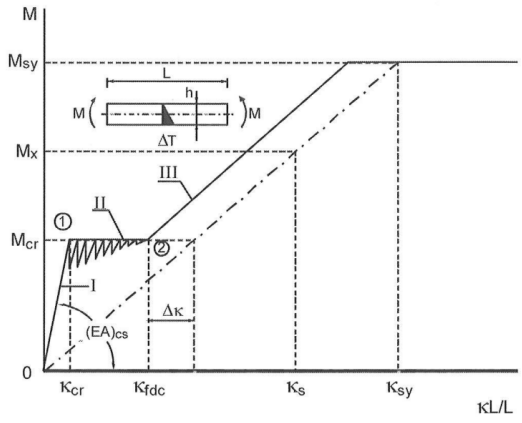

Figure A.6: M-κ diagram of a flexural member

$$\kappa = \frac{M}{EI_{red}}$$

$$\kappa_{cr} = \frac{2\varepsilon_{cr}}{h}$$

$$\kappa_{fdc} = \frac{\varepsilon_{fdc}}{d - X_m} = \frac{2M_{cr}}{E_c b X_m^2 \left(d - \frac{X_m}{3}\right)}$$

$$X_m = d\left(-\alpha_e \alpha_{ts} \rho_{eff} + \sqrt{\left(\alpha_e \alpha_{ts} \rho\right)^2 + 2\alpha_e \alpha_{ts} \rho}\right)$$

$$\alpha_{ts} = \frac{\sigma_{s,cr}}{\sigma_{sm}}$$

$$\kappa_{sy} = \frac{\left|\varepsilon_{cu3}\right| + \varepsilon_s}{d}$$

$$\Delta\kappa = \frac{M}{EI_{red}}$$

Loading sequence

Effect of Loading sequence on crack width

For the crack width calculation, it is important to take into account the loading sequence. The loading combination can result in different final steel stresses. Therefore the calculation of the steel stress at the first crack and for the final situation is given in this section. The imposed deformation results in a tensile force in the slab until its cracks. The maximum axial force by shrinkage is thus limited by the cracking forces of the concrete. When the slab is also loaded by external loads, the combined loading might initiate cracking at the location of the load. The steel stress due to the loading can be calculated on the basis of equilibrium in the cross-section. With the steel stress and the crack-width due to the tensile force, the maximum crack width of the combined

loading can be calculated according to:

$$w_{max} = \gamma_s \gamma_\infty w_{mf} = \gamma_s \gamma_\infty w_{mo} 1.8 \left(\frac{\sigma_s}{\sigma_{s,cr}} - 0.5 \right) \tag{A.16}$$

The loading sequence of the external load and the restrained deformation does influence the outcome of the crack width calculations. The calculation methods depend on which loads are applied first and if this first load results in cracking of the concrete. The following situations are relevant to the research.

Bending moment M followed by an imposed strain or curvature
The crack pattern will be fully developed if the bending moment results in a cracked cross-section. The imposed strain will lead to a widening of the already existing cracks. When the applied bending moment is below the cracking moment, the cracking is likely to be caused by the imposed deformation. The crack pattern can be assumed to be not fully developed. A fully developed crack pattern is only possible by a very large imposed deformation. The equations for this situation are given despite the unlikelihood of appearing.

Restrained deformation followed by an external load.
When the imposed strain results in a fully developed crack pattern, the bending moment will contribute to higher steel stress in the crack, which results in larger crack width. If the crack pattern is not fully developed or the structure is un-cracked, the additional moment will likely result in a fully developed crack pattern. Also, for this situation, the resulting steel stress of the combined loading is used for the calculation of the crack width and spacing.

Example
In the literature, an example is given for the same situation. Only the assumption of cracking is different. The conclusion is that first cracking due to an external followed by shrinkage is more beneficial. Because external loads result in fully developed crack patterns and therefore the maximum amount of cracks are present. The additional opening of the crack due to the shrinkage is therefore smaller.

Imposed curvature and external bending moment
Not fully developed crack pattern when $M_{Ed} << M_{cr}$ and $\kappa_{cr} < \kappa_{Ed} < \kappa_{fdc}$:

$$w_m = w_{mo(M_{cr})} \tag{A.17}$$

Fully developed crack pattern:

$$w_m = w_{mo(M_{cr})} 1.8 \left(\frac{\sigma_s}{\sigma_{s,cr}} - 0.5 \right) \tag{A.18}$$

Where the steel stress σ_s is:

$$\sigma_s = \frac{M_{Ed}}{zA_s} + \kappa_{Ed} \left(d - \frac{h}{2} \right) E_s \qquad \text{If} \quad M_{Ed} > M_{cr} \quad \text{Followed by} \, \kappa_{Ed} \tag{A.19}$$

$$\sigma_s = \sigma_{s(\kappa_{Ed})} + \frac{M_{Ed}}{zA_s} \qquad \text{If} \quad \kappa_{Ed} > \kappa_{fdc} \quad \text{Followed by} \, M_{Ed} \tag{A.20}$$

$$\sigma_s = \sigma_{s,cr(M_{cr})} + \frac{M_{Ed}}{zA_s} \qquad \text{If} \quad \kappa_{Ed} < \kappa_{fdc} \quad \text{Followed by} \, M_{Ed} \tag{A.21}$$

Imposed strain and external bending moment
Not fully developed crack pattern when $M_{Ed} << M_{cr}$ and $\varepsilon_{cr} < \varepsilon_{Ed} < \varepsilon_{fdc}$

$$w_m = w_{mo(N_{cr})} \tag{A.22}$$

Fully developed crack pattern

$$w_m = w_{mo} 1.8 \left(\frac{\sigma_s}{\sigma_{s,cr}} - 0.5 \right) \tag{A.23}$$

Where the steel stress σ_s and w_{mo} is:

$$\sigma_s = \frac{M_{Ed}}{zA_s} + \sigma_{s(\varepsilon_{Ed})} \quad \text{and} \quad w_{mo} = w_{mo(M_{cr})} \quad \text{If} \quad M_{Ed} > M_{cr} \quad \text{Followed by } \varepsilon_{Ed} \tag{A.24}$$

$$\sigma_s = \sigma_{s(\varepsilon_{Ed})} + \frac{M_{Ed}}{zA_s} \quad \text{and} \quad w_{mo} = w_{mo(N_{cr})} \quad \text{If} \quad \varepsilon_{Ed} > \varepsilon_{fdc} \quad \text{Followed by } M_{Ed} \tag{A.25}$$

$$\sigma_s = \sigma_{s,cr(N_{cr})} + \frac{M_{Ed}}{zA_s} \quad \text{and} \quad w_{mo} = w_{mo(N_{cr})} \quad \text{If} \quad \varepsilon_{Ed} < \varepsilon_{fdc} \quad \text{Followed by } M_{Ed} \tag{A.26}$$

Appendix B

Failure survey

Survey - F. Narin and Wiklund

Four site surveys were performed by F. Narin and Wiklund to investigate the shrinkage behaviour of slab on ground with piles. The different foundation method results in a slightly different restraint of the concrete slab. Cracks caused by the pile foundation are left out and the focus is on the shrinkage cracking of the concrete slab. The objects are given with a description of the cracks. Besides the cracks, the concrete cover is also measured. The outcome of the survey is summarised at the end.

Object 1

Only three cracks were found during the survey. The cracks are likely due to shrinkage. Locally higher restraint from the joints in combination with a rectangular shape are assumed to be the reason for cracking. The crack widths are within the performance requirement and thus not reported as failure. Interesting to notice is that the mean cover value is higher then the design value of 25 mm. The hogging capacity is therefore lower than designed which can result in failure. It also leads to a lower reinforcement ratio in the toplayer. The reinforcement becomes less effective to reduce the cracks width. In section D there was found a crazed surface and exposed aggregate. The surface is affected by drying of the surface layer, Figure B.1. This can come from casting in windy/sunny conditions and not covering the slab in time. Crazing indicate a construction error instead of design errors. Also a deviating in concrete mixture quality can be the reason. Nevertheless the floor is in good condition.

(a) Overview

Crack number	Concrete cover - mean value [mm]	Crack width - max value [mm]	Crack width - mean value [mm]
1	48.8	0.25	0.14
2	24.6	0.20	0.14
3	38.3	0.15	0.11

(b) Cracks

(c) Surface damage

(d) Crazing

Figure B.1: Object 1

Object 2

Many cracks were observed during the survey. Four cracks are reported with a significant width. Crack one and two are identified in zone C and are a result of overloading by *M.H.E.*. Crack three and four are indicated as shrinkage cracks because of the aspect ratio is way above the advised value of 1.15. During execution, it was decided to add a joint. It would be better if the joint was placed in the middle and perpendicular to its current position. The reasons for its final locations are not known.

The crack widths exceed the recommendation values, but the client didn't have high aesthetic demands and wanted a cheap floor. Therefore it is possible that the crack widths are within the acceptable design range. Crack widths larger than 1 mm are found, which can result in additional damage by *M.H.E.* by spalling of the concrete at the edge. This already happened at the constructed joints shown in figure B.2. At the joints, height different is measured, which resulted in the joint damage.

During the survey, crazing was found around the complete slab. The overall quality, particularly the visual appearance, was not very satisfying. Besides the crazing and cracks, the detailing of the joints was found not to be carefully executed. The final joint location is not always as designed and the quality of the joints is low. The overall quality of the floor is poor but accepted by the client.

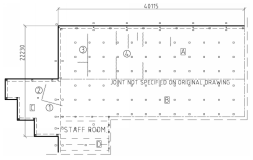

(a) Overview

Crack number	Concrete cover - mean value [mm]	Crack width - max value [mm]	Crack width - mean value [mm]
1	36.4	1.20	0.96
2	36.4	1.10	0.88
3	23.0	1.10	0.74
4	30.5	1.00	0.64

(b) Cracks

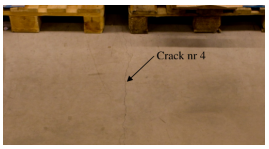

(c) Shrinkage crack

(d) Joint deterioration

Figure B.2: Object 2

Object 3

In bay D cracks one to three looks like shrinkage cracking created by the restraint of the earlier poured section C. The extra restraint from the large foundation pad can be the reason why these cracks only occurred at this location. Crack widths of 2 mm were found above the pile group. A combination of a hogging moment due to settlement, in-between pile loading and shrinkage is the reason for large crack width. In zone E, G and H the settlement difference between piles and soil resulted also in excessive cracking. Due to the heavy loaded zone, large hogging moments arise and resulted in cracking. For slabs on grade this can also occur when the soil stiffness is inhomogeneous or stiff pad foundations are used for the columns.

In some places, plastic settlement cracking is defined with the same spacing as the reinforcement. The mean cover, 19 mm, in this area is at the lower bound of the nominal value,20 mm, which can be the reason for the settlement cracking. The presence of multiple crack types with large crack width indicates poor execution in combination with an insufficient overall design.

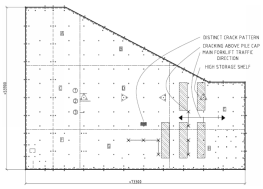

(a) Overview

Crack number	Concrete cover - mean value [mm]	Crack width - max value [mm]	Crack width - mean value [mm]
1	45	0.80	0.59
2	45	2.00	1.20
3	45	0.40	0.29

(b) Cracks

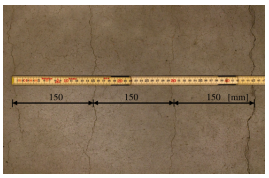

(c) Plastic shrinkage

(d) Overloading:hogging moment

Figure B.3: Object 3

Object 4

A relative small warehouse with no joints is investigated. Local thickening is applied at the perimeter and at the internal piles. This resulted in long rectangular areas with very high edge restraints. Due to the long strips with edge restraints, typical shrinkage cracks were found. Joints should have been applied to reduce the aspects ratio of the restrained slabs. Crack widths of 1.1 mm with a maximum mean value of 0.7 are measured. This is above the advised crack width and also not wanted by the client/user. The cracks were repaired by filling it with epoxy-based materialB.4. Cracks 2,5 and 9 are probably from the traffic loading, which creates a hogging moment over the thickened perimeter. The average crack widths, 0.30-0.38 mm, are within the advised value and, therefore, as designed. The overall surface had no defects or extensive crazing. Besides the larger cracks, the aesthetics were good.

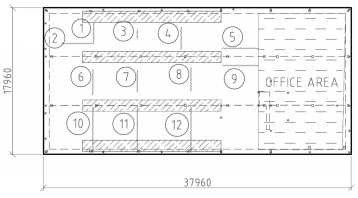

(a) Overview

Crack number	Concrete cover - mean value [mm]	Crack width -max value [mm]	Crack width -mean value [mm]
1	69.4	1.10	0.60
2	62.4	0.50	0.30
3	54.2	0.50	0.28
4	86.3	0.50	0.31
5	72.6	0.50	0.31
6	-	1.00	0.64
7	-	1.00	0.59
8	-	1.00	0.69
9	62.6	0.50	0.38
10	-	1.00	0.66
11	-	0.60	0.45
12	-	1.00	0.67

(b) Cracks

(c) Shrinkage crack (repaired)

Figure B.4: Object 4

Survey - J. Hedebratt and J. Silfwerbrand

A long-term study on several industrial floors, age varies from 6 to 11 years, mainly constructed with steel fibre reinforcement was performed by J. Hedebratt and J. Silfwerbrand. In total, 25 floors are examined and eleven of them have extensive cracking. Two floors have shown levelness problems and only one has issues with joints. It is found that cracks are often near or due to the joints and thereby caused by them. On two floors, there was severe damage reported by overloading. This seems to be an unusual case. During the survey, twelve floors reported no damages, but it can not be concluded that there is no cracking on these floors. The owner only values the imperfections, and there consequences not as a failure.

The majority of the cracking in the floor is likely to be caused by segregation and plastic settlement of the concrete and or subsoil. This can come from too much plasticizer and high consistency class to increase the workability. During the casting of the floor, local soil settlement can occur, resulting in higher tensile stresses above the reinforcement. After power floating the top surface can be repaired, but after some shrinkage, the crack can resurface.[21]

Survey - Tampere University

A study performed by Tampere University investigated six industrial floors with centric reinforcement with a thickness of 120-130 mm. Cracks widths of 0.1 to 1 mm and crack spacing of 300 to 1000 mm are measured. Noticeable is that for small crack widths, the crack spacing is small and larger cracks have larger spacing. Also it is found that the location of the reinforcement is not always as designed. Sometimes the reinforcement was found in the bottom layer of the slab. With joint spacing larger than ten meters many shrinkage cracks occurred in the floors. Most cracks were found near columns of the building frame. Radial cracks were found around the columns which can indicate settlement differences of the floor and the column foundation.[62]

Survey - Garber

The levelness of the subbase is sometimes more off than designed. A study by John Kelly lasers 1989 showed that a typically graded subbase ready for placement had a standard deviation of 14.9 mm. Which results in that 10% of the floor is 25 mm above or below the design grade. The floor surface can also vary more than many suppose. Satisfactory floor surfaces with a variation of 20 mm around the design grade can be found. When the two situations come together, a floor thickness reduction of 45 mm is possible after execution [4].

Appendix C

Diana Finite Element Analysis

Mesh sensitivity analysis

The mesh size has an influence on the behaviour in finite element analysis. Therefore, it is important to investigate the effect of the mesh size on the analysis. The notched tensile member is analysed with a coarse and fine mesh of respectively $\frac{h}{7}$ and $\frac{h}{14}$. With a smaller mesh size, the analyses are more smooth because the strains and stresses can be calculated at a smaller scale. The development of the minimum and maximum axial forces and steel stress is shown in Fig: C.1a. The maximum and minimum axial concrete forces are found in respectively the uncracked and cracked zone. The steel stresses are found contrary to that. The global behaviour of the tensile members is similar. Only the amount of forces and stresses are different. The crack relaxation effect in more present in the coarser mesh. Also, crack localisation occurs more rapidly with the coarse mesh. In the finer mesh, a cracking period is present before a dominant crack is formed. It can be seen that the contribution of the concrete in the crack is larger when a fine mesh is used. The tensile member acts stiffer during cracking because the tension stiffening effect is more present. This results in lower steel stress in the crack. When looking at the crack width based on the average strain and the element, Fig: C.1b and Fig:C.1c, method it can be concluded that the higher axial force or steel stress does not result in a large crack width difference. The crack width development based on the average strain method in both model is equal Fig:C.1d.

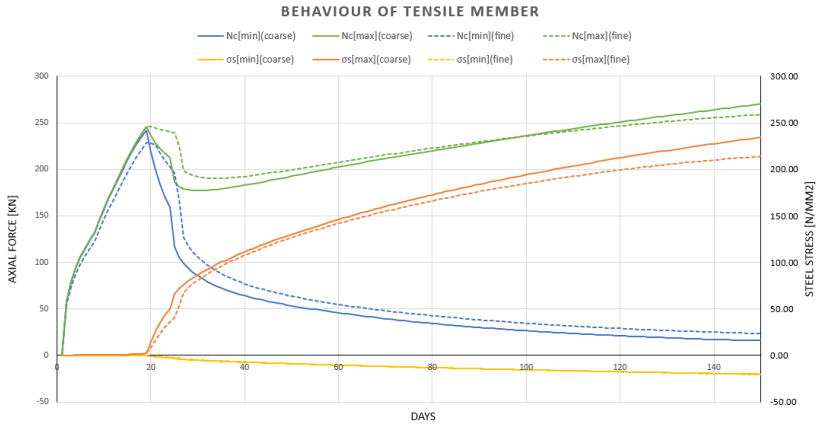

(a) Behaviour in tensile member

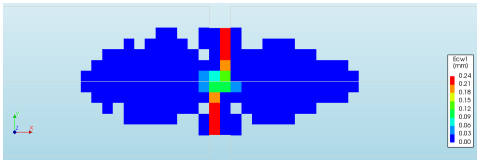

(b) Crack width fine mesh

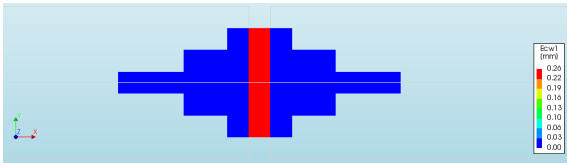

(c) Crack width coarse mesh

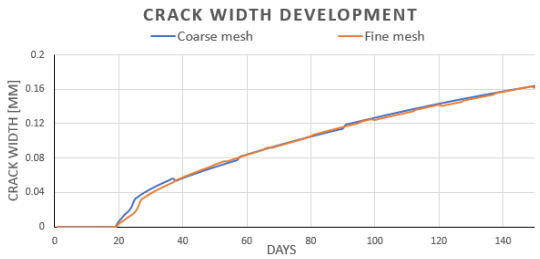

(d) Crack width average strain based

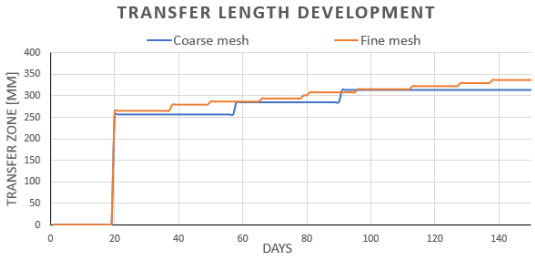

(e) Influence on transfer length

Figure C.1: Random field for changing α_{th}

Random field

As mentioned in the report, the correlation function suggested in the literature is between 0.5 and 5 m. The exponential and squared exponential correlation functions are both suggested to use. The coefficient of variation is between 0.1 and 0.3 for the normal, truncated normal and log-normal distribution types. A study is performed to investigate the effect of the α_{var} and L_{cor} on the cracking behaviour.

During the research of *R. van der Have*, it is concluded that the CMD method is the most accurate for class 1 but becomes less efficient for models with more than 1000 nodes. No significant difference between the exponential and squared exponential correlation function was found. The research also concluded that the random field might improve the numerical stability of *N.L.F.E.A.*. When the random field is used, the area with cracking strains becomes smaller. Cracking is more localised, which improves the numerical stability. The growth of cracked integration points is more gradual when spatial varying material properties are used. The downside is that when the random field is applied in *N.L.F.E.A.*, it is not known when the cracking starts because the weakest point in the structure is not known prior. This required a larger zone with smaller load steps and, thus, a more intensive model. In this research, the used methods are based on the suggestions by *R. van der Have* [53].

Random field parameter analysis

To get a better insight into the generation of the random field, the parameters are analysed. The focus of the analysis was on the variation in the tensile strength and the number of imperfection in a slab of ten meters long. The number of imperfections indicates the number of localised cracks and, therefore, the crack spacing. The imperfections are determined as the number of the area which has the lowest values in the legend. It can occur during the crack analysis that cracking is initiated in more weak spots, and thus, a lower crack spacing can be found.

Variation coefficient α_{var}

The variation of concrete properties according to the *JCSS* model in DIANA FEA is 0.06, 0.30, 0.15 and 0.15 for respectively compression, tension, Young's modulus and ultimate strain. Therefore the extreme values in the range of 0.05 to 0.3 for the variation coefficient α_{var} are investigated. In Tab: C.1 the results are shown. An increase of α_{var} has a trend to reduce the crack spacing. Higher variation tends to lead to more weak spots in the slab, but no final conclusion can be drawn from the results. On the other hand, it can be concluded that an increase in α_{var} significantly increases the deviation of the variable property.

Table C.1: Analysis of variation coefficient α_{var}

α_{var}	Min f_{ctm}	deviation factor	Max f_{ctm}	deviation factor	ave. crack spacing
0.05	1.67	0.96	1.83	1.05	6.7
0.1	1.56	0.89	1.91	1.10	4.4
0.2	1.50	0.86	2.14	1.23	5.0
0.3	1.29	0.74	2.39	1.38	2.7

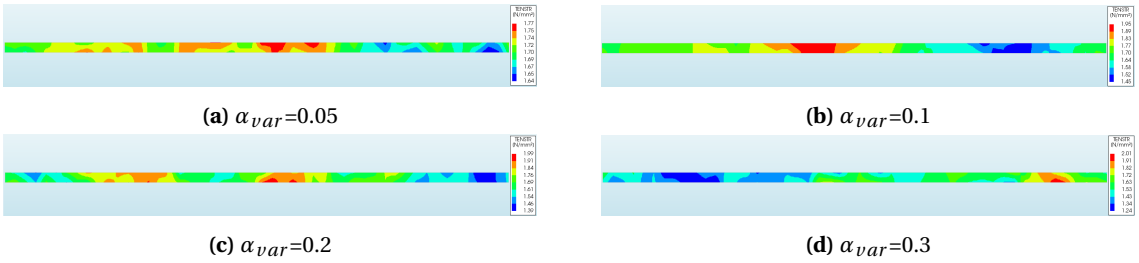

(a) α_{var}=0.05 **(b)** α_{var}=0.1

(c) α_{var}=0.2 **(d)** α_{var}=0.3

Figure C.2: Random field for changing α_{var}

The tensile strength variation from multiple random fields is analysed and compared with the characteristic values in the *E.C. 2*. The average upper and lower bound tensile strength values calculated with the recom-

mended variation coefficient of 0.3 are given in Tab: C.2. It can be seen that there is a large variation in the deviation factor.

Table C.2: Analysis of strength variation

	f_{ctm}	Min f_{ctm}	deviation factor	Max f_{ctm}	deviation factor
E.C. 2	2.90	2.0	0.7	3.8	1.3
α_{cr}=1.0	2.90	2.38	0.82	3.60	1.24
α_{cr}=0.8	2.32	1.76	0.76	2.86	1.24
α_{cr}=0.6	1.74	1.26	0.73	2.51	1.44

In this research, a variation coefficient of 0.3 in combination with chosen for the cracking analysis based on the advised variation on the tensile strength.

Correlation length L_{cor}

Extreme values in the range of 0.1 to 5 meters for the correlation length L_{cor} are investigated. In Tab: C.3 the results are shown. An increase of L_{cor} has the trend to reduce the standard deviation of the variable. The upper and lower bound zones are wider, which will result in larger cracking zones. A large correlation length will not lead to crack localisation. The chosen correlation length also has a significant influence on the crack spacing. A larger L_{cor} will increase the crack spacing. The designer should be aware that the chosen L_{cor} determines the crack spacing.

Table C.3: Analysis of correlation length L_{cor}

L_{cor}	Min f_{ctm}	deviation factor	Max f_{ctm}	deviation factor	ave. crack spacing
0.1	1.62	0.93	1.87	1.08	1.8
0.5	1.62	0.93	1.85	1.06	2.5
1.0	1.66	0.95	1.84	1.06	2.9
2.0	1.67	0.96	1.83	1.05	6.7
5.0	1.64	0.94	1.78	1.02	10.0

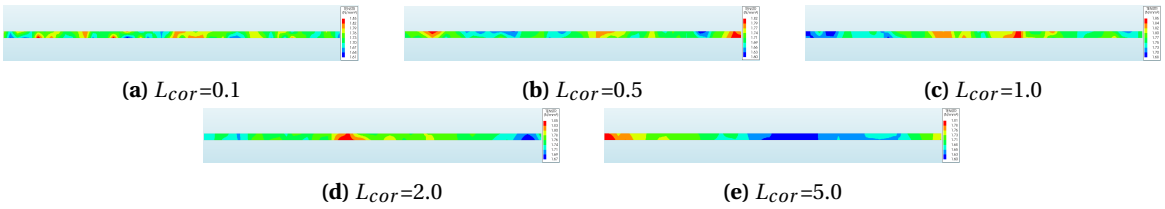

(a) L_{cor}=0.1 **(b)** L_{cor}=0.5 **(c)** L_{cor}=1.0

(d) L_{cor}=2.0 **(e)** L_{cor}=5.0

Figure C.3: Random field for changing L_{cor}

The advised correlation length of five meter results in too large crack spacing. Therefore, a correlation length of 1.0 meter is chosen because it results in simulate crack spacing found in practice. The assumed crack spacing from the random fields is defined in Tab: C.3. From practice, it is found that the crack spacing varies between 0.5 and 3 meters.

Variation points n_{var_l} and n_{var_h}

There are no recommendations found for the number of variation points per plane. A higher number of variation points result in smaller and more localised weak spots. Also, the variation within the weak zone is more present with a higher n_{var_l}. A smaller n_{var_l} result in substantial larger crack spacing. Fewer but larger cracking zones are present for small values of n_{var_l}. The same effect occurs for large correlation lengths. Therefore the n_{var_l} has a large influence on the crack behaviour in the model. For this research, the ratio of $\frac{2 \cdot L_{slab}}{h}$, resulting in approximately 100 variation points per ten meters, give the most satisfying result. In Fig: C.5 the variation of n_{var_h} is shown. For n_{var_h}=1, cracking over the full height will occur in the weak zones. This will result in a sudden large increase in the cracked elements, which leads to convergence problems. An increase of n_{var_h} result in smaller weak zones, which will decrease the likelihood of the formation of full depth cracks. To initiate

a more gradual cracking behaviour but also to realise pull depth cracking, two variation points over the height of the slab give the best result. For both the n_{var_l} and n_{var_h}, one variation point for every 100 mm hight or width is advised. This value is assumed during the research

Table C.4: Analysis of correlation length α_{var}

n_{var_l}	Min f_{ctm}	deviation factor	Max f_{ctm}	deviation factor	ave. crack spacing
10	1.65	0.95	1.81	1.04	6.7
50	1.66	0.95	1.84	1.06	2.9
100	1.65	0.94	1.85	1.06	2.2
250	1.64	0.94	1.84	1.06	2.4

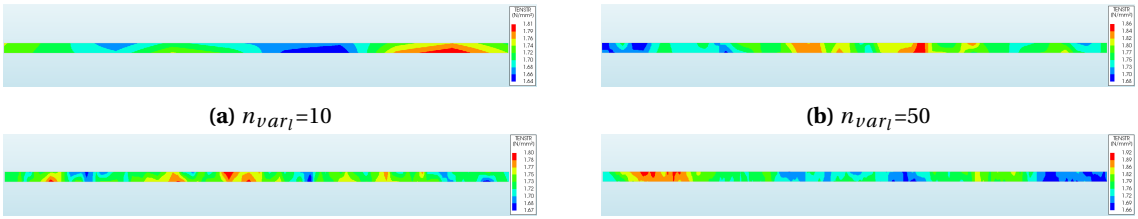

(a) n_{var_l}=10 **(b)** n_{var_l}=50

(c) n_{var_l}=100 **(d)** n_{var_l}=250

Figure C.4: Random field for changing n_{var_l}

Table C.5: Analysis of correlation length n_{var_h}

n_{var_h}	Min f_{ctm}	deviation factor	Max f_{ctm}	deviation factor	ave. crack spacing
1	1.64	0.94	1.83	1.05	2.5
2	1.65	0.95	1.85	1.06	2.2
5	1.62	0.93	1.83	1.05	2.9
10	1.64	0.94	1.89	1.09	3.1

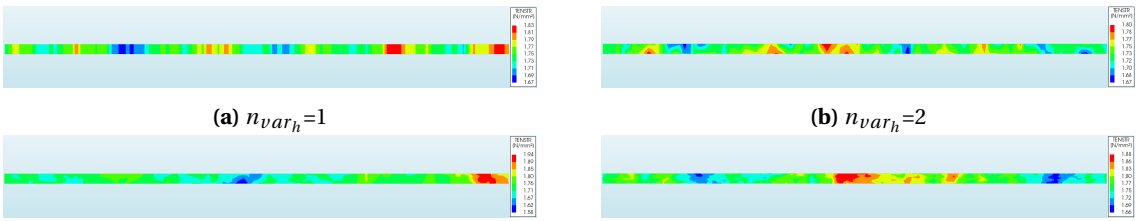

(a) n_{var_h}=1 **(b)** n_{var_h}=2

(c) n_{var_h}=5 **(d)** n_{var_h}=10

Figure C.5: Random field for changing n_{var_h}

Threshold value α_{th}

In studies a threshold value between 0 and 0.5 is often used. With the use of a threshold value the variation between the point is smoother. Downside is that a higher α_{th} result in a less accurate random field. A threshold value of 1.0 result in errors in DIANA FEA. For concrete material a threshold value of 0.5 is advised. In Tab: C.6 it can been seen that a higher α_{th} result in a slightly lower deviation factor. The influence is low because the coefficient of variation is also taken low during the analysis. In this research, the threshold value is taken as zero because it have significant influence and it reduces the accuracy of the random field.

Table C.6: Analysis of threshold valueα_{th}

α_{th}	**Min** f_{ctm}	**deviation factor**	**Max** f_{ctm}	**deviation factor**	**ave. crack spacing**
0	1.65	0.95	1.84	1.04	2.2
0.25	1.65	0.95	1.84	1.06	3.1
0.50	1.67	0.96	1.82	1.05	2.9
0.75	1.66	0.95	1.76	1.01	2.7

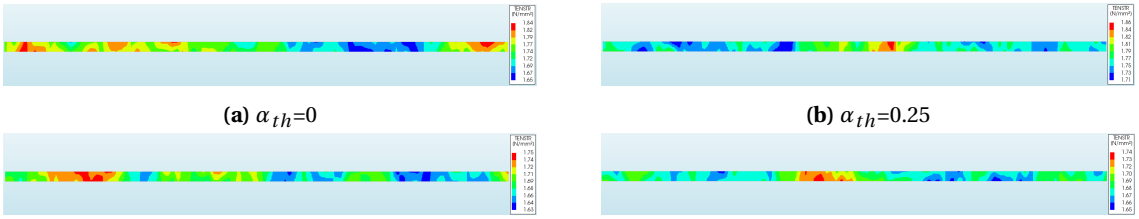

(a) α_{th}=0 **(b)** α_{th}=0.25

(c) α_{th}=0.50 **(d)** α_{th}=0.75

Figure C.6: Random field for changing α_{th}

Effect of random field on crack behaviour

During the analysis of the random field, it is concluded that the input parameters can predetermine the crack spacing in the model. The chosen maximum value of the concrete tensile strength can also have large influence on the stress development in the member. The partial stronger member is generated with the random-field field α_{var} of 0.3. For both models the tensile strength variation and the stress development are shown in Fig: C.7. In Tab:C.7 the axial forces and steel stresses in the governing crack are given. From the diagram and the table it can be concluded that the a higher tensile strength of the concrete result in higher forces and stresses in the crack. The axial force in the uncracked zone is higher and therefore the force in the crack will also be higher. To approach the real cracking and stress behaviour of *S.o.G.* in a *N.L.F.E.A.* the upperbound of the concrete tensile strength have to be taken into account.

Table C.7: Analysis of tensile strength variation: *Gilbert* v.s. *F.E.M.*

	Gilbert				*F.E.M.*		
Range f_{ctm}	N_{cr}	$N_{c_{(t)}}$	ψ_{crack}	$\sigma_{s,cr}$	Max. $N_{c_{(t)}}$	Max. ψ_{crack}	Max. $\sigma_{s,cr}$
1.67-1.88	337	230	0.68	132	274	0.81	253
1.58-3.21	331	244	0.74	180	304	0.92	274

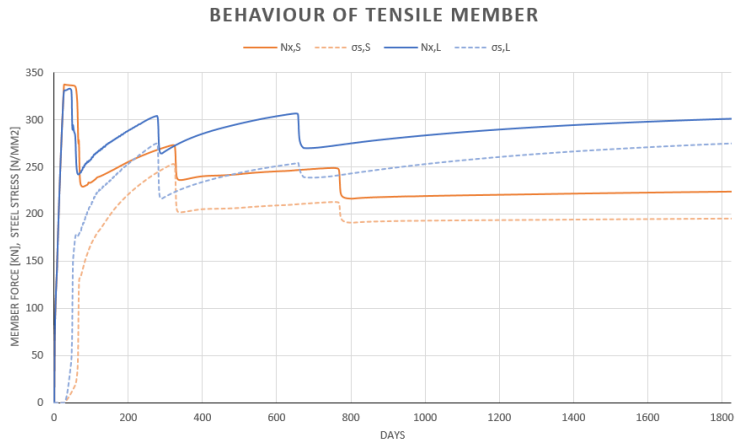

(a) Stress development of small and large range of concrete tensile strength

(b) Small range of concrete tensile strength

(c) Large range of concrete tensile strength

Figure C.7: Force and steel stress development in tensile member

Quantification of the transfer length is difficult in the *F.E.M.* because of the variation of the concrete properties. The transfer length for three runs with the same parameters, but different random fields were in the order of respectively 150, 180, and 220 mm for embedded reinforcement.

Post-analysis crack width methods

The post-analysis crack width methods, one based on stress and the second on the average strain, are compared and the results are shown in Tab:C.8. The results are from a five meter long single cracked restraint element after 100 days of shrinkage. The average strain method is based on equilibrium. Because the model parameters are constant and there is only one single crack, all the applied strain load (minus the elastic strain of concrete) is concentrated in the cracking zone. In the case of imposed deformation, the bad bonding properties result in a larger transfer area but with a lower average strain. Therefore the crack widths are almost equal in the model. For external loading, for example, bending of a beam under a point load, the steel strain in the cracked zone is approximately the same for every bonding type. If the reinforced concrete has bad bonding properties, which result in a longer transfer length, the crack width will be wider for bad compared to good or fully bonding. The difference is that a single crack from shrinkage loading is in the *N.F.D.C.P.* and the external loading cracks in the *F.D.C.P.*. During the analysis, it is noticed that the transfer length in the *N.F.D.C.P.* depends on the amount of force in the crack. Therefore the transfer length has to be determined per crack during the post-analysis checks. For conservative results, the maximum transfer length according to the *E.C. 2* can be used.

Table C.8: Analysis of bond slip at t=100

			F.E.M.	Crack width	methods:	
Bonding	ψ_{crack}	l_t	$\sigma_{s,cr}$	w_{max} **Ave. element**	w_{max} **Ave strain**	w_{max} **Max steel stress**
Fully	0.84	129	196	0.17	0.13	0.09
Good	0.72	157	195	0.19	0.13	0.09
Bad	0.58	221	134	0.22	0.13	0.05
Analytical- Good	0.70	160	190	0.11 (*Gilbert*)	0.13 (*M.C. 2010*)	0.08 (*Van Breugel*)
Analytical- Bad	0.45	240	121	0.13 (*Gilbert*)	0.05 (*M.C. 2010*)	0.04 (*Van Breugel*)

The chosen crack width calculation method for the post-analysis checks greatly influence the final design crack width. The crack widths of the average strain and average element method are significantly wider than the steel stress-based method. When the crack width is calculated with the analytical models, the design crack

width variates between 0.08 and 0.13 mm. By increasing the transfer length due to bad bonding, the steel stress reduces according to the *Gilbert*. The *M.C. 2010* and *Van Breugel* are based on the steel stress in the crack and therefore, the crack width decreases. This is contrary to the findings in the *F.E.M.*. Experiments have to be performed to validate the results of the assumed post-analysis crack width calculation method for imposed deformation in the *N.F.D.C.P.*. When the crack widths are determined with the use of the average steel strain over the transfer length, it is important to take into account the bond-slip behaviour. For crack width calculation based on the maximum steel stress in the crack, the bond-slip behaviour is less relevant. For the steel stress method, the embedded reinforcement is advised because of this result in slightly higher steel stresses and thus more safe results. With the average element method, the crack width at every location can easily be checked. No additional calculation is required to calculate the crack width at the top surface, which makes it easier for design purposes.

Creep model with bond-slip interface

Modelling the cracking behaviour with the creep compliance function in combination with the bond-slip interface result in significant cracking along the rebar. The cracking stress along the rebar is reached sooner than the cracking stress in the uncracked zones due to the concrete relaxation. Therefore no additional cracking occurs in the member, which results in one large dominant crack. The same effect is found when the *A.A.E.M* is applied in the *N.L.F.E.A.* instead of the compliance function. The cracking along the rebar gives the same behaviour of failure of the bond-slip interface. In reality, this slipping phenomenon is less present because the stresses along the rebar are gradually increasing and the concrete relaxation is already present after minutes of loading. In the *F.E.M.*, the strain load increment represents one day of shrinkage load. The concrete relaxation effect is only present on day two, according to the compliance model. The strain increments of one day result in peak stresses along the rebar, which are higher than the cracking stresses. The bond-slip interface distributes the stresses over a longer area and which results in a long cracking area along the rebar. With embedded reinforcement, only local cracking along the rebar occurs with eventually a secondary crack perpendicular to the reinforcement. In Fig:C.9, the crack pattern after 500 days of loading for embedded and bond-slip reinforcement is shown for both creep models. It can also be seen that bond-slip results in crack localisation. In the embedded tensile member, two cracks appear simultaneously close to each other, which results in lower peak steel stresses.

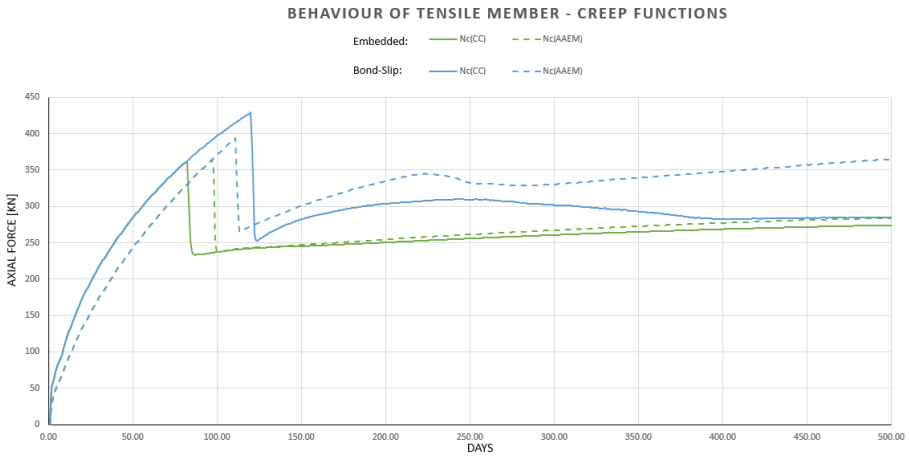

Figure C.8: Comparison of creep function in *F.E.M.*

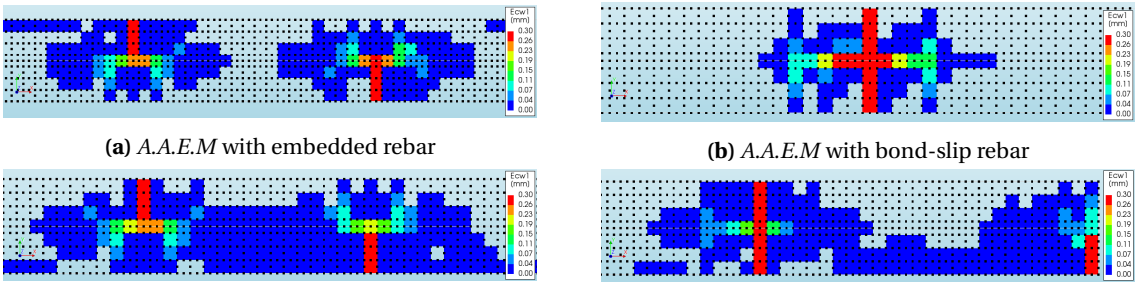

(a) *A.A.E.M* with embedded rebar

(b) *A.A.E.M* with bond-slip rebar

(c) Compliance with embedded rebar

(d) Compliance with bond-slip rebar

Figure C.9: Cracking after 500 days

Validation of *F.E.M.*

Stress behaviour

Validation of finite element models is important to ensure the model behaviour. In the research of *T. Seo* and *J. Kim* the behaviour of concrete in the uncracked region after cracking under restrained drying shrinkage in a notched tensile member is investigated[55]. This research is used to check the developed *F.E.M.*. The theoretical strain distribution and the experimental set-up of the research are shown in Fig:C.10a and Fig:C.10a. Half of the specimen is modelled in *DIANA FEA* based on symmetry in the middle of the beam. The material properties obtained from the experiment, which are applied in the *F.E.M.*, are shown in Tab:C.9. During the research, it has come forward that the quantification of the concrete relaxation effect is complex and depends mainly on the concrete age at the time of loading t_0. This experiment is used to find an appropriate t_0, which can be applied in further research. The *CUR-36* advises t_0 at the start of loading. During the investigation of the Analytical Model (*A.M.*), it was found that the 28-day properties give the best agreement. Both concrete ages are analysed and compared in the research. The curing time in the experiment is seven days and therefore t_0=7 according to the *CUR-36* recommendation.

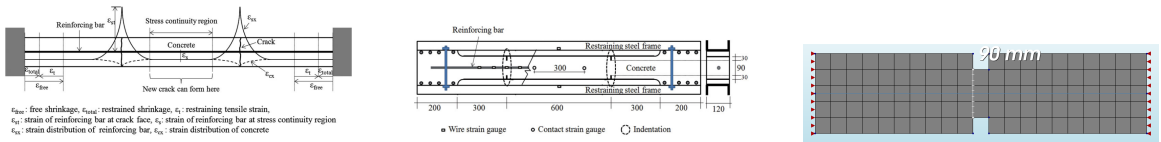

(a) Theoretical model

(b) Experimental model

(c) *F.E.M.*

Figure C.10: Restrained notched tensile model

Table C.9: Material properties experiment per specimen

Specimen	E_{cm}	f_{ctm}	σ_{cr}	$\varnothing$	$e_{c(t=80)}$
RD10	24000	2.1	1.47	9.53	0.00043
RD13	24000	2.0	1.4	12.70	0.00032

Both specimens are analysed, and the results are compared. The stress behaviour in the concrete from the experiment and *F.E.M.* are shown in Fig: C.11. The crack relaxation effect in the *F.E.M.* is significantly less than the experimental results. In the *F.E.M.*, the residual tensile stress based on the cracking energy determines the stress behaviour greatly during cracking. A cracking stage of approximately ten days is visible where the crack formation in the experiment is instant. The simulate this instant crack formation, the fracture energy G_{f_c} of the concrete is reduced by a factor 5. In the reduced G_{f_c} analysis, the stress behaviour is more similar to the experiment. The models with the G_{f_c} from the provisions result in significantly higher stresses after cracking. In the *F.E.M.* non-ageing concrete with 28-day properties is used. In the experiment, the concrete properties can be lower, which results in lower stresses.

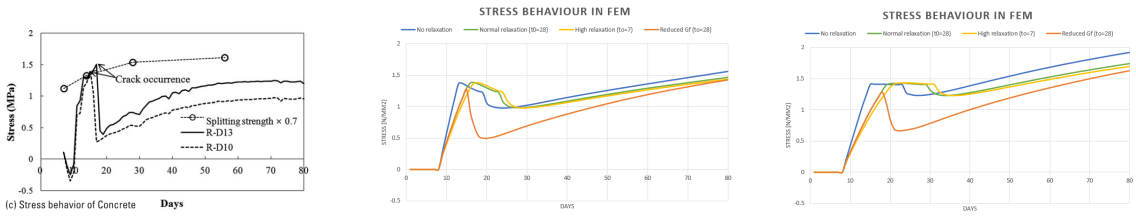

(a) Experiment **(b)** RD10 specimen FEM **(c)** RD13 specimen FEM

Figure C.11: Stress behaviour in concrete

The concrete stress development in the uncracked region is compared by assuming the concrete stress after cracking zero. Therefore the stress development after cracking can be compared. In Fig: C.12, it can be seen that the stresses in the uncracked zone are significantly higher than the experiment. Even the large concrete relaxation model (t0=7) overestimates the concrete stress after cracking with ±40% resulting in ψ of 0.31 and 0.36. The concrete relaxation is more present in the RD13 specimen but still not in the order of the experiment.

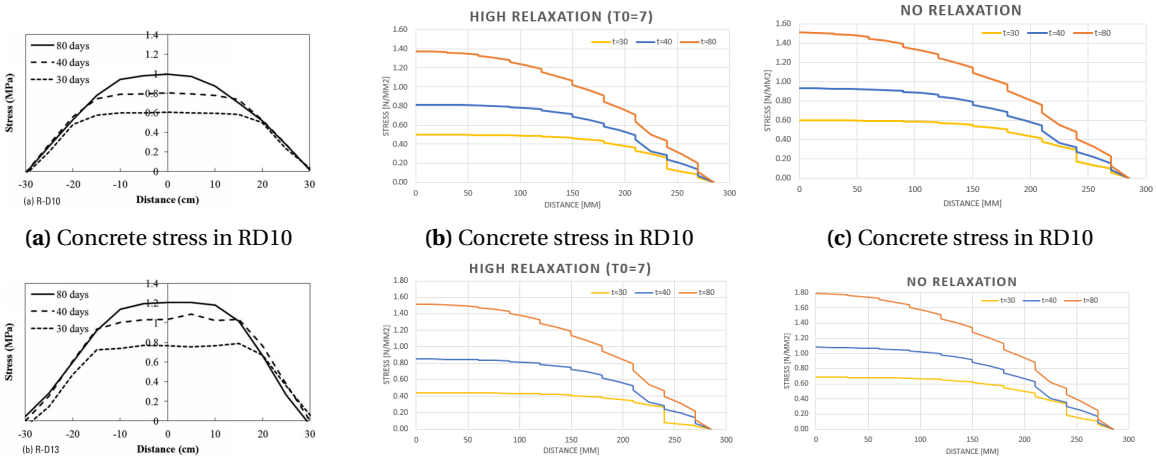

(a) Concrete stress in RD10 **(b)** Concrete stress in RD10 **(c)** Concrete stress in RD10

(d) Concrete stress in RD13 **(e)** Concrete stress in RD13 **(f)** Concrete stress in RD13

Figure C.12: Stress behaviour in concrete

The stress difference in the concrete can come from the method how the stress is determined from the *F.E.M.*. The concrete stress is not everywhere constant. During this analysis, the axial force is calculated and divided by the concrete area in the notch. The stress difference in the concrete can also come from different stress-strain behaviour in the reinforcement. For example bad bond-slip properties will results in large crack relaxation and thus lower concrete stresses. Therefore the strain development in the reinforcement are compared and shown in Fig: C.13. The development of the transfer zone in the *F.E.M.* and the experiment are in good agreement. The maximum values are also in good agreement. The non-relaxated models have a slightly higher steel strain than the relaxation models because the force in the member is higher.

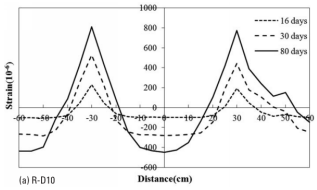

(a) Steel strain in RD10

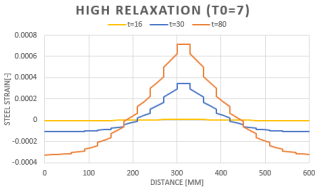

(b) Steel strain in RD10

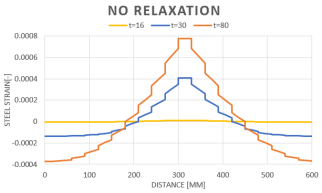

(c) Steel strain in RD10

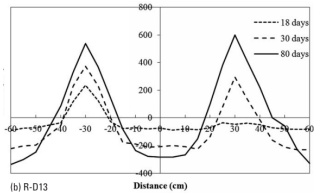

(d) Steel strain in RD13

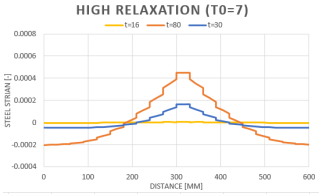

(e) Steel strain in RD13

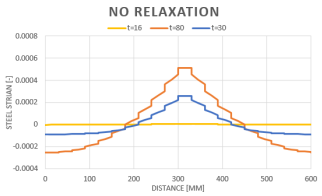

(f) Steel strain in RD13

Figure C.13: Strain behaviour in reinforcement

From the comparison analysis, is can be concluded that detailed finite element modelling of an experiment always results in an estimation of the structural behaviour. Modelling crack relaxation effects in a concrete structure is complex. It is found that that the tensile softening behaviour based on the cracking energy overestimate the concrete contribution in the direct tensile cracks. In the experiment, crack relaxation factors of approximately 0.22 and 0.27 are found for respectively specimen RD10 and RD13. Where for the finite element models with high relaxation, crack relaxation factors of 0.72 and 0.86 are found. The crack relaxation factors according to the analytical model of *Gilbert* are 0.14 and 0.35 for respectively RD10 and RD13. The *Gilbert* model is in better agreement to determine the crack relaxation effect but still not precise. To realise accurate calculations, the exact material properties, such as bond-slip, should be taken into account.

Relaxation model

The linear and relaxed stresses for the *F.E.M.* and *Bazant* are compared. For the finite element model the build-in material models based on the *M.C. 2010* and *E.C. 2* are also added for validation. No significant difference is found for both the linear and relaxed stresses(Fig:C.14a). All the models are in good agreement Most concrete properties are time-dependent. When non-ageing analysis are performed in *DIANA FEA*, the 28-days material properties are assumed as standard values. The relaxation behaviour is highly dependable on the nominal creep φ_0. As discussed, the concrete age at loading significantly influences the creep coefficient. Older concrete results in a smaller creep coefficient. In Fig:C.14b, it can be seen that the assumed 28-day properties give the best agreement with the analytical method of *Bazant*, which takes into account the ageing of concrete.

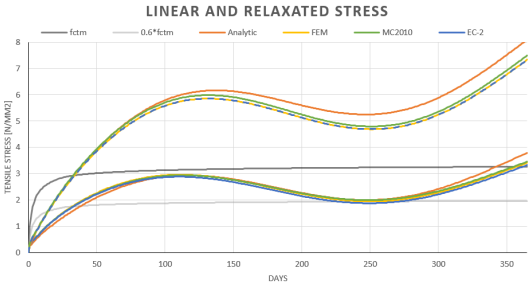

(a) Stress development

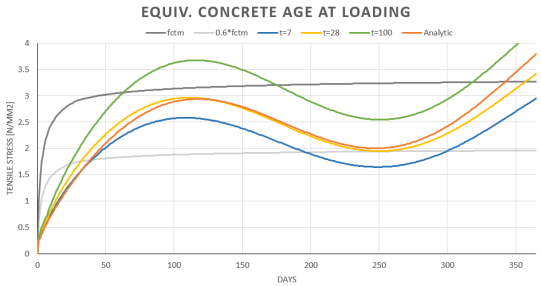

(b) Relaxated stresses

Figure C.14: Model comparison

Appendix D

Degree of restraint

Soil friction

Slabs on grade will always be submitted to frictional restraint with the sub-base when the slab undergoes horizontal movement. For large industrial floor, these restraints will likely result in a fully restrained section R=1 of the floor. In the *CUR-36* a constant horizontal shear stress τ_{max} is assumed. The shear force increases linearly from the slab edge towards the slab centre. When the shear force is equal to the internal shrinkage force, the movement of the slab is prevented. The middle section is then fully restraint. The minimum required length of $L_{friction}$ is calculated for different foundation types. The *CUR-36* model does not take into account the slip effect when the maximum shear stress is reached. Therefore, the model is compared with a Coulomb friction model based on the Mohr-Coulomb theory shown in Fig:D.1b. The tension cut off is set to zero in the Coulomb model. No tension and shear stresses can be transferred when there is an opening at the interface.

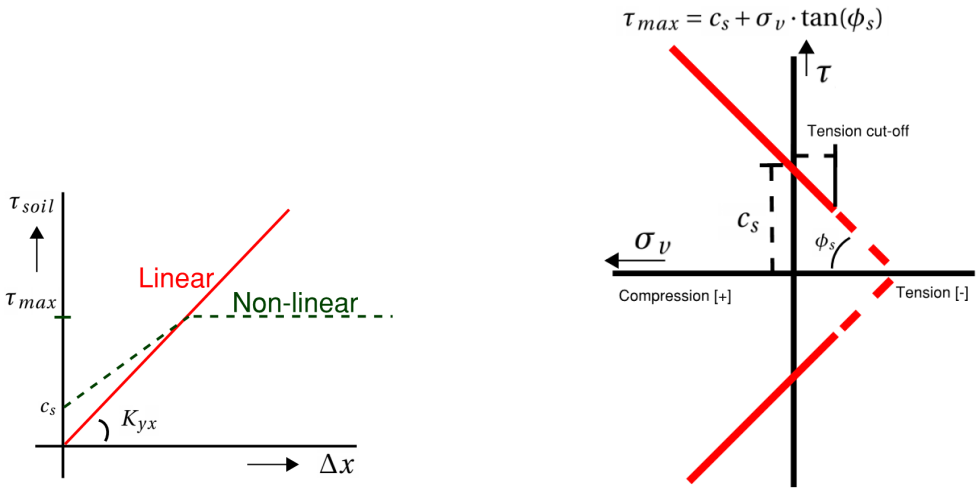

(a) Stress displacement graph of soil models

(b) Morh coulomb friction

Figure D.1: Friction model

For the calculation, two methods are compared. The first method is based on the linear shear stiffness, the second on the maximum shear stress presented in the *CUR-36*. For the linear shear stiffness method, an average displacement is assumed. The assumed average slab edge displacement is checked with finite element calculations. The *CUR-36* states that the force in the slab can never be higher then N_{cr}. When this force can be mobilised by the sub-base, a fully restrained midsection is present. The maximum restraint length $L_{friction}$ can be calculated with the following formula when free movement (K_{yx}=0) at the slab edge is assumed

Formulae

$$L_{friction} = \sqrt{\frac{2E_{cm}\psi h}{K_{yx}}} \tag{D.1}$$

$$\Delta x_{mean} = \frac{\varepsilon_c L_{friction}}{2} \tag{D.2}$$

$$F_{restriant} = \Delta x_{mean} L_{friction} K_{yx} \tag{D.3}$$

$$F_{restriant} = \frac{\varepsilon_c K_{yx} L_{friction}^2}{2} \tag{D.4}$$

$$F_{slab} = \varepsilon_c E_{cm} \psi h \tag{D.5}$$

$$F_{restriant} = F_{slab} \tag{D.6}$$

$$\frac{\varepsilon_c K_{yx} L_{friction}^2}{2} = \varepsilon_c E_{cm} \psi h \tag{D.7}$$

$$L_{friction} = \sqrt{\frac{2E_{cm}\psi h}{K_{yx}}} \tag{D.8}$$

$$\tag{D.9}$$

Graphs

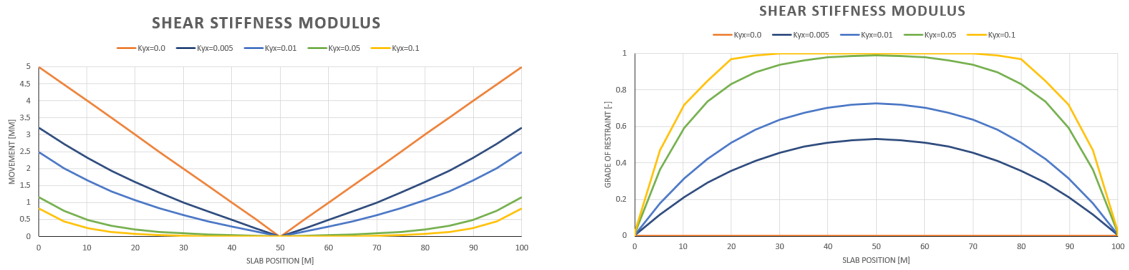

(a) Slab movement **(b)** degree of restraint

Figure D.2: Linear friction model with variation of K_{yx}

(a) Slab movement based on K_{yx} **(b)** degree of restraint based on K_{yx} **(c)** degree of restraint based on c_s

Figure D.3: Coulomb friction model

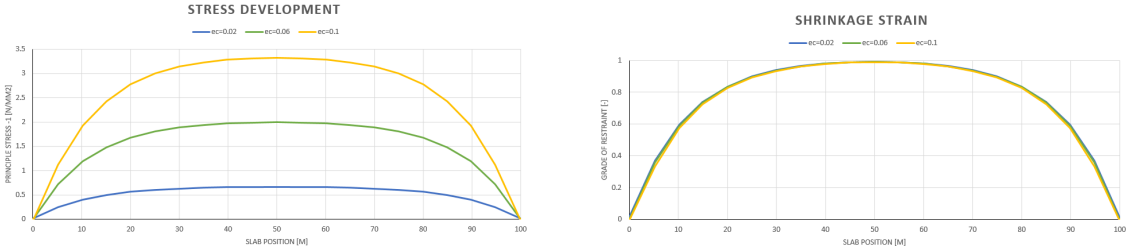

(a) Stress development **(b)** degree of restraint

Figure D.4: Effect of shrinkage

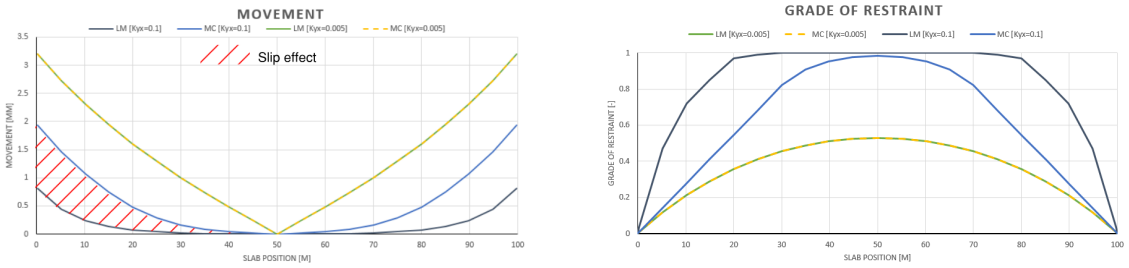

(a) Stress development

(b) degree of restraint

Figure D.5: Comparison of models: LM vs CM

Parameters

For the comparison analysis, different sub-base types are compared. In practice a common assumption is that the shear stiffness modulus K_{yx} is $\frac{1}{10}$ of the normal stiffness modulus k_{mod}. Test performed by *Pettersons* showed an asymptotic growth of the shear stress towards the maximum shear reached at a certain slip. Thus the shear stiffness is very high at the beginning and decreases to zero for large slip values. From the test results the average shear stiffness of 0.034 and 0.035 $N^3\,mm^{-1}$ are be derived for respectively sand and gravel, Fig: D.6. The values are 3-5 times higher than commonly assumed in practice. A plastic slip membrane decreases the shear stiffness approximately by 50%, but this is not investigated further-on.

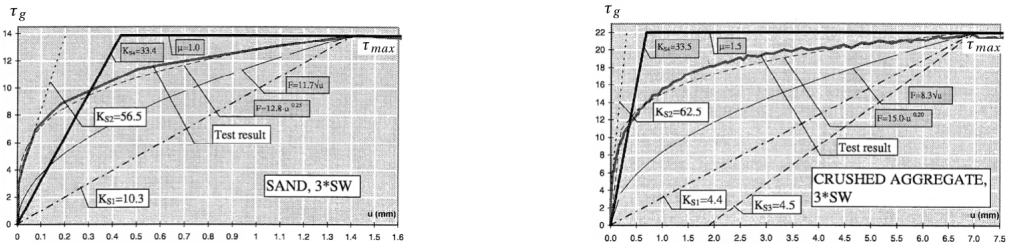

(a) Sand

(b) gravel

Figure D.6: Friction tests

The maximum shear stress τ_{max} for the Coulomb friction model depends on the cohesion c_s, friction angle ϕ_s and the vertical load q_v. The *CUR-36* calculates τ_{max} with the use of a friction coefficient μ_0. For comparison the equivalent μ_0 for the Coulomb is calculated with $\mu_0 = \tan(\phi_s)$. As mentioned τ_{max} depends on the vertical stress. In practice it is common to take the vertical stress as of 50% of the *U.D.L.*. For design calculation the uniform load have to be reduced according to the NEN-EN 1990 depending on the design lifetime, consequence class and loading category. For storage loading ψ_{UDL} = 0.8 taken from the *NEN-EN 1990: Table NB.2 – A1.1.* Therefore $q_v = \psi_{UDL} \cdot UDL + SW$. Indicative values found in the *CUR-36* for different foundation types used in this research are given in Tab: D.1 [1] [18]. Two sub-base types are compared for a 250 mm thick slab, concrete class C30/37 with σ_{cr}=f_{ctm}. The load on the slab is three times its self-weight. Also *F.E.M.* calculations with coulomb friction interfaces are performed for comparison. In the *F.E.M.*,$L_{friction}$ is determined from the edge until the point were the horizontal displacement is lower than 0.1 mm.

Table D.1: Friction Parameters

Foundation type	k_{mod}	K_{yx}	c_s	ϕ_s	$\mu_{0CUR-35}$	$\tau_{maxCUR-36}$	$\mu_{0Coulomb}$	τ_{maxFEM}
Sand	0.070	0.033	0.010	30	0.58	0.026	0.8	0.017
Gravel	0.100	0.034	0.015	35	0.70	0.041	1.2	0.029

Friction length $L_{friction}$

An extensive study on the friction length is performed by *Petersons* in 1992 and 1998. In the study of *F. Narin* and *O. Wiklund* the frictional length is investigated with the use of non-linear friction calculations and com-

[1] Units according to symbol list

pared with *Petersons* results[6].

Case nr	Case	Force equation on the form $F = B \cdot u^n$	Stress equation on the form $\tau = C \cdot s^n$	Slip at fully developed friction s_{max} [mm]
1	Sand	$F = 12.8 \cdot u^{0.25}$	$\tau = 13.33 \cdot s^{0.25}$	1.4
2	Crushed aggregate	$F = 15.0 \cdot u^{0.20}$	$\tau = 15.63 \cdot s^{0.20}$	6.7
3	Crushed aggregate + plastic	$F = 9.0 \cdot u^{0.16}$	$\tau = 9.34 \cdot s^{0.16}$	2.4

(a) Sand

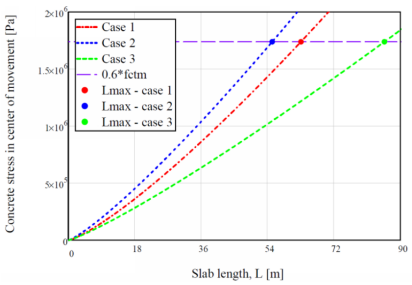

(b) gravel

Case nr	Case	Allowed maximum slab length according to calculations [m]	s_{end} [mm]
1	Sand	63.0	8.9
2	Crushed aggregate	55.2	7.9
3	Crushed aggregate + plastic	85.6	12.4

(c) gravel

Figure D.7: Results from *F. Narin*

It is concluded that the friction coefficient method of Petersons overestimates the friction because the slip behaviour is not taken into account. When taking into account the slip behaviour, the slab length can increase with approximately 70%. The results of this study are compared with the calculation method provided in the *CUR-36* and *F.E.M.*. In Tab: D.2 it can been seen that the *CUR-36* method is the most conservative. When the slip behaviour is taken into account, $L_{friction}$ increases significantly. It is important to keep in mind that only the frictional restraint is taken into account.

In Tab: D.2 practical values are given for $L_{friction}$ based on the *CUR-36* method and Coulomb friction method. For clarification, τ_{max} per method and the edge movement are shown. The edge movement is calculated at the moment of cracking with and without the concrete relaxation effect ψ=0.5.

Table D.2: Friction length values

Situation	$L_{frictionCUR36}$	$\tau_{maxCUR36}$	$L_{frictionFEM}$	τ_{maxFEM}	Δ_x	$\Delta_x\psi$
Sand - Unloaded	26	0.014	39	0.014	0.98	3.00
Sand - Heavily loaded	13	0.030	34.3	0.026	0.80	1.97
Gravel - Unloaded	17	0.021	28.1	0.019	0.75	2.42
Gravel - Heavily loaded	8	0.045	26.2	0.032	0.66	1.56

Temperature differentials

When a concrete structure rapidly changes in temperature, which often occurs during hardening, a temperature difference ΔT arises in the concrete. The ΔT result in restrained stresses known as *eigenstresses*. The stresses are in equilibrium over the cross-section, but high tensile stresses at the surface or at the centre can result in cracking from receptively heating and cooling of the structure. When cracking occurs, the restrained stresses substantially decreases. And when cracking does not occur, the Young's modulus is very low, the creep is high, and therefore, the restrained stresses are rapidly relieved. Research recommends a restraint factor of 0.42 for this effect[58]. Assuming the concrete properties at t=1 the temperature difference ΔT should be at least 34 °C to initiate cracking. This temperature increment is not likely to occur for industrial floor because of the relative thin concrete structure. In combination with the rapidly relieving stresses the *eigenstresses* are therefore not taken into account in this study.

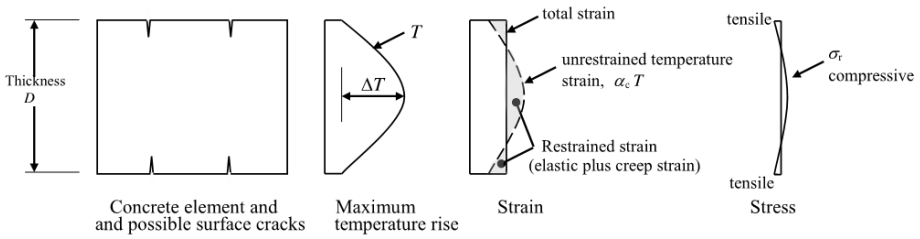

Figure D.8: Eigenstresses

Rotational restraint $L_{curvature}$

Due to the linear gradient shrinkage profile the slab wants to curl upwards. The self-weight of the concrete restraint the movement and therefore stresses occurs in the slab mentioned in section **??**. The slab is fully restraint by this effect when the bending moment from the restraint $M_{restriant}$ is equal to the maximum bending moment in the slab M_{slab}. The $L_{curvature}$ can be derived from this equilibrium situation. *Pettersson* found an equation which gives the critical length of the curled slab. [19]

$$L_{curvature,petterson} = \sqrt{\frac{4\varepsilon_c E_c h}{5\rho_c g f}} \tag{D.10}$$

$$M_{restriant} = \frac{q_v L_{curvature}^2}{2} \tag{D.11}$$

$$M_{slab} = \frac{\varepsilon_c E_{cm} \psi h^2}{6} \tag{D.12}$$

$$M_{restriant} = M_{slab} \tag{D.13}$$

$$\frac{q_v L_{curvature}^2}{2} = \frac{\varepsilon_c E_{cm} \psi h^2}{6} \tag{D.14}$$

$$L_{curvature} = \sqrt{\frac{\varepsilon_c E_{cm} \psi h^2}{3 q_v}} \tag{D.15}$$

$$\tag{D.16}$$

Appendix E

Sensitivity analysis: stresses

The results from the sensitivity analysis for the concrete properties, strains, creep, relaxation and stresses are given. The formulae, values and graphs are shown per subject.

Concrete properties

Formulae

$$E_{cm} = \alpha_E 22000 \left(\frac{f_{cm}}{10} \right)^{0.3} \tag{E.1}$$

$$E_{cm}(t) = \left(\frac{f_{cm}(t)}{f_{cm}} \right)^{0.3} E_{cm} \tag{E.2}$$

$$E_{cm,mc2010} = 21500 \left(\frac{f_{cm}}{10} \right)^{\frac{1}{3}} \tag{E.3}$$

$$f_{cm} = f_{ck} + \Delta f \tag{E.4}$$

$$f_{cm}(t) = \beta_{cc}(t) f_{cm} \tag{E.5}$$

$$\beta_{cc}(t) = \exp\left(s_{cc} \left(1 - \frac{28}{t}^{0.5} \right) \right) \tag{E.6}$$

$$\Delta f = 8 \tag{E.7}$$

$$f_{ctk} = 0.7 f_{ctm} \tag{E.8}$$

$$f_{ctm} = 0.3 f_{ck}^{\frac{2}{3}} \tag{E.9}$$

$$f_{ctm}(t) = \beta_{cc}(t)^{\alpha} f_{ctm} \tag{E.10}$$

$$\alpha = 1 for\ t < 28 \tag{E.11}$$

$$\alpha = 2/3 for\ t > 28 \tag{E.12}$$

$$G_f = 73 f_{cm}^{0.18} \tag{E.13}$$

$$G_c = 250 \cdot G_f \tag{E.14}$$

$$\tag{E.15}$$

Comparison of tensile strength formulae

$$f_{ctm,0} = 0.9 \left(1.0 + 0.05 \cdot f_{ccm} \right) \tag{E.16}$$

$$f_{ctm,0[EC2]} = 0.3 f_{ck}^{\frac{2}{3}} \tag{E.17}$$

$$f_{ctm,\infty} = 0.7 \cdot 0.9 \left(1.0 + 0.05 \cdot f_{ccm} \right) \tag{E.18}$$

$$F_{bm,\infty} = 2 \cdot \frac{0.7 \cdot (1.05 + 0.05 \cdot f_{cck})}{1.4} \tag{E.19}$$

$$\sigma_{cr,\infty} = \alpha_{cr} \cdot f_{ctm} \tag{E.20}$$

$$f_{cr,3} = 0.24 \cdot \sqrt{f_{cm}} \tag{E.21}$$

$$f_{cr,28} = 0.40 \cdot \sqrt{f_{cm}} \tag{E.22}$$

$$\tag{E.23}$$

Values

Table E.1: Analysis Young's Modulus E_{cm} development

Cement type	$\beta_{cc}(t=1)$ [-]	[% of N]	$\beta_{cc}(t=7)$ [-]	[% of N]	$\beta_{cc}(t=365)$ [-]	[% of N]
S	0.61	85	0.89	96	1.06	102
N	0.72	100	0.93	100	1.04	100
R	0.77	1.07	0.94	102	1.03	99

Table E.2: Analysis Young's Modulus E_{cm} properties

Concrete Class	$E_{cm}(t=1)$ [MPa]	$E_{cm}(t=7)$ [MPa]	$E_{cm}(t=28)$ [MPa]	$E_{cm}(t=365)$ [MPa]	[% of C30/37]
C20/25	21716	27797	29962	31065	91
C25/30	22814	29201	31476	32635	96
C30/37	23800	30464	32837	34045	100
C35/45	24699	31615	34077	35332	104

Table E.3: Analysis Young's Modulus E_{cm} properties

Aggregate type	$E_{cm}(t=1)$ [MPa]	$E_{cm}(t=7)$ [MPa]	$E_{cm}(t=28)$ [MPa]	$E_{cm}(t=365)$ [MPa]	[% of C30/37]
Bazalt	28560	36557	39404	40854	120
Standard	23800	30464	32837	34045	100
Limestone	21420	27418	29553	30641	90
Sandstone	16660	21325	22986	23832	70

Tensile strength comparison

The different tensile strength values are calculated and compared. *R. I. Gilbert* suggest a direct tensile cracking stress $f_{cr,3}$ and $f_{cr,28}$ for t=3 and t≥28 to calculate the early age and long-term crack width[58]. In the old dutch codes *(VBC)* there was a specific the long-term tensile strength $f_{bm,\infty}$ defined for crack width calculation. In Tab: E.4 an overview is given of the short and long-term tensile strength for different provisions. For this research, the mean tensile strength f_{ctm} given by the *E.C. 2* are used. This values is almost equal to the long-term tensile strength $f_{bm,\infty}$ for crack width calculation according to the *VBC*.

Table E.4: Comparison of tensile strength of concrete [N/mm2]

Concrete class	$f_{ctm,0[EC2]}$	$f_{ctm,0[MC2010]}$	$f_{cr,3}$	$f_{bm,\infty}$	$f_{ctm,\infty}$	$\sigma_{cr,\infty}$	$f_{cr,\geq 28}$
C20/25	**2.2**	2.4	1.27	2.3	1.7	1.5	2.12
C25/30	**2.6**	2.7	1.38	2.6	1.9	1.6	2.30
C30/37	**2.9**	3.0	1.48	2.9	2.1	1.8	2.47
C35/45	**3.2**	3.3	1.57	3.3	2.3	2.0	2.62

Next to the many different tensile strength presented in the provisions, there is also a different strength relation between uniaxial en flexural stresses. The flexural stresses increase when the height of the slab increases. The flexural stresses can be determined by the multiplying f_{ctm} with the factor $\left(\frac{1600-h}{1000}\right)$ with h in mm and $\left(\frac{1600-h}{1000}\right) \not< 1$. Fatigue also has an influence on the tensile strength when relative large cyclic loading is present during the structure's lifetime. Fatigue is not addressed in this research.

Table E.5: Analysis Tensile strength f_{ctm} development

Cement type	$\beta_{cc}^{(}\alpha)(t=1)$ [-]	[% of N]	$\beta_{cc}^{(}\alpha)(t=7)$ [-]	[% of N]	$\beta_{cc}^{(}\alpha)(t=365)$ [-]	[% of N]
S	0.20	57	0.68	88	1.20	106
N	0.34	100	0.78	100	1.13	100
R	0.42	124	0.82	105	1.10	98

Table E.6: Analysis Tensile strength f_{ctm} properties

Concrete Class	$f_{ctm}(t=1)$ [MPa]	$f_{ctm}(t=7)$ [MPa]	$f_{ctm}(t=28)$ [MPa]	$f_{ctm}(t=365)$ [MPa]	[% of C30/37]
C20/25	0.76	1.72	2.21	2.49	76
C25/30	0.88	2.00	2.56	2.89	89
C30/37	0.99	2.26	2.90	3.27	100
C35/45	1.10	2.50	3.21	3.62	111

Graphs

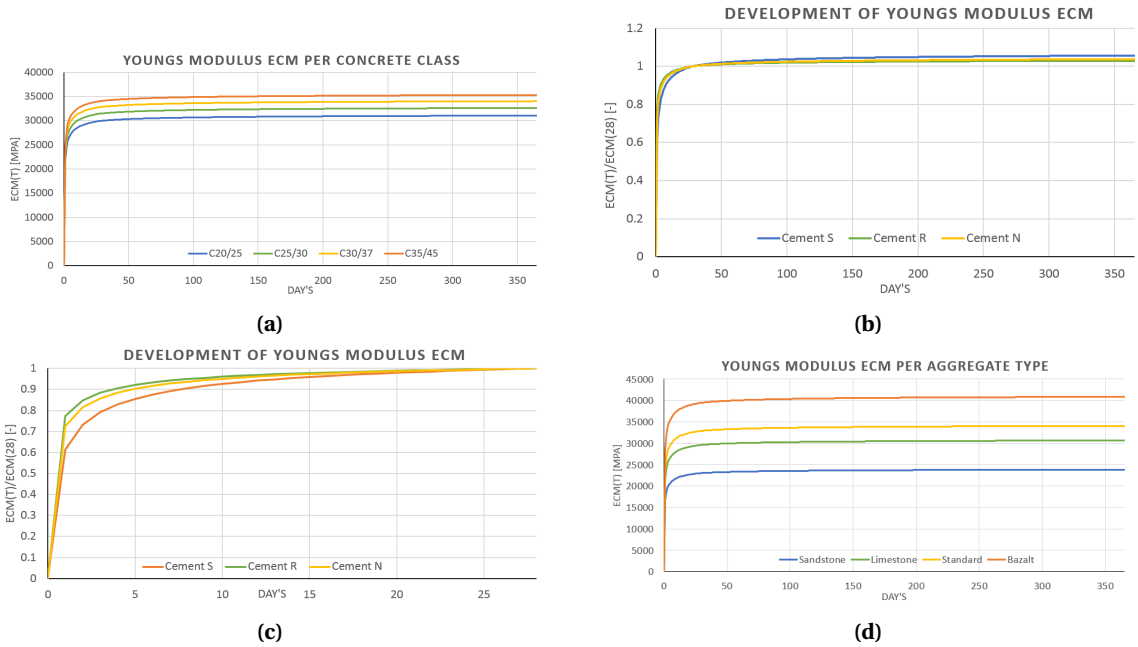

Figure E.1: Concrete Young's modulus

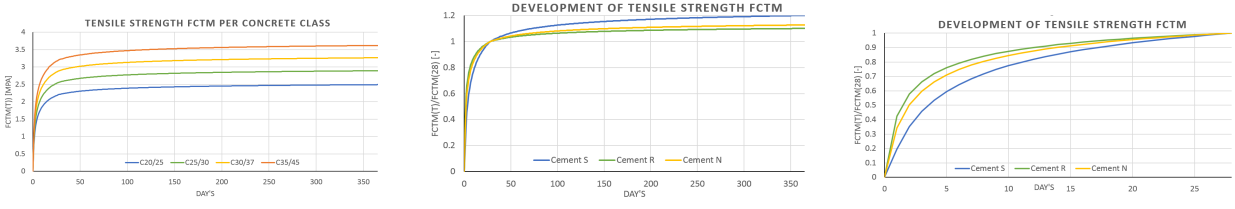

Figure E.2: Concrete tensile strength

Creep

For the relaxed stress calculation, the time-dependent creep factor $\varphi_{t,to}$ is required. The creep factor can be calculated according to the *E.C. 2*. The equation is given below:

Formulae

$$\varphi(t,t_0) = \varphi_0 \beta_c(t,t_0) \tag{E.24}$$

$$\varphi_0 = \varphi_{RH} \beta(f_{cm}) \beta(t_0) \tag{E.25}$$

$$\varphi_{RH} = 1 + \frac{1 - RH/100}{0.1\sqrt[3]{h_0}} \qquad for\, f_{cm} \leq 35 \tag{E.26}$$

$$\varphi_{RH} = \left(1 + \left(\frac{1 - RH/100}{0.1\sqrt[3]{h_0}}\right)\alpha_1\right)\alpha_2 \qquad for\, f_{cm} > 35 \tag{E.27}$$

$$\beta(f_{cm}) = \frac{16.8}{\sqrt{f_{cm}}} \tag{E.28}$$

$$\beta(t_0) = \frac{1}{\left(0.1 + t_0^{0.2}\right)} \tag{E.29}$$

$$\beta_c(t,t_0) = \left(\frac{(t - t_0)}{\beta_H + t - t_0}\right)^{o.3} \tag{E.30}$$

$$\beta_H = 1.5\left(1 + (0.012RH)^{18})\right) h_0 + 250 \leq 1500 \qquad for\, f_{cm} \leq 35 \tag{E.31}$$

$$\beta_H = 1.5\left(1 + (0.012RH)^{18})\right) h_0 + 250\alpha_3 \leq 1500\alpha_3 \qquad for\, f_{cm} > 35 \tag{E.32}$$

$$\alpha_3 = \sqrt{\frac{35}{f_{cm}}} \tag{E.33}$$

$$\varepsilon_{cc(t)} = \frac{1}{E_{cm}} \sum_{i=0}^{n} \Delta\sigma_i \varphi_{t,t_i} \text{Boltmann} \tag{E.34}$$

$$E_{cm,eff} = \frac{E_{cm}}{1 + \varphi} \text{A.A.E.M.} \tag{E.35}$$

$$\varepsilon_{cc(t)} = \frac{\sigma_{(t)}}{E_{cm,eff}} \tag{E.36}$$

$$\varepsilon_{cc(t)} = \frac{\sigma_0}{\frac{E_{cm}}{1+\varphi}} + \frac{\Delta\sigma_{(t)}}{\frac{E_{cm}}{1+\chi_{age}\varphi}} \qquad \text{Trost} \tag{E.37}$$

$$\varepsilon_{cc(t)} = \sigma_{t_0} \cdot J_{(t)} = \sigma_{t_0}\left[\frac{1}{E_{cm(t_0)}} + \frac{\varphi_{(t,t_0)}}{E_{cm(28)}}\right] \qquad \text{M.C.2010} \tag{E.38}$$

Values

Table E.7: Analysis of creep coefficient

Parameter		**Creep** $\varphi_0, t = \infty$ [-]	[%]	**Creep** $\varphi_{t=365}$ [-]	**Development after 1 year**[%]
Concrete strength F_{ck}	20	4.45	121	3.10	70
[MPa]	25	4.10	111	2.86	70
	30	3.69	100	2.57	70
	35	3.29	89	2.30	70
Cement type	S	4.18	113	2.91	70
[%]	N	3.69	100	2.57	70
	R	2.86	77	1.98	69
Relative Humidity	40	4.31	117	3.00	70
[%]	60	3.69	100	2.57	70
	80	3.06	83	2.00	65
Slab height	150	3.81	103	2.76	72
[mm]	200	3.69	100	2.57	70
	250	3.60	98	2.42	67
Age of concrete when loaded	1	7.37	200	5.16	70
[day]	28	3.69	100	2.58	70
	365	2.42	66	1.69	70

Graphs

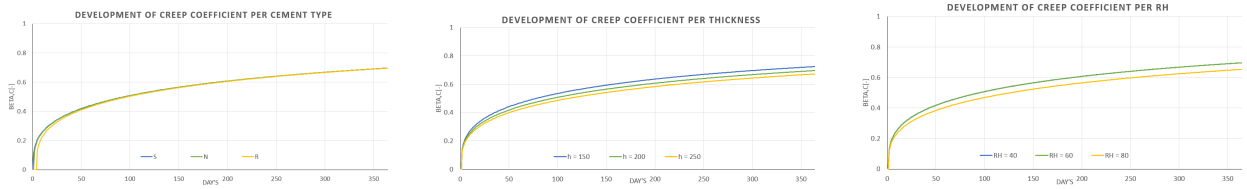

(a) Cement type **(b)** Slab thickness **(c)** Relative humidity

Figure E.3: Development of creep

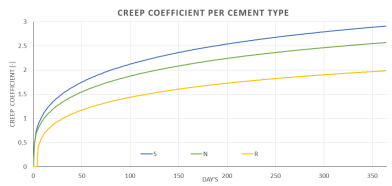

(a) Cement type

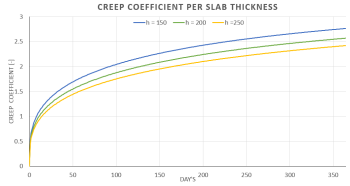

(b) Slab thickness

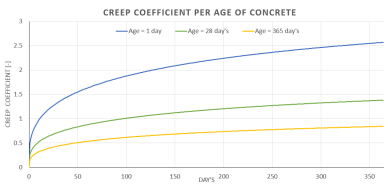

(c) Age of concrete at loading

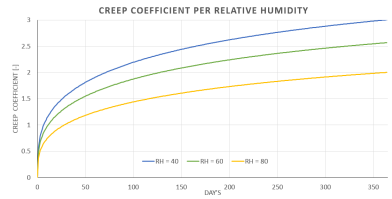

(d) Relative humidity

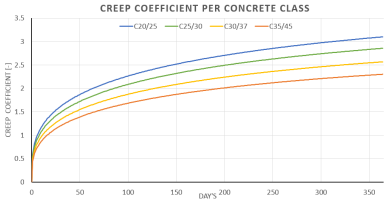

(e) Concrete class

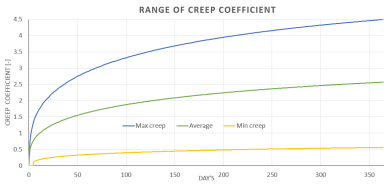

(f) Minimum and maximum value

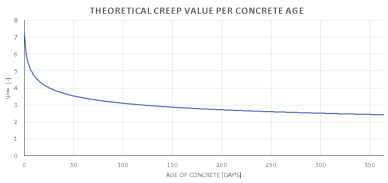

(g) Final creep value per concrete age at loading

Figure E.4: Creep coefficient

The influence of the parameters is investigated and the following conclusions can be drawn.

- The slab thickness has a minor effect on the development of creep in time. The variation after one year is ±2% per 50 mm slab thickness change.
- A very high *R.H.* (>75%) reduces the development of the creep coefficient.
- After one year, the creep is ≈ 70% developed.
- Cement types S increases and R decreases the final creep coefficient with ≈ 13% compared with type N.
- The age of concrete at the moment of loading has a significant influence on the final creep coefficient. Applying a load on older concrete results in a decrease of the creep coefficient. Concrete loaded after one day and a year leads to an increment of 100% and a reduction of 34% compared to respectively 28 days old loaded concrete.
- Slab thickness has a minor effect on the final creep coefficient. ±2% per 50 mm of slab thickness change.
- A higher concrete class leads to a reduction of the creep coefficient. ±11% per concrete class.
- A higher *R.H.* leads to a reduction of the final creep coefficient. ±17% per 20% of *R.H.* change.

Relaxation

Formulae

$$\psi_{gradual} = \frac{1}{\left(1 + \chi_{age}\varphi(t,t_o)\right)} \tag{E.39}$$

$$\psi_{instant} = 1 - \frac{\varphi(t,t_o)}{\left(1 + \chi_{age}\varphi(t,t_o)\right)} \tag{E.40}$$

$$\psi_{CUR36} = \frac{\left(1 - \exp(-\varphi(t,t_o))\right)}{\varphi(t,t_o)} \tag{E.41}$$

Values

Table E.8: Analysis of relaxation calculation method

Parameter		**ψ for t_l=7**	**ψ for t_l=28**	**ψ for t_l=365**
χ_{age}	0.6	0.63	0.50	0.25
	0.8	0.66	0.55	0.34
	1.0	0.68	0.59	0.42
Function	CUR-36	0.80	0.72	0.54
	Gradually	0.73	0.64	0.48
	Instant	0.66	0.55	0.34
Creep coefficient φ_0	0.5	0.90	0.85	0.74
	2.0	0.67	0.56	0.35
	4.0	0.48	0.35	0.15
Concrete age t_0	1	0.49	0.36	0.16
	28	0.66	0.55	0.34
	365	0.77	0.68	0.50

Graphs

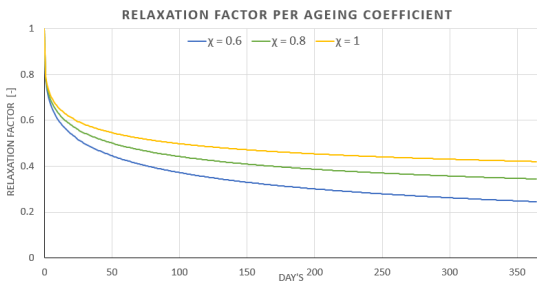

(a) Ageing coefficient

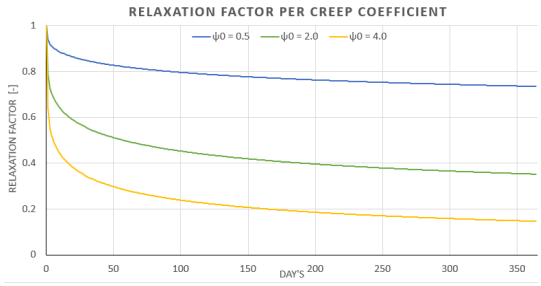

(b) Creep coefficient

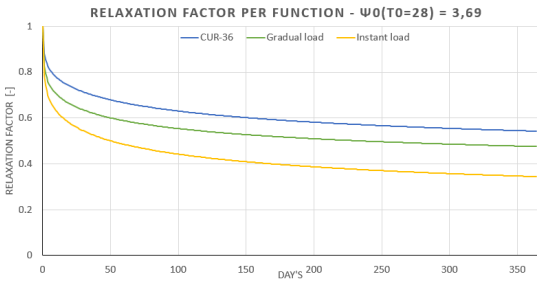

(c) Relaxation function

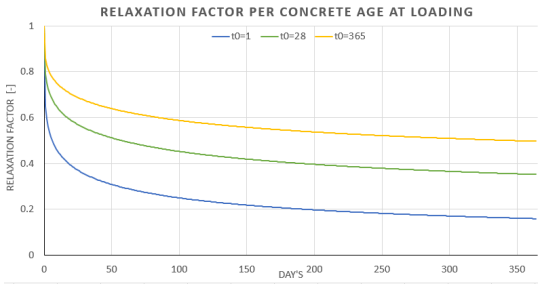

(d) Concrete age at loading

Figure E.5: Relaxation factor

Drying shrinkage

Formulae

$$\varepsilon_{cs}(t) = \varepsilon_{cd}(t) + \varepsilon_{ca}(t) \tag{E.42}$$

$$\varepsilon_{cd,0} = 0.85\left(\left(220 + 110\alpha_{ds1}\right)\exp\left(-\alpha_{ds2}\frac{f_{cm}}{f_{cm0}}\right)\right)\beta_{RH} * 10^{-6} \tag{E.43}$$

$$\beta_{RH} = 1.55\left(1 - \left(\frac{RH}{RH_0}\right)^3\right) \tag{E.44}$$

$$\beta_{ds}(t, ts) = \frac{\left(t - t_s\right)}{\left(t - t_s\right) + 0.04\sqrt{h_0^3}} \tag{E.45}$$

$$k_h = k_{h500} + \frac{500 - h_0}{500 - 300}(0.75 - 0.70) \tag{E.46}$$

α_{ds1} is 4 for cement class N
α_{ds2} is 0.12 for cement class N
f_{cm0} is 10 MPa
RH_0 is 100 %

Values

Table E.9: Analysis of drying shrinkage

Parameter		$\varepsilon_{cd,0,t=\infty}$ [mm m^{-1}]	**[%]**	$\varepsilon_{cd,t=365}$ [mm m^{-1}]	**[%]**	**Development after one year**[%]
F_{ck}	20	0.49	113	0.19	113	38
[MPa]	25	0.46	106	0.18	106	38
	30	0.43	100	0.17	100	38
	35	0.41	94	0.16	94	38
RH	40	0.52	119	0.20	119	38
[%]	60	0.43	100	0.17	100	38
	80	0.27	62	0.10	62	38
Slab height	150	0.43	100	0.21	124	47
[mm]	200	0.43	100	0.17	100	38
	250	0.43	100	0.13	81	31
Curing time	0	0.43	100	0.17	100	39
[day's]	7	0.43	100	0.17	100	38
	28	0.43	100	0.16	99	37
Cement Type	S	0.35	80	0.13	80	38
[-]	N	0.43	100	0.17	100	38
	R	0.60	138	0.23	138	38

Graphs

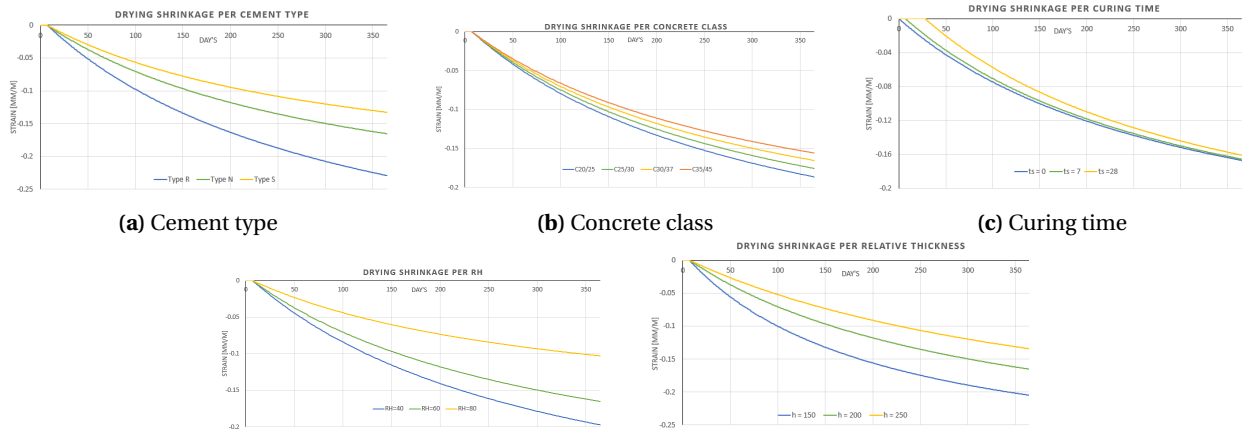

(a) Cement type **(b)** Concrete class **(c)** Curing time

(d) Relative humidity **(e)** Slab thickness

Figure E.6: Drying shrinkage

Autogenous shrinkage

Formulae

$$\varepsilon_{ca}(t) = \beta_{as}(t)\varepsilon_{ca}(\infty) \tag{E.47}$$

$$\beta_{as}(t) = 1 - \exp\left(-0.2t^{0.5}\right) \tag{E.48}$$

$$\varepsilon_{ca}(\infty) = 2.5\left(f_{ck} - 10\right)10^{-6} \tag{E.49}$$

(E.50)

Values

Table E.10: Analysis of autogenous shrinkage

Parameter		$\varepsilon_{ca,\infty}$ [mm m^{-1}]	[%]	$]\varepsilon_{ca,t=365}$ [mm m^{-1}]	**Development after one year** [%]
Concrete strength F_{ck}	20	0.025	50	0.024	98
[MPa]	25	0.038	75	0.037	98
	30	0.050	100	0.049	98
	35	0.063	125	0.061	98

Graphs

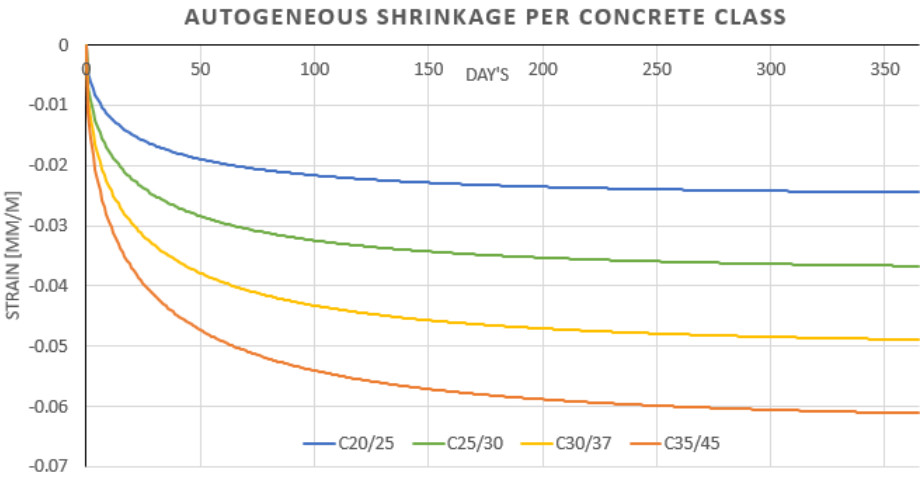

Figure E.7: Autogenous shrinkage per concrete class

Hydration temperature analysis

In a different study, the stress development in concrete structures from ground restraint is examined. In Fig: E.8b, the stresses from a model calculation in the newly cast concrete for a *S.o.G.* with a joint spacing of 140 m is shown. After two days of curing, the stresses start to develop. First, the concrete expands and then due to cooling tensile stresses develop.

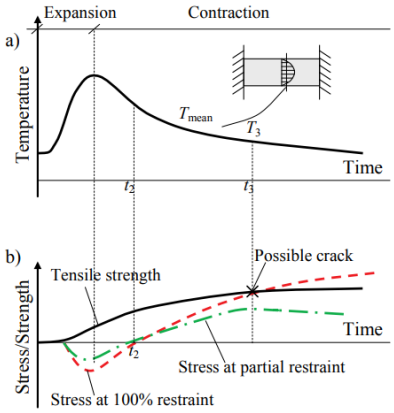

(a) principle

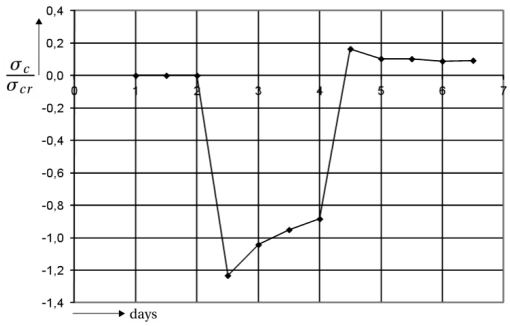

(b) Stress development in 140 m long *S.o.G.*

Figure E.8: Early age stress behaviour

For the investigated in this research, four temperature profiles are created. The profiles are a combination of peak temperature with rapid or slow cooling. The profiles are based on the measured temperature profiles in the survey *Bishop*[19]. The linear and relaxed stresses are calculated with the *Bazant* method.

Values

Table E.11: Analysis of hardening temperature

Temperature	**Profile**	$\sigma_{t=365}$ [MPa]	% of σ_{cr}
Dt=10 °C	Rapid cooling	0.18	6
Dt=10 °C	Slow cooling	0.27	8
Dt=15 °C	Rapid cooling	0.27	8
Dt=15 °C	Slow cooling	0.40	12
Dt=20 °C	Rapid cooling	0.36	11
Dt=20 °C	Slow cooling	0.53	16

Graphs

(a) dT = 10 °C

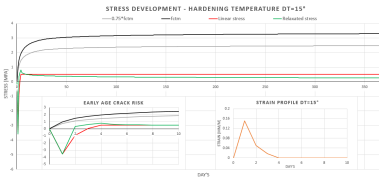

(b) dT = 15 °C

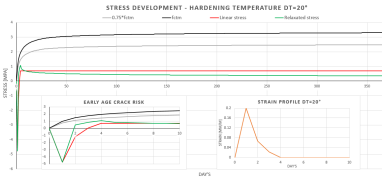

(c) dT = 20 °C

Figure E.9: Hydration effect - rapid cooling

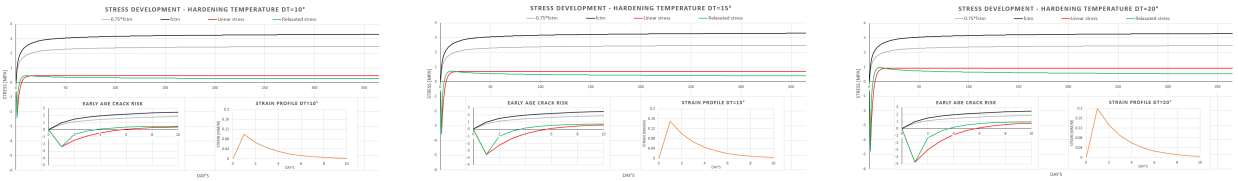

(a) dT = 10 °C **(b)** dT = 15 °C **(c)** dT = 20 °C

Figure E.10: Hydration effect - slow cooling

Seasonal temperature

The seasonal temperature changes are analysed with four sinus strain profiles. The temperature change per season is shown below the graphs. The results found in the literature are also given.

Graphs

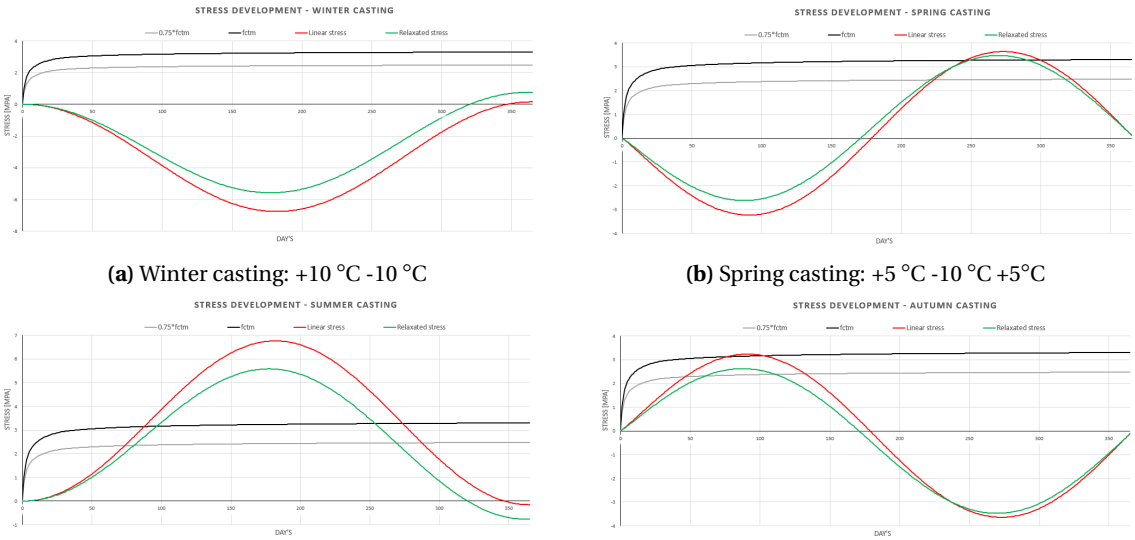

(a) Winter casting: +10 °C -10 °C **(b)** Spring casting: +5 °C -10 °C +5°C

(c) Summer casting: -10 °C +10 °C **(d)** Autumn casting: -5 °C +10 °C -5°C

Figure E.11: Seasonal temperature effect

In Fig: E.12, the stresses are shown from the model calculation to illustrate the effect of the surrounding temperature. The crack risk (ratio between the concrete stress and tensile capacity $\frac{\sigma_c}{\sigma_{cr}}$) is plotted on the vertical axis with the days on the horizontal axis. Different situations are analysed with the model calculation. The surrounding temperature T_{sur} during casting and the cooling temperature gradient are changed. The crack risk is plotted for joint spacing from 10 to 100 meters.

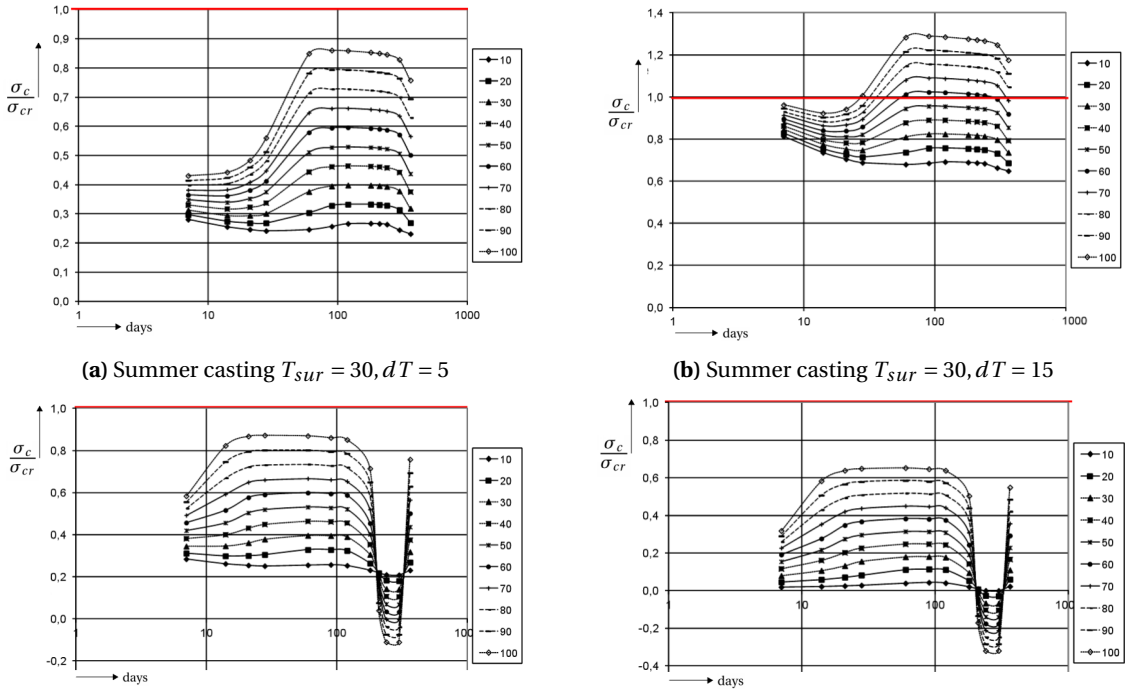

(a) Summer casting $T_{sur} = 30, dT = 5$

(b) Summer casting $T_{sur} = 30, dT = 15$

(c) Winter casting $T_{sur} = 10, dT = 5$

(d) Winter casting $T_{sur} = 10, dT = 0$

Figure E.12: Temperature stresses in *S.o.G.*

Daily temperature

Values

Table E.12: Analysis of daily temperature

Daily temperature change [°C]	σ_{daily}	% of f_{ctm}
+/- 0.5	+/- 0.20	6
+/- 1	+/- 0.40	12

Graphs

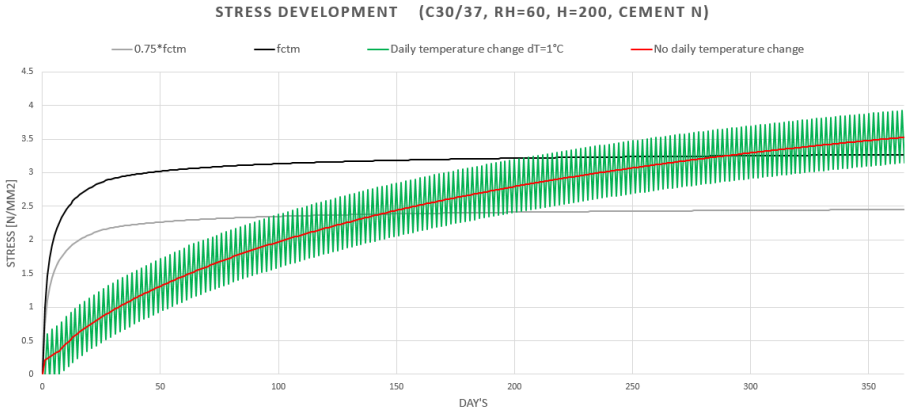

Figure E.13: Daily temperature change

degree of restraint

Values

Table E.13: Analysis of degree of restraint

degree of restraint R	σ_{max}	% of f_{ctm}
0.25	1.13	35
0.50	2.72	70
0.75	3.40	105
1.00	4.54	140

Graphs

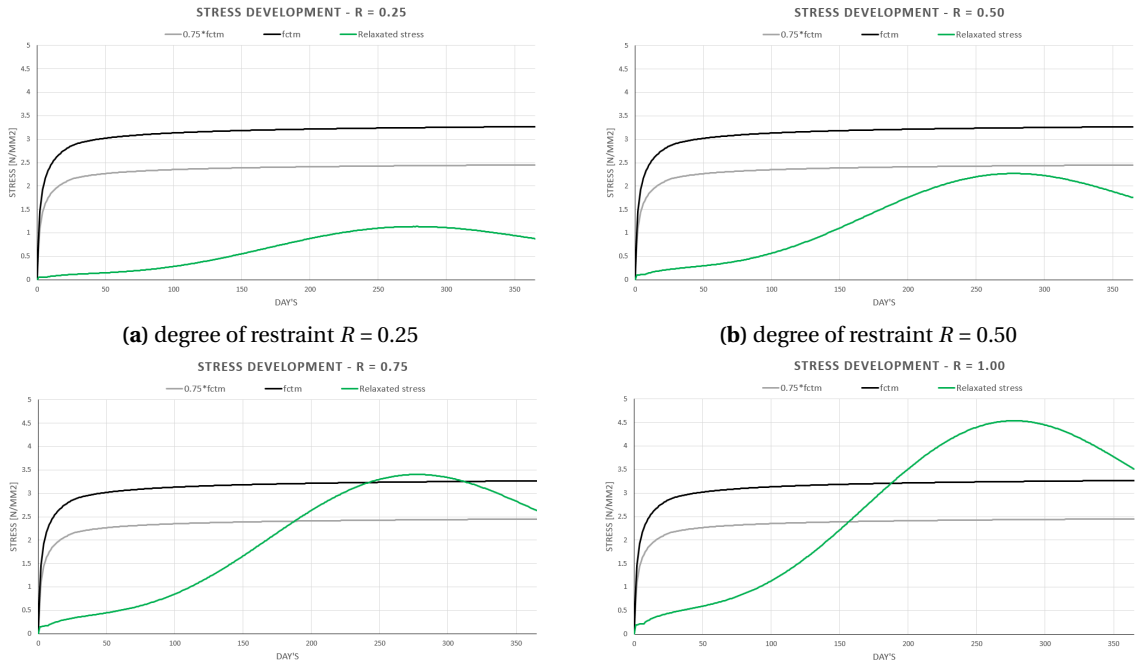

(a) degree of restraint R = 0.25

(b) degree of restraint R = 0.50

(c) degree of restraint R = 0.75

(d) degree of restraint R = 1.00

Figure E.14: Stress development with different degree of restraint

Appendix F

Sensitivity analysis: cracking

Effect of slab boundaries

Values

Table F.1: Analysis of stresses and crack width

		Breugel	Gilbert					Breugel		Gilbert			*M.C. 2010*		CUR-65	Stufib-11
Parameter	t	N_{cr}	$N_{c_{(t)}}$	ψ_{crack}	$\sigma_{c1_{(t)}}$	$\sigma_{s1_{(t)}}$	$\sigma_{s,cr}$	w_{mo}	w_{max}	Cracks	s_m	w_{max}	l_t	w_{max}	w_{max}	w_{max}
h=150	**34**	271	239	0.88	1.6	-1.0	315.2	0.12	0.22	1	-	0.28	**182**	**0.35**	0.29	0.27
	3650	311	**257**	0.83	2.0	-57.5	340.7	0.12	0.24	48	1.0	0.30	182	0.34	0.32	
h=200	**49**	371	326	0.88	1.6	-1.0	323.4	0.13	0.23	1	-	0.35	**207**	**0.41**	0.32	0.27
	3650	414	**344**	0.83	2.0	-53.7	342.3	0.12	0.24	45	1.1	0.30	207	0.39	0.35	
h=250	**65**	471	415	0.88	1.7	-1.0	328.9	0.13	0.24	1	-	0.36	**231**	**0.46**	0.35	0.27
	3650	518	**432**	0.83	2.0	-49.9	343.9	0.12	0.25	42	1.2	0.30	231	0.45	0.38	
$L_{restraint}$=5	49	371	199	**0.53**	1.0	-6.2	195.5	0.05	**0.09**	1	-	0.17	207	0.12	0.32	0.27
	3650	414	317	0.76	1.9	-56.0	313.2	0.10	0.18	**5**	1	0.28	207	0.34	0.35	
$L_{restraint}$=25	49	371	298	**0.80**	1.5	-1.8	294.1	0.11	**0.18**	1	-	0.29	207	0.36	0.32	0.27
	3650	414	339	0.82	2.0	-54.2	336.6	0.12	0.23	**23**	1.1	0.30	207	0.38	0.35	
$L_{restraint}$=50	49	371	326	**0.88**	1.6	-1.0	323.4	0.13	**0.23**	1	-	0.35	207	0.41	0.32	0.27
	3650	414	344	0.83	2.0	-53.7	342.3	0.12	0.24	**45**	1.1	0.30	207	0.39	0.35	
$L_{restraint}$=100	49	371	343	**0.92**	1.7	-0.5	340.3	0.14	**0.28**	1	-	0.45	207	0.43	0.32	0.27
	3650	414	351	0.85	2.0	-53.4	349.7	0.12	0.26	**88**	1.1	0.31	207	0.41	0.35	
τ_g=0.0075	49	371	326	0.88	1.6	-1.0	324.6	0.13	0.24	1	-	0.35	207	0.41	0.32	0.27
	3650	414	344	0.83	2.0	-53.7	**343.0**	0.12	0.25	45	1.1	0.30	207	0.39	0.35	
τ_g=0.021	49	371	326	0.88	1.6	-1.0	323.4	0.13	0.23	1	-	0.35	207	0.41	0.32	0.27
	3650	414	344	0.83	2.0	-53.7	**342.3**	0.12	0.24	45	1.1	0.30	207	0.39	0.35	
τ_g=0.069	49	371	326	0.88	1.6	-1.0	320.7	0.12	0.23	1	-	0.35	207	0.40	0.32	0.27
	3650	414	344	0.83	2.0	-53.7	**340.7**	0.12	0.24	45	1.1	0.30	207	0.39	0.35	
R.H.=40	**42**	367	323	0.88	1.6	-1.0	320.2	0.12	0.23	1	-	0.33	207	0.40	0.32	0.28
	3650	414	336	0.81	2.0	-64.9	**333.9**	0.11	0.22	**54**	0.9	**0.31**	207	0.37	0.35	
R.H.=60	**49**	371	326	0.88	1.6	-1.0	323.4	0.13	0.23	1	-	0.35	207	0.41	0.32	0.27
	3650	414	344	0.83	2.0	-53.7	**342.3**	0.12	0.24	**45**	1.1	**0.30**	207	0.39	0.35	
R.H.=80	**76**	380	334	0.88	1.7	-1.0	331.2	0.13	0.24	1	-	0.40	207	0.42	0.33	0.27
	3650	414	361	0.87	2.0	-31.8	**359.3**	0.13	0.29	**27**	1.9	**0.30**	207	0.42	0.35	
α_{sra}=0.6	78	384	343	0.89	1.7	-1.0	340.2	0.13	0.26	1	-	0.38	207	0.42	0.33	0.16
	3650	418	374	0.89	2.0	-30.3	371.5	0.14	0.33	25	2.0	0.30	207	0.46	0.35	0.27
α_{sra}=0.8		379	338	0.89	1.7	-1.0	335.2	0.13	0.26	1	-	0.34	207	0.41	0.32	0.16
	3650	418	357	0.86	2.0	-41.9	354.4	0.13	0.27	35	1.4	0.30	207	0.42	0.35	0.27
α_{sra}=1.0	49	371	326	0.88	1.6	-1.0	323.4	0.13	0.23	1	-	0.35	207	0.41	0.32	0.27
	3650	414	344	0.83	2.0	-53.7	342.3	0.12	0.24	45	1.1	0.30	207	0.39	0.35	0.37
ΔT=10	**37**	364	321	0.88	1.6	-1.0	317.5	0.12	0.23	1	-	0.29	207	0.40	0.31	0.28
	3650	414	330	**0.80**	2.0	-73.8	**327.4**	0.11	**0.21**	61	0.8	**0.31**	207	0.36	0.35	
ΔT=20	**30**	358	316	0.88	1.6	-0.9	312.6	0.12	0.22	1	-	0.25	207	0.39	0.31	0.29
	3650	414	307	**0.74**	2.0	-93.9	**304.7**	0.10	**0.17**	78	0.6	**0.31**	207	0.31	0.35	

Graphs

Soil friction after cracking

(a) Dominant cracks after 5 years

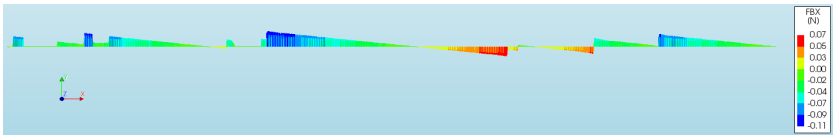

(b) Soil friction force after cracking

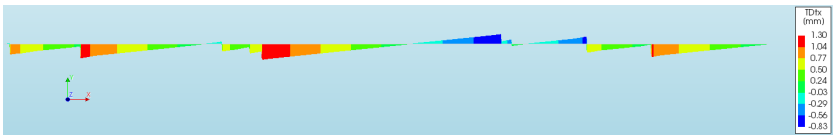

(c) Horizontal displacement after cracking

Figure F.1: Soil behaviour in tensile member after cracking

Effect of reinforcement

Values

Table F.2: Analysis of stresses and crack width

		Breugel	Gilbert					Breugel		Gilbert			*M.C. 2010*		CUR-65	Stufib-11
Parameter	t	N_{cr}	$N_{c_{(t)}}$	ψ_{crack}	$\sigma_{c1_{(t)}}$	$\sigma_{s1_{(t)}}$	$\sigma_{s,cr}$	w_{mo}	w_{max}	Cracks	s_m	w_{max}	l_t	w_{max}	w_{max}	w_{max}
ρ_s=0.32	49	368	288	0.78	1.5	-2.1	435.0	0.24	1.22	1	-	0.67	270	-	0.64	0.57
	3650	411	352	0.86	1.9	-54.4	-	-	-	19	2.6	0.71	270	-	0.71	
ρ_s=0.50	49	371	326	0.88	1.6	-1.0	323.4	0.13	0.23	1	-	0.35	207	0.41	0.32	0.27
	3650	414	344	0.83	2.0	-53.7	342.3	0.12	0.24	45	1.1	0.30	207	0.39	0.35	
ρ_s=1.00	49	380	349	0.92	1.8	-0.3	174.2	0.04	0.07	1	-	0.16	151	0.15	0.13	0.09
	3650	423	297	0.70	2.0	-53.2	147.8	0.03	0.05	176	0.3	0.08	151	0.10	0.14	
∅=6	49	371	337	0.91	1.7	-0.7	335.2	0.09	0.19	1	-	0.26	170	0.34	0.26	0.19
	3650	414	346	0.83	2.0	-53.5	344.5	0.09	0.18	67	0.7	0.20	170	0.32	0.28	
∅=9	49	371	326	0.88	1.6	-1.0	323.4	0.13	0.23	1	-	0.35	207	0.41	0.32	0.27
	3650	414	344	0.83	2.0	-53.7	342.3	0.12	0.24	45	1.1	0.30	207	0.39	0.35	
∅=12	49	371	316	0.85	1.6	-1.3	312.0	0.15	0.27	1	-	0.43	242	0.46	0.38	0.35
	3650	414	342	0.83	2.0	-53.9	339.8	0.15	0.30	34	1.5	0.41	242	0.48	0.42	
Eccentricity=0	49	371	326	0.88	1.6	-1.0	323.4	0.13	0.23	1	-	0.35	207	0.41	0.32	0.27
	3650	414	344	0.83	2.0	-53.7	342.3	0.12	0.24	45	1.1	0.30	207	0.39	0.35	
Eccentricity=25	49	371	326	0.88	1.6	-1.0	256.3	0.08	0.14	1	-	0.28	182	0.23	0.22	0.19
	3650	414	344	0.83	2.0	-53.7	270.1	0.08	0.13	45	1.1	0.24	182	0.22	0.24	
Eccentricity=50	49	371	326	0.88	1.6	-1.0	212.8	0.06	0.10	1	-	0.23	157	0.13	0.16	0.14
	3650	414	344	0.83	2.0	-53.7	224.4	0.06	0.10	45	1.1	0.20	157	0.12	0.17	

Graphs

Influence of bonding quality

A low bonding quality can result in slipping of the reinforcement with one dominant crack in the tensile member. The slipping behaviour of the reinforcement is shown in Fig: F.3 for the red marked points in Fig: F.2a. In Fig: F.2b the crack width development is given for the different calculation methods. It can be seen that a dominant crack results in an undesirable crack width of 0.8 mm after 300 days.

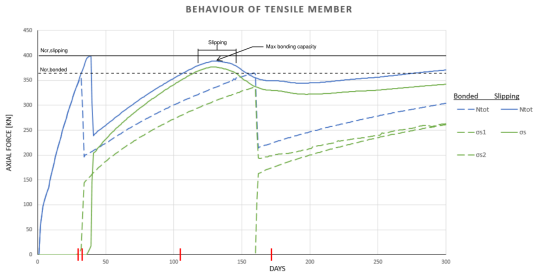

(a) Stress behaviour of slipping and bonded reinforcement

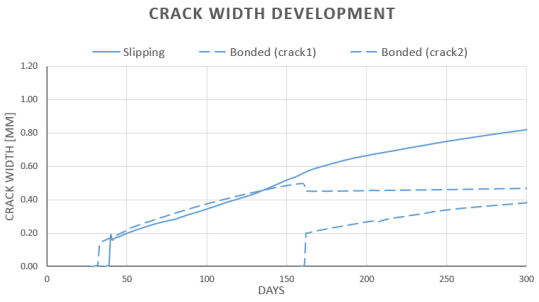

(b) Crack width of slipping and bonded reinforcement

Figure F.2: Behaviour of slipping and bonded reinforcement

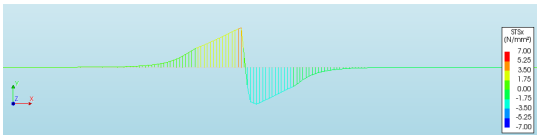

(a) Bond stress at t=39, start cracking

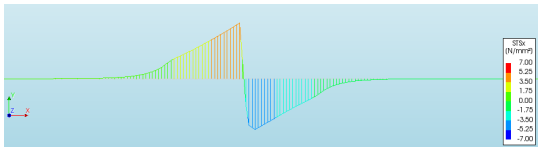

(b) Bond stress at t=43, after cracking

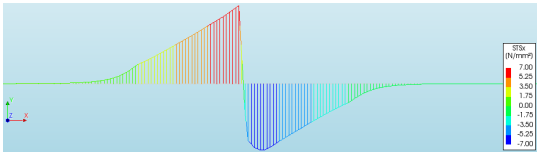

(c) Bond stress at t=124, before slipping

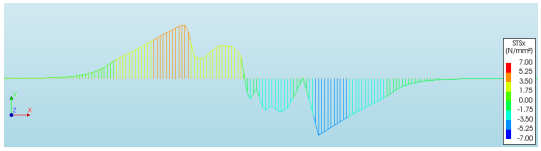

(d) Bond stress at t=170, start slipping

Figure F.3: Bond stress behaviour in dominant crack

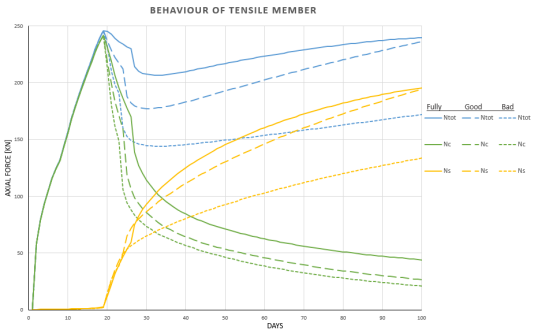

(a) Stress behaviour in *N.T.M.*

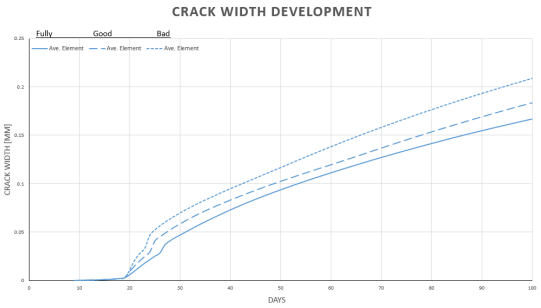

(b) Crack width development

Figure F.4: Effect of bonding quality in *N.T.M.*

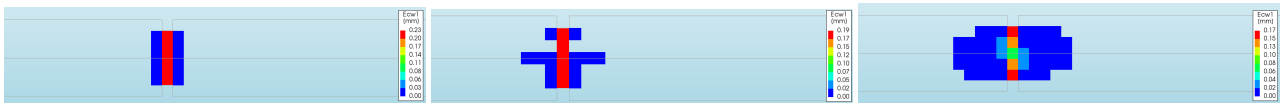

(a) Bad bonding

(b) Good bonding

(c) Fully bonded

Figure F.5: Crack pattern in *N.T.M.*

Influence of eccentricity

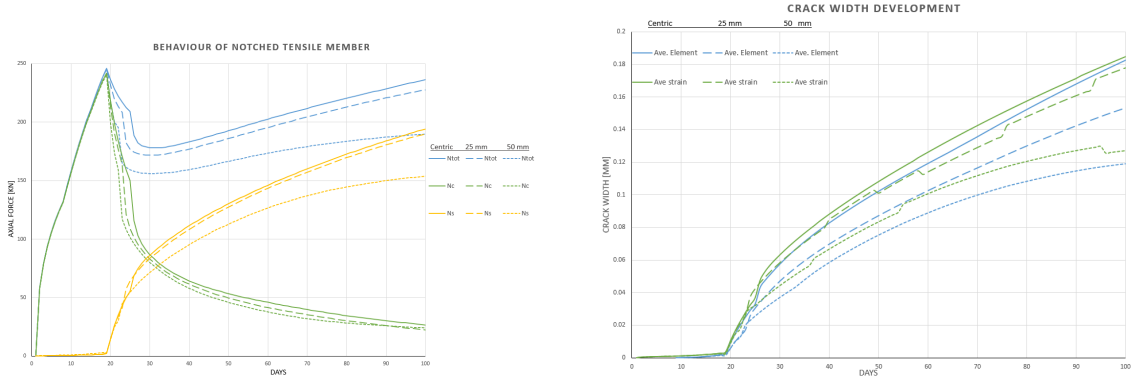

(a) Stresses in *N.T.M.* **(b)** Crack width in *N.T.M.*

Figure F.6: Eccentricity effect in *N.T.M.*

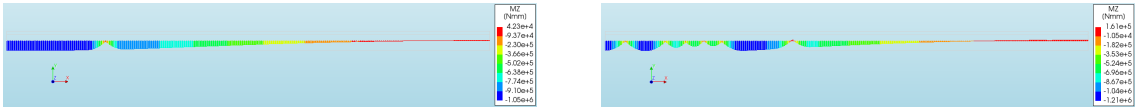

(a) After the first crack **(b)** After 3 years

Figure F.7: Bending moments in eccentric reinforced *R.T.M.*

Behaviour of low ρ_s in eccentric reinforced *R.T.M.*

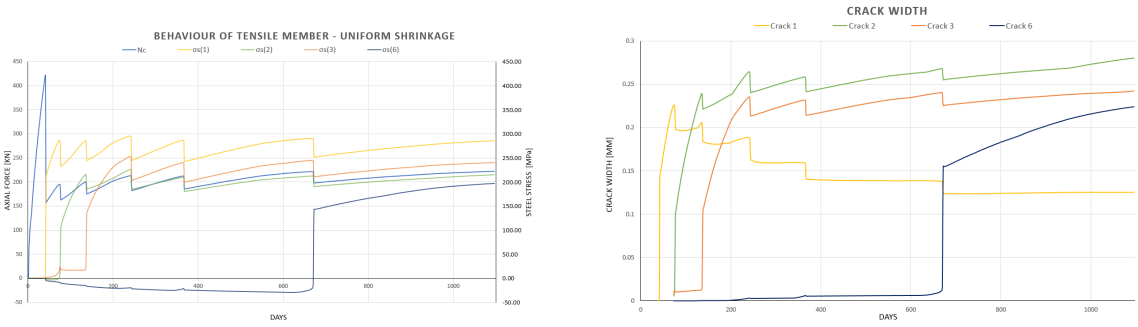

(a) Stresses in *R.T.M.* **(b)** Crack width in *R.T.M.*

Figure F.8: low reinforcement ratio in *R.T.M.*

Effect of concrete mixture

Values

Table F.3: Analysis of stresses and crack width

		Breugel	Gilbert					Breugel		Gilbert			*M.C. 2010*		CUR-65	Stufib-11
Parameter	t	N_{cr}	$N_{c_{(t)}}$	ψ_{crack}	$\sigma_{c1_{(t)}}$	$\sigma_{s1_{(t)}}$	$\sigma_{s,cr}$	w_{mo}	w_{max}	Cracks	s_m	w_{max}	l_t	w_{max}	w_{max}	w_{max}
C20/25	51	285	252	0.88	1.3	-0.8	249.3	0.10	0.18	1	-	0.27	207	0.31	0.25	0.23
	3650	317	250	0.79	1.5	-58.3	248.1	0.09	0.15	63	0.8	0.24	207	0.27	0.28	
C30/37	49	371	326	0.88	1.6	-1.0	323.4	0.13	0.23	1	-	0.35	207	0.41	0.32	0.27
	3650	414	344	0.83	2.0	-53.7	342.3	0.12	0.24	45	1.1	0.30	207	0.39	0.35	
C35/45	46	409	359	0.88	1.8	-1.1	355.8	0.13	0.28	1	-	0.37	207	0.45	0.35	0.28
	3650	458	392	0.86	2.2	-51.9	391.1	0.13	0.37	39	1.3	0.34	207	0.46	0.39	
Basalt	35	361	314	0.87	1.6	-0.9	310.1	0.12	0.21	1	-	0.27	207	0.39	0.31	0.27
	3650	412	343	0.83	2.0	-56.2	341.1	0.12	0.24	47	1.1	0.30	207	0.39	0.35	
Quartz	49	371	326	0.88	1.6	-1.0	323.4	0.13	0.23	1	-	0.35	207	0.41	0.32	0.27
	3650	414	344	0.83	2.0	-53.7	342.3	0.12	0.24	45	1.1	0.30	207	0.39	0.35	
Sandstone	93	389	347	0.89	1.7	-1.0	344.6	0.13	0.27	1	-	0.48	207	0.42	0.33	0.28
	3650	419	356	0.85	2.0	-47.1	354.1	0.13	0.27	39	1.3	0.31	207	0.40	0.35	
Cement S	63	387	340	0.88	1.7	-1.0	337.3	0.13	0.25	1	-	0.43	207	0.42	0.33	0.27
	3650	448	395	0.88	2.2	-41.9	394.7	0.14	0.40	32	1.6	0.33	207	0.47	0.38	
Cement N	49	371	326	0.88	1.6	-1.0	323.4	0.13	0.23	1	-	0.35	207	0.41	0.32	0.27
	3650	414	344	0.83	2.0	-53.7	342.3	0.12	0.24	45	1.1	0.30	207	0.39	0.35	
Cement R	37	363	319	0.88	1.6	-1.0	316.2	0.12	0.23	1	-	0.31	207	0.40	0.31	0.28
	3650	402	314	0.78	2.0	-76.0	311.2	0.11	0.19	65	0.8	0.30	207	0.34	0.34	
α_{cr}=0.6	49	371	326	0.88	1.6	-1.0	323.4	0.13	0.23	1	-	0.35	207	0.41	0.32	0.27
	3650	414	344	0.83	2.0	-53.7	342.3	0.12	0.24	45	1.1	0.30	207	0.39	0.35	
α_{cr}=0.8	82	509	447	0.88	2.3	-1.3	435.0	0.45	2.28	1	-	0.53	207	-	0.44	0.44
	3650	552	476	0.86	-	-	-	-	-	-	-	0.40	207	-	0.47	
α_{cr}=1.0	125	648	569	0.88	-	-	-	-	-	-	-	0.73	207	-	0.56	0.65
	3650	690	622	0.90	-	-	-	-	-	-	-	0.50	207	-	0.59	
ψ=0.50	102	396	355	0.90	1.8	-1.1	352.3	0.13	0.29	1	-	0.50	207	0.42	0.33	0.27
	3650	426	379	0.89	2.0	-24.2	375.7	0.14	0.34	20	2.5	0.31	207	0.40	0.35	
ψ=0.75	49	375	334	0.89	1.7	-1.0	331.2	0.13	0.25	1	-	0.35	207	0.41	0.32	0.27
	3650	418	348	0.83	2.0	-48.8	344.4	0.12	0.25	41	1.2	0.30	207	0.39	0.35	
ψ=1.00	29	357	315	0.88	1.6	-0.9	311.8	0.12	0.22	1	-	0.25	207	0.38	0.31	0.27
	3650	414	341	0.82	2.0	-57.3	336.8	0.12	0.23	48	1.0	0.30	207	0.39	0.35	
t	49	371	326	0.88	1.6	-1.0	323.4	0.13	0.23	1	-	0.35	207	0.41	0.32	0.27
	100	385	363	0.94	1.9	-8.9	361.0	0.14	0.30	8	6.3	0.27	207	0.44	0.33	0.27
	365	401	358	0.89	1.9	-29.0	356.6	0.13	0.29	25	2.0	0.29	207	0.43	0.34	0.27
	1825	412	352	0.86	2.0	-49.4	350.8	0.13	0.27	41	1.2	0.30	207	0.41	0.35	0.27
	3650	414	344	0.83	2.0	-53.7	342.3	0.12	0.24	45	1.1	0.30	207	0.39	0.35	0.27

Graphs

Influence of relaxation

The effect of relaxation on cracking in the *N.L.F.E.A.* is investigated in the *N.T.M.* with a constant predescribed strain load. The analysis showed that relaxation delays the moment of cracking. A higher strain load is required to initiate cracking in the concrete. The effect is shown in Fig: F.9

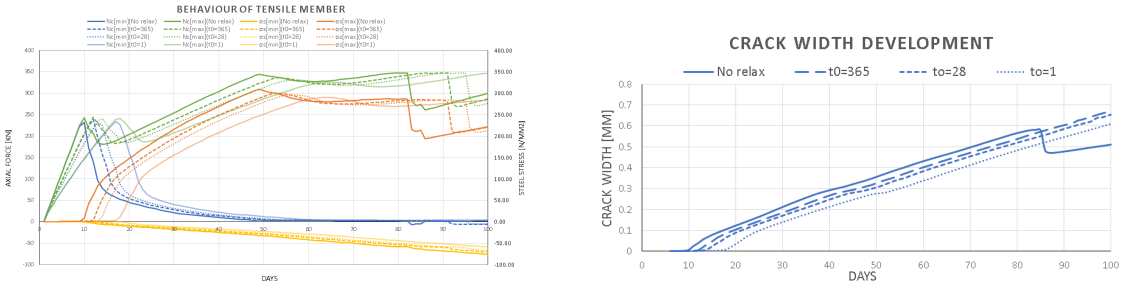

(a) Stresses in *N.T.M.*

(b) Crack width in *N.T.M.*

Figure F.9: Relaxation effect in *N.T.M.*

Influence of concrete mixture

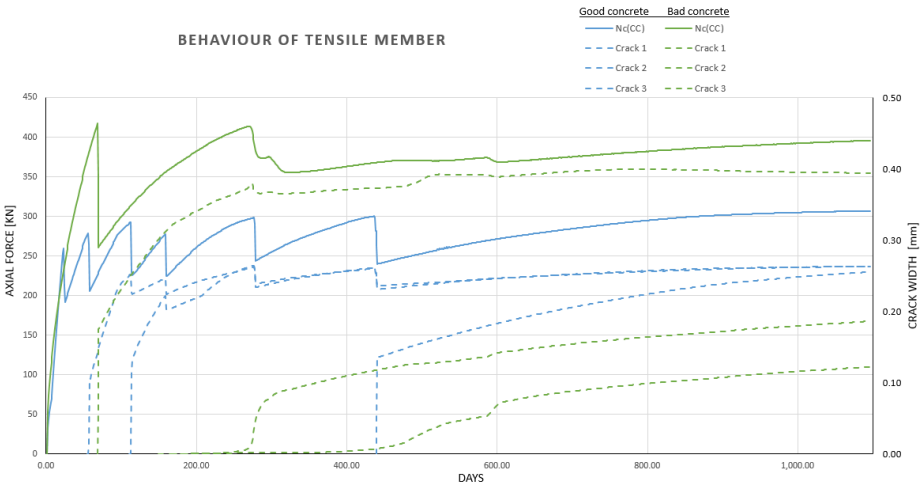

Figure F.10: Behaviour for different concrete mixtures

Effect of *S.F.R.C.*

Properties

The many parameters result in a large variation of *S.F.R.C.* properties. In Tab:F.4 and F.5 the assumed properties for this research are shown. Some values are received from a steel fibre supplier(bold). The properties used in this research are solely for comparison studies and can not be used for design purposes.

Table F.4: Properties 3D *S.F.R.C.*

3D 65/60BG	V_f	f_{r1}	σ_{r1}	f_{r3}	σ_{r3}
C20/25	30	**2.90**	1.32	**3.00**	1.10
	40	3.91	1.76	4.16	1.54
C25/30	30	3.18	1.43	3.16	1.17
	40	4.33	1.95	4.57	1.69
C30/37	30	**3.20**	1.45	**3.30**	1.16
	40	4.51	2.03	4.70	1.74
C35/45	30	3.20	1.44	3.03	1.12
	40	4.62	2.08	4.76	1.76

Table F.5: Properties 4D *S.F.R.C.*

4D 65/60BG	V_f	f_{r1}	σ_{r1}	f_{r3}	σ_{r3}
C20/25	30	**3.40**	1.54	**4.30**	1.54
	40	4.40	1.98	5.35	1.98
C25/30	30	3.76	1.69	4.57	1.69
	40	4.91	2.21	5.97	2.21
C30/37	30	**3.90**	1.74	**4.70**	1.74
	40	5.16	2.32	6.27	2.32
C35/45	30	3.91	1.76	4.76	1.76
	40	5.33	2.4	6.49	2.40

Formulae

The *E.C. 2* does not give formulae for the crack width calculation of hybrid structures. The suggested method of the *E.C. 2* is altered by many researchers to take into account the steel fibre reinforcement. The crack spacing is often reduced with a factor. *RELIM TC 162 TDF* suggested a reduction factor based on the fibre aspect ration λ_f, Eq:F.3[69]. The weakness of this model is that the fibre amount is not taken into account. *Moffat* suggested a method based on the residual stress, Eq: F.2[35].

$$w_m = s_{r,max} \cdot \left(\varepsilon_{sm} - \varepsilon_{cm}\right) \tag{F.1}$$

$$s_{m,Moffat} = k_3 * c + k_1 \cdot k_2 \cdot k_4 \cdot \frac{\varnothing}{\omega_{eff}} \cdot \left(1 - \frac{\sigma_{R1}}{\sigma_{cr}}\right) \tag{F.2}$$

$$s_{m,RELIM} = \beta \left(k_3 + k_1 \cdot k_2 \cdot k_4 \cdot \frac{\varnothing}{\omega_{eff}}\right) \cdot \left(k_5 \lambda_f\right) \tag{F.3}$$

$$\varepsilon_{sm} - \varepsilon_{cm} = \frac{\sigma_s - k_t \frac{f_{ct,eff}}{\rho_s}\left(1 + \alpha_e \cdot \rho_s\right)}{E_s} \tag{F.4}$$

Values

Table F.6: Analysis of stresses and crack width

		Breugel	Gilbert					Breugel		Gilbert			*M.C. 2010*		CUR-65	**Stufib-11**
Parameter	t	N_{cr}	$N_{c_{(t)}}$	ψ_{crack}	$\sigma_{c1_{(t)}}$	$\sigma_{s1_{(t)}}$	$\sigma_{s,cr}$	w_{mo}	w_{max}	Cracks	s_m	w_{max}	l_t	w_{max}	w_{max}	w_{max}
K_{fibre}=600	49	375	347	**0.93**	1.7	-0.5	**286.4**	0.10	0.17	1	-	0.23	154	0.33	0.10	0.01
	3650	418	348	0.83	2.0	-53.7	288.7	0.09	0.15	88	0.57	0.15	159	0.32	0.13	
K_{fibre}=800	49	375	347	0.93	1.7	-0.5	**273.4**	0.09	0.16	1	-	0.23	154	0.31	0.10	0.01
	3650	418	348	0.83	2.0	-53.7	275.6	0.08	0.14	88	0.57	0.15	159	0.30	0.13	
K_{fibre}=1000	49	375	347	0.93	1.7	-0.5	**262.1**	0.09	0.15	1	-	0.23	154	0.29	0.10	0.01
	3650	418	348	0.83	2.0	-53.7	264.9	0.08	0.13	88	0.57	0.15	159	0.28	0.13	
ρ_s=0.50	49	371	326	0.88	1.6	-1.0	323.4	0.13	0.23	1	-	0.35	207	0.41	0.32	0.27
	3650	414	344	0.83	2.0	-53.7	342.3	0.12	0.24	45	1.1	0.30	207	0.39	0.35	
3D-30, ρ_s=0.50	49	375	347	0.93	1.7	-0.5	273.4	0.09	0.16	1	-	0.23	154	0.31	0.10	0.01
	3650	418	348	0.83	2.0	-53.7	275.6	0.08	0.14	**88**	0.57	0.15	**159**	0.30	0.13	
4D-30, ρ_s=0.50	49	375	349	0.83	1.8	-0.4	275.6	0.09	0.16	1	-	0.20	142	0.31	0.07	-
	3650	418	349	0.83	2.0	-53.7	276.3	0.08	0.14	**112**	0.45	0.12	**149**	0.30	0.09	
3D-40, ρ_s=0.50	49	375	352	0.94	1.8	-0.3	262.1	0.09	0.15	1	-	0.17	132	0.29	0.04	-
	3650	418	350	0.84	2.0	-53.7	263.0	0.07	0.13	**146**	0.34	0.09	**140**	0.28	0.06	
4D-40, ρ_s=0.50	49	375	354	0.95	1.8	-0.3	263.2	0.09	0.15	1	-	0.15	120	0.28	0.01	-
	3650	418	350	0.84	2.0	-53.7	262.1	0.07	0.13	**198**	0.25	0.07	**130**	0.28	0.04	

Research is performed on the crack width behaviour of *S.F.R.C.* to investigated the the effect of the fibre volume V_f and fibre aspect ratio λ_f on the maximum crack width. Different types of fibres are analysed. The performance of the fibres regarding crack width depends greatly on the volume and aspect ratio shown in Fig: F.11.

Type vezel Steel fibres	Fibre volume V_f (%)	$V_f \lambda_f$	Time of first crack (days)	Maximum crack width w_{max} (mm)
Crimped	0,25	8,3	18	0,21
l_f = 38 mm	0,50	16,7	21	0,12
Crimped	0,125	11,0	18	0,16
l_f = 50 mm	0,25	21,9	22	0,14
Hooked end	0,25	11,8	18	0,25
l_f = 50 mm	0,50	23,6	23	0,11
Flat end	0,125	6,3	18	0,33
l_f = 30 mm	0,25	12,5	18	0,22
Profiled	0,125	3,2	14	0,49
l_f = 20 mm	0,25	6,4	18	0,24
	0,50	12,8	25	0,10

Figure F.11: Crack width analysis on *S.F.R.C.*

Graphs

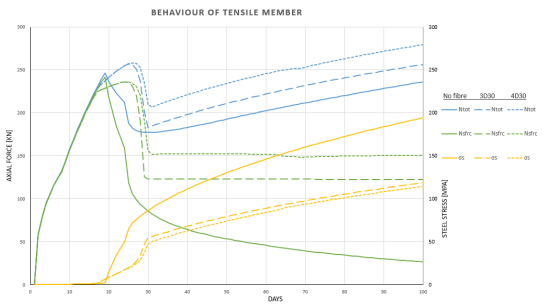

(a) Stresses in *N.T.M.*

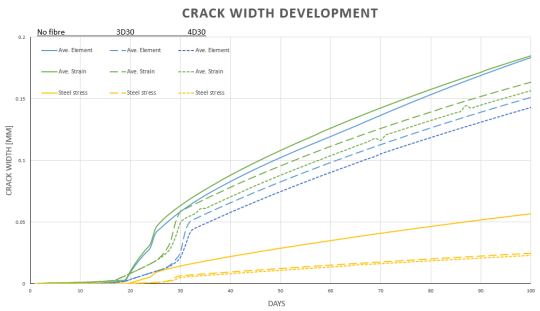

(b) Crack width in *N.T.M.*

Crack width behaviour in time

Table F.7: Comparison of calculation method for eccentric reinforced member

				Breugel	Gilbert		*M.C. 2010*	CUR-65	Stufib-11		
t	N_c	ψ_{crack}	$\sigma_{s,cr}$	w_{max}	Cracks	w_{max}	w_{max}	$\sigma_{s,cr}$	w_{max}	$\sigma_{s,cr}$	w_{max}
57	144	0.27	172	0.07	1	0.24	-	340	0.42	655	0.44
100	169	0.89	208	0.09	2	0.10		349	0.43	224	0.12
150	136	0.70	166	0.06	4	0.10	-	354	0.44	224	0.12
200	140	0.72	172	0.06	5	0.10	-	358	0.44	224	0.12
250	167	0.85	205	0.09	5	0.11	-	360	0.44	224	0.12
300	155	0.79	190	0.07	6	0.11	-	362	0.44	224	0.12
350	171	0.86	210	0.09	6	0.11	-	363	0.45	225	0.12
400	155	0.78	190	0.07	7	0.11	-	364	0.45	225	0.12
450	165	0.83	202	0.08	7	0.11	-	365	0.45	225	0.12
500	149	0.75	182	0.07	8	0.11	-	366	0.45	225	0.12
550	155	0.78	190	0.07	8	0.11	-	366	0.45	225	0.12
600	161	0.80	197	0.08	8	0.11	-	367	0.45	226	0.12
650	166	0.83	204	0.08	8	0.12	-	367	0.45	226	0.12
700	149	0.74	182	0.07	9	0.11	-	368	0.45	226	0.12
750	153	0.76	187	0.07	9	0.11	-	368	0.45	226	0.12
800	156	0.78	191	0.07	9	0.11	-	368	0.45	226	0.12
850	159	0.79	195	0.08	9	0.12	-	369	0.45	226	0.12
900	162	0.80	198	0.08	9	0.12	-	369	0.45	226	0.12
950	164	0.81	201	0.08	9	0.12	-	369	0.45	226	0.12
1000	147	0.73	180	0.07	10	0.11	-	370	0.45	226	0.12
1100	151	0.75	185	0.07	10	0.11	-	370	0.45	226	0.12
1200	154	0.76	189	0.07	10	0.12	-	370	0.45	227	0.12
1300	157	0.78	192	0.07	10	0.12	-	371	0.46	227	0.12
1400	159	0.79	195	0.08	10	0.12	-	371	0.46	227	0.12
1500	161	0.80	198	0.08	10	0.12	-	371	0.46	227	0.12
1600	163	0.81	201	0.08	10	0.12	-	372	0.46	227	0.12
1700	147	0.73	180	0.07	11	0.11	-	372	0.46	227	0.12
1800	149	0.73	182	0.07	11	0.11	-	372	0.46	227	0.12
1900	150	0.74	184	0.07	11	0.12	-	372	0.46	227	0.12

Appendix G

External loading

Elastic approach

The elastic design method for *S.o.G.* is based on the pioneering work of Westergaard in 1925. The principles, modifications and the formula's found in the literature are given below.

Westergaard principle

For the calculation of the maximum stresses in a *S.o.G.* the pioneering work of Westergaard in 1925 is still used in current guidelines. The calculations are based on the assumption that a slab acts as a homogeneous, isotropic and elastic solid in equilibrium. The slab is supported on an elastic Winkler foundation defined by the modulus of subgrade reaction. The subgrade reaction is assumed to be vertical only and proportionally with the deflection of the slab.

In 1926 Westergaard presented a mathematical analysis for the design of slab on ground pavements.[70] Westergaard's work was based on the pioneering work of Winkler(1867)[71], Hertz(1984)[72] and Foppl(1922)[73]. Before the work of Westergaard, two prominent engineers in the early 1920s tried to solve the problem of corner breaks in concrete pavements. The investigation of Goldbeck(1919)[74] and Older(1924)[75] is stated as ''the most important single step in the investigation of the mechanics of road slabs" by Ioannides et al. (1985)[76]. Westergaard solutions were available for three critical positions, namely: corner, edge and interior. Besides the stresses, Westergaard also presented formulae for the deflection of the slab under the point-load. The solution was first solely developed for the design of (semi) infinite pavements and runways to take wheel loads. Westergaard equations can now be used for dimensioning industrial floors by taking the maximum stress equal to the stress capacity of the concrete. Many experiments showed a large difference between the cracking load and the theoretical cracking load according to the Westergaard formula's[77]. It is generally admitted that Westergaard solution overestimates the values of deflection and the bending stress in the slab.[64] Nowadays, the Westergaard method is also used for the industrial ground-floor slabs. During the years, the original formula is refined, improved and expanded by Westergaard many times(1927,1933,1939,1943,1948). Also, other researchers have come up with a modification to make the solution more applicable and accurate. Different modified equations are used in guidelines. This research will compare the given Westergaard equation in the publications of *CUR-36*[18], *J. Knapton*[10], the Institution of Civil Engineers (*I.C.E.*)[78] and *A. Abbas* [5]. An overview of the calculation methods from the past century is given below.

Stresses

The design methods of the guidelines/proposals which are compared in this research will be elaborated.

Knapton [10]

In his book *Ground Bearing Concrete Slabs J. Knapton* presents the original Westergaard equation from 1926 formulated in a convenient matter. In the original equations, the contact area of the load is used. For the corner load, the length from the corner to the midpoint of the circular contact area is applied. Knapton also presents the formula of the distance $x_{max,corner}$ from the corner to the maximum tensile stress in the upper surface.

$$\sigma_{Knapton,mid} = \frac{0.31625F}{h^2} \cdot \log_{10}\left(\frac{0.36E_c h^3}{k r_{eq}^4}\right) \tag{G.1}$$

$$\sigma_{Knapton,edge} = \frac{0.57185F}{h^2} \cdot \log_{10}\left(\frac{0.20E_c h^3}{k r_{eq}^4}\right) \tag{G.2}$$

$$\sigma_{Knapton,cor} = \frac{3F}{h^2} \cdot \left(1.0 - \left(\frac{\sqrt{2}r_{eq}}{l_{rs}}\right)^{0.6}\right) \tag{G.3}$$

$$x_{max,corner} = 2 \cdot \sqrt{r_{eq}\sqrt{2}l_{rs}} \tag{G.4}$$

ICE - design and practice guide [78]

The calculation methods given in *I.C.E.* is a mixture of different researches. The cone of equivalent distribution area is now applied. For the interior load the rewritten form ,performed by *Bradbury* in 1938[79], of the equation presented by Westergaard in 1933 is used.

The edge situation is based on the work of *Kelley*. *Kelley* proposed an empirical modification of the version written by *Bradbury*. Kelley assumed a half-circle loading area at the edge with an equivalent loading area of the interior load. This gives that for the edge situation r_{eq} becomes $r_{eq} \cdot \sqrt{2}$. The adopted assumption by *Kelley* results in the lower-bound values. Furthermore, the second $\log_{10}$ term in the brackets is not dimensionless and have in this formulation the unit mm.[80] *Pickett* studied the corner situation and proposed a formula for the maximum stress with the circular contact area radius and takes into account the effect of curling at the corner.[81]

$$\sigma_{ICE,mid} = \frac{0.31625F}{h^2} \cdot \left(4 \cdot \log_{10}\left(\frac{l_{rs}}{b_{cone}} + 1.069\right)\right) \tag{G.5}$$

$$b_{cone,edge} = \sqrt{1.6(r_{eq} \cdot \sqrt{2})^2 + h^2} - 0.675h \qquad \text{for} \quad r_{eq} \cdot \sqrt{2} < 1.724h \tag{G.6}$$

$$b_{cone,edge} = r_{eq} \cdot \sqrt{2} \qquad \text{for} \quad r_{eq} \cdot \sqrt{2} \geq 1.724h \tag{G.7}$$

$$\sigma_{ICE,edge} = \frac{0.57185F}{h^2} \cdot \left(4 \cdot \log_{10}\left(\frac{l_{rs}}{b_{cone,edge}} + \log_{10}\left(\frac{b_{cone,edge}}{25.4}\right)\right)\right) \tag{G.8}$$

$$\sigma_{ICE,cor} = \frac{4.2F}{h^2} \cdot \left(1.0 - \left(\frac{\sqrt{\frac{r_{eq}}{l_{rs}}}}{0.925 + 0.22\frac{r_{eq}}{l_{rs}}}\right)\right) \tag{G.9}$$

(G.10)

CUR 36 [18]

The Dutch guideline *CUR-36* is focused on the work of *Ioannides et al* carried out in 1985[76]. They re-examined the original Westergaard solutions with the use of a *L.F.E.A.* and concluded that the formulas Westergaard presented in 1948 should be used for the interior and especially the edge situation. For the interior situation the formula of 1948 is expanded with an additional part due to a larger loading area which Westergaard presented in 1939.[**?**] *Ioannides et al.* also suggested a modified solution based on the original Westergaard solution for the corner situation. In the recommendation *CUR-36*, there is an extra step for the calculation of the equivalent radius. Instead of r_{eq}, it is proposed to use the circular loading area $a_{eq}{}^*$ in the calculations, which increases the ratio with half the slab height. The equation is given below.

$$a_{eq} = r_{eq} + 0.5h \tag{G.11}$$

$$b_{cone} = \sqrt{1.6a_{eq}^2 + h^2} - 0.675h \quad \text{for} \quad a_{eq} < 1.724h \tag{G.12}$$

$$b_{cone} = a_{eq} \quad \text{for} \quad a_{eq} \geq 1.724h \tag{G.13}$$

$$\sigma_{CUR36,mid} = \frac{0.55F}{h^2} \cdot \ln\left(\frac{l_{rs}}{b_{cone}} + 0.62\right) + \frac{0.05F}{h^2} \cdot \left(\frac{{b_{cone}}^2}{l_{rs}}\right) \tag{G.14}$$

$$\sigma_{CUR36,edge} = \frac{0.35F}{h^2} \cdot \left(\ln\frac{E_c h^3}{100ka_{eq}^4} + 2.07 + 1.53\frac{a_{eq}}{l_{rs}}\right) \tag{G.15}$$

$$\sigma_{CUR36,cor} = \frac{3F}{h^2} \cdot \left(1.0 - \left(\frac{a_{eq}\sqrt{\pi}}{l_{rs}}\right)^{0.72}\right) \tag{G.16}$$

***Notation**

During the literature study it is found that there is no agreement with the formulas in the *CUR-36* report with other documents. The formula of the cone of equivalent distribution area is likely presented wrong. The dimensions are not in agreement, $mm^2 + mm = mm$, and is it differs from the original formula found in many different articles. Below are the original, *CUR-36* and assumed correct *CUR-36* formulas shown.

$$b_{original} = \sqrt{1.6r_{eq}^2 + h^2} - 0.675h \quad \text{for} \quad r_{eq} < 1.724h \tag{G.17}$$

$$b_{original} = r_{eq} \quad \text{for} \quad r_{eq} \geq 1.724h \tag{G.18}$$

$$b_{cur36} = \sqrt{1.6r_{eq}^2} + h^2 - 0.675h + 0.5h \quad \text{for} \quad r_{eq} < 1.724h \tag{G.19}$$

$$b_{cur36} = a_{eq} \quad \text{for} \quad r_{eq} \geq 1.724h \tag{G.20}$$

$$b_{assumed} = \sqrt{1.6(r_{eq} + 0.5h)^2 + h^2} - 0.675h \quad \text{for} \quad r_{eq} < 1.724h \tag{G.21}$$

$$b_{assumed} = a_{eq} \quad \text{for} \quad r_{eq} \geq 1.724h \tag{G.22}$$

Also some questions arise according to the a_{eq}. Nowhere in the literature the assumption of a beneficial larger radius is found. Assumed is that a_{eq} is the equivalent radius in the centreline of the slab which is maybe the assumption of Westergaard calculations.

LFEA - Abbas

With the use of *L.F.E.A. A. Abbas* presented optimised equations of the Westergaard methode. Multiple analyses resulted in stress and deflection equations for the three main load situations. With the analysis, correct factors are taken from the standard values for b_{100} and r_{50}. The original equations are based on the length, l_{width}, of a square patch load. For comparison reasons r_{eq} is used in the equations below. *A. Abbas* compared the results

with guidelines and concluded that the formulas are in agreement and produce more economical results.

$$\sigma_{LFEA,mid} = 1.0186 \cdot \left(1.1301 - 0.1362 \frac{r_{eq}\sqrt{\pi}}{b_{100}}\right) \frac{F}{h^2} \cdot \left(\log_{10}\left(\frac{l_{rs}}{b_{100}}\right)\right) \tag{G.23}$$

$$\sigma_{LFEA,edge} = 2.1982 \cdot \left(1.2135 - 0.2163 \frac{r_{eq}\sqrt{\pi}}{b_{100}}\right) \frac{F}{h^2} \cdot \left(\log_{10}\left(\frac{l_{rs}}{b_{100}}\right)\right) \tag{G.24}$$

$$\sigma_{LFEA,cor} = 3.2053 \cdot \left(1.1652 - 0.1651 \frac{r_{eq}}{r_{50}}\right) \frac{F}{h^2} \cdot \left(1 - \frac{r_{50}\sqrt{2}}{l_{rs}}\right)^{3.20} \tag{G.25}$$

$$b_{100} = 100 \tag{G.26}$$

$$r_{50} = 50 \cdot \sqrt{2} \tag{G.27}$$

$$M_{Ed} = \frac{\sigma_{mid} h^2 B}{6(1-\nu^2)} \cdot 10^{-6} \tag{G.28}$$

Deflection

In 1925 Westergaard also included formulae for deflection due to a point load. After further research, Westergaard changed the formula in 1939 for the interior load to allow larger load area's. *Childs* and *Kapernick* carried out experimental tests and concluded that for flat slabs Westergaards solutions are in good agreement with the load-deflection test results.[82] Also, the results from the *L.FE.A.* by Abbas are close to Westergaard equations. The produced equations of Westergaard and Abbas are given below.

Westergaard

$$\delta_{wes1925,mid} = \frac{0.125F}{k_{mod} l_{rs}^2} \tag{G.29}$$

$$\delta_{wes1938,mid} = \frac{0.125F}{k_{mod} l_{rs}^2} \cdot \left(1 + \left(0.3665 \log_{10} \frac{r_{eq}}{l_{rs}} - 0.2174\right) \cdot \left(\frac{r_{eq}}{l_{rs}}\right)^2\right) \tag{G.30}$$

$$\delta_{wes1925,edge} = \frac{0.433F}{k_{mod} l_{rs}^2} \tag{G.31}$$

$$\delta_{wes1925,cor} = \left(1.1 - 0.88 \frac{r_{eq}\sqrt{2}}{l_{rs}}\right) \frac{F}{k_{mod} l_{rs}^2} \tag{G.32}$$

LFEA - Abbas

$$\delta_{LFEA,mid} = \text{CFWLA} \cdot \frac{0.1236F}{k_{mod} l_{rs}^2} \quad \text{with} \tag{G.33}$$

$$\text{CFWLA} = 1.0 \quad \text{for } 0 \le b_{cone} \le 250\text{mm} \tag{G.34}$$

$$\text{CFWLA} = 1.2439 - 0.1038 \frac{b_{cone}}{b_{100}} \quad \text{for } b_{cone} > 250\text{mm} \tag{G.35}$$

$$\delta_{LFEA,edge} = 0.4016 \cdot \left(1.0376 - 0.0434 \frac{b_{cone}}{b_{100}}\right) \frac{F}{k_{mod} l_{rs}^2} \tag{G.36}$$

$$\delta_{LFEA,cor} = 2.2708 \cdot \left(1.048 - 0.0643 \frac{r_{eq}}{r_{50}}\right) \left(0.5775 - \frac{r_{eq}\sqrt{2}}{l_{rs}}\right) \frac{F}{k_{mod} l_{rs}^2} \tag{G.37}$$

Influence length

All the equations are based on the same principle and parameters, which are introduced by *Westergaard*. The most important parameter is known as the radius of relative stiffness l_{rs}. The relative stiffness is the relation

between the flexural rigidity of the slab D and the subgrade modulus of the soil k_{mod}. Where E_{cm} is the Young's modulus of concrete, h height of the slab and υ the Poisson ratio taken as 0.15 for concrete.

$$l_{rs} = \sqrt[4]{\frac{D}{k_{mod}}} \quad \text{with} \quad D = \frac{E_c h^3}{12(1-\upsilon^2)} \quad \Longrightarrow \quad l_{rs} = \sqrt[4]{\frac{E_c h^3}{12(1-\upsilon^2)k_{mod}}} = \sqrt[4]{\frac{E_c h^3}{11.73 k_{mod}}} \tag{G.38}$$

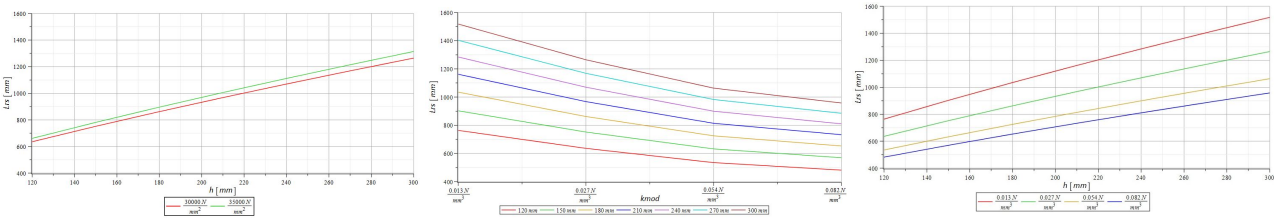

(a) Influence of E_{cm} on l_{rs} (k_{mod}=0.027) **(b)** Influence of h on l_{rs} (E_{cm}=30000) **(c)** Influence of k_{mod} on l_{rs} (E_{cm}=30000)

Figure G.1: Influence relative stiffness radius l_{rs}

Besides the above-mentioned parameters, the maximum stresses depend on the loading area and the force. The maximum stress in the slab is proportional to the point-load, for example, from a wheel or rack, $\sigma_{max} \propto F$. For the loading area, Westergaard assumed a circular patch load with uniform stress distribution. In practice, the patch loads will be rectangular, but these assumptions lead to minor errors and are conservative[10]. An improvement by Westergaard was to introduce a non zero cone of equivalent distribution of pressure b_{cone} at the bottom of the slab to overcome singularity problems when the load is concentrated i.e., a point-load. The expression is based on an equivalent circular contact area of the load r_{eq} and the height of the slab h. The value of b_{cone} is governed by the relation between r_{eq} and h. The improvement of Westergaard is used by the methods of *I.C.E.*, *CUR-36* and *A. Abbas*. *J. Knapton* presents in his book the formula's based on the equivalents contact radius r_{eq}. The equivalent contact radius is based on the length l_{length} and width l_{width} of the rectangular loading area.

$$r_{eq} = \sqrt{\frac{l_{lengt} \cdot l_{width}}{\pi}} \tag{G.39}$$

$$b_{cone} = \sqrt{1.6 r_{eq}^2 + h^2} - 0.675h \qquad \text{for} \quad r_{eq} < 1.724h \tag{G.40}$$

$$b_{cone} = r_{eq} \qquad \text{for} \quad r_{eq} \geq 1.724h \tag{G.41}$$

The loading area differs slightly per guideline. Also, some guidelines present formulas to calculated the position of the maximum corner stress. These deviations and additions will be elaborated when needed. In general, the maximum tensile stress occurs at the bottom of the slab under the patch load for corner and edge loads. The maximum tensile stress for the corner situation arises at the top of the slab at a certain distance from the corner.

Slab stresses

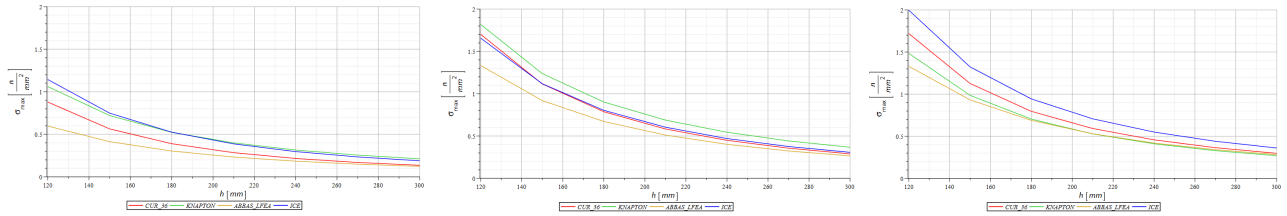

(a) σ_{max} for interior load **(b)** σ_{max} for edge load **(c)** σ_{max} for corner load

Figure G.2: σ_{max} per location for (E_{cm}=30000,k_{mod}=0.027,A_{load}=10000)

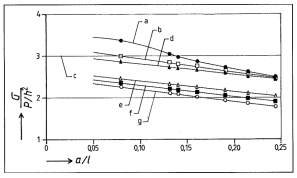

(a) Overview corner calculation methods(a= *I.C.E.*, g=*Knapton*, f=*L.F.E.A.*)

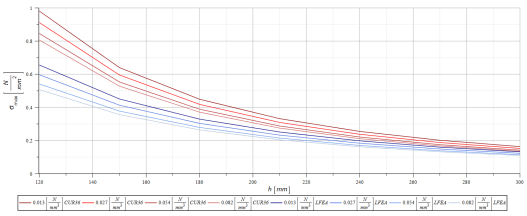

(b) Soil stiffness k_{mod}

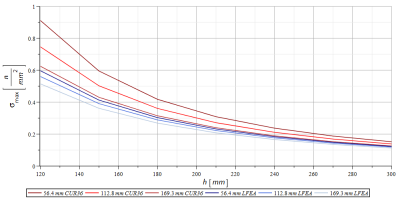

(c) Load area

Figure G.3: Influence on stress

N.L.F.E.A.

Point loads

Table G.1: Analysis of point loads

	k_{mod}=0.01	k_{mod}=0.05	k_{mod}=0.10	E_{cm}=10000	E_{cm}=20000	E_{cm}=30000	h=120	h=180	h=240	C20/25	C30/37	σ_c<σ_{cr}	σ_c»σ_{cr}	Unit
σ_{cr}	1.76	1.76	1.73	1.8	1.76	1.74	1.63	1.76	2.1	1.12	1.76	1.60	1.98	Mpa
$M_{z,cr}$	9.50	9.50	9.34	9.72	9.50	9.40	3.91	9.50	20.16	6.05	9.50	8.64	10.69	kNmm^{-1}
l_{rs}	999	668	562	562	668	739	493	668	829	668	668	668	668	mm
$\sigma_{LFEA,mid}$	2.73	2.26	2.05	2.05	2.26	2.38	4.26	2.26	1.41	2.26	2.26	2.26	2.26	MPa
σ_{Sxx}	5.16	5.27	5.14	5.12	5.27	5.34	11.60	5.27	2.97	5.27	5.27	2.64	10.55	MPa
F_{equ}	170	210	226	225	210	202	245	210	189	210	210	105	420	kN
$M_{z,cr}$	19.0	16.3	14.9	14.6	16.3	16.9	16.8	16.3	28.0	17.1	16.3	14.1	33.1	kNmm^{-1}
$M_{z,uncr}$	-16.9	-11.2	-11.2	-11.4	-11.2	-11.5	-11.1	-11.2	-9.5	-10.7	-11.2	-3.2	-22.0	kNmm^{-1}
N_{uncr}	-176	-134	-117	-123	-134	-140	-165	-134	-13	-136	-134	-0.64	-311	kNm^{-1}
$\sigma_{s,cr}$	59.5	46.8	32.4	65.3	46.8	32.9	166.6	46.8	-18.9	41.1	46.8	-13.9	82.5	MPa
d_Y	4	2	1	3	2	2	4	2	1	2	2	1	4	mm
Scale factor	1.24	1.00	0.93	0.94	1.00	1.04	0.86	1.00	1.11	1.00	1.00	2.00	0.50	-
$M_{z,cr}$	23.5	16.3	13.9	13.7	16.3	17.6	14.4	16.3	31.1	17.1	16.3	28.2	16.6	kNmm^{-1}
$M_{z,uncr}$	-20.9	-11.2	-10.4	-10.7	-11.2	-12.0	-9.5	-11.2	-10.6	-10.7	-11.2	-6.4	-11.0	kNmm^{-1}
N_{uncr}	-218	-134	-109	-115	-134	-146	-142	-134	-14	-136	-134	-1	-156	kNm^{-1}
$\sigma_{s,cr}$	73.6	46.8	30.2	61.1	46.8	34.2	143.0	46.8	-21.0	41.1	46.8	-27.8	41.3	MPa
d_Y	6	2	1	3	2	2	3	2	1	2	2	2	2	mm

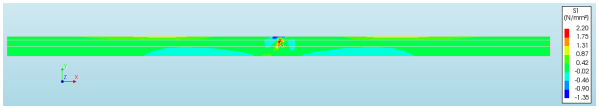

(a) Principal stress 1

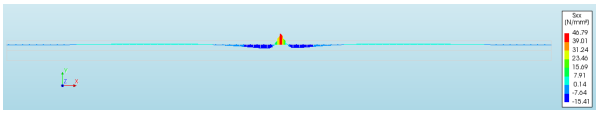

(b) Steel stress

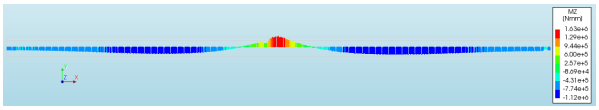

(c) Bending moment

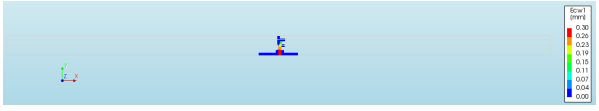

(d) Cracking behaviour

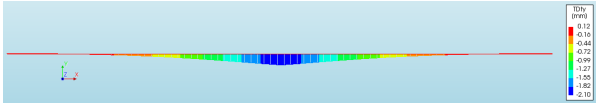

(e) Slab settlement

Figure G.4: C30/37

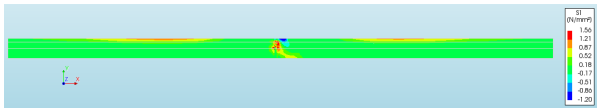

(a) Principal stress 1

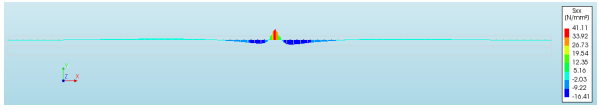

(b) Steel stress

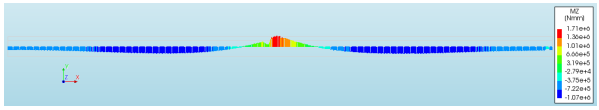

(c) Bending moment

(d) Cracking behaviour

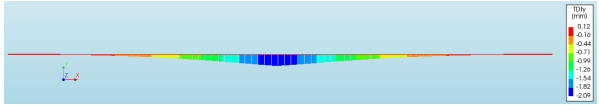

(e) Slab settlement

Figure G.5: C20/25

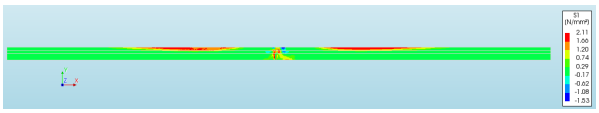

(a) Principal stress 1

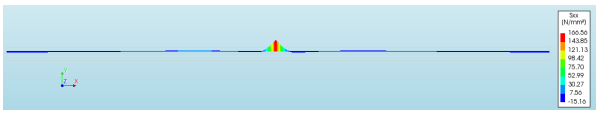

(b) Steel stress

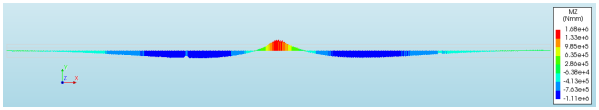

(c) Bending moment

(d) Cracking behaviour

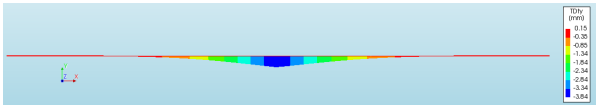

(e) Slab settlement

Figure G.6: h = 120 mm

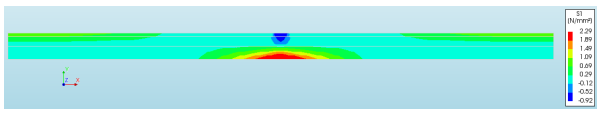

(a) Principal stress 1

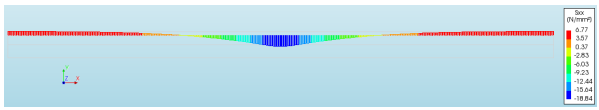

(b) Steel stress

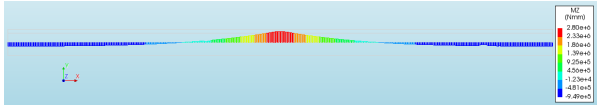

(c) Bending moment

(d) Cracking behaviour

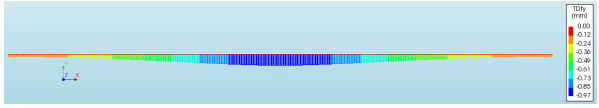

(e) Slab settlement

Figure G.7: h = 240 mm

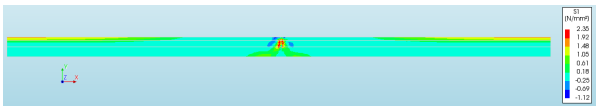

(a) Principal stress 1

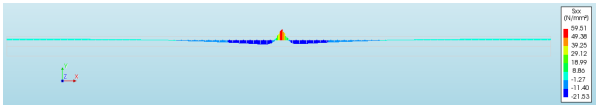

(b) Steel stress

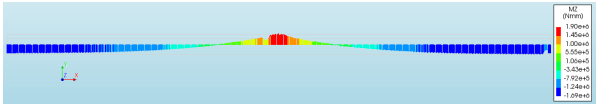

(c) Bending moment

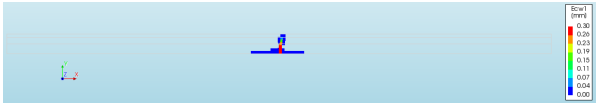

(d) Cracking behaviour

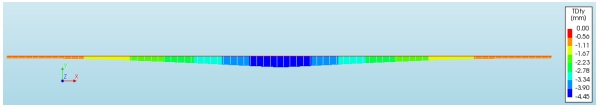

(e) Slab settlement

Figure G.8: k_{mod} = 0.01 N mm^{-3}

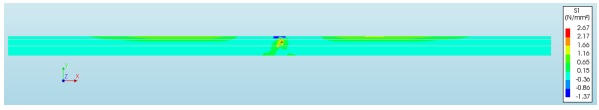

(a) Principal stress 1

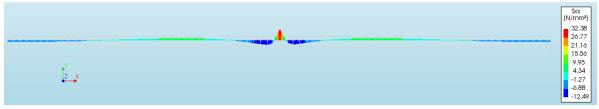

(b) Steel stress

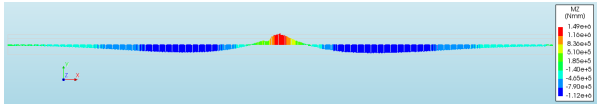

(c) Bending moment

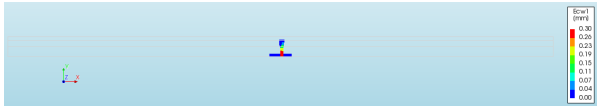

(d) Cracking behaviour

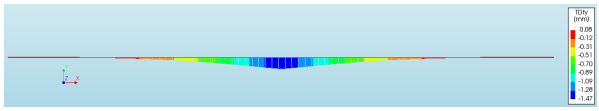

(e) Slab settlement

Figure G.9: k_{mod} = 0.1 N mm^{-3}

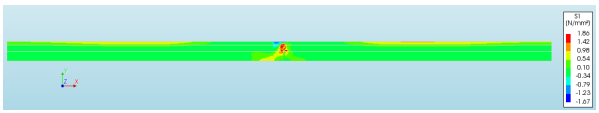

(a) Principal stress 1

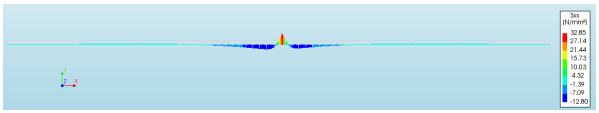

(b) Steel stress

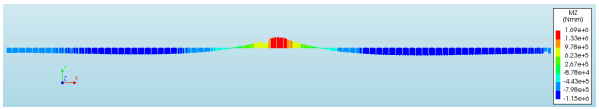

(c) Bending moment

(d) Cracking behaviour

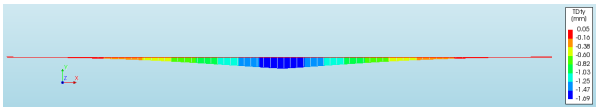

(e) Slab settlement

Figure G.10: E_{cm} = 30000 MPa

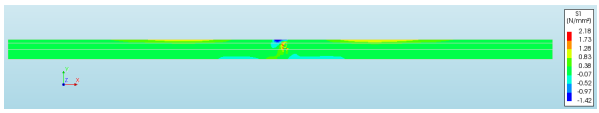

(a) Principal stress 1

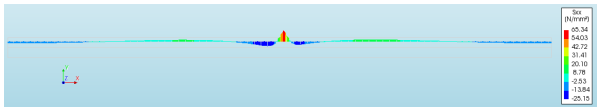

(b) Steel stress

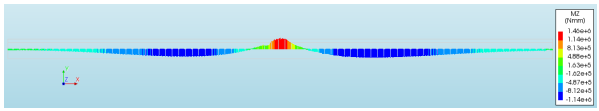

(c) Bending moment

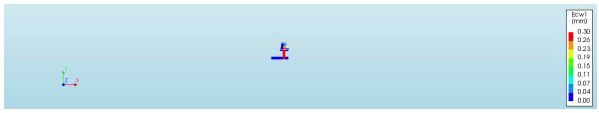

(d) Cracking behaviour

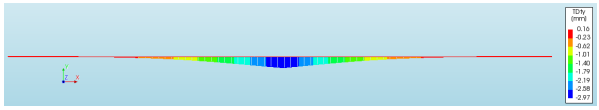

(e) Slab settlement

Figure G.11: E_{cm} = 10000 MPa

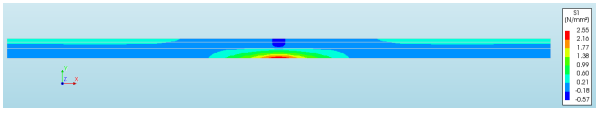

(a) Principal stress 1

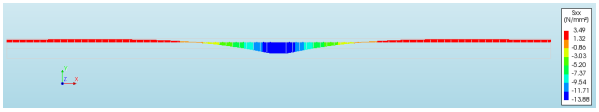

(b) Steel stress

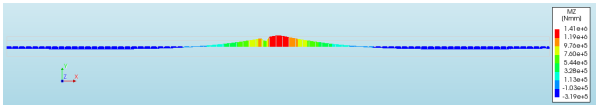

(c) Bending moment

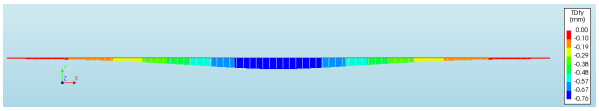

(d) Slab settlement

Figure G.12: low loaded slab F_{eqv}= 105 kN

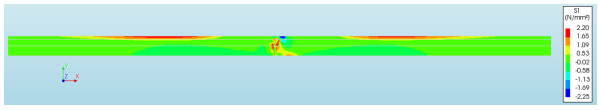

(a) Principal stress 1

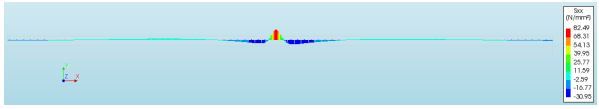

(b) Steel stress

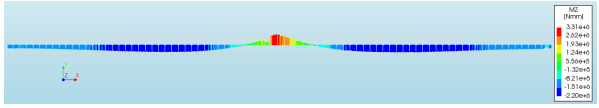

(c) Bending moment

(d) Cracking behaviour

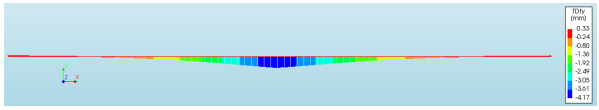

(e) Slab settlement

Figure G.13: Heavy loaded slab F_{eqv}= 360 kN

Combined loading

- Situation 1: *S.R.A.* concrete with low racking load
- Situation 2: Normal concrete with low racking load
- Situation 3: *S.R.A.* concrete with high racking load
- Situation 4: Normal concrete with high racking load
- Situation 5: *S.R.A.* concrete with low racking load with C20/25

- Situation 6: *S.R.A.* concrete with low racking load on slab of 120 mm thick
- Situation 7: Hybrid normal concrete with low racking load

Values

Table G.2: Analysis of combined loads

	Parameter	Situation 1	Situation 2	Situation 3	Situation 4	Situation 5	Situation 6	Situation 7	Unit
L.F.E.A.	$\sigma_{LFEA,mid}$	2.54	2.96	4.84	4.45	2.40	4.43	2.42	MPa
	F_{eqv}	109	116	208	174	103	102	104	kN
N.L.F.E.A.	σ_{cr}	2.54	2.47	2.35	2.61	1.86	2.58	2.38	MPa
	M_{uncr}	-14.5	-12.5	-18.2	-16.0	-11.4	-6.3	-13.8	kN m m^{-1}
	N_{uncr}	114	168	154	119	93	103	240	kN
	$\sigma_{s,cr}$	216	228	183	245	191	266	121	MPa
	w_{mo}	0.15	0.25	0.14	0.25	0.11	0.17	0.01	mm
	Cracks	2	6	8	6	6	4	1	
	l_t	159	128	150	155	130	120	100	mm
	d_Y	7	6	12	10	7	10	6	mm
Scaled values	Factor	0.91	0.86	0.48	0.57	0.97	0.98	0.96	-
	M_{uncr}	-13.3	-10.8	-8.7	-9.2	-11.0	-6.1	-13.2	kN m m^{-1}
	N_{uncr}	104	145	7	68	90	101	230	kN
	$\sigma_{s,cr}$	198	196	88	142	185	260	116	MPa
	w_{mo}	0.14	0.22	0.07	0.14	0.11	0.17	0.01	mm
	Cracks	2	5	4	3	6	4	1	-
	l_t	145	110	72	89	126	117	96	mm
	d_Y	6	5	6	6	7	9	6	mm
Analytical	Models								
Gilbert	l_t	187	187	187	187	187	135	136	mm
	$\sigma_{s,cr}$	214	290	226	282	246	266	286	MPa
CUR-65	w_{max}	0.36	0.35	0.33	0.37	0.26	0.21	0.17	mm
	$\sigma_{s,cr}$	317	313	293	329	236	265	213	MPa
Stu*fib*-11	w_{max}	0.36	0.35	0.31	0.38	0.28	0.22	0.10	mm
	$\sigma_{s,cr}$	434	429	401	451	320	335	210	MPa

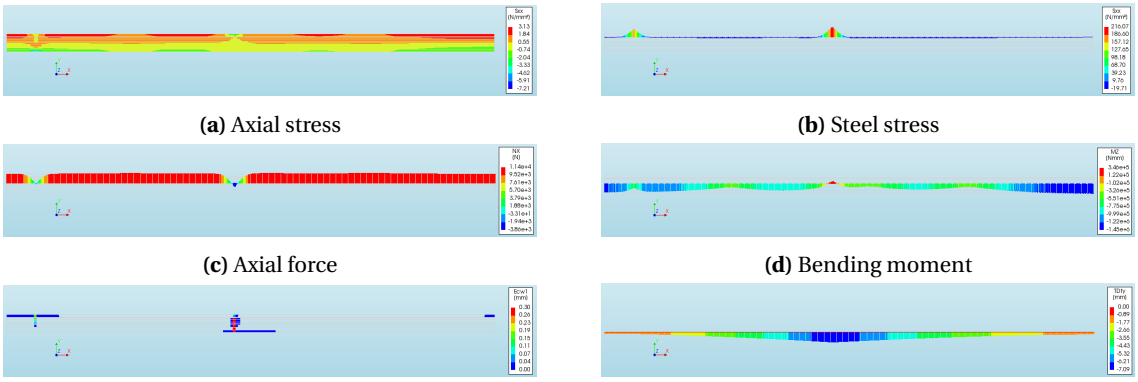

(a) Axial stress

(b) Steel stress

(c) Axial force

(d) Bending moment

(e) Cracking behaviour

(f) Slab settlement

Figure G.14: Situation 1: SRA concrete with low racking loads

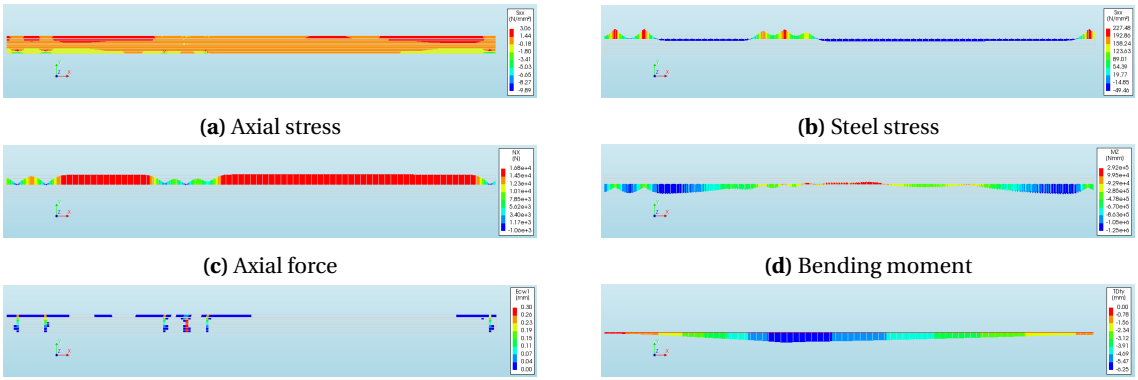

(a) Axial stress

(b) Steel stress

(c) Axial force

(d) Bending moment

(e) Cracking behaviour

(f) Slab settlement

Figure G.15: Situation 2: Normal concrete with low racking loads

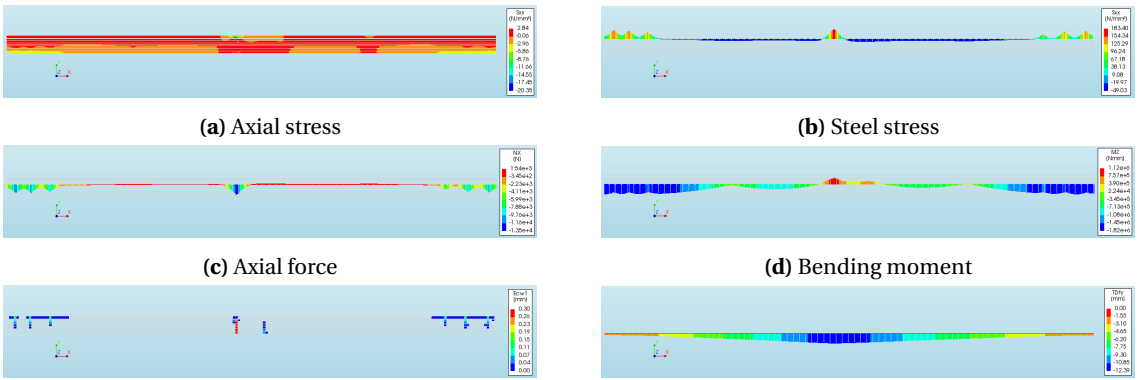

(a) Axial stress

(b) Steel stress

(c) Axial force

(d) Bending moment

(e) Cracking behaviour

(f) Slab settlement

Figure G.16: Situation 3: SRA concrete with high racking loads

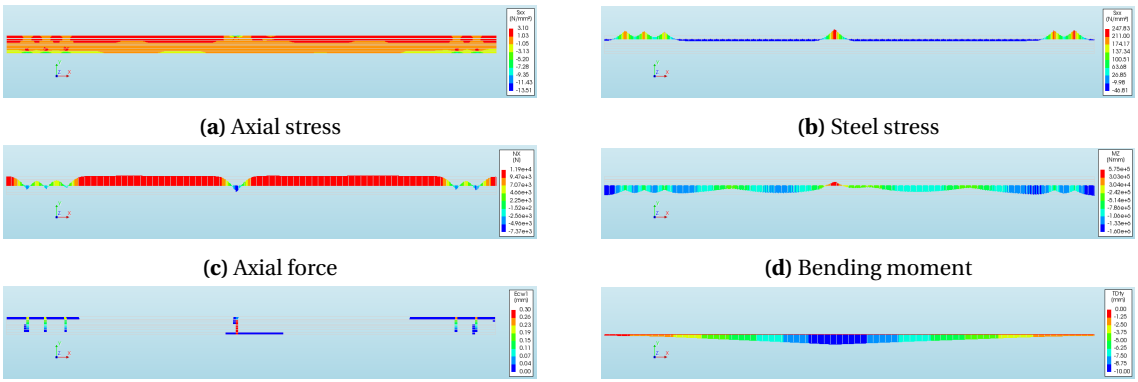

(a) Axial stress

(b) Steel stress

(c) Axial force

(d) Bending moment

(e) Cracking behaviour

(f) Slab settlement

Figure G.17: Situation 4: Normal concrete with high racking loads

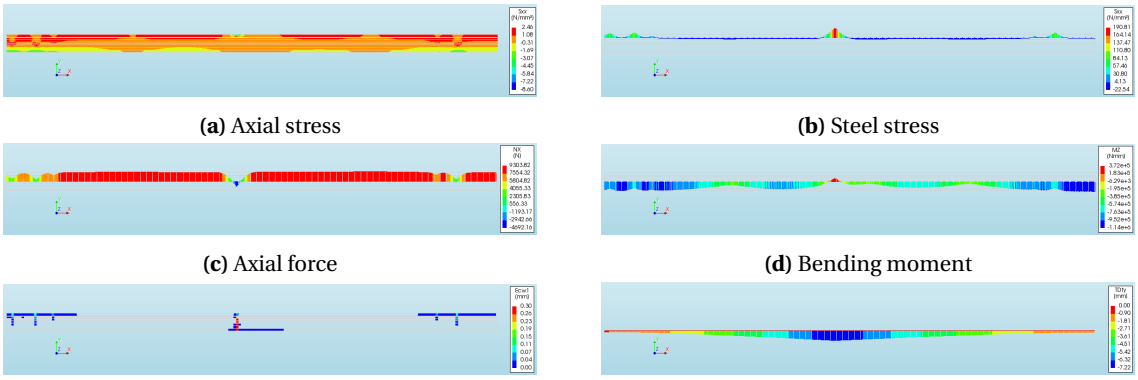

(a) Axial stress

(b) Steel stress

(c) Axial force

(d) Bending moment

(e) Cracking behaviour

(f) Slab settlement

Figure G.18: Situation 5: C20/25

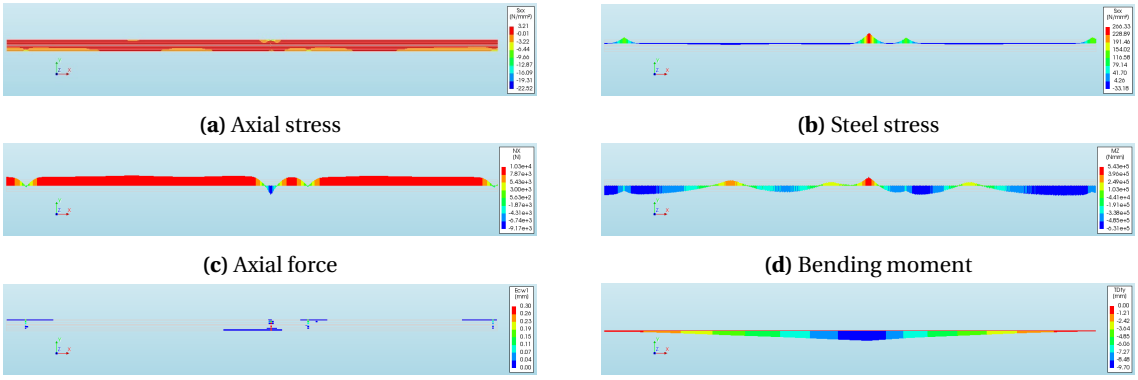

(a) Axial stress

(b) Steel stress

(c) Axial force

(d) Bending moment

(e) Cracking behaviour

(f) Slab settlement

Figure G.19: Situation 6: h=120 mm

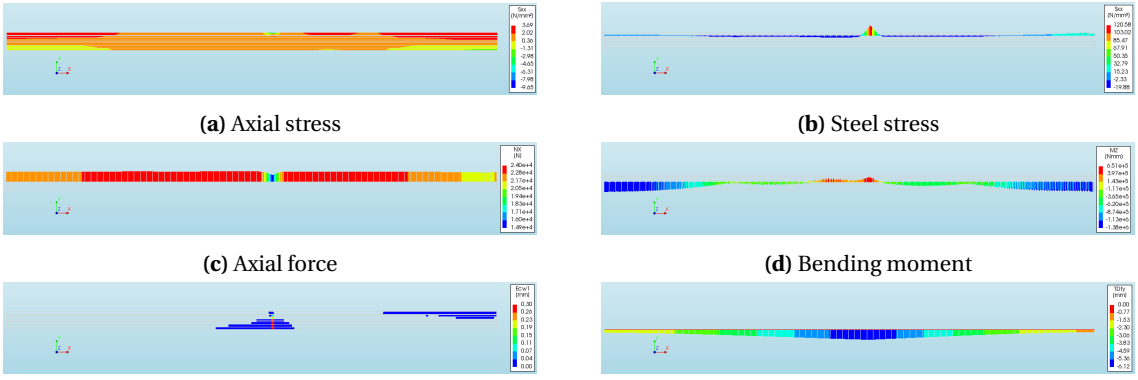

(a) Axial stress

(b) Steel stress

(c) Axial force

(d) Bending moment

(e) Cracking behaviour

(f) Slab settlement

Figure G.20: Situation 7: Hybrid concrete

Appendix H

Soil calculation models

Pasternak

The Fig: H.1 the effect of the soil shear interaction is shown. The ζ represents the shear capacity of the soil in the Pasternak model. An increasing ζ increases the shear capacity and this reduces the deflection and stresses in the slab.

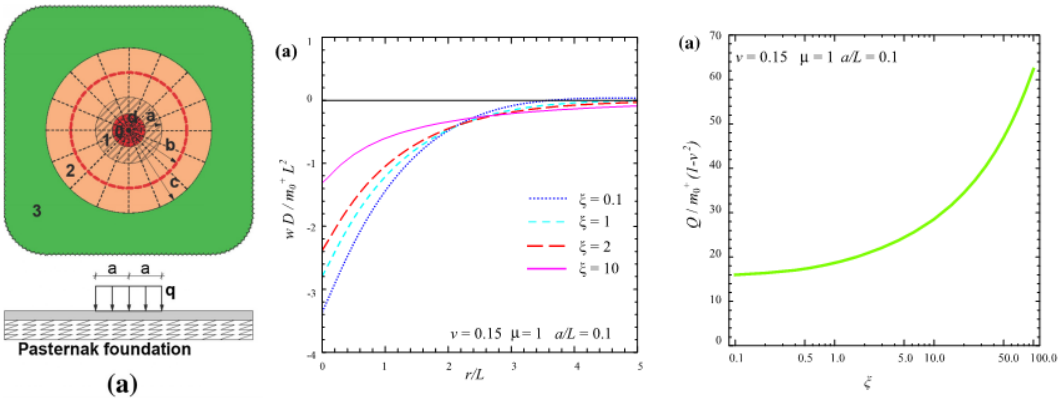

(a) Overview **(b)** Displacement **(c)** Stresses

Figure H.1: Analysis of the Pasternak model

Studies of soil models

Model comparison

Walker and Holland investigated the subgrade modulus value. They stated that there should be three different types of subgrade modulus used for calculating *S.o.G.*. The subgrade modulus is not a fixed soil property and is a function of the soil elastic properties, loading intensity, loading area and stiffness of the slab[48]. The initial response and the long-term response due to soil consolidation from the sustained loading influence the elastic soil properties. The loading intensity has an effect on the long-term consolidation settlement. The loading area determines the area over which the load is applied. Wider and larger loading areas will involve the consolidation of the deeper soil layers. Finally, the slab stiffness influence the distribution of the soil bearing pressure.

Because, in practice, it is a widespread misunderstanding that the subgrade reaction is a single value, it is important to state the limitations with a certain subgrade modulus. The researchers mentioned that both the structural and the geotechnical engineers are responsible for the correct use of the subgrade modulus.

According to them the structural engineer is responsible for the type of loading and the intensity of it. He also should provide the amount and size of the slab surface area's that will be loaded. And should include the length of loading time. Make clear that to the owner's that slabs are sensitive to cracking, soil settlement and slab sloping due to the settlement. The geotechnical engineer is responsible for providing recommendations for the subgrade modulus to be used for the different load cases.

The geotechnical engineer should use the information provided by the structural engineer and the site soil properties determined with tests. Finally, he should recommend any testing that needs to be performed to support the provided subgrade reaction values. For industrial slabs there should be two types of subgrade reaction given by the geotechnical engineer. First, the short term loading (plate) subgrade modulus. Secondly, the long-term loading subgrade modulus for loads like wide area rack or uniform storage loads.

With the use of two computer models representing a coupled soil (Pasternak) and an uncoupled (Winkler), the values are compared. The Winkler parameter is iteratively determined to create the same stresses in the concrete slab as the solid soil model. The value is approximately 35% of the plate subgrade reaction, which is according to many published reductions.

The model represents a concrete slab of 152 mm supporting rack post loads of 32 kN. From the model it is found that uniform stress distribution is reached at 4.27 meter shown in figure H.2a. Settlements above this line will produce stresses in the slab. The settlement due to the uniform stresses only produces uniform displacement of the slab. In figure H.2b the total displacement of the slabs are given. Noticeable is that the Winkler model only produces differential deflections. The solid soil model also produces uniform (long-term) settlement of 30 mm. The differential settlement for the solid model (0.78 mm) and spring model (0.61 mm) is not the same because the springs in the subgrade reaction model are uncoupled.

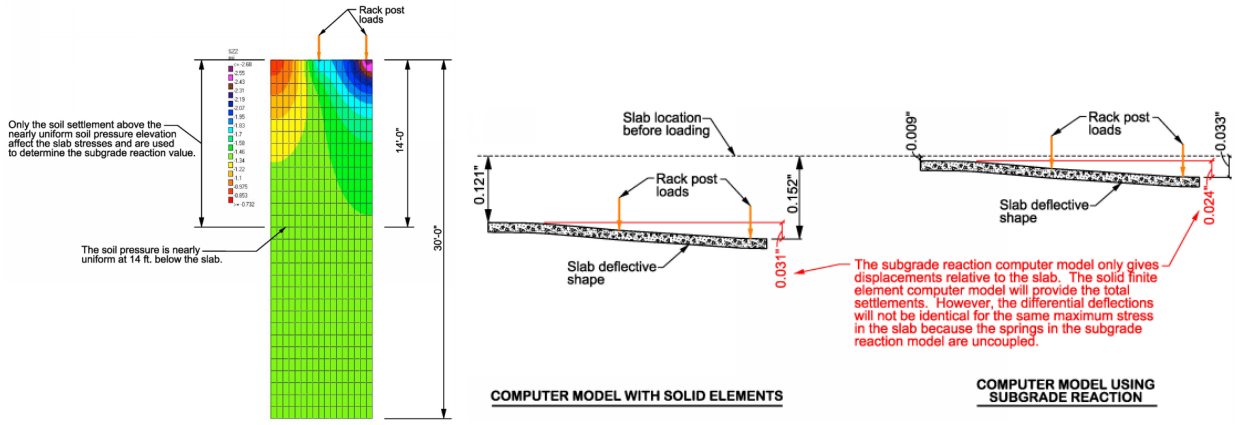

(a) Vertical soil stress **(b)** slab displacement models

Figure H.2: Model results

The values of the different types of subgrade reaction modules are calculated for standard soil types. In figure H.3 general value are given which can only be used for industrial floors on grade. [1000 psi = 6.9 $\mathrm{N\,mm^{-2}}$, 1000 PCI = 0.272 $\mathrm{N\,mm^{-3}}$].

These values are shown for information only and should not be used for slab designs with these types of soils. The K_{ws} values should be used for these types of soils.

Table 1 – Subgrade Reaction Design Values

Soil Type	E_s (psi)	μ	K_p (PCI)	K_w (PCI)	Ratio $\frac{K_w}{K_p}$	K_{ws} (PCI	Ratio $\frac{K_{ws}}{K_p}$
Clay Soft	2,000	0.45	110	70	0.64	50	0.45
Medium	4,800	0.35	230	130	0.57	80	0.35
Hard	10,600	0.20	470	260	0.55	140	0.30
Sandy	15,600	0.25	710	390	0.55	200	0.28
Sand Silty	2,000	0.30	90	70	0.78	---	---
Loose	2,500	0.30	120	80	0.67	---	---
Dense	9,500	0.35	460	240	0.52	---	---

Plate subgrade reaction design values used for short-term loadings over small areas, such as vehicle wheel loads.

Subgrade reaction design values reduced for wide area storage loadings, such as uniform or rack loads. Typically, sandy soils have mostly initial elastic settlements and little long-term soil consolidation. Therefore, these values are not reduced for long-term soil consolidation.

Subgrade reaction design values reduced for wide area storage loadings, such as uniform or rack loads, and reduced due to long-term soil consolidation settlements typical of clay types of soils.

Figure H.3: Subgrade modulus k_{mod} values

Soil comparison

Barros researched the effect of different soil types on a point loaded *S.o.G.*. Wire reinforced concrete (142 $mm^2\,m^{-1}$) and equivalent *S.FR.C.* (40 $kg\,m^{-3}$) are compared for failure load, crack pattern and displacement. The steel fibre reinforcement represents the same maximum resisting moment as the wire reinforcement but works positive as well as negative. It's equivalent to the conventionally reinforced slab in both faces. The properties are given in Fig: H.4a. The results for internal loading are shown in Fig:H.4. The blue represents the SFRC and the red the wire-reinforced slab. The contact-loss line represents a non-linear spring element that can not take over tension stresses[83].

Concrete	Soil
E_c =30 000 MPa υ =0.15 f_{ck} =20 MPa f_{ctk} =1.6 MPa l_h =square root of the Gauss point area[10] Plain concrete: G_f =0.06 N.mm α =0.3; ξ =0.1 (bilinear softening diagram) *SFRC*: G_f =2.068 N.mm α_1 =0.55; ξ_1 =0.004, α_2 =0.25; ξ_2 =0.2	k_s =0.06 N/mm^3, β p_{su} = 0.036 MPa soil 1: p_{su} = 0.4 MPa, β = 0.09, a_{su} = 13.33 mm soil 2: p_{su} = 0.1 MPa, β = 0.36, a_{su} = 3.33 mm
Reinforcement	
f_{syd} =500 MPa E_s =200 000 MPa	

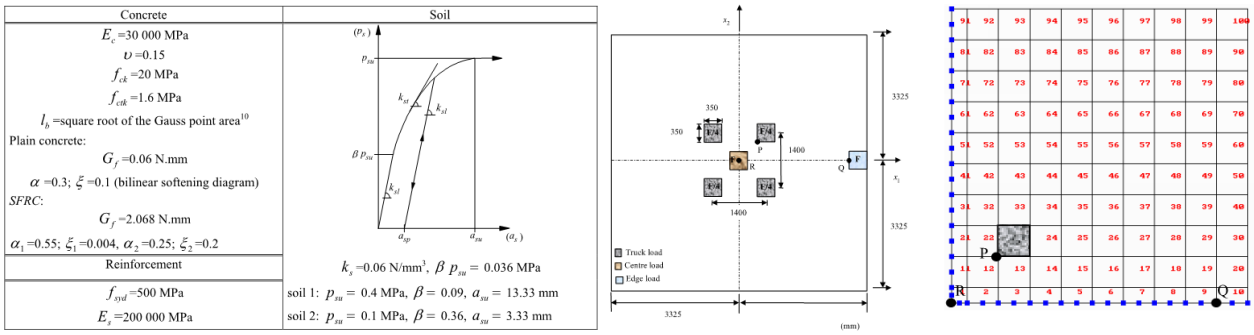

(a) Properties **(b)** FEM

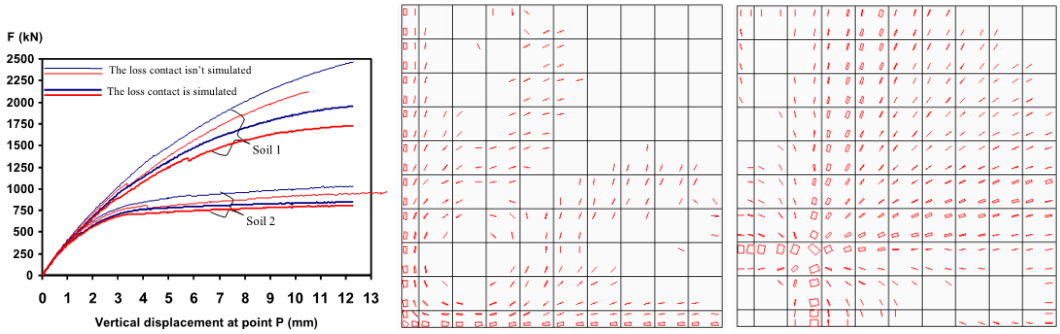

(c) **(d)** Crack pattern: Top **(e)** Crack pattern: bottom

Figure H.4: Behaviour of *S.o.G.* by point load

From the research, the following can be concluded:

- Simulating contact loss between the slab and soil results in lower maximum load-bearing capacity.
- Contact loss effect increases with an increase in soil load-bearing capacity.
- Soil properties have a big influence on the crack pattern and the maximum load-bearing capacity.